

Walther-Straub-Institute for Pharmacology and Toxicology,
Ludwig-Maximilians-Universität zu München



Dissertation

zum Erwerb des Doctor of Philosophy (Ph.D.) an der
Medizinischen Fakultät der
Ludwig-Maximilians-Universität zu München

***Investigation of potencies, selectivities and
binding modes of nicotinic acetylcholine
receptor modulators***

vorgelegt von:

Yves Haufe

aus:

Meißen, Deutschland

Jahr:

2022

Mit Genehmigung der Medizinischen Fakultät der
Ludwig-Maximilians-Universität zu München

First supervisor: Prof. Dr. Annette Nicke

Second supervisor: Prof. Dr. Ingrid Boekhoff

Third supervisor: Prof. Dr. med Stephan Kröger

Dean: Prof. Dr. med. Thomas Gudermann

Datum der Verteidigung:

20.07.2022

Affidavit



LUDWIG-
MAXIMILIANS-
UNIVERSITÄT
MÜNCHEN

Promotionsbüro
Medizinische Fakultät



Affidavit

Haufe, Yves

Surname, first name

Nussbaumstrasse 26

Street

80336, Munich, Germany

Zip code, town, country

I hereby declare, that the submitted thesis entitled:

Investigation of potencies, selectivities and binding modes of nicotinic acetylcholine receptor modulators

is my own work. I have only used the sources indicated and have not made unauthorised use of services of a third party. Where the work of others has been quoted or reproduced, the source is always given.

I further declare that the submitted thesis or parts thereof have not been presented as part of an examination degree to any other university.

Munich, 15.03.2022

place, date

Yves Haufe

Signature doctoral candidate

Confirmation of congruency



Confirmation of congruency between printed and electronic version of the doctoral thesis

Haufe, Yves

Surname, first name

Nussbaumstrasse 26

Street

80336, Munich, Germany

Zip code, town, country

I hereby declare, that the submitted thesis entitled:

Investigation of potencies, selectivities and binding modes of nicotinic acetylcholine receptor modulators

is congruent with the printed version both in content and format.

Munich, 15.03.2022

place, date

Yves Haufe

Signature doctoral candidate

Table of content

Affidavit	3
Confirmation of congruency	4
Table of content	5
List of abbreviations	7
List of publications	9
1. Introductory summary	10
1.1 Nicotinic acetylcholine receptors (nAChR)	10
1.2 Physiological and therapeutic relevance	13
1.3 Substances that modulate nAChRs function	15
1.3.1 Neurotoxins.....	15
1.3.2 Conotoxins.....	15
1.3.3 Pesticides	17
1.3.4 Organophosphates.....	18
1.3.5 Channel blockers	18
1.3.6 Allosteric modulators	19
1.4 Aim of this work.....	20
2. Publications: Short summary and personal contribution	21
2.1 Publication I: Backbone Cyclization Turns a Venom Peptide into a Stable and Equipotent Ligand at Both Muscle and Neuronal Nicotinic Receptors.....	21
2.2 Publication II: Synthesis, Structural and Pharmacological Characterizations of CIC, a Novel α -Conotoxin with an Extended N-Terminal Tail	23
2.3 Publication III: Interaction of $\alpha 9\alpha 10$ Nicotinic Receptors With Peptides and Proteins From Animal Venoms (additional contribution Supplementary A)	24
2.4 Publication IV: Acute effects of the imidacloprid metabolite desnitro-imidacloprid on human nACh receptors relevant for neuronal signaling (additional contribution, Supplementary B)	25
2.5 Unpublished manuscript: Symmetrical bispyridinium compounds act as open channel blockers of cation-selective ion channels (additional contribution, Supplementary C)	26
2.6 Unpublished work: Validation of FEP-based predictions on selectivity of α -conotoxins with LvIA mutants (additional contribution)	27
2.7 Unpublished work: Investigation of the molecular determinants for the toxin-resistance of the $\alpha 4\beta 2$ nAChR (additional contribution).....	29
3. References	30
4. Publication I	50
5. Publication II	73
6. Supplementary A: Publication III	85
7. Supplementary B: Publication IV	98

8. Supplementary C: Publication V (unpublished manuscript)	121
Acknowledgements	164
Curriculum vitae	Error! Bookmark not defined.

List of abbreviations

α-Btx	α -Bungarotoxin
α-Ctx	α -Cobratoxin
Aβ	Amyloid beta
ACh	Acetylcholine
AChBP	Acetylcholine binding protein
AChE	Acetylcholine esterase
ALS	Amyotrophic lateral sclerosis
APP	Amyloid precursor protein
BPC	Bispyridinium compounds
Cryo-EM	Cryo-electron microscopy
DN-IMI	Desnitro-Imidacloprid
EC₅₀	half maximal effective concentration
ECD	Extracellular domain
ELIC	<i>Erwinia</i> ligand-gated ion channel
FEP	Free-energy perturbation
FRET	Fluorescence resonance energy transfer
GABA	Gamma-aminobutyric acid
GLIC	<i>Gloeobacter</i> ligand-gated ion channel
IC₅₀	half maximal inhibitory concentration
ICD	Intracellular domain
IL-10	Interleukin-10
IMI	Imidacloprid
IMI-olefin	Imidacloprid-olefin
LPS	Lipopolysaccharide
LUHMES	human neuronal precursor cell line
mAChR	Muscarinic acetylcholine receptor
MEC	Mecamylamine
MLA	Methyllycaconitine
MS	Mass spectrometry
nAChR	Nicotinic acetylcholine receptor
OP	Organophosphate
OPP	Organophosphate poisoning
PAM	Positive allosteric modulator
pLGIC	Pentameric ligand-gated ion channel

PNU-120596	1-(5-chloro-2,4- dimethoxy-phenyl)-3-(5-methyl-isoxazol-3-yl)-urea
SAR	Structure-activity-relationship
TEVC	Two-Electrode voltage clamp
TMD	Transmembrane domain
VGCC	Voltage-gated calcium channel
WT	Wild type
ZAC	Zinc-activated

List of publications

This thesis is based on the following publications:

I. Backbone Cyclization Turns a Venom Peptide into a Stable and Equipotent Ligand at Both Muscle and Neuronal Nicotinic Receptors

Julien Giribaldi*, **Yves Haufe***, Edward R.J. Evans, Muriel Amar, Anna Durner, Casey Schmidt, Adèle Faucherre, Hamid Moha Ou Maati, Christine Enjalbal, Jordi Molgó, Denis Servent, David T. Wilson, Norelle L. Daly, Annette Nicke, Sébastien Dutertre

Journal of Medicinal Chemistry, 2020, 63(21): 12682-12692

II. Synthesis, Structural and Pharmacological Characterizations of CIC, a Novel α -Conotoxin with an Extended N-Terminal Tail

Julien Giribaldi, **Yves Haufe**, Edward R.J. Evans, David T. Wilson, Norelle L. Daly, Christine Enjalbal, Annette Nicke, Sébastien Dutertre

Marine Drugs, 2021, 19(3):141

Additional publications (included as supplementary material):

III. Interaction of $\alpha 9\alpha 10$ Nicotinic Receptors With Peptides and Proteins From Animal Venoms

Victor Tsetlin, **Yves Haufe**, Valentina Safronova, Dmitriy Serov, PranavKumar Shadamrshan, Lina Son, Irina Shelukhina, Denis Kudryavtsev, Elena Kryukova, Igor Kasheverov, Annette Nicke, Yuri Utkin

Frontiers in Cellular Neuroscience, 2021, 15:765541

IV. Acute effects of the imidacloprid metabolite desnitro-imidacloprid on human nACh receptors relevant for neuronal signaling

Dominik Loser, Karin Grillberger, Maria G. Hinojosa, Jonathan Blum, **Yves Haufe**, Timm Danker, Ylva Johansson, Clemens Möller, Annette Nicke, Susanne H. Bennekou, Iain Gardner, Caroline Bauch, Paul Walker, Anna Forsby, Gerhard F. Ecker, Udo Kraushaar, Marcel Leist

Archives of Toxicology, 2021, 95(12):3695-3716

V. Symmetrical bispyridinium compounds act as open channel blockers of cation-selective ion channels

Yves Haufe, Dominik Loser, Karin V. Niessen, Thomas Seeger, Timm Danker, Annette Nicke

Manuscript prepared for submission

* indicates shared first authorship

1. Introductory summary

Acetylcholine (ACh) is a signaling molecule that is conserved throughout evolution. It is present in bacteria, archaea, eukaryotic unicellular organisms, fungi, plants, invertebrates and vertebrates. In invertebrates and vertebrates, it activates muscarinic G protein-coupled metabotropic receptors (mAChRs) and ionotropic ligand-gated nicotinic receptors (nAChRs) and is inactivated by the ACh degrading esterase (AChE). nAChRs represent a diverse family of ion channels with complex subunit composition that mediates excitatory neurotransmission. Their dysregulation is linked to conditions such as nicotine addiction, Parkinson's Disease, Alzheimer's Disease, Schizophrenia, and Myasthenia gravis, to only name a few. Their essential roles in the central and peripheral (somatic and autonomic) nervous systems become also apparent through the large variety of natural compounds that target this receptor as defense or prey strategies. This work focuses on muscle-type and neuronal nAChR subtypes, with distinct homomeric and heteromeric assemblies, and natural and synthetic molecules that target these receptors.

1.1 Nicotinic acetylcholine receptors (nAChR)

nAChRs are non-selective cation channels that belong to the cys-loop superfamily of pentameric ligand-gated ion channels (pLGIC) together with the GABA_A, glycine, 5-HT₃ and zinc-activated (ZAC) receptors, as well as homologues prokaryotic ion channels (GLIC, ELIC). The cys-loop is a common motive in the extracellular domain with two cysteine residues, that lie 13 residues apart in the case of the mammalian nAChR subunits. There are 16 mammalian nAChR subunits known: $\alpha 1 - \alpha 7$, $\alpha 9$, $\alpha 10$, $\beta 1 - \beta 4$, δ , γ and ϵ . The α -subunits are characterized by a pair of adjacent cysteine residues in loop C that is required for agonist binding (Albuquerque et al., 2009; Karlin et al., 1986). These subunits form functional pentamers in different assemblies. The nAChR subtype found post-synaptically in efferent neurons of skeletal muscles is referred to as muscle-type nAChR and consists of two $\alpha 1$ subunits with the $\beta 1$, δ and γ subunit. In mammals, the γ subunit is replaced by ϵ during adolescence. The $\alpha 7$ and the $\alpha 9$ are able to form homomeric pentamers and the $\alpha 9$ forms additionally functional receptors with the $\alpha 10$ subunit (Elgoyhen et al., 2001). All other nAChRs require at least one principle α -subunit ($\alpha 2$, $\alpha 3$, $\alpha 4$, $\alpha 6$, $\alpha 7$) and one complementary β -subunit ($\beta 2$ or $\beta 4$) to form functional receptors. However, more complex assemblies containing several α - or β -subunits are described and also an assembly of the $\alpha 7$ with the $\beta 2$ subunit was found (J. Wu et al., 2016; Zoli et al., 2015). These α or α/β subunit combinations are historically classified as neuronal subtypes and expressed in post- and presynaptic nerve terminals, although expression of some of these receptors in non-neuronal cells (e.g. in immune cells) has also been described (Gahring & Rogers, 2005; Kawashima & Fujii, 2003; Morley et al., 2018; Zoli et al., 2018). The ACh binding site is formed by the (+) face of an α -subunit and the (-) face of the adjacent subunit, resulting in five potential α/α -interfaces in homomers and the $\alpha 9\alpha 10$ receptor and two or three α/β -interfaces (depending on the subunit stoichiometry) in the other neuronal nAChRs. In case of the muscle-type, the binding sites are at the α/δ or $\alpha/\gamma(\epsilon)$ -interfaces which show distinct affinities for ligands. $\alpha 5$ and $\beta 3$ subunits do not contribute to the formation of these orthosteric binding sites and seem to function as structural subunits (similar to the $\beta 1$ and $\alpha 10$ subunits (Elgoyhen & Katz, 2012), mainly to regulate the function and localization of the receptor (Broadbent et al., 2006; Groot-Kormelink et al., 2001).

While biochemical and electrophysiological studies provided already a principle idea about the basic structure of nAChRs (and consequently that of the other pLGIC family members) the successful crystallization of the acetylcholine binding protein (AChBP) from *Lymnaea stagnalis* revealed the first molecular structure at atomic resolution (Brejc et al., 2001). This pentameric soluble protein has a high homology with the extracellular domain of pLGICs and especially with

nAChRs and was used as a surrogate for early SAR (structure activity relationship) studies of ligand binding. Cryo-electron microscopy (cryo-EM) studies of the *Torpedo* electric ray nAChR in its skin, resulted in the first three-dimensional structure of the transmembrane domain from eukaryotic pLGIC (Miyazawa et al., 2003) and led to the modelling of a full-length structure with a 4 Å resolution (Unwin, 2005). Each subunit consists of a large extracellular, β -sandwich N-terminus (ECD), followed by four α -helical transmembrane domains (M1-4) that are connected by loops and a short extracellular C-terminus. The intracellular domain connects M3 and M4 and is longer than the other loops, highly flexible, and shows the least sequence homology and the highest variability in residue number among the subunits (Stokes et al., 2015). Five subunits form the functional receptor with their M2 helices lining the channel pore, surrounded by M1, M3, and M4. M4 is the most peripheral helix and has extensive interactions with the membrane (Hénault et al., 2019).

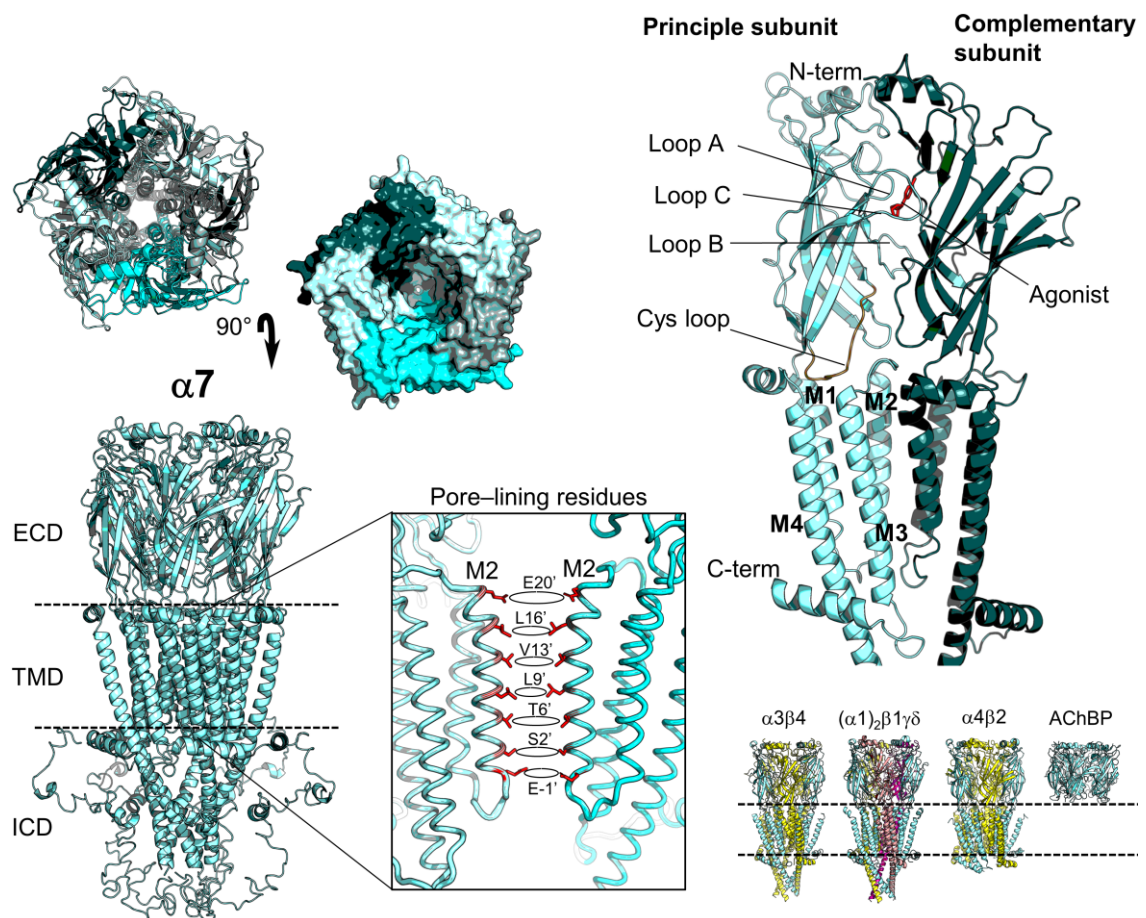


Figure 1: The molecular structure of different nAChR subtypes. The cryo-EM structure of the $\alpha 7$ nAChR in resting state is shown as an example. α -subunits are in blue (different shades for better separation of subunits). In the heteromeric nAChR the β -subunits are in yellow, γ in magenta and δ in light orange. PDB IDs: $\alpha 7$ resting state (7KOO aligned with 7RPM), AChBP (PDB: 1I9B), $\alpha 4\beta 2$ (PDB: 5KXI), $\alpha 3\beta 4$ (PDB: 6PV8), *Torpedo* muscle-type (6UWZ)

The first full length X-ray structure of the pLGIC in high resolution (2-3 Å) were obtained using the prokaryotic homologues *Erwinia* ligand-gated ion channel, ELIC (Hilf & Dutzler, 2008) and *Gloeobacter* ligand-gated ion channel, GLIC (Bocquet et al., 2008). These structures were the first models to computationally investigate ion permeation and gating. Further advances in the field of cryo-EM provided later the first high-resolution, full length structures of the human $\alpha 4\beta 2$ (Morales-Perez et al., 2016), human $\alpha 3\beta 4$ nAChRs (Gharpure et al., 2019) and *Torpedo* muscle-type (Rahman et al., 2020). These experimental structures eventually confirmed the conserved structure of nAChRs and experimental studies for their function. Additionally, these structures provided the

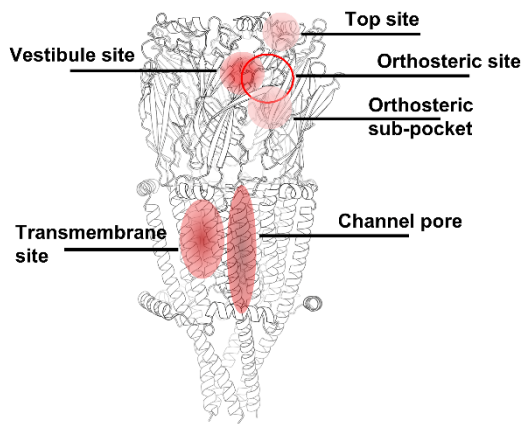


Figure 2: Described binding sites for modulators of the $\alpha 7$ nAChR. The stronger the color the higher evidence for the described site so far. The orthosteric site is only red circled.

basis for improved homology modelling and better tools for SAR-studies regarding subtype selectivity. By using appropriate stabilizing ligands, distinct functional states of the $\alpha 7$ (Noviello et al., 2021; Y. Zhao et al., 2021) and the torpedo muscle-type nAChR (Zarkadas et al., 2022) were most recently obtained, opening new possibilities for structure-function studies. The distinct states allow a more precise computational modelling of the ion flux through the pore and the structural motions that are necessary for channel activation. The agonist-mediated motion between resting and open confirmation links the binding of the extracellular ligand to a movement within the transmembrane domain, that finally opens the channel. Comparison of the different states confirmed a general twisting and flattening (“blooming”) of the

transmembrane domain, mediated by the closing of the loop C upon agonist binding, resulting in the opening of the resting gate in the transmembrane domain (Gay & Yakel, 2007). This is followed by a reversed twisting and stretching that leads to a closing of the receptor, release of the agonist and return of the receptor to the apo state. However, the exact atomic changes seem to be unique among the different nAChRs, probably explaining their distinct desensitization characteristics (Noviello et al., 2021; Zarkadas et al., 2022).

The ACh binding site is called orthosteric ligand binding site. It consists of aromatic residues, which form an “aromatic box” that chelates the charged ammonium-group of ACh and stabilizes it via cation- π interactions. The aromatic residues are provided by loop A, B and C from the principle subunit and additional residues from the complementary subunit (Cecchini & Changeux, 2015; Zhong et al., 1998). Competitive antagonists compete with agonists for this binding site. Apart from the orthosteric site, many allosteric binding sites have been described. Allosteric binding sites describe all other ligand binding sites that result in the functional modulation of the receptor, usually via conformational changes. A physiological allosteric modulator for some neuronal nAChRs is calcium, which binds to a pocket beneath the orthosteric binding site and seems to act as endogenous potentiator (Galzi et al., 1996; Mulle et al., 1992). A homologue binding site was also found in the prokaryotic GLIC (Zimmermann & Dutzler, 2011). Several other allosteric binding sites are described for the extracellular domain, such as the agonist sub-site, the top-site and the vestibule site (Spurny et al., 2015). The last one has recently led to the discovery of allosteric agonists of the $\alpha 7$ nAChR (Quadri et al., 2018). Additional allosteric binding sites have been found within the transmembrane domain for many members of the pLGIC family that modulate receptor function (as positive or negative allosteric modulators) of different members in a different extent. Ethanol binds close to the pore in the upper transmembrane part (Sauguet et al., 2013) and general anesthetics bind in the upper transmembrane part orientated towards the membrane (Nury et al., 2011) close to the ivermectin binding site (Krause et al., 1998). The binding site for synthetic modulators like PNU-120596 and TQS is wedged in the transmembrane helices M1 and M3 (Young et al., 2008) and seems to be exclusive for the $\alpha 7$ nAChR. Some of these allosteric binding sites seem to be conserved among the structurally tightly related pLGICs (Changeux, 2018), while others seem to be specific for certain members and have great prospects for the discovery of new therapeutic approaches (Haskell-Luevano & Meanwell, 2018; Papke & Horenstein, 2021; Wenthur et al., 2014). Another binding site is the channel pore itself, which is formed by stacked rings of lipophilic residues. Antagonists that act here are referred to as channel blockers and, depending on the characteristic of the compound, can bind throughout the entire pore (Cecchini & Changeux, 2015).

1.2 Physiological and therapeutic relevance

The muscle-type nAChR is expressed in the postsynaptic membrane of the neuromuscular-junction and is crucial for controlled skeletal muscle movement. It is the target of many animal toxins, for example from snakes and snails. Antibodies against this receptor cause the autoimmune disease myasthenia gravis. Curare alkaloids, like d-Tubocurarine are derived from plants and act as competitive antagonists of the muscle-type nAChR. They are non-depolarizing muscle relaxants and represent essential drugs in general anesthesia and surgery (Bowman, 2006; Rossman, 2011). Another clinically widely used muscle relaxant is the depolarizing succinylcholine, the mode of action of which is not fully understood but it seems to interact on the muscle-type nAChR as well (Jonsson et al., 2006). The depolarizing succinylcholine displays more post-operative complications than the non-depolarizing muscle relaxants (X. Zhang et al., 2019). The muscle-type nAChR exists in two distinct assemblies, the fetal $(\alpha 1)_2\beta 1\delta\gamma$ and the adult $(\alpha 1)_2\beta 1\delta\varepsilon$ form. The γ/ε switch occurs in the first post-natal weeks, but the γ subunit persists partly in the multiply innervated slow fibers of extraocular muscle until adulthood (Kalamida et al., 2007). Both subtypes are differently affected by muscle relaxants, a feature with clinical importance. Amyotrophic lateral sclerosis (ALS) is a devastating disease characterized by neuron degeneration, leading to progressive paralysis. Recent evidence strengthens the evidence that pathogenic events in the progress of the disease target the neuromuscular junction and Riluzole, the only approved drug against ALS, seems to affect the muscle-type nAChR (Palma et al., 2016).

Neuronal nAChRs are primarily expressed in the nervous system, with $\alpha 7$ and $\alpha 4\beta 2$ being the most abundant subtypes in the brain (Taly et al., 2009). The exact subtype contribution is less understood for neuronal nAChRs. They have been identified in the pre-, peri- and post-synaptic areas (Lena et al., 1993; Wonnacott, 1997) where they probably co-regulate neurotransmission via agonist-induced cation-influx that results in membrane depolarization, or in the case of $\alpha 7$, in calcium dependent signaling cascades, and subsequent activation of voltage-gated calcium channels (VGCCs) (Kulak et al., 2001; Sharma & Vijayaraghavan, 2003; Soliakov & Wonnacott, 1996). They are linked with essential functions in the autonomic nervous system in sympathetic and parasympathetic neurons, in the regulation of respiration (Shao & Feldman, 2009), in innervation of smooth muscle cells (endothelium and gut) and the fast-excitatory transmission in peripheral ganglia. In the central nervous system, they are believed to modulate the release of major neurotransmitters such as dopamine, γ -aminobutyric acid, glutamate, serotonin, norepinephrine and ACh itself, and to participate in complex behaviors such as learning, memory, emotions and reward feeling (Brunzell et al., 2015; Picciotto et al., 2012). The dysfunction of nAChRs has been linked to the development of several diseases and they therefore represent promising drug targets. Below are some examples of associated diseases and involved nAChRs.

Among other neurological symptoms, Parkinson's Disease is characterized by severe motoric dysfunction as a consequence of the degeneration of dopaminergic neurons. There is evidence for an interplay between the cholinergic and dopaminergic systems involving the $\alpha 7$, $\alpha 4\beta 2$, $\alpha 6\beta 2$ and more complex assemblies with $\alpha 5$ and $\beta 3$ nAChR subunits. These subunits are found in dopaminergic terminals as well as in afferent neurons. Interestingly, nicotine has been shown to have neuroprotective effects, in accordance with an epidemiologic link between smoking and a lower incidence of Parkinson's disease. (Quik & Wonnacott, 2011)

Alzheimer's disease is characterized by cognitive dysfunctions and progressive loss of memory. The involvement of neuronal nAChRs in cognition and memory has been demonstrated (Paterson & Nordberg, 2000) and a reduction of $\alpha 7$ and $\alpha 4\beta 2$ nAChRs in the hippocampus and cerebral cortex of Alzheimer patients is reported. A complex interaction of these subtypes together with the $\alpha 7\beta 2$ nAChR with the Amyloid beta ($A\beta$) is described in the literature (Arora et al., 2013; Dineley et al., 2002; Liu et al., 2012; Olivero et al., 2014). A recent study found that specific

fragments of the amyloid precursor protein (APP) modulate $\alpha 7$ nAChR as positive allosteric modulator (Richter et al., 2018). Weak choline esterase inhibitors, such as Donepezil, Rivastigmine and Galantamine have shown to be beneficial in treatment of cognition and behavioral symptoms in Alzheimer's Disease and are widely used (Goh et al., 2011; Wilcock et al., 2003). Galantamine was reported to act additionally as positive allosteric modulator on the $\alpha 7$ and $\alpha 4\beta 2$ nAChRs, but these findings were recently disproved (Kowal et al., 2018).

Addiction is a complex field of research, that is associated with learning and reward feeling by the abusive compound, resulting in molecular changes in synaptic structures and altered neurotransmitter release, referred to as synaptic plasticity. This process involves several distinct regions of the brain and is associated with alterations in dopamine-release, but seems to be partly distinct depending on the abusive compound. As already described with Parkinson's Disease, nAChRs seem to regulate dopamine function and several neuronal nAChRs involving $\alpha 3$, $\alpha 4$, $\alpha 6$, $\alpha 7$ and $\beta 2$, but also complex assemblies with $\alpha 5$ and $\beta 3$, are described to be involved in addiction (Feduccia et al., 2012). One of these addictive compounds is nicotine which directly targets some nAChRs as agonists, with high evidence for the $\alpha 4\beta 2$ and $\alpha 7$ subtypes. Exposure to nicotine causes an increase of these two subtypes in several brain regions, which is believed to be a compensation for the fast desensitization it causes (Govind et al., 2009). Specific polymorphism in $\alpha 3^*$, $\alpha 5^*$ and $\beta 4$ (*indicates varying complementary subunits) are linked with a higher risk for nicotine dependence, with strong experimental evidence for the $\alpha 5^*$ (Morel et al., 2014; Wojas-Krawczyk et al., 2012). Varenicline is a common drug to treat nicotine addiction that acts as a partial agonist of the $\alpha 4\beta 2$ nAChR (Tonstad et al., 2020).

The nervous system is not the only place of expression for neuronal nAChRs. Many neuronal nAChR subunits have been found in mRNA level or in immunolocalization in skin (Grando, 2014), immune cells, muscle fibers (Wessler & Kirkpatrick, 2008), various parts of the lung (Diabasana et al., 2020), oligodendrocytes, astrocytes (Höslí et al., 1988; Picciotto & Kenny, 2013) and endothelial cells (Abbruscato et al., 2002). The absence of VGCC in non-excitabile cells highlights the intrinsic potential of some nAChRs such as the $\alpha 7$ and $\alpha 9^*$ subtypes to increase intracellular calcium (Fucile et al., 2006; Zia et al., 2000), as well as their capabilities of metabotropic regulation of second messenger signaling (Bondarenko et al., 2022; King et al., 2015; Stokes et al., 2015). In lung cancer, the $\alpha 5$ and more recently the $\alpha 7$ subunits are used as a major genetic biomarker and described to be involved in tumorigenic processes including proliferation, angiogenesis and metastasis and are considered as potential treatment targets (S. Wang & Hu, 2018). The metabotropic signaling of $\alpha 9^*$ subtypes are connected with proliferation, progression and metastatic processes in various cancer types such as lung cancer, breast cancer, melanoma and gliomas, rendering the $\alpha 9^*$ nAChRs promising candidates as biomarkers, screening tools or even potential drug targets (Pucci et al., 2022).

Opioids are the primarily described drugs against chronic pain, induced by various underlying conditions such as nerve-injuries, chemotherapy, cancer and diabetes. Their usage comes with major side effects (Jitpakdee & Mande, 2014) and high risk for addiction (Darcq & Kieffer, 2018). Antagonism of the $\alpha 9\alpha 10$ has been shown to display antinociceptive and antihyperalgesic actions (Vincler et al., 2006) and to be involved in the modulation of pain sensation (Hone et al., 2018), presenting a promising alternative in the treatment of neuropathic pain (X. Li et al., 2021; Pacini et al., 2016; Romero et al., 2017; H. Wang et al., 2019).

Other nAChR-associated diseases are Schizophrenia (Freedman, 2014), attention-deficit/hyperactivity disorder (Wilens & Decker, 2007) and front lobe epilepsy (Becchetti et al., 2015).

1.3 Substances that modulate nAChRs function

Many of the aspects presented under 1.1 and 1.2 already highlight the need for compounds that can differentiate between the diverse nAChR subtypes and can be used as pharmacological tools and/or modulate their action and can be developed into drugs. In the following, I will describe the ligands that were the focus of my research and their usage.

1.3.1 Neurotoxins

The first toxin family of great interest for nAChR research, are α -neurotoxins. They are components of the toxin cocktail in snakes of the family *Elapidae*, like cobras and sea snakes. They share a so called “three-finger” motive and target nAChRs. However, other snake venom proteins sharing this characteristic folding, can also target other proteins such as multiple ion channels, G protein-coupled receptors or transporter proteins (Tsetlin, 2015). Interestingly, the Ly-6/uPAR protein superfamily, endogenous regulators of nAChRs conserved from insects to mammals, adopts the same folding and might have served as blueprint for these toxins (Anderson et al., 2020; Loughner et al., 2016). In principle, α -neurotoxins are divided into two classes: The short-chain α -neurotoxins are usually selective competitive antagonists for the muscle-type nAChR, while the long-chain α -neurotoxins target additionally the $\alpha 7$ and, more recently discovered, $\alpha 9^*$ containing nAChRs (Tsetlin, 2015). α -neurotoxins played essential roles in the study of nAChRs. The most prominent members of this family are α -bungarotoxin (α -Btx) and α -cobratoxin (α -Ctx). The first one was isolated by Chang and Lee in 1963 (Chang & Lee, 1963) and proven to efficiently block the impulse transmission on neuromuscular-junctions. Later, it was also shown to effectively block a receptor in the brain (later identified as the $\alpha 7$ nAChR) and for decades nAChRs were differentiated into α -Btx-sensitive and insensitive. The high affinity and virtually irreversible binding (similar to antibodies) enabled the first isolation of a nAChR (muscle-type nAChR-like) from the electric organ of *Torpedo marmorata* skin (Karlsson et al., 1972), using affinity chromatography columns with α -Ctx. Their clear selectivity for $\alpha 7$ and muscle-type nAChRs, two subtypes without overlapping expression, made them invaluable tools for structure-function analysis (Levandoski et al., 1999; Zouridakis et al., 2014), as labeled derivatives for diagnostic purposes (Pestronk et al., 1985), as standard pharmacological tools for binding studies in cell and tissue (Clarke et al., 1985; Guan et al., 2002) and even for detection in western-blot and imaging (Kryukova et al., 2013; Quik et al., 2007). Until today, these toxins are established and essential tools in nAChR research (Brun et al., 2022; Kem et al., 2022; Noviello et al., 2021; Sun et al., 2022). However, α -neurotoxins are not selective for specific neuronal nAChR subtypes and some α -neurotoxins have been shown to cross-react with GABA receptors (McCann et al., 2006; L. Zhang et al., 2012) and the muscarinic M4 receptor (Mordvintsev et al., 2009; L. Zhang et al., 2012). The identification of new α -neurotoxins and identification of their critical molecular determinants for ion channel binding can help to guide the *de-novo* design for new subtype specific ligands.

1.3.2 Conotoxins

In terms of neuronal nAChRs subtype specificity, α -conotoxins are the superior pharmacological tools. Conotoxins or conopeptides are small disulfide-rich peptides in the venomous cocktail of Cone-snails, marine carnivores that use these peptides in different hunting or defense strategies (Olivera et al., 2015). Each cone-snail species is estimated to produce more than thousand conopeptides with as little as 5% of overlap between different species (Davis et al., 2009; McIntosh et al., 1999) and with an estimated total amount of 1 million distinct bioactive conotoxins, of which only around 1% have been identified so far (Jin et al., 2019). These peptides target mainly the

fast ligand- and voltage-gated ion channels involved in the excitatory and neuromuscular transmission, but also G protein-coupled receptors and transport proteins, typically resulting in a fast immobilization of prey or aggressor. Conopeptides are classified according to three different features: a) the signal sequence of the precursor peptide defining the gene superfamily (A-Y), b) the complex cysteine framework in the mature peptide (I - XXXIII) and c) the pharmacological target (differentiated by Greek letters) (Kaas et al., 2010, 2012), (<https://www.conoserver.org>). In each cone-snail species, at least one conotoxin has been identified that targets nAChRs. Most of the nAChR-targeting conotoxins belong to the α -conotoxin family (some also to the distinct α A, α O and ψ groups) which are competitive nAChR antagonists and generally belong to the A superfamily (Kasheverov et al., 2022; McIntosh et al., 1999). The α -conotoxins usually have the cysteine framework I (CC-C-C, lines indicate different numbers of amino acids other than cysteine) and rarely IV (CC-C-C-C-C). However, non-classical α -conotoxins targeting nAChRs have also been identified and belong to the superfamilies B, D, J, L, M, O1, S, T with at least 7 more cysteine frameworks (Dutertre et al., 2017; Kasheverov et al., 2022). The nomenclature for α -conotoxins starts with one to two letters for the conus species, followed by the Roman number I for the cysteine framework type I and a Latin letter in descending order indicating the order of discovery, e.g. CIB was the second type I α -conotoxin isolated from *C. catulus* (McIntosh et al., 1999). α -Conotoxins with framework I form disulfide bridges between Cys1-Cys3 and Cys2-Cys5, thus creating two loops. This disulfide bond pattern is defined as “globular” folding and is considered to be the native folding. When chemically synthesized, two different folding patterns can form, ribbon (Cys1-Cys4, Cys2-Cys3) and bead (Cys1-Cys2, Cys3-Cys4). For a long time, these folding were considered unusable (Y. Wu et al., 2014), but recent literature proposes activity for these alternative foldings as well (Ho et al., 2021a; X. Wu et al., 2021). Based on the number of amino acids within the loops formed by the disulfide-bridges, α -conotoxins can be further sub-grouped. Interestingly, the number of amino acids in the loops in most cases already determines the subtype selectivity: 3/5 α -conotoxins for muscle-type nAChR, 4/3 α -conotoxins for α 7 or α 9* nAChRs and 4/4, 4/6, and 4/7 α -conotoxins for neuronal nAChRs (Dutertre et al., 2017).

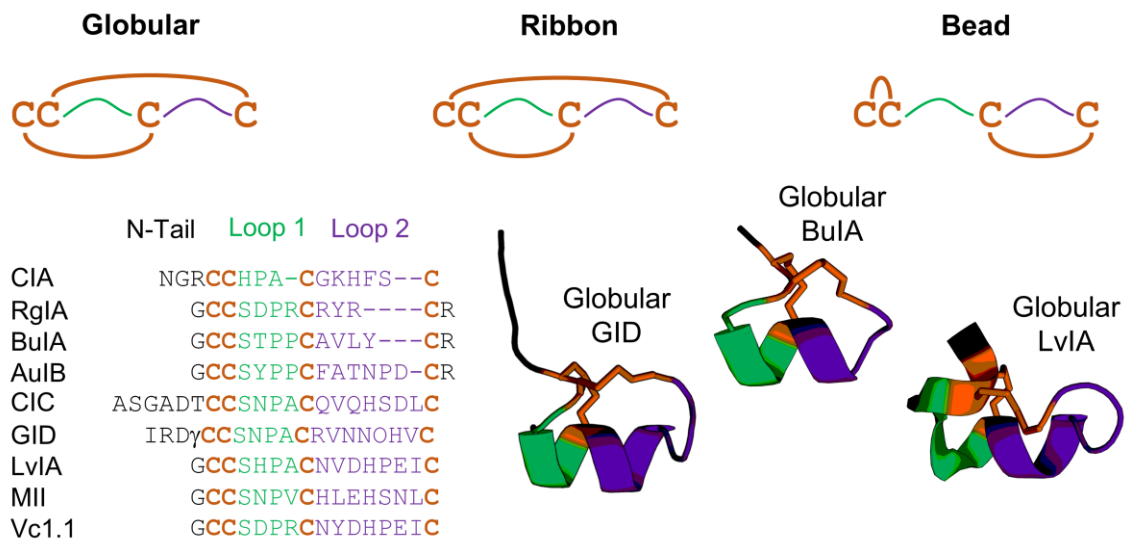


Figure 3: Principle structure of α -conotoxins with cysteine framework type I and possible cysteine bridge patterns. Selected examples of amino acid sequences (one letter code) and molecular structures. Note the highly conserved backbone structure. Selectivity is supposed to be mainly determined by the side chains. globular GID (PDB: 1MTQ), globular BulA (PDB: 2I28), globular LvIA (PDB: 2MDQ)

α -Conotoxins are generally competitive antagonists but few examples of different modes of actions are described as well (Gulsevini et al., 2021; Ho et al., 2021b). Alanine scanning mutagenesis of α -conotoxins, in combination with computational modelling based on three-dimensional

structures (Everhart et al., 2004; Huynh et al., 2020; Leffler et al., 2017), provided detailed information regarding the structure-function relationship and molecular details about the diverse modes of ligand binding on nAChRs (Ho et al., 2020). The identification of critical residues involved in ligand binding allowed the design of mutated, non-natural α -conotoxins as improved tools to study the involvement and function of distinct nAChR subtypes in many of the physiological and pathophysiological processes introduced under 1.2. Examples of such α -conotoxins are the $\alpha 6^*$ -selective [H9A,L15A]MII, the $\alpha 9\alpha 10$ specific RgIA4, and the $\alpha 7$ -selective [V11L,V16D]ArIB (Dutertre et al., 2017). In particular for investigation of $\alpha 9^*$ and $\alpha 6^*$ receptors, α -conotoxins are the only and best selective ligands available so far and provide essential insights into the biological roles of these subtypes (Dutertre et al., 2017; X. Li et al., 2021). Next to their crucial role as pharmacological tools, few α -conotoxins are also developed for diagnostic purposes, pesticides or even therapeutics. However, the common issue of bioavailability and *in-vivo* stability limit their therapeutic or diagnostic use (Durek & Craik, 2015). To address these issues, many research groups applied chemical modifications, including the optimization of the disulfide bridge against oxidation and breakdown by proteases (Chen et al., 2014; van Lierop et al., 2013; R. Zhao et al., 2020), the backbone cyclization to increase stability and membrane permeability (Clark et al., 2010; Giribaldi et al., 2020; Khatri et al., 2019; X. Li et al., 2020; Zheng et al., 2020) and the coupling to polyethylene glycol or lipophilic groups like the lipoamino acid 2-amino-D,L-dodecanoic acid to increase bioavailability (Blanchfield et al., 2003; Wan et al., 2015). Another modification of high interest is the coupling of conotoxins to fluorophores in order to advance the read-out possibilities in *in-vitro* and *in-vivo* experiments. This modification enables the study of the neuroanatomic contribution of nAChRs, allows sophisticated structure-function studies (e.g. FRET-based) and potentially contributes to the generation of new diagnostic imaging tools (Muttenthaler et al., 2020; Vishwanath & McIntosh, 2006). Despite the previously mentioned limitations, a synthetic derivative of the ω -conotoxin MVIIA (Ziconitide or SNX-111) targeting N-type calcium channels is an available alternative to opioids for the treatment of chronic pain. However, it requires intrathecal application and a thorough dose adjustment due to the small therapeutic window (Pope & Deer, 2013). The first α -conotoxin, a derivative of RgIA4 (KCP-506) was patented by Kineta in cooperation with Genetech (Roche) as a promising additional option to treat chronic neuropathic pain (Bordon et al., 2020; Kineta, 2021) and a phase I clinical trial (NL9581 in the Netherlands) was finished in November 2021 but without any details on the outcome so far (NTR, 2021).

1.3.3 Pesticides

Pesticides are chemicals used to fight unwanted species (pests) mostly in agriculture and human health protection (e.g. malaria, dengue fever, bilharzia). They are also widely used in urban green-areas, sport-fields, buildings, wide areas or even in pet shampoos to prevent the presence of these unwanted species (Nicolopoulou-Stamati et al., 2016). Insecticides are all the chemicals that specifically target insects within these applications. The essential functions of nAChRs throughout evolutions are highlighted by their importance as insecticide targets. Currently, there are 34 classes of insecticides, grouped by their mode of action, of which four classes either directly (competitive antagonists, channel blocker, allosteric modulators) or indirectly (AChE-inhibitors) target nAChRs. These classes include some of the largest and most widely used groups of insecticides worldwide, such as neonicotinoids (Costas-Ferreira & Faro, 2021; Ihara & Matsuda, 2018) and organophosphates (Rezende-Teixeira et al., 2022). The latter are a compound class of high concern, introduced in more detail under 1.3.4. Neonicotinoids are synthetic derivatives of the pyridine alkaloid nicotine, a natural secondary metabolite used by the Tabaco plant as defense mechanism against insects and was used as the first commercial insecticide (Schmeltz, 1971; Steppuhn et al., 2004). Nicotine and derivatives are specific agonists of nAChRs.

All insecticides share some common concerns regarding their environmental impacts (Aktar et al., 2009) and impact on not targeted insect species (Grünewald & Siefert, 2019; Hahn et al., 2015; Mulé et al., 2017). Optimization or *de-novo* synthesis of new insecticides is necessary (Casida, 2018) but efforts are hampered mainly because of their poor expression in heterologous expression systems and mostly unclear native nAChR subunit assembly (French-Constant et al., 2016; Millar, 2009). Additionally, safety concerns for humans by occupational and dietary exposure to insecticides are raised (Faro et al., 2019; Loser, Hinojosa, et al., 2021) and so far, the effects of metabolites of the active substances are understudied (Loser, Grillberger, et al., 2021).

1.3.4 Organophosphates

Organophosphates (OP) are a chemical group of phosphate esters used in two applications, as insecticides and as chemical warfare agents. They were developed as insecticides in the 1930s and were employed as nerve agents already during world war II. They were used again during the Gulf War and most recently, despite the attempt by the United Nations to prohibit their usage (*Chemical Weapons Convention* | OPCW) in the war in Syria (John et al., 2018) and in individual assaults and terroristic actions (Franca et al., 2019; Haslam et al., 2021). They are divided in three groups, the G series (sarin, soman tabun) developed by the Germans, the V series (VE, VM, VX, etc.) developed by the British and the novichok series developed in the former Soviet Union. Some of the most important OP insecticides used until today are Parathion, Chlorpyrifos and Malathion (Lerro et al., 2015). Even though banned from the European market, OP-insecticides are still widely used in South-America, Africa and Asia and pose a threat via occupational and dietary exposure. Sadly, they are also often used in these countries for suicidal attempts due to their low cost and easy accessibility (Eddleston et al., 2008; Hung et al., 2015).

These compounds inhibit choline esterases (Aldridge & Reiner, 1969) by occupying the active site and forming a covalent link with the catalytically important serine residue. The resulting triester is chemically unstable and the enzyme-phosphoester complex can spontaneously hydrolyze to a stable diester, resulting in an irreversibly blocked enzyme, a process referred to as “aging” (Fukuto, 1990). Especially warfare OPs age fast, with half-life times of the triester of a few minutes (H. Li et al., 2007). The most sensitive esterases towards OPs are the acetylcholine esterase and serum choline esterases (butyrylcholinesterase and acylpeptide hydrolase). The latter ones represent important biomarkers to detect potential OP poisoning (OPP) (Marsillach et al., 2011). The inhibition of the AChE results in the accumulation of the neurotransmitter ACh and the subsequent overstimulation of the cholinergic system. The mAChRs mediate effects such as bradycardia, hypersalivation, nausea and blurred vision, while nAChRs mediate effects such as muscle hypertension, fasciculations, cramping and paralysis. The first-line antidotes are atropine, a competitive mAChR antagonist and oximes as AChE-reactivator of enzymes that have not yet undergone aging. However, the use of oximes is limited and efficiency depends on the time past exposure and the OP in question (Worek et al., 2020). There is no current treatment targeting the desensitization of nAChRs and the induced paralysis and respiratory failure, which represents the most common cause of death in OPP. An adequate oxygenation is clinically important and ventilation is often required for weeks (EPA, 2014; Thiermann et al., 2013).

1.3.5 Channel blockers

The third group of nAChR-modulating compounds are channel blockers. After the original identification and isolation of nAChRs, these compounds were used to characterize nAChRs and in particular, to investigate the gating process, the essential functional process of ion channels. Channel blockers are non-competitive antagonists which physically occlude the channel pore and

thereby prevent ion flux. They are characterized by their use- and voltage-dependent block which is believed to result from the binding within the electric field of the membrane, hence within the channel pore (Woodhull, 1973). These characteristics were already early noticed for common drugs targeting ion channels besides nAChRs, such as lidocaine-derivates (QX-222, QX-314), thiopentone, amylobarbitone, and methohexitone barbiturates (Adams, 1976). This made them (especially QX-222) useful tools for the early studies of structure of the nAChR pore (Imoto et al., 1988; Leonard et al., 1988) as well as of the gating mechanism (Heidmann & Changeux, 1986; Purohit & Grosman, 2006) before atomic structures of pLGIC were obtained. Most of the identified channel blockers show a general inhibition of all nAChRs with some selectivity for specific subtypes, addressing specific differences in the gating and residues within the pore. The dual-gating mechanism, meaning the existence of two distinct gates regulating the activation and desensitization, was postulated via open channel blockers (Auerbach & Akk, 1998) and later confirmed and extended as a general gating mechanism in pLGIC (Gielen & Corringer, 2018; Noviello et al., 2021). Open channel blockers of various ion channels are still widely used as anesthetic, anti-arrhythmic and antiepileptic drugs (Ågren et al., 2019; S. Zhang et al., 1999). Interestingly, some of these drugs that target other receptors/channels have shown off-target effects as open channel blocker on nAChRs. Such drugs are: Lamotrigine (Lamictal) that is prescribed to treat epilepsy and stabilize mood in bipolar disorders (Vallés et al., 2007), Amphetamine as a central nervous stimulant (Spitzmaul et al., 1999), Chlorpromazine, which is used to treat distinct psychotic disorders (Xu et al., 2006), Fluoxetine as a typical antidepressant (García-Colunga et al., 1997) and Memantine, used to treat moderate symptoms in Alzheimer's Disease (Buisson & Bertrand, 1998; Maskell et al., 2003). Channel blockers have been proposed as potential treatment for OPP (Tattersall, 1993).

1.3.6 Allosteric modulators

Allosteric modulators have already been introduced under 1.1. The principle of functional modulation via allosteric sites has been described for many members of the pLGICs (Hansen et al., 2018; Olsen, 2018; Yevenes & Zeilhofer, 2011) including nAChRs. The majority of specific allosteric modulators for nAChRs are found for the $\alpha 7$ subtype, with some of the most striking observations for positive allosteric modulators (PAMs) for this receptor (Papke & Horenstein, 2021). The $\alpha 7$ nAChR displays a low opening probability and a characteristic very fast desensitization (Papke & Porter Papke, 2002; Williams et al., 2011). Two basic types of PAMs for the $\alpha 7$ nAChR are described in the literature. PAM type I (PAM I) synergize with orthosteric ligands to increase channel activation resulting in larger currents observed in electrophysiological recordings, without changing the desensitization significantly (Timmermann et al., 2007). PAM type II (PAM II) not only increase the activation of $\alpha 7$, but additionally overcome the desensitization (Hurst et al., 2005) and are able to reactivate desensitized channels (Papke et al., 2009). Their ability to enhance nAChRs function only in presence of endogenous agonist without changing physiological activation pattern makes them interesting drug candidates (Papke & Horenstein, 2021; v. Uteshev, 2016). These modulators are already experimentally tested, together with the recently identified agonistic PAMs, so called ago-PAMs that can activate $\alpha 7$ without orthosteric ligands (Papke et al., 2014), in models of neuroinflammation (Mizrachi et al., 2021), Schizophrenia (X. Wang et al., 2021) and cognitive deficits (Verma et al., 2021). There are only few other PAMs described for the $\alpha 4\beta 2$ (Deba et al., 2020; Dineley et al., 2015) but so far none for other members of the nAChRs including the muscle-type. PAM II would provide a potential treatment to overcome desensitization overserved in OPP.

1.4 Aim of this work

nAChRs are essential ion channels in excitatory neuromuscular and neuronal transmission and non-neuronal processes. Their crucial physiological role is evident by the number of natural compounds targeting this ion channel family and different subtypes have been associated with neurological deficits and tumour establishment and progression. However, the involvement of specific subtypes and their composition is incompletely understood. With my contributions to the studies presented in this work I aim to:

1. improve the stability and bioavailability of peptide ligands for a better application in *in-vivo* assays and as a crucial step towards their potential application as diagnostic tools or drug leads (Chapter 2.1)
2. contribute to the identification and characterization of new peptide and protein ligands as pharmacological tools for nAChR subtype differentiation and thereby help to understand nAChR subtype involvement in neurotransmission and immune cell function (Chapter 2.2, 2.3, 2.7, 2.6)
3. evaluate the effects of metabolites of insecticides on nAChR subtypes to improve the risk assessment for insecticides for humans (Chapter 2.4)
4. determine the potency and the mode of action of a series of bispyridinium analogues on nAChRs to further evaluate their potential as treatment against organophosphate poisoning (Chapter 2.5)

2. Publications: Short summary and personal contribution

2.1 Publication I: Backbone Cyclization Turns a Venom Peptide into a Stable and Equipotent Ligand at Both Muscle and Neuronal Nicotinic Receptors

Julien Giribaldi*, Yves Haufe*, Edward R.J. Evans, Muriel Amar, Anna Durner, Casey Schmidt, Adèle Faucherre, Hamid Moha Ou Maati, Christine Enjalbal, Jordi Molgó, Denis Servent, David T. Wilson, Norelle L. Daly, Annette Nicke, Sébastien Dutertre

Journal of Medicinal Chemistry, 2020, 63(21): 12682-12692

*indicates equal contribution, shared first authorship

One important issue with bioactive peptides as potential tools for *in-vivo* studies or even drug leads is their limited stability and bioavailability. This also applies to α -conotoxins, which are prone to degradation and proteolytic breakdown, despite their two disulfide bonds, mainly from the termini. Their strong polarity and molecular weight additionally decrease membrane permeation. Head-to-tail cyclization has been shown to not only improve the stability but also the membrane permeability of peptides (C. K. Wang & Craik, 2018), however changed structural features might affect biological activity. In this study, we aimed to investigate whether the properties of α -CIA, a recently characterized 3/5 α -conotoxin with selectivity for the muscle-type nAChR (Giribaldi et al., 2018), change upon head-to-tail cyclisation. Three cyclic derivatives were synthesized, using two (AG), three (AAG) or four (GAAG) amino acids as linker sequence. All three cyclic analogs maintained their high potency for the fetal muscle-type (IC_{50} values 3-9 nM), but displayed slower dissociation from the receptor, with the cyclic analogue with the three amino acids linker (cCIA-3), needing 45 min to fully dissociate. Comparison of the adult and the fetal muscle-type with cCIA-3 revealed a 20-fold higher, sub-nanomolar potency and long-lasting inhibition (only 30 % recovery of the receptor within 45 min) of the adult-muscle-type. Surprisingly and atypical for a 3/5 α -conotoxins, the cyclic analogs displayed an up to 52-fold (cCIA-3) increase in potency at the neuronal $\alpha 3\beta 2$ nAChR (IC_{50} for CIA and cCIA-3 were 68.2 nM and 1.30 nM, respectively), but with a remarkably fast off-rate. We employed a competition assay on the $\alpha 3\beta 2$ nAChR with the α -conotoxin MII and confirmed a competitive mode of action. cCIA-3 showed a 7-fold lower potency towards the closely related $\alpha 6/\alpha 3\beta 2\beta 3$ receptor, that often shows cross-reactivity (McIntosh et al., 2004). All three cyclic analogues showed higher proteolysis-resistance in blood serum and experiments with zebrafish confirmed a highly paralytic action upon injection and improved bioavailability when applied into the water. These analogs represent the first stable, highly-equipotent inhibitors for a neuronal and muscle-type nAChR and offer a unique tool for specific pharmacological studies like the Train-of-Four fading, which is commonly observed in clinics with non-depolarizing muscle relaxants. In addition, they provide a useful basis for further structure function analysis with the aim to understand determinants of subtype selectivity and design of improved peptides.

For this study, I constructed the previously described $\alpha 6/\alpha 3$ Chimera (Kuryatov et al., 2000) using Gibson assembly (Gibson et al., 2009). I employed the two-electrode voltage-clamp (TEVC) technique using *Xenopus laevis* oocytes as expression system and determined the potency and off-rate of four α -conotoxins on the $\alpha 3\beta 2$ and fetal muscle-type nAChRs, resulting in figure 1 of the manuscript and supplementary figures S2, S3 and S4. I characterized cCIA-3 additionally on the

$\alpha 6/\alpha 3\beta 2\beta 3$ and adult muscle-type nAChRs, shown in supplementary figures S6 and S7. The by me performed competition assay for cCIA-3 with MII is shown in supplementary figures S5. I screened cCIA-3 on seven additional nAChRs shown in supplementary table S1. I analyzed and visualized all above-mentioned data for the publication and wrote parts of the manuscript concerning my work. I also participated in proof-reading and editing of the manuscript.

The project was initiated and led by a cooperation partner of our group, who designed and synthesized the α -conotoxins investigated in this study. Because of the essential and substantial contribution of the electrophysiological data for the feasibility and interpretation of the whole study, all authors agreed commonly on a shared first authorship.

2.2 Publication II: Synthesis, Structural and Pharmacological Characterizations of CIC, a Novel α -Conotoxin with an Extended N-Terminal Tail

Julien Giribaldi, Yves Haufe, Edward R.J. Evans, David T. Wilson, Norelle L. Daly, Christine Enjalbal, Annette Nicke, Sébastien Dutertre

Marine Drugs, 2021, 19(3):141

In this study, the synthesis, structure and functional characterization of the novel α -conotoxin CIC is described. CIC was previously identified in a MS-based proteotranscriptome study of the toxin cocktail of *Conus catus* (Himaya et al., 2015) and belongs to the group of 4/7 α -conotoxin that display usually a high selectivity for neuronal $\alpha 7$ and $\alpha 3$ -containing nAChRs. α -CIC contains a unusual extended N-terminal amino acid sequence. Only one other typical 4/7 α -conotoxin, α -GID has a similarly extended N-terminus and here, the N-terminus was shown to confer potency to the $\alpha 4\beta 2$ nAChR, a subtype that is not targeted by other conotoxins (Nicke et al., 2003; X. Wu et al., 2021). Another α -conotoxin with an extended N-terminal, PI168 has an atypical 4/8 framework and did not show inhibition of either nAChR, calcium or sodium channels (Wilson et al., 2020). We therefore tested if the N-terminal sequence of CIC is important for its subtype selectivity. However, CIC only inhibited $\alpha 3\beta 2$ nAChR with low potency (IC_{50} 3.51 μ M) in the micro-molar range but the $\alpha 6/\alpha 3\beta 2\beta 3$ receptors with a 3-fold higher potency (IC_{50} 1.03 μ M). CIC showed a fast dissociation from both receptors. Interestingly, as shown for GID at the $\alpha 3\beta 2$ nAChR subtype (Nicke et al., 2003), the removal of the N-terminal tail did not alter the potency at the $\alpha 3\beta 2$ or $\alpha 6/\alpha 3\beta 2\beta 3$ receptors. This observation indicates that the tail is not important for binding to these subtypes. It is possible that CIC is selective for nAChRs in cone snail prey, which are structurally distinct from mammalian receptors. In addition, there is the possibility that some of the N-terminal extended α -conotoxins are selective for a different mammalian receptor family or serve specific physiological functions in the cone snail.

For this study, I screened two α -conotoxins (CIC and truncated CIC) on ten different nAChRs subtypes using TEVC and *Xenopus laevis* oocytes as expression system to define their subtype selectivity (Table 1 in the manuscript). I further determined the potency of CIC on $\alpha 3\beta 2$ and $\alpha 6/\alpha 3\beta 2$ combinations. The dose response analysis is shown together with representative recordings in Figure 2. A part of this experimental work was done by Fiona Mandausch, a student assistant, under my supervision. I analyzed and visualized all above-mentioned data for the publication and wrote parts of the manuscript concerning my work. I also participated in proof-reading and editing of the manuscript.

2.3 Publication III: Interaction of $\alpha 9\alpha 10$ Nicotinic Receptors With Peptides and Proteins From Animal Venoms (additional contribution Supplementary A)

Victor Tsetlin, Yves Haufe, Valentina Safronova, Dmitriy Serov, PranavKumar Shadamarsan, Lina Son, Irina Shelukhina, Denis Kudryavtsev, Elena Kryukova, Igor Kasheverov, Annette Nicke, Yuri Utkin

Frontiers in Cellular Neuroscience, 2021, 15:765541

$\alpha 9$ -containing ($\alpha 9^*$) nAChRs are found to show a limited RNA-level in the peripheral cochlea, the *pars tuberalis* of the pituitary (Elgoyhen et al., 1994), the vestibular inner hair cells (Simmons & Morley, 2011) but no RNA expression was detected in the brain (Morley et al., 2018). Interestingly, this nAChR subtype was also found in the bone marrow (L. Luo et al., 1998), cancer cells (Pucci et al., 2022) and various immune cells (Galvis et al., 2006; Peng et al., 2004; Safronova et al., 2021). $\alpha 9$ -containing nAChRs have been shown to be involved in pain modulation (Hone et al., 2018) and inflammatory processes (Grau et al., 2019) and their presence in immune cells is linked with these findings. $\alpha 9$ -selective α -conotoxins, such as PeIA (McIntosh et al., 2005), α -O-conotoxin GeXIVA (S. Luo et al., 2015), Vc1.1 (Clark et al., 2006) and RgIA4 (Romero et al., 2017) have been proven essential functional and biochemical tools in these studies and displayed analgesic and anti-inflammatory activity. Another prominent tool in nAChR research are snake venom-derived α -neurotoxins. There are reports, that some members of the long-chain α -neurotoxins target the $\alpha 9\alpha 10$ nAChR (Barber et al., 2013) besides their high potency for the muscle-type and $\alpha 7$ nAChR. In this study we aimed to contribute to the knowledge about the functional role of $\alpha 9^*$ nAChRs in immune cells and to further characterize long-chain α -neurotoxins regarding their selectivity for $\alpha 9^*$ nAChRs. To this aim, we isolated granulocytes from murine bone marrow and challenged these with LPS and several $\alpha 9$ -selective α -conotoxins. Interestingly, all tested $\alpha 9$ -selective α -conotoxins induced IL-10 release, an interleukin associated with analgesic and anti-inflammatory actions (da Silva et al., 2015). We further investigated the potency of eight different snake toxins on the human $\alpha 9\alpha 10$ nAChRs using TEVC. We found that the all five long-chain α -neurotoxin inhibited the $\alpha 9\alpha 10$ nAChR with low nanomolar potency (IC_{50} 30-166 nM), but only Tx-NM2 (Son et al., 2021) displayed a remarkable slow off-rate. To our knowledge this is the first reported α -neurotoxin with slow dissociation from $\alpha 9^*$ nAChRs. Identification of the causal structural determinants could provide essential leads for the optimization of selective ligands for the $\alpha 9^*$ nAChRs.

For this study, I established a measuring protocol for the human $\alpha 9\alpha 10$ nAChR using TEVC and *Xenopus laevis* oocytes as expression system. I determined the potency and off-rate of eight α -neurotoxins on this subtype, resulting in Figure 2 of the publication. I further determined the nAChR subtype selectivity of all toxins on five additional nAChR subtypes, resulting in Table 1 of the publication. Additionally, I confirmed that the chosen incubation time gives a reliable estimation of the real potency of the toxins (supplementary figure 1). Parts of the experimental work were done by PranavKumar Shadamarsan, a student assistant, under my supervision. I analyzed and visualized the results for the publication and wrote parts of the manuscript. I also participated in proof-reading and editing of the manuscript.

2.4 Publication IV: Acute effects of the imidacloprid metabolite desnitro-imidacloprid on human nACh receptors relevant for neuronal signaling (additional contribution, Supplementary B)

Dominik Loser, Karin Grillberger, Maria G. Hinojosa, Jonathan Blum, Yves Haufe, Timm Danker, Ylva Johansson, Clemens Möller, Annette Nicke, Susanne H. Bennekou, Iain Gardner, Caroline Bauch, Paul Walker, Anna Forsby, Gerhard F. Ecker, Udo Kraushaar, Marcel Leist

Archives of Toxicology, 2021, 95(12):3695-3716

Many plants are known to produce compounds that specifically target nAChRs and are believed to have evolved as protection mechanism against insects and herbivores (Millar & Denholm, 2007). Many natural and synthetic agonists and antagonists of nAChRs have been developed and are used by humans as pest control. The highly conserved nature of the cholinergic system has consequently led to challenges because of cross-activity on vertebrate nAChRs. One of the biggest groups of nAChR-targeting insecticides are synthetic nitromethylene compounds, similar to nicotine, referred to as neonicotinoids (Soloway et al., 1978). Imidacloprid was the first worldwide distributed neonicotinoid and is still an important insecticide (Elbert et al., 1998). Even though neonicotinoids are developed to be selective for insect nAChRs, which is primarily attributed to their nitro-group that prevents crossing of the blood-brain barrier (Tomizawa & Casida, 2000), there is raising evidence that they adversely affect mammals in a concentration that can be reached by dietary exposure (Loser, Hinojosa, et al., 2021). Furthermore, they are prone to metabolization, forming a set of understudied metabolites, some of which have been reported to be persistent in crops. In this study, we aimed to investigate the effects of two imidacloprid (IMI) metabolites, desnitro-imidacloprid (DN-IMI) and imidacloprid-olefin (IMI-olefin), on human nAChR function. To this aim, we employed the human neuronal precursor (LUHMES) and SH-SY5Y cell lines, both commonly used models to study neurotoxicity for humans, in a calcium-imaging assay and investigated the human $\alpha 7$, $\alpha 3\beta 4$, and $\alpha 4\beta 2$ nAChR subtypes expressed in *X. laevis* in TEVC. Only DN-IMI effectively induced calcium signals in both cell lines in a concentration-dependent manner ($EC_{50} \sim 1\mu M$). IMI-olefin induced only small calcium signals similar to the parent compound IMI. DN-IMI-induced calcium signals could be inhibited with the non-selective competitive nAChR antagonists (+)-tubocurarine and the non-selective non-competitive antagonist mecamylamine (MEC), supporting that nAChRs induce the calcium flux. The potentiation of the calcium signal by the $\alpha 7$ -selective PAM II, PNU-120596, and the inhibition by the $\alpha 7$ -selective competitive antagonist methyllycaconitine (MLA) clearly identified that at least a part of the observed effects is mediated by the $\alpha 7$ nAChR. The investigation of $\alpha 7$, $\alpha 3\beta 4$, and $\alpha 4\beta 2$ nAChR subtypes expressed in *X. laevis* oocytes confirmed that DN-IMI acts as agonist on the $\alpha 7$ and $\alpha 3\beta 4$ nAChRs with a slightly higher potency than the well-studied neurotoxicant nicotine. Interestingly, it acted as partial antagonist at the $\alpha 4\beta 2$ nAChR. The binding of DN-IMI to the orthosteric binding site was supported by molecular docking. The present study describes the hazardous potential of desnitro- metabolites from neonicotinoids and highlights the need to extend toxicological evaluations on metabolites.

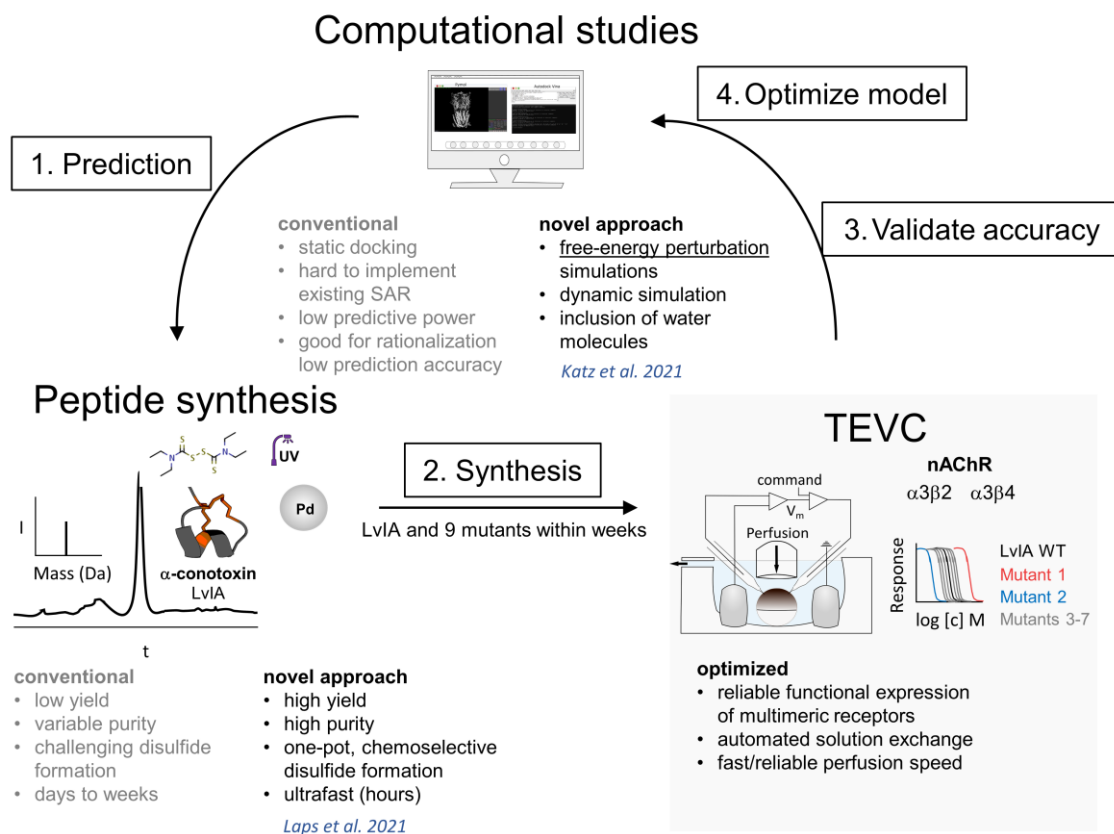
For this study, I designed a cloning strategy and subcloned the human $\alpha 3$, $\alpha 4$, $\beta 2$ and $\beta 4$ subunits into the oocyte expression vector pNKS2. I synthesized cRNA of all subunits and validated the formation of functional $\alpha 7$, $\alpha 3\beta 4$, and $\alpha 4\beta 2$ receptors by TEVC and then provided the plasmids to Dominik Loser. Additionally, I provided advice for recordings and analysis. I also participated in proof-reading of the manuscript.

2.5 Unpublished manuscript: Symmetrical bispyridinium compounds act as open channel blockers of cation-selective ion channels (additional contribution, Supplementary C)

Organophosphates are a class of phosphate esters that are used as warfare agents and pesticides and still represent a major threat for human health. Upon OOP, nAChRs are over-activated and desensitized, leading subsequently to a depolarization block and life-threatening conditions. There is currently no treatment for nAChR-mediated effects such as muscle fasciculation, cramps, paralysis, dyspnea, tachycardia, hypertension and disturbances in consciousness and only palliative treatment of the nAChR-mediated symptoms with e.g. benzodiazepam or ventilation is available (Thiermann et al., 2010). Advances in the development of therapeutic approaches have been limited over the last decades (Worek et al., 2020). Non-oxime bispyridinium compounds (BPC) have shown beneficial effects in animal experiments (Kassa et al., 2020; Turner et al., 2011) and induced recovery of muscle contraction in mammalian muscle preparations (Seeger et al., 2012; Tattersall, 1993). The mode of action of these structurally very similar compounds is ambiguous and several mechanisms are currently discussed. Action as open channel blockers was found on native muscle-type nAChR (Tattersall, 1993), action as positive allosteric modulators of $\alpha 7$ nAChR stably expressed in CHO cells (Scheffel et al., 2018) and competitive interactions based on radioligand-competition assay on membrane preparations of *Torpedo* electric ray (Niessen et al., 2018) and molecular dynamic simulations on a homology model of the human muscle-type nAChR (Epstein et al., 2021). In this study, we aim to clarify the pharmacological effects of several BPCs on oocyte-expressed muscle and $\alpha 7$ nAChR. We show a general inhibition of nAChRs, with IC_{50} -values in the low nanomolar range for the most potent derivate PTM0022. Further analysis revealed a non-competitive, voltage-dependent inhibition that agrees with a channel block as mode of action. Using the $\alpha 7$ nAChR as model receptor, we employ a combination of molecular docking, generation of chimeric receptors and site-directed mutagenesis to exclude the ECD as binding area. We identify critical residues for BPC binding in the transition zone from ECD to TMD within the channel as well as a critical involvement of the negatively charged ring formed by E258 (E20') close to the ECD. Interestingly, the same region seems to be involved in the channel-blocking effect of ACh in high concentrations. Investigation of other cation-selective channels suggest a rather unspecific inhibition of pentameric cation channels by BPCs with a selectivity for $\alpha 7$ and muscle-type nAChRs. The potential usage in the treatment of OPP requires further investigation.

For this study, I established an optimized TEVC setup with fast and reproducible perfusion, low volume of perfused solution and Teflon tubing to reduce unspecific binding of ligands. I further established recording protocols for allosteric modulators on nAChRs, to identify channel blockers on nAChRs, and for fast-gating, voltage-activated sodium channels. In the course of this study, I investigated the potency of nine BPCs on the $\alpha 7$ and muscle-type nAChR and characterized two of them in detail regarding their orthosteric competitiveness, voltage-dependency and interaction with a positive allosteric modulator PNU-120596. I further created eight receptor chimeras and ten mutants, performed molecular docking to study the binding site on the $\alpha 7$ nAChR, and performed a complex ACh-induced desensitization protocol to test for potential recovery by BPCs. I analyzed and visualized all of the results, which I summarized in nine figures and five tables in the main manuscript and additional five figures and five tables in the supplementary material. I conceived and designed major parts of the study and wrote the first draft of the manuscript together with Prof. Annette Nicke. Small parts of the molecular cloning were done by Veronika Iskra, a student assistant, under my supervision.

2.6 Unpublished work: Validation of FEP-based predictions on selectivity of α -conotoxins with Lv1A mutants (additional contribution)

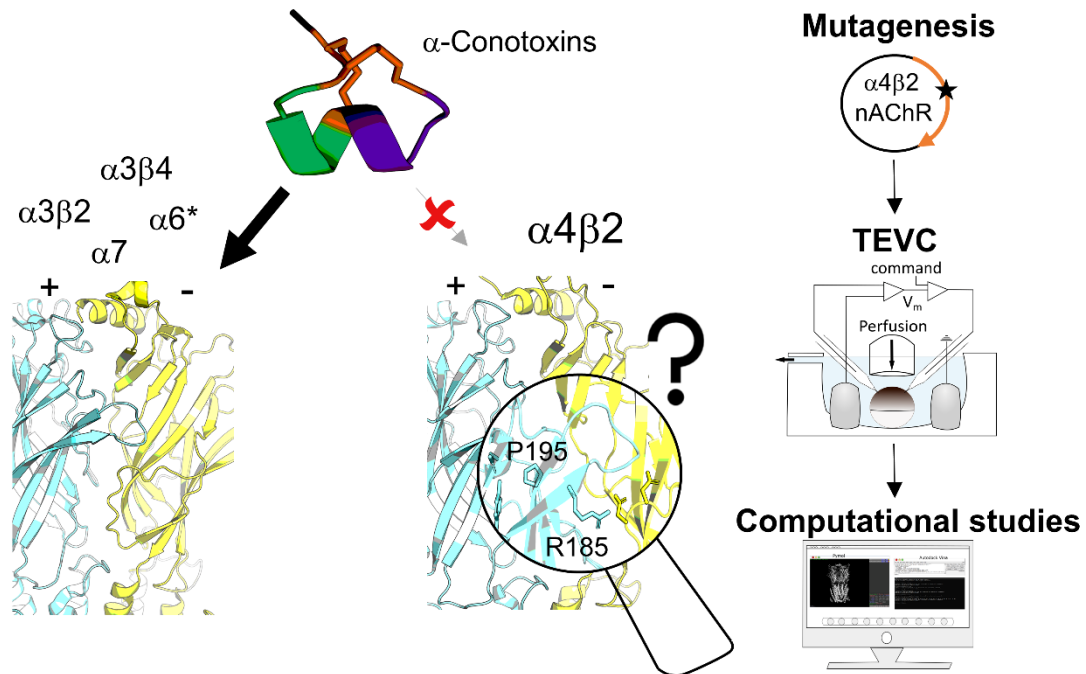


α -Conotoxins are competitive antagonists of nAChRs, that display a natural selectivity for specific subtypes (see 1.3.2). To identify selectivity-enhancing point mutations is a desired goal in order to optimize α -conotoxins as pharmacological tools and potential drug leads. Alanine-scanning mutagenesis (Grishin et al., 2013; Kompella et al., 2015; Ning et al., 2018) is a common approach to identify crucial residue positions for the potency of α -conotoxins. Identified residues could theoretically be exchanged by all 20 amino acids (not Cys) in order to investigate their influence on the potency and to identify more selective mutants. The synthesis, hampered by the challenge of achieving correct folding of α -conotoxins (Banerjee et al., 2013) and biological evaluation of the necessary number of peptides is labor, cost and time extensive. Computational docking studies would greatly decrease the number of peptides that would need to be synthesized and tested, but due to the low number of three-dimensional structures of nAChR/ α -conotoxins complexes and weak predictive power, their use is still limited (Leffler et al., 2017). In this project we aim to validate the accuracy of the free-energy perturbation (FEP) method for the prediction of potency and selectivity of α -conotoxins mutants. FEP is a molecular dynamic based approach that mutates the residue of interest under consideration of receptor/ligand interaction and water molecules (Ross et al., 2020). A trained FEP-model (Katz et al., 2021) was recently established to exchange every non-cysteine residue in Lv1A (α -conotoxins with a natural 10-fold selectivity for α 3 β 2 over α 3 β 4 nAChR) with every other possible amino acid, except for cysteine and to predict the selectivity for α 3 β 2 over α 3 β 4 nAChR. Lv1A WT and three already described alanine mutants (Zhu et al., 2020) were chosen as control for the electrophysiological measurements and additional six new predicted mutants to evaluate the accuracy of the FEP-prediction. The peptides were synthesized employing a recently discovered new synthesis strategy with regioselective and ultrafast

disulfide formation (Laps et al., 2021), using disulfiram activation of cysteine side chains and UV-light/Platinum catalyzed chemoselective disulfide formation. The mutants were successfully synthesized with correct folding in high yield and purity within a few weeks. All 10 LvIA mutants are currently studied regarding their potency and binding kinetics on the rat $\alpha 3\beta 2$ and $\alpha 3\beta 4$ nAChRs employing TEVC to evaluate the prediction accuracy of the FEP-model.

For this project, I participated in conceiving the main hypothesis and I supervised and participated in the electrophysiological measurements (dose-response analysis and kinetics) of the ten LvIA mutants on the two nAChR subtypes, assisted by Gonxhe Lokaj and PranavKumar Shadamarshan, colleagues in my group.

2.7 Unpublished work: Investigation of the molecular determinants for the toxin-resistance of the $\alpha 4\beta 2$ nAChR (additional contribution)



The $\alpha 4\beta 2$ nAChR is one of the most abundant nAChR in the brain and linked with physiological processes like cognition, mood, reward-feeling and nociception (Picciotto et al., 2001; Rueter et al., 2006; Taly et al., 2009) and has also been found in the lung (Diabasana et al., 2020). This nAChR exists in two stoichiometries, $2(\alpha 4)3(\beta 2)$ only forms α/β -interfaces but $3(\alpha 4)2(\beta 2)$ forms an additional α/α -interface that displays a distinct pharmacology (Indurthi et al., 2016; Mazzaferro et al., 2017). Despite the variety of already identified nAChR-targeting α -conotoxins, there has not been an α -conotoxin discovered that selectively targets either of the two interfaces of this nAChR (Dutertre et al., 2017). GID is the only described conotoxin that actually targets the $\alpha 4\beta 2$ subtype with good potency in the higher nanomolar range, but displays even higher potency on the $\alpha 7$ and $\alpha 3\beta 2$ subtypes (Millard et al., 2009; Nicke et al., 2003). This creates a lack of selective tools to study and potentially drug the $\alpha 4\beta 2$ nAChR. In a previous work (Beissner et al., 2012), our group identified two essential residues in the $\alpha 4$ subunit (R185 and P195), that prevent efficient binding of α -conotoxins to this receptor. In this ongoing project, we aim to understand the molecular reason for this apparent toxin-resistance and to provide insights to guide the optimization of ligands to selectively target the $\alpha 4\beta 2$ nAChR. We employed computational docking, molecular dynamics and site-directed mutagenesis to study the possible involvement of ionic interactions in the accessibility of α -conotoxins to the binding site. Therefore, we created more than 15 $\alpha 4\beta 2$ nAChR mutants, in which we removed and introduced several charged residues within and around loop C. We characterized the affinity toward ACh for these mutants and investigated the binding of [A10L]Tx1A and MII employing the TEVC and *X. laevis* as expression system.

The majority of the $\alpha 4\beta 2$ mutants were constructed by my colleague Anna Durner and other members of my group. I determined for 15 $\alpha 4\beta 2$ mutants the affinity for ACh and characterized the potency of [A10L]Tx1A using TEVC. Part of these measurements were done by Lukas Sassenbach, a student assistant, under my supervision. Currently I am preparing the first draft of the manuscript for this project.

3. References

- Abbruscato, T. J., Lopez, S. P., Mark, K. S., Hawkins, B. T., & Davis, T. P. (2002). Nicotine and cotinine modulate cerebral microvascular permeability and protein expression of ZO-1 through nicotinic acetylcholine receptors expressed on brain endothelial cells. *Journal of Pharmaceutical Sciences*, *91*(12), 2525–2538. <https://doi.org/10.1002/jps.10256>
- Adams, P. R. (1976). Drug blockade of open end-plate channels. *The Journal of Physiology*, *260*(3), 531–552. <https://doi.org/10.1113/JPHYSIOL.1976.SP011530>
- Ågren, R., Nilsson, J., & Århem, P. (2019). Closed and open state dependent block of potassium channels cause opposing effects on excitability – a computational approach. *Scientific Reports*, *9*(1), 1–10. <https://doi.org/10.1038/s41598-019-44564-x>
- Aktar, W., Sengupta, D., & Chowdhury, A. (2009). Impact of pesticides use in agriculture: their benefits and hazards. *Interdisciplinary Toxicology*, *2*(1), 1. <https://doi.org/10.2478/V10102-009-0001-7>
- Albuquerque, E. X., Pereira, E. F. R., Alkondon, M., & Rogers, S. W. (2009). Mammalian nicotinic acetylcholine receptors: From structure to function. In *Physiological Reviews* (Vol. 89, Issue 1, pp. 73–120). NIH Public Access. <https://doi.org/10.1152/physrev.00015.2008>
- Aldridge, W. N., & Reiner, E. (1969). Acetylcholinesterase. Two types of inhibition by an organophosphorus compound: one the formation of phosphorylated enzyme and the other analogous to inhibition by substrate. *Biochemical Journal*, *115*(2), 147. <https://doi.org/10.1042/BJ1150147>
- Anderson, K. R., Hoffman, K. M., & Miwa, J. M. (2020). Modulation of cholinergic activity through lynx protoxins: Implications for cognition and anxiety regulation. *Neuropharmacology*, *174*, 108071. <https://doi.org/10.1016/j.neuropharm.2020.108071>
- Arora, K., Alfulajj, N., Higa, J. K., Panee, J., & Nichols, R. A. (2013). Impact of sustained exposure to β -amyloid on calcium homeostasis and neuronal integrity in model nerve cell system expressing $\alpha 4\beta 2$ nicotinic acetylcholine receptors. *The Journal of Biological Chemistry*, *288*(16), 11175–11190. <https://doi.org/10.1074/JBC.M113.453746>
- Auerbach, A., & Akk, G. (1998). Desensitization of Mouse Nicotinic Acetylcholine Receptor Channels A Two-Gate Mechanism. *Journal of General Physiology*, *112*(2), 181–197. <https://doi.org/10.1085/JGP.112.2.181>
- Banerjee, J., Gyanda, R., Chang, Y. P., & Armishaw, C. J. (2013). The chemical synthesis of α -conotoxins and structurally modified analogs with enhanced biological stability. *Methods in Molecular Biology*, *1081*, 13–34. https://doi.org/10.1007/978-1-62703-652-8_2
- Barber, C. M., Isbister, G. K., & Hodgson, W. C. (2013). Alpha neurotoxins. In *Toxicon* (Vol. 66, pp. 47–58). Pergamon. <https://doi.org/10.1016/j.toxicon.2013.01.019>
- Becchetti, A., Aracri, P., Meneghini, S., Brusco, S., & Amadeo, A. (2015). The role of nicotinic acetylcholine receptors in autosomal dominant nocturnal frontal lobe epilepsy. *Frontiers in Physiology*, *6*(FEB). <https://doi.org/10.3389/FPHYS.2015.00022>
- Beissner, M., Dutertre, S., Schemm, R., Danker, T., Sporning, A., Grubmüller, H., & Nicke, A. (2012). Efficient binding of 4/7 α -conotoxins to nicotinic $\alpha 4\beta 2$ receptors is prevented by Arg185 and Pro195 in the $\alpha 4$ subunit. *Molecular Pharmacology*, *82*(4), 711–718. <https://doi.org/10.1124/mol.112.078683>
- Blanchfield, J. T., Dutton, J. L., Hogg, R. C., Gallagher, O. P., Craik, D. J., Jones, A., Adams, D. J., Lewis, R. J., Alewood, P. F., & Toth, I. (2003). Synthesis, structure elucidation, in vitro

- biological activity, toxicity, and Caco-2 cell permeability of lipophilic analogues of α -conotoxin MII. *Journal of Medicinal Chemistry*, 46(7), 1266–1272. https://doi.org/10.1021/JM020426J/SUPPL_FILE/JM020426J_S.PDF
- Bocquet, N., Nury, H., Baaden, M., le Poupon, C., Changeux, J. P., Delarue, M., & Corringer, P. J. (2008). X-ray structure of a pentameric ligand-gated ion channel in an apparently open conformation. *Nature* 2008 457:7225, 457(7225), 111–114. <https://doi.org/10.1038/nature07462>
- Bondarenko, V., Wells, M. M., Chen, Q., Tillman, T. S., Singewald, K., Lawless, M. J., Caporoso, J., Brandon, N., Coleman, J. A., Saxena, S., Lindahl, E., Xu, Y., & Tang, P. (2022). Structures of highly flexible intracellular domain of human $\alpha 7$ nicotinic acetylcholine receptor. *Nature Communications*, 13(1), 793. <https://doi.org/10.1038/s41467-022-28400-x>
- Bordon, K. de C. F., Cologna, C. T., Fornari-Baldo, E. C., Pinheiro-Júnior, E. L., Cerni, F. A., Amorim, F. G., Anjolette, F. A. P., Cordeiro, F. A., Wiesel, G. A., Cardoso, I. A., Ferreira, I. G., Oliveira, I. S. de, Boldrini-França, J., Pucca, M. B., Baldo, M. A., & Arantes, E. C. (2020). From Animal Poisons and Venoms to Medicines: Achievements, Challenges and Perspectives in Drug Discovery. *Frontiers in Pharmacology*, 11, 1132. <https://doi.org/10.3389/FPHAR.2020.01132>
- Bowman, W. C. (2006). Neuromuscular block. *British Journal of Pharmacology*, 147(Suppl 1), S277. <https://doi.org/10.1038/SJ.BJP.0706404>
- Brejč, K., van Dijk, W. J., Klaassen, R. v., Schuurmans, M., van der Oost, J., Smit, A. B., & Sixma, T. K. (2001). Crystal structure of an ACh-binding protein reveals the ligand-binding domain of nicotinic receptors. *Nature*, 411(6835), 269–276. <https://doi.org/10.1038/35077011>
- Broadbent, S., Groot-Kormelink, P. J., Krashia, P. A., Harkness, P. C., Millar, N. S., Beato, M., & Sivilotti, L. G. (2006). Incorporation of the $\beta 3$ subunit has a dominant-negative effect on the function of recombinant central-type neuronal nicotinic receptors. *Molecular Pharmacology*, 70(4), 1350–1357. <https://doi.org/10.1124/mol.106.026682>
- Brun, O., Zoukimian, C., Oliveira-Mendes, B., Montnach, J., Lauzier, B., Ronjat, M., Bérout, R., Lesage, F., Boturn, D., & de Waard, M. (2022). Chemical Synthesis of a Functional Fluorescent-Tagged α -Bungarotoxin. *Toxins*, 14(2). <https://doi.org/10.3390/TOXINS14020079>
- Brunzell, D. H., Stafford, A. M., & Dixon, C. I. (2015). Nicotinic receptor contributions to smoking: insights from human studies and animal models. *Current Addiction Reports*, 2(1), 33. <https://doi.org/10.1007/S40429-015-0042-2>
- Buisson, B., & Bertrand, D. (1998). Open-channel blockers at the human $\alpha 4\beta 2$ neuronal nicotinic acetylcholine receptor. *Molecular Pharmacology*, 53(3), 555–563. <https://doi.org/10.1124/mol.53.3.555>
- Casida, J. E. (2018). Neonicotinoids and Other Insect Nicotinic Receptor Competitive Modulators: Progress and Prospects. *Annual Review of Entomology*, 63(1), 125–144. <https://doi.org/10.1146/annurev-ento-020117-043042>
- Cecchini, M., & Changeux, J. P. (2015). The nicotinic acetylcholine receptor and its prokaryotic homologues: Structure, conformational transitions & allosteric modulation. *Neuropharmacology*, 96(PB), 137–149. <https://doi.org/10.1016/J.NEUROPHARM.2014.12.006>
- Chang, C., & Lee, C. (1963). Isolation of neurotoxins from the venom of bungarus multicinctus and their modes of neuromuscular blocking action. *Archives Internationales de Pharmacodynamie et de Thérapie*, 144, 241–257. <https://pubmed.ncbi.nlm.nih.gov/14043649/>

- Changeux, J. P. (2018). The nicotinic acetylcholine receptor: A typical 'allosteric machine.' In *Philosophical Transactions of the Royal Society B: Biological Sciences* (Vol. 373, Issue 1749). Royal Society Publishing. <https://doi.org/10.1098/rstb.2017.0174>
- Chemical Weapons Convention | OPCW*. (n.d.). Retrieved March 9, 2022, from <https://www.opcw.org/chemical-weapons-convention>
- Chen, S., Gopalakrishnan, R., Schaer, T., Marger, F., Hovius, R., Bertrand, D., Pojer, F., & Heinis, C. (2014). Dithiol amino acids can structurally shape and enhance the ligand-binding properties of polypeptides. *Nature Chemistry* 2014 6:11, 6(11), 1009–1016. <https://doi.org/10.1038/nchem.2043>
- Clarke, P. B. S., Schwartz, R. D., Paul, S. M., Pert, C. B., & Pert, A. (1985). Nicotinic binding in rat brain: Autoradiographic comparison of [3H]acetylcholine, [3H]nicotine, and [125I]- α -bungarotoxin. *Journal of Neuroscience*, 5(5), 1307–1315. <https://doi.org/10.1523/jneurosci.05-05-01307.1985>
- Clark, R. J., Fischer, H., Nevin, S. T., Adams, D. J., & Craik, D. J. (2006). The synthesis, structural characterization, and receptor specificity of the alpha-conotoxin Vc1.1. *The Journal of Biological Chemistry*, 281(32), 23254–23263. <https://doi.org/10.1074/JBC.M604550200>
- Clark, R. J., Jensen, J., Nevin, S. T., Callaghan, B. P., Adams, D. J., & Craik, D. J. (2010). The Engineering of an Orally Active Conotoxin for the Treatment of Neuropathic Pain. *Angewandte Chemie International Edition*, 49(37), 6545–6548. <https://doi.org/10.1002/A-NIE.201000620>
- Costas-Ferreira, C., & Faro, L. R. F. (2021). Neurotoxic effects of neonicotinoids on mammals: What is there beyond the activation of nicotinic acetylcholine receptors?—A systematic review. *International Journal of Molecular Sciences*, 22(16). <https://doi.org/10.3390/ijms22168413>
- Darcq, E., & Kieffer, B. L. (2018). Opioid receptors: drivers to addiction? *Nature Reviews Neuroscience* 2018 19:8, 19(8), 499–514. <https://doi.org/10.1038/s41583-018-0028-x>
- Davis, J., Jones, A., & Lewis, R. J. (2009). Remarkable inter- and intra-species complexity of conotoxins revealed by LC/MS. *Peptides*, 30(7), 1222–1227. <https://doi.org/10.1016/J.PEPTIDES.2009.03.019>
- Deba, F., Ramos, K., Vannoy, M., Munoz, K., Akinola, L. S., Imad Damaj, M., & Hamouda, A. K. (2020). Examining the Effects of (α 4) β 2 Nicotinic Acetylcholine Receptor-Selective Positive Allosteric Modulator on Acute Thermal Nociception in Rats. *Molecules* 2020, Vol. 25, Page 2923, 25(12), 2923. <https://doi.org/10.3390/MOLECULES25122923>
- Diabasana, Z., Perotin, J. M., Belgacemi, R., Ancel, J., Mulette, P., Delepine, G., Gosset, P., Maskos, U., Polette, M., Deslée, G., & Dormoy, V. (2020). Nicotinic receptor subunits atlas in the adult human lung. *International Journal of Molecular Sciences*, 21(20), 1–15. <https://doi.org/10.3390/ijms21207446>
- Dineley, K. T., Bell, K. A., Bui, D., & Sweatt, J. D. (2002). beta -Amyloid peptide activates alpha 7 nicotinic acetylcholine receptors expressed in *Xenopus* oocytes. *The Journal of Biological Chemistry*, 277(28), 25056–25061. <https://doi.org/10.1074/JBC.M200066200>
- Dineley, K. T., Pandya, A. A., & Yakel, J. L. (2015). Nicotinic ACh Receptors as Therapeutic Targets in CNS Disorders. *Trends in Pharmacological Sciences*, 36(2), 96. <https://doi.org/10.1016/J.TIPS.2014.12.002>
- Durek, T., & Craik, D. J. (2015). Therapeutic conotoxins: a US patent literature survey. <http://dx.doi.org/10.1517/13543776.2015.1054095>, 25(10), 1159–1173. <https://doi.org/10.1517/13543776.2015.1054095>

- Dutertre, S., Nicke, A., & Tsetlin, V. I. (2017). Nicotinic acetylcholine receptor inhibitors derived from snake and snail venoms. In *Neuropharmacology* (Vol. 127, pp. 196–223). Elsevier Ltd. <https://doi.org/10.1016/j.neuropharm.2017.06.011>
- Eddleston, M., Buckley, N. A., Eyer, P., & Dawson, A. H. (2008). Management of acute organophosphorus pesticide poisoning. *Lancet (London, England)*, 371(9612), 597–607. [https://doi.org/10.1016/S0140-6736\(07\)61202-1](https://doi.org/10.1016/S0140-6736(07)61202-1)
- Elbert, A., Nauen, R., & Leicht, W. (1998). Imidacloprid, a Novel Chloronicotinyl Insecticide: Biological Activity and Agricultural Importance. *Insecticides with Novel Modes of Action*, 50–73. https://doi.org/10.1007/978-3-662-03565-8_4
- Elgoyhen, A. B., Johnson, D. S., Boulter, J., Vetter, D. E., & Heinemann, S. (1994). $\alpha 9$: An acetylcholine receptor with novel pharmacological properties expressed in rat cochlear hair cells. *Cell*, 79(4), 705–715. [https://doi.org/10.1016/0092-8674\(94\)90555-X](https://doi.org/10.1016/0092-8674(94)90555-X)
- Elgoyhen, A. B., & Katz, E. (2012). The efferent medial olivocochlear-hair cell synapse. *Journal of Physiology, Paris*, 106(1–2), 47–56. <https://doi.org/10.1016/J.JPHYSPARIS.2011.06.001>
- Elgoyhen, A. B., Vetter, D. E., Katz, E., Rothlin, C. v., Heinemann, S. F., & Boulter, J. (2001). $\alpha 10$: A determinant of nicotinic cholinergic receptor function in mammalian vestibular and cochlear mechanosensory hair cells. *Proceedings of the National Academy of Sciences of the United States of America*, 98(6), 3501–3506. <https://doi.org/10.1073/pnas.051622798>
- EPA. (2014). Recognition and Management of Pesticide Poisonings: Sixth Edition: 2013: Chapter 5 Organophosphates. *Recognition and Management of Pesticide Poisonings: Sixth Edition*, 49–52. https://www.epa.gov/sites/default/files/documents/rmpp_6thed_ch5_organophosphates.pdf
- Epstein, M., Bali, K., Piggot, T. J., Green, A. C., Timperley, C. M., Bird, M., Tattersall, J. E. H., Bermudez, I., & Biggin, P. C. (2021). Molecular determinants of binding of non-oxime bispyridinium nerve agent antidote compounds to the adult muscle nAChR. *Toxicology Letters*, 340, 114–122. <https://doi.org/10.1016/j.toxlet.2021.01.013>
- Everhart, D., Cartier, G. E., Malhotra, A., Gomes, A. v., McIntosh, J. M., & Luetje, C. W. (2004). Determinants of Potency on α -Conotoxin MII, a Peptide Antagonist of Neuronal Nicotinic Receptors. *Biochemistry*, 43(10), 2732–2737. <https://doi.org/10.1021/bi036180h>
- Faro, L. R. F., Tak-Kim, H., Alfonso, M., & Durán, R. (2019). Clothianidin, a neonicotinoid insecticide, activates $\alpha 4\beta 2$, $\alpha 7$ and muscarinic receptors to induce in vivo dopamine release from rat striatum. *Toxicology*, 426. <https://doi.org/10.1016/j.tox.2019.152285>
- Feduccia, A. A., Chatterjee, S., & Bartlett, S. E. (2012). Neuronal nicotinic acetylcholine receptors: Neuroplastic changes underlying alcohol and nicotine addictions. *Frontiers in Molecular Neuroscience*, 0(AUG 2012), 83. <https://doi.org/10.3389/FNMOL.2012.00083/BIBTEX>
- French-Constant, R. H., Williamson, M. S., Davies, T. G. E., & Bass, C. (2016). Ion channels as insecticide targets. In *Journal of Neurogenetics* (Vol. 30, Issues 3–4, pp. 163–177). Taylor and Francis Ltd. <https://doi.org/10.1080/01677063.2016.1229781>
- Franca, T. C. C., Kitagawa, D. A. S., Cavalcante, S. F. de A., da Silva, J. A. V., Nepovimova, E., & Kuca, K. (2019). Novichoks: The Dangerous Fourth Generation of Chemical Weapons. *International Journal of Molecular Sciences*, 20(5). <https://doi.org/10.3390/IJMS20051222>
- Freedman, R. (2014). $\alpha 7$ -nicotinic acetylcholine receptor agonists for cognitive enhancement in schizophrenia. *Annual Review of Medicine*, 65, 245–261. <https://doi.org/10.1146/ANNUREV-MED-092112-142937>

- Fucile, S., Sucapane, A., & Eusebi, F. (2006). Ca²⁺ permeability through rat cloned $\alpha 9$ -containing nicotinic acetylcholine receptors. *Cell Calcium*, 39(4), 349–355. <https://doi.org/10.1016/J.CECA.2005.12.002>
- Fukuto, T. R. (1990). Mechanism of action of organophosphorus and carbamate insecticides. *Environmental Health Perspectives*, 87, 245–254. <https://doi.org/10.1289/ehp.9087245>
- Gahring, L. C., & Rogers, S. W. (2005). Neuronal nicotinic acetylcholine receptor expression and function on nonneuronal cells. *The AAPS Journal 2005 7:4*, 7(4), E885–E894. <https://doi.org/10.1208/AAPSJ070486>
- Galvis, G., Lips, K. S., & Kummer, W. (2006). Expression of nicotinic acetylcholine receptors on murine alveolar macrophages. *Journal of Molecular Neuroscience 2006 30:1*, 30(1), 107–108. <https://doi.org/10.1385/JMN:30:1:107>
- Galzi, J. L., Bertrand, S., Corringer, P. J., Changeux, J. P., & Bertrand, D. (1996). Identification of calcium binding sites that regulate potentiation of a neuronal nicotinic acetylcholine receptor. *The EMBO Journal*, 15(21), 5824. <https://doi.org/10.1002/j.1460-2075.1996.tb00969.x>
- García-Colunga, J., Awad, J. N., & Miledi, R. (1997). Blockage of muscle and neuronal nicotinic acetylcholine receptors by fluoxetine (Prozac). *Proceedings of the National Academy of Sciences of the United States of America*, 94(5), 2041–2044. <https://doi.org/10.1073/pnas.94.5.2041>
- Gay, E. A., & Yakel, J. L. (2007). Gating of nicotinic ACh receptors; new insights into structural transitions triggered by agonist binding that induce channel opening. *The Journal of Physiology*, 584(Pt 3), 727. <https://doi.org/10.1113/JPHYSIOL.2007.142554>
- Gharpure, A., Teng, J., Zhuang, Y., Noviello, C. M., Walsh, R. M., Cabuco, R., Howard, R. J., Zaveri, N. T., Lindahl, E., & Hibbs, R. E. (2019). Agonist Selectivity and Ion Permeation in the $\alpha 3\beta 4$ Ganglionic Nicotinic Receptor. *Neuron*, 104(3), 501–511.e6. <https://doi.org/10.1016/j.neuron.2019.07.030>
- Gibson, D. G., Young, L., Chuang, R. Y., Venter, J. C., Hutchison, C. A., & Smith, H. O. (2009). Enzymatic assembly of DNA molecules up to several hundred kilobases. *Nature Methods*, 6(5), 343–345. <https://doi.org/10.1038/NMETH.1318>
- Gielen, M., & Corringer, P. J. (2018). The dual-gate model for pentameric ligand-gated ion channels activation and desensitization. In *Journal of Physiology* (Vol. 596, Issue 10, pp. 1873–1902). J Physiol. <https://doi.org/10.1113/JP275100>
- Giribaldi, J., Haufe, Y., Evans, E. R. J., Amar, M., Durner, A., Schmidt, C., Faucherre, A., Moha Ou Maati, H., Enjalbal, C., Molgó, J., Servent, D., Wilson, D. T., Daly, N. L., Nicke, A., & Dutertre, S. (2020). Backbone Cyclization Turns a Venom Peptide into a Stable and Equipotent Ligand at Both Muscle and Neuronal Nicotinic Receptors. *Journal of Medicinal Chemistry*, 63(21), 12682–12692. <https://doi.org/10.1021/acs.jmedchem.0c00957>
- Giribaldi, J., Wilson, D., Nicke, A., el Hamdaoui, Y., Laconde, G., Faucherre, A., Maati, H. M. O., Daly, N. L., Enjalbal, C., & Dutertre, S. (2018). Synthesis, structure and biological activity of CIA and CIB, two α -conotoxins from the predation-evoked venom of *Conus catus*. *Toxins*, 10(6). <https://doi.org/10.3390/toxins10060222>
- Goh, C. W., Aw, C. C., Lee, J. H., Chen, C. P., & Browne, E. R. (2011). Pharmacokinetic and pharmacodynamic properties of cholinesterase inhibitors donepezil, tacrine, and galantamine in aged and young Lister hooded rats. *Drug Metabolism and Disposition: The Biological Fate of Chemicals*, 39(3), 402–411. <https://doi.org/10.1124/DMD.110.035964>

- Govind, A. P., Vezina, P., & Green, W. N. (2009). Nicotine-induced upregulation of nicotinic receptors: Underlying mechanisms and relevance to nicotine addiction. *Biochemical Pharmacology*, *78*(7), 756–765. <https://doi.org/10.1016/J.BCP.2009.06.011>
- Grando, S. A. (2014). Connections of nicotine to cancer. In *Nature Reviews Cancer* (Vol. 14, Issue 6, pp. 419–429). Nat Rev Cancer. <https://doi.org/10.1038/nrc3725>
- Grau, V., Richter, K., Hone, A. J., & Michael McIntosh, J. (2019). Conopeptides [V11L;V16D]Arib and RGIA4: Powerful tools for the identification of novel nicotinic acetylcholine receptors in monocytes. *Frontiers in Pharmacology*, *9*(JAN), 1499. <https://doi.org/10.3389/fphar.2018.01499>
- Grishin, A. A., Cuny, H., Hung, A., Clark, R. J., Brust, A., Akondi, K., Alewood, P. F., Craik, D. J., & Adams, D. J. (2013). Identifying key amino acid residues that affect α -conotoxin AulB inhibition of $\alpha 3\beta 4$ nicotinic acetylcholine receptors. *Journal of Biological Chemistry*, *288*(48), 34428–34442. <https://doi.org/10.1074/jbc.M113.512582>
- Groot-Kormelink, P. J., Boorman, J. P., & Sivilotti, L. G. (2001). Formation of functional $\alpha 3\beta 4\alpha 5$ human neuronal nicotinic receptors in *Xenopus* oocytes: A reporter mutation approach. *British Journal of Pharmacology*, *134*(4), 789–796. <https://doi.org/10.1038/sj.bjp.0704313>
- Grünewald, B., & Siefert, P. (2019). Acetylcholine and Its Receptors in Honeybees: Involvement in Development and Impairments by Neonicotinoids. *Insects*, *10*(420), 1–12. <https://doi.org/10.3390/insects10120420>
- Guan, Z. Z., Nordberg, A., Mousavi, M., Rinne, J. O., & Hellström-Lindahl, E. (2002). Selective changes in the levels of nicotinic acetylcholine receptor protein and of corresponding mRNA species in the brains of patients with Parkinson's disease. *Brain Research*, *956*(2), 358–366. [https://doi.org/10.1016/S0006-8993\(02\)03571-0](https://doi.org/10.1016/S0006-8993(02)03571-0)
- Gulsevin, A., Papke, R. L., Stokes, C., Tran, H. N. T., Jin, A. H., Vetter, I., & Meiler, J. (2021). The allosteric activation of $\alpha 7$ nAChR by α -conotoxin Mrlc is modified by mutations at the vestibular site. *Toxins*, *13*(8). <https://doi.org/10.3390/toxins13080555>
- Hahn, M., Schotthöfer, A., Schmitz, J., Franke, L. A., & Brühl, C. A. (2015). The effects of agrochemicals on Lepidoptera, with a focus on moths, and their pollination service in field margin habitats. *Agriculture, Ecosystems & Environment*, *207*, 153–162. <https://doi.org/10.1016/J.AGEE.2015.04.002>
- Hansen, K. B., Yi, F., Perszyk, R. E., Furukawa, H., Wollmuth, L. P., Gibb, A. J., & Traynelis, S. F. (2018). Structure, function, and allosteric modulation of NMDA receptors. *Journal of General Physiology*, *150*(8), 1081–1105. <https://doi.org/10.1085/JGP.201812032>
- Haskell-Luevano, C., & Meanwell, N. A. (2018). Allosteric Modulators of Drug Targets. *Journal of Medicinal Chemistry*, *62*(1), 1–2. <https://doi.org/10.1021/ACS.JMEDCHEM.8B01902>
- Haslam, J. D., Russell, P., Hill, S., Emmett, S. R., & Blain, P. G. (2021). Chemical, biological, radiological, and nuclear mass casualty medicine: a review of lessons from the Salisbury and Amesbury Novichok nerve agent incidents. *British Journal of Anaesthesia*. <https://doi.org/10.1016/J.BJA.2021.10.008>
- Heidmann, T., & Changeux, J. P. (1986). Characterization of the transient agonist-triggered state of the acetylcholine receptor rapidly labeled by the noncompetitive blocker [3H]chlorpromazine: additional evidence for the open channel conformation. *Biochemistry*, *25*(20), 6109–6113. <https://doi.org/10.1021/BI00368A041>
- Hénault, C. M., Govaerts, C., Spurny, R., Brams, M., Estrada-Mondragon, A., Lynch, J., Bertrand, D., Pardon, E., Evans, G. L., Woods, K., Elberson, B. W., Cuello, L. G., Brannigan, G., Nury, H., Steyaert, J., Baenziger, J. E., & Ulens, C. (2019). A lipid site shapes the agonist response

- of a pentameric ligand-gated ion channel. *Nature Chemical Biology*, *15*(12), 1156–1164. <https://doi.org/10.1038/s41589-019-0369-4>
- Hilf, R. J. C., & Dutzler, R. (2008). X-ray structure of a prokaryotic pentameric ligand-gated ion channel. *Nature* *2008* *452*:7185, *452*(7185), 375–379. <https://doi.org/10.1038/nature06717>
- Himaya, S. W. A., Jin, A. H., Dutertre, S., Giacomotto, J., Mohialdeen, H., Vetter, I., Alewood, P. F., & Lewis, R. J. (2015). Comparative Venomics Reveals the Complex Prey Capture Strategy of the Piscivorous Cone Snail *Conus catus*. *Journal of Proteome Research*, *14*(10), 4372–4381. <https://doi.org/10.1021/ACS.JPROTEOME.5B00630>
- Hone, A. J., Servent, D., & McIntosh, J. M. (2018). α 9-containing nicotinic acetylcholine receptors and the modulation of pain. *British Journal of Pharmacology*, *175*(11), 1915–1927. <https://doi.org/10.1111/BPH.13931>
- Hösli, L., Hösli, E., Briotta, G. della, Quadri, L., & Heuss, L. (1988). Action of acetylcholine, muscarine, nicotine and antagonists on the membrane potential of astrocytes in cultured rat brainstem and spinal cord. *Neuroscience Letters*, *92*(2), 165–170. [https://doi.org/10.1016/0304-3940\(88\)90054-7](https://doi.org/10.1016/0304-3940(88)90054-7)
- Ho, T. N. T., Abraham, N., & Lewis, R. J. (2020). Structure-Function of Neuronal Nicotinic Acetylcholine Receptor Inhibitors Derived From Natural Toxins. *Frontiers in Neuroscience*, *14*. <https://doi.org/10.3389/FNINS.2020.609005>
- Ho, T. N. T., Abraham, N., & Lewis, R. J. (2021a). Rigidity of loop 1 contributes to equipotency of globular and ribbon isomers of α -conotoxin AusIA. *Scientific Reports*, *11*(1). <https://doi.org/10.1038/S41598-021-01277-4>
- Ho, T. N. T., Abraham, N., & Lewis, R. J. (2021b). Unique Pharmacological Properties of α -Conotoxin OmlA at α 7 nAChRs. *Frontiers in Pharmacology*, *12*. <https://doi.org/10.3389/FPHAR.2021.803397>
- Hung, D. Z., Yang, H. J., Li, Y. F., Lin, C. L., Chang, S. Y., Sung, F. C., & Tai, S. C. W. (2015). The Long-Term Effects of Organophosphates Poisoning as a Risk Factor of CVDs: A Nationwide Population-Based Cohort Study. *PLoS ONE*, *10*(9). <https://doi.org/10.1371/JOURNAL.PONE.0137632>
- Hurst, R. S., Hajós, M., Raggenbass, M., Wall, T. M., Higdon, N. R., Lawson, J. A., Rutherford-Root, K. L., Berkenpas, M. B., Hoffmann, W. E., Piotrowski, D. W., Groppi, V. E., Allaman, G., Ogier, R., Bertrand, S., Bertrand, D., & Arneric, S. P. (2005). A novel positive allosteric modulator of the α 7 neuronal nicotinic acetylcholine receptor: in vitro and in vivo characterization. *The Journal of Neuroscience: The Official Journal of the Society for Neuroscience*, *25*(17), 4396–4405. <https://doi.org/10.1523/JNEUROSCI.5269-04.2005>
- Huynh, P. N., Harvey, P. J., Gajewiak, J., Craik, D. J., & Michael McIntosh, J. (2020). Critical residue properties for potency and selectivity of α -Conotoxin RglA towards α 9 α 10 nicotinic acetylcholine receptors. *Biochemical Pharmacology*, *181*, 114124. <https://doi.org/10.1016/j.bcp.2020.114124>
- Ihara, M., & Matsuda, K. (2018). Neonicotinoids: molecular mechanisms of action, insights into resistance and impact on pollinators. *Current Opinion in Insect Science*, *30*, 86–92. <https://doi.org/10.1016/J.COIS.2018.09.009>
- Imoto, K., Busch, C., Sakmann, B., Mishina, M., Konno, T., Nakai, J., Bujo, H., Mori, Y., Fukuda, K., & Numa, S. (1988). Rings of negatively charged amino acids determine the acetylcholine receptor channel conductance. *Nature*, *335*(6191), 645–648. <https://doi.org/10.1038/335645a0>

- Indurthi, D. C., Lewis, T. M., Ahring, P. K., Balle, T., Chebib, M., & Absalom, N. L. (2016). Ligand Binding at the $\alpha 4$ - $\alpha 4$ Agonist-Binding Site of the $\alpha 4\beta 2$ nAChR Triggers Receptor Activation through a Pre-Activated Conformational State. *PLoS ONE*, *11*(8). <https://doi.org/10.1371/JOURNAL.PONE.0161154>
- Jin, A. H., Muttenthaler, M., Dutertre, S., Himaya, S. W. A., Kaas, Q., Craik, D. J., Lewis, R. J., & Alewood, P. F. (2019). Conotoxins: Chemistry and Biology. *Chemical Reviews*, *119*(21), 11510–11549. <https://doi.org/10.1021/ACS.CHEMREV.9B00207>
- Jitpakdee, T., & Mande, S. (2014). Strategies for preventing side effects of systemic opioid in postoperative pediatric patients. *Paediatric Anaesthesia*, *24*(6), 561–568. <https://doi.org/10.1111/PAN.12420>
- John, H., van der Schans, M. J., Koller, M., Spruit, H. E. T., Worek, F., Thiermann, H., & Noort, D. (2018). Fatal sarin poisoning in Syria 2013: forensic verification within an international laboratory network. *Forensic Toxicology*, *36*(1), 61–71. <https://doi.org/10.1007/s11419-017-0376-7>
- Jonsson, M., Dabrowski, M., Gurley, D. A., Larsson, O., Johnson, E. C., Fredholm, B. B., & Eriksson, L. I. (2006). Activation and inhibition of human muscular and neuronal nicotinic acetylcholine receptors by succinylcholine. *Anesthesiology*, *104*(4), 724–733. <https://doi.org/10.1097/00000542-200604000-00017>
- Kaas, Q., Westermann, J. C., & Craik, D. J. (2010). Conopeptide characterization and classifications: an analysis using ConoServer. *Toxicon: Official Journal of the International Society on Toxinology*, *55*(8), 1491–1509. <https://doi.org/10.1016/J.TOXICON.2010.03.002>
- Kaas, Q., Yu, R., Jin, A. H., Dutertre, S., & Craik, D. J. (2012). ConoServer: updated content, knowledge, and discovery tools in the conopeptide database. *Nucleic Acids Research*, *40*(Database issue). <https://doi.org/10.1093/NAR/GKR886>
- Kalamida, D., Poulas, K., Avramopoulou, V., Fostieri, E., Lagoumintzis, G., Lazaridis, K., Sideri, A., Zouridakis, M., & Tzartos, S. J. (2007). Muscle and neuronal nicotinic acetylcholine receptors. *The FEBS Journal*, *274*(15), 3799–3845. <https://doi.org/10.1111/J.1742-4658.2007.05935.X>
- Karlin, A., Cox, R. N., Dipaola, M., Holtzman, E., Kao, P. N., Lobel, P., Wang, L., & Yodh, N. (1986). Functional Domains of the Nicotinic Acetylcholine Receptor. *Annals of the New York Academy of Sciences*, *463*(1 Second Colloq), 53–69. <https://doi.org/10.1111/j.1749-6632.1986.tb21503.x>
- Karlsson, E., Heilbronn, E., & Widlund, L. (1972). Isolation of the nicotinic acetylcholine receptor by biospecific chromatography on insolubilized *Naja naja* neurotoxin. *FEBS Letters*, *28*(1), 107–111. [https://doi.org/10.1016/0014-5793\(72\)80688-4](https://doi.org/10.1016/0014-5793(72)80688-4)
- Kasheverov, I., Kudryavtsev, D., Shelukhina, I., Nikolaev, G., Utkin, Y., & Tsetlin, V. (2022). Marine Origin Ligands of Nicotinic Receptors: Low Molecular Compounds, Peptides and Proteins for Fundamental Research and Practical Applications. In *Biomolecules* (Vol. 12, Issue 2, p. 189). Multidisciplinary Digital Publishing Institute. <https://doi.org/10.3390/biom12020189>
- Kassa, J., Timperley, C. M., Bird, M., Green, A. C., & Tattersall, J. E. H. (2020). Influence of experimental end point on the therapeutic efficacy of the antinicotinic compounds MB408, MB442 and MB444 in treating nerve agent poisoned mice—a comparison with oxime-based treatment. *Toxicol. Mech. Methods*, *30*(9), 703–710. <https://doi.org/10.1080/15376516.2020.1817218>

- Katz, D., DiMattia, M. A., Sindhikara, D., Li, H., Abraham, N., & Leffler, A. E. (2021). Potency- and Selectivity-Enhancing Mutations of Conotoxins for Nicotinic Acetylcholine Receptors Can Be Predicted Using Accurate Free-Energy Calculations. *Marine Drugs*, *19*(7), 367. <https://doi.org/10.3390/md19070367>
- Kawashima, K., & Fujii, T. (2003). The lymphocytic cholinergic system and its contribution to the regulation of immune activity. *Life Sciences*, *74*(6), 675–696. <https://doi.org/10.1016/J.LFS.2003.09.037>
- Kem, W. R., Andrud, K., Bruno, G., Xing, H., Soti, F., Talley, T. T., & Taylor, P. (2022). Interactions of Nereistoxin and Its Analogs with Vertebrate Nicotinic Acetylcholine Receptors and Molluscan ACh Binding Proteins. *Marine Drugs*, *20*(1). <https://doi.org/10.3390/MD20010049>
- Khatri, B., Nuthakki, V. R., & Chatterjee, J. (2019). Strategies to Enhance Metabolic Stabilities. *Methods in Molecular Biology (Clifton, N.J.)*, *2001*, 17–40. https://doi.org/10.1007/978-1-4939-9504-2_2
- Kineta, Inc. 2022. (n.d.). *Neuroscience – Kineta Inc.* Retrieved February 27, 2022, from <https://kinetabio.com/neuroscience/>
- King, J. R., Nordman, J. C., Bridges, S. P., Lin, M. K., & Kabbani, N. (2015). Identification and Characterization of a G Protein-binding Cluster in $\alpha 7$ Nicotinic Acetylcholine Receptors. *The Journal of Biological Chemistry*, *290*(33), 20060–20070. <https://doi.org/10.1074/JBC.M115.647040>
- Kompella, S. N., Cuny, H., Hung, A., & Adams, D. J. (2015). Molecular basis for differential sensitivity of α -conotoxin RegIIA at rat and human neuronal nicotinic acetylcholine receptors. *Molecular Pharmacology*, *88*(6), 993–1001. <https://doi.org/10.1124/mol.115.100503>
- Kowal, N. M., Ahring, P. K., Liao, V. W. Y., Indurti, D. C., Harvey, B. S., O'Connor, S. M., Chebib, M., Olafsdottir, E. S., & Balle, T. (2018). Galantamine is not a positive allosteric modulator of human $\alpha 4\beta 2$ or $\alpha 7$ nicotinic acetylcholine receptors. *British Journal of Pharmacology*, *175*(14), 2911–2925. <https://doi.org/10.1111/bph.14329>
- Krause, R. M., Buisson, B., Bertrand, S., Corringer, P. J., Galzi, J. L., Changeux, J. P., & Bertrand, D. (1998). Ivermectin: A Positive Allosteric Effector of the $\alpha 7$ Neuronal Nicotinic Acetylcholine Receptor. *Molecular Pharmacology*, *53*(2), 283–294. <https://doi.org/10.1124/MOL.53.2.283>
- Kryukova, E. v., Shelukhina, I. v., Kozina, E. A., Ugrumov, M. v., & Tsetlin, V. I. (2013). Expression of acetylcholine receptors in the brain of mice at the presymptomatic stage of Parkinson's disease. *Doklady Biochemistry and Biophysics*, *449*(1), 69–71. <https://doi.org/10.1134/S1607672913020038>
- Kulak, J. M., McIntosh, J. M., Yoshikami, D., & Olivera, B. M. (2001). Nicotine-evoked transmitter release from synaptosomes: functional association of specific presynaptic acetylcholine receptors and voltage-gated calcium channels. *Journal of Neurochemistry*, *77*(6), 1581–1589. <https://doi.org/10.1046/J.1471-4159.2001.00357.X>
- Kuryatov, A., Olale, F., Cooper, J., Choi, C., & Lindstrom, J. (2000). Human $\alpha 6$ AChR subtypes: Subunit composition, assembly, and pharmacological responses. *Neuropharmacology*, *39*(13), 2570–2590. [https://doi.org/10.1016/S0028-3908\(00\)00144-1](https://doi.org/10.1016/S0028-3908(00)00144-1)
- Laps, S., Atamleh, F., Kamnesky, G., Sun, H., & Brik, A. (2021). General synthetic strategy for regioselective ultrafast formation of disulfide bonds in peptides and proteins. *Nature Communications*, *12*(1), 1–9. <https://doi.org/10.1038/s41467-021-21209-0>
- Leffler, A. E., Kuryatov, A., Zebroski, H. A., Powell, S. R., Filipenko, P., Hussein, A. K., Gorson, J., Heizmann, A., Lyskov, S., Tsien, R. W., Poget, S. F., Nicke, A., Lindstrom, J., Rudy, B.,

- Bonneau, R., & Holford, M. (2017). Discovery of peptide ligands through docking and virtual screening at nicotinic acetylcholine receptor homology models. *Proceedings of the National Academy of Sciences of the United States of America*, *114*(38), E8100–E8109. <https://doi.org/10.1073/pnas.1703952114>
- Lena, C., Changeux, J. P., & Mulle, C. (1993). Evidence for “preterminal” nicotinic receptors on GABAergic axons in the rat interpeduncular nucleus. *Journal of Neuroscience*, *13*(6), 2680–2688. <https://doi.org/10.1523/jneurosci.13-06-02680.1993>
- Leonard, R. J., Labarca, C. G., Charnet, P., Davidson, N., & Lester, H. A. (1988). Evidence That the M2 Membrane-Spanning Region Lines the Ion Channel Pore of the Nicotinic Receptor. *Science*, *242*(4885), 1578–1581. <https://doi.org/10.1126/SCIENCE.2462281>
- Lerro, C. C., Koutros, S., Andreotti, G., Friesen, M. C., Alavanja, M. C., Blair, A., Hoppin, J. A., Sandler, D. P., Lubin, J. H., Ma, X., Zhang, Y., & Freeman, L. E. B. (2015). Organophosphate insecticide use and cancer incidence among spouses of pesticide applicators in the Agricultural Health Study. *Occupational and Environmental Medicine*, *72*(10), 736. <https://doi.org/10.1136/OEMED-2014-102798>
- Levandoski, M. M., Lin, Y., Moise, L., McLaughlin, J. T., Cooper, E., & Hawrot, E. (1999). Chimeric Analysis of a Neuronal Nicotinic Acetylcholine Receptor Reveals Amino Acids Conferring Sensitivity to α -Bungarotoxin. *Journal of Biological Chemistry*, *274*(37), 26113–26119. <https://doi.org/10.1074/JBC.274.37.26113>
- Li, H., Schopfer, L. M., Nachon, F., Froment, M. T., Masson, P., & Lockridge, O. (2007). Aging pathways for organophosphate-inhibited human butyrylcholinesterase, including novel pathways for isomalathion, resolved by mass spectrometry. *Toxicological Sciences*, *100*(1), 136–145. <https://doi.org/10.1093/toxsci/kfm215>
- Liu, Q., Huang, Y., Shen, J., Steffensen, S., & Wu, J. (2012). Functional $\alpha 7 \beta 2$ nicotinic acetylcholine receptors expressed in hippocampal interneurons exhibit high sensitivity to pathological level of amyloid β peptides. *BMC Neuroscience*, *13*(1). <https://doi.org/10.1186/1471-2202-13-155>
- Li, X., Tae, H. S., Chu, Y., Jiang, T., Adams, D. J., & Yu, R. (2021). Medicinal chemistry, pharmacology, and therapeutic potential of α -conotoxins antagonizing the $\alpha 9 \alpha 10$ nicotinic acetylcholine receptor. *Pharmacology & Therapeutics*, *222*. <https://doi.org/10.1016/J.PHARMTHERA.2020.107792>
- Li, X., Wang, S., Zhu, X., Zhangsun, D., Wu, Y., & Luo, S. (2020). Effects of Cyclization on Activity and Stability of α -Conotoxin Tx1B. *Marine Drugs*, *18*(4). <https://doi.org/10.3390/MD18040180>
- Loser, D., Grillberger, K., Hinojosa, M. G., Blum, J., Haufe, Y., Danker, T., Johansson, Y., Möller, C., Nicke, A., Bennekou, S. H., Gardner, I., Bauch, C., Walker, P., Forsby, A., Ecker, G. F., Kraushaar, U., & Leist, M. (2021). Acute effects of the imidacloprid metabolite desnitro-imidacloprid on human nACh receptors relevant for neuronal signaling. *Archives of Toxicology*, *95*(12), 3695–3716. <https://doi.org/10.1007/s00204-021-03168-z>
- Loser, D., Hinojosa, M. G., Blum, J., Schaefer, J., Brüll, M., Johansson, Y., Suci, I., Grillberger, K., Danker, T., Möller, C., Gardner, I., Ecker, G. F., Bennekou, S. H., Forsby, A., Kraushaar, U., & Leist, M. (2021). Functional alterations by a subgroup of neonicotinoid pesticides in human dopaminergic neurons. *Archives of Toxicology*, *95*(6), 2081–2107. <https://doi.org/10.1007/s00204-021-03031-1>
- Loughner, C. L., Bruford, E. A., McAndrews, M. S., Delp, E. E., Swamynathan, S., & Swamynathan, S. K. (2016). Organization, evolution and functions of the human and mouse

- Ly6/uPAR family genes. *Human Genomics* 2016 10:1, 10(1), 1–19. <https://doi.org/10.1186/S40246-016-0074-2>
- Luo, L., Bennett, T., Jung, H. H., & Ryan, A. F. (1998). Developmental expression of alpha 9 acetylcholine receptor mRNA in the rat cochlea and vestibular inner ear. *The Journal of Comparative Neurology*, 393(3), 320–331. <http://www.ncbi.nlm.nih.gov/pubmed/9548553>
- Luo, S., Zhangsun, D., Harvey, P. J., Kaas, Q., Wu, Y., Zhu, X., Hu, Y., Li, X., Tsetlin, V. I., Christensen, S., Romero, H. K., McIntyre, M., Dowell, C., Baxter, J. C., Elmslie, K. S., Craik, D. J., & McIntosh, J. M. (2015). Cloning, synthesis, and characterization of α O-conotoxin GeXIVA, a potent α 9 α 10 nicotinic acetylcholine receptor antagonist. *Proceedings of the National Academy of Sciences of the United States of America*, 112(30), E4026–E4035. <https://doi.org/10.1073/PNAS.1503617112>
- Marsillach, J., Richter, R. J., Kim, J. H., Stevens, R. C., MacCoss, M. J., Tomazela, D., Suzuki, S. M., Schopfer, L. M., Lockridge, O., & Furlong, C. E. (2011). Biomarkers of organophosphorus (OP) exposures in humans. *NeuroToxicology*, 32(5), 656–660. <https://doi.org/10.1016/j.neuro.2011.06.005>
- Maskell, P. D., Speder, P., Newberry, N. R., & Bermudez, I. (2003). Inhibition of human α 7 nicotinic acetylcholine receptors by open channel blockers of N-methyl-D-aspartate receptors. *British Journal of Pharmacology*, 140(7), 1313–1319. <https://doi.org/10.1038/sj.bjp.0705559>
- Mazzaferro, S., Bermudez, I., Sine, S. M., & Stephenson, F. A. (2017). α 4 β 2 Nicotinic Acetylcholine Receptors; relationships between subunit stoichiometry and function at the single channel level. *Journal of Biological Chemistry*, 292(7), 2729–2740. <https://doi.org/10.1074/jbc.M116.764183>
- McCann, C. M., Bracamontes, J., Steinbach, J. H., & Sanes, J. R. (2006). The cholinergic antagonist α -bungarotoxin also binds and blocks a subset of GABA receptors. *Proceedings of the National Academy of Sciences*, 103(13), 5149–5154. <https://doi.org/10.1073/PNAS.0600847103>
- McIntosh, J. M., Azam, L., Staheli, S., Dowell, C., Lindstrom, J. M., Kuryatov, A., Garrett, J. E., Marks, M. J., & Whiteaker, P. (2004). Analogs of α -Conotoxin MII Are Selective for α 6-Containing Nicotinic Acetylcholine Receptors. *Molecular Pharmacology*, 65(4), 944–952. <https://doi.org/10.1124/mol.65.4.944>
- McIntosh, J. M., Plazas, P. v., Watkins, M., Gomez-Casati, M. E., Olivera, B. M., & Elgoyhen, A. B. (2005). A novel alpha-conotoxin, PeIA, cloned from *Conus pergrandis*, discriminates between rat α 9 α 10 and α 7 nicotinic cholinergic receptors. *The Journal of Biological Chemistry*, 280(34), 30107–30112. <https://doi.org/10.1074/JBC.M504102200>
- McIntosh, J. M., Santos, A. D., & Olivera, B. M. (1999). *Conus* peptides targeted to specific nicotinic acetylcholine receptor subtypes. In *Annual Review of Biochemistry* (Vol. 68, pp. 59–88). Annual Reviews 4139 El Camino Way, P.O. Box 10139, Palo Alto, CA 94303-0139, USA. <https://doi.org/10.1146/annurev.biochem.68.1.59>
- Millard, E. L., Nevin, S. T., Loughnan, M. L., Nicke, A., Clark, R. J., Alewood, P. F., Lewis, R. J., Adams, D. J., Craik, D. J., & Daly, N. L. (2009). Inhibition of neuronal nicotinic acetylcholine receptor subtypes by alpha-Conotoxin GlD and analogues. *The Journal of Biological Chemistry*, 284(8), 4944–4951. <https://doi.org/10.1074/JBC.M804950200>
- Millar, N. S. (2009). A review of experimental techniques used for the heterologous expression of nicotinic acetylcholine receptors. *Biochemical Pharmacology*, 78(7), 766–776. <https://doi.org/10.1016/j.bcp.2009.06.015>

- Millar, N. S., & Denholm, I. (2007). Nicotinic acetylcholine receptors: Targets for commercially important insecticides. *Invertebrate Neuroscience*, 7(1), 53–66. <https://doi.org/10.1007/s10158-006-0040-0>
- Miyazawa, A., Fujiyoshi, Y., & Unwin, N. (2003). Structure and gating mechanism of the acetylcholine receptor pore. *Nature* 2003 423:6943, 423(6943), 949–955. <https://doi.org/10.1038/nature01748>
- Mizrachi, T., Marsha, O., Brusin, K., Ben-David, Y., Thakur, G. A., Vaknin-Dembinsky, A., Treinin, M., & Brenner, T. (2021). Suppression of neuroinflammation by an allosteric agonist and positive allosteric modulator of the $\alpha 7$ nicotinic acetylcholine receptor GAT107. *Journal of Neuroinflammation*, 18(1), 99. <https://doi.org/10.1186/s12974-021-02149-4>
- Morales-Perez, C. L., Noviello, C. M., & Hibbs, R. E. (2016). X-ray structure of the human $\alpha 4\beta 2$ nicotinic receptor. *Nature*, 538(7625), 411–415. <https://doi.org/10.1038/nature19785>
- Mordvintsev, D. Y., Polyak, Y. L., Rodionov, D. I., Jakubik, J., Dolezal, V., Karlsson, E., Tsetlin, V. I., & Utkin, Y. N. (2009). Weak toxin WTX from *Naja kaouthia* cobra venom interacts with both nicotinic and muscarinic acetylcholine receptors. *The FEBS Journal*, 276(18), 5065–5075. <https://doi.org/10.1111/J.1742-4658.2009.07203.X>
- Morel, C., Fattore, L., Pons, S., Hay, Y. A., Marti, F., Lambalez, B., de Biasi, M., Lathrop, M., Fratta, W., Maskos, U., & Faure, P. (2014). Nicotine consumption is regulated by a human polymorphism in dopamine neurons. *Molecular Psychiatry*, 19(8), 930–936. <https://doi.org/10.1038/MP.2013.158>
- Morley, B. J., Whiteaker, P., & Elgoyhen, A. B. (2018). Commentary: Nicotinic Acetylcholine Receptor $\alpha 9$ and $\alpha 10$ Subunits Are Expressed in the Brain of Mice. *Frontiers in Cellular Neuroscience*, 12. <https://doi.org/10.3389/FNCEL.2018.00104>
- Mulé, R., Sabella, G., Robba, L., & Manachini, B. (2017). Systematic review of the effects of chemical insecticides on four common butterfly families. *Frontiers in Environmental Science*, 5(JUN), 32. <https://doi.org/10.3389/FENVS.2017.00032/BIBTEX>
- Mulle, C., Léna, C., & Changeux, J. P. (1992). Potentiation of nicotinic receptor response by external calcium in rat central neurons. *Neuron*, 8(5), 937–945. [https://doi.org/10.1016/0896-6273\(92\)90208-U](https://doi.org/10.1016/0896-6273(92)90208-U)
- Muttenthaler, M., Nevin, S. T., Inserra, M., Lewis, R. J., Adams, D. J., & Alewood, P. F. (2020). On-resin strategy to label α -conotoxins: Cy5-RgIA, a potent $\alpha 9\alpha 10$ nicotinic acetylcholine receptor imaging probe. *Australian Journal of Chemistry*, 73(4), 327–333. <https://doi.org/10.1071/CH19456>
- Nicke, A., Loughnan, M. L., Millard, E. L., Alewood, P. F., Adams, D. J., Daly, N. L., Craik, D. J., & Lewis, R. J. (2003). Isolation, structure, and activity of GID, a novel $\alpha 4/7$ -conotoxin with an extended N-terminal sequence. *The Journal of Biological Chemistry*, 278(5), 3137–3144. <https://doi.org/10.1074/jbc.M210280200>
- Nicolopoulou-Stamati, P., Maipas, S., Kotampasi, C., Stamatis, P., & Hens, L. (2016). Chemical Pesticides and Human Health: The Urgent Need for a New Concept in Agriculture. *Frontiers in Public Health*, 4, 148. <https://doi.org/10.3389/FPUBH.2016.00148/BIBTEX>
- Niessen, K. V., Seeger, T., Rappenglück, S., Wein, T., Höfner, G., Wanner, K. T., Thiermann, H., & Worek, F. (2018). In vitro pharmacological characterization of the bispyridinium non-oxime compound MB327 and its 2- and 3-regioisomers. *Toxicology Letters*, 293, 190–197. <https://doi.org/10.1016/j.toxlet.2017.10.009>

- Ning, J., Li, R., Ren, J., Zhangsun, D., Zhu, X., Wu, Y., & Luo, S. (2018). Alanine-Scanning mutagenesis of α -Conotoxin GI reveals the residues crucial for activity at the muscle acetylcholine receptor. *Marine Drugs*, *16*(12). <https://doi.org/10.3390/md16120507>
- Noviello, C. M., Gharpure, A., Mukhtasimova, N., Cabuco, R., Baxter, L., Borek, D., Sine, S. M., & Hibbs, R. E. (2021). Structure and gating mechanism of the $\alpha 7$ nicotinic acetylcholine receptor. *Cell*, *184*(8), 2121–2134.e13. <https://doi.org/10.1016/j.cell.2021.02.049>
- NTR. (2021). Retrieved February 27, 2022, from <https://www.trialregister.nl/trial/9581>
- Nury, H., van Renterghem, C., Weng, Y., Tran, A., Baaden, M., Dufresne, V., Changeux, J. P., Sonner, J. M., Delarue, M., & Corringer, P. J. (2011). X-ray structures of general anaesthetics bound to a pentameric ligand-gated ion channel. *Nature*, *469*(7330), 428–431. <https://doi.org/10.1038/NATURE09647>
- Olivera, B. M., Seger, J., Horvath, M. P., & Fedosov, A. E. (2015). Prey-Capture Strategies of Fish-Hunting Cone Snails: Behavior, Neurobiology and Evolution. *Brain, Behavior and Evolution*, *86*(1), 58–74. <https://doi.org/10.1159/000438449>
- Olivero, G., Grilli, M., Chen, J., Preda, S., Mura, E., Govoni, S., & Marchi, M. (2014). Effects of soluble β -amyloid on the release of neurotransmitters from rat brain synaptosomes. *Frontiers in Aging Neuroscience*, *6*(JUL), 166. <https://doi.org/10.3389/FNAGI.2014.00166/BIBTEX>
- Olsen, R. W. (2018). GABA A receptor: Positive and negative allosteric modulators. *Neuropharmacology*, *136*(Pt A), 10–22. <https://doi.org/10.1016/J.NEUROPHARM.2018.01.036>
- Pacini, A., Micheli, L., Maresca, M., Branca, J. J. V., McIntosh, J. M., Ghelardini, C., & di Cesare Mannelli, L. (2016). The $\alpha 9\alpha 10$ nicotinic receptor antagonist α -conotoxin RglA prevents neuropathic pain induced by oxaliplatin treatment. *Experimental Neurology*, *282*, 37–48. <https://doi.org/10.1016/J.EXPNEUROL.2016.04.022>
- Palma, E., Reyes-Ruiz, J. M., Lopergolo, D., Roseti, C., Bertollini, C., Ruffolo, G., Cifelli, P., Onesti, E., Limatola, C., Miledi, R., & Inghilleri, M. (2016). Acetylcholine receptors from human muscle as pharmacological targets for ALS therapy. *Proceedings of the National Academy of Sciences of the United States of America*, *113*(11), 3060–3065. <https://doi.org/10.1073/pnas.1600251113>
- Papke, R. L., & Horenstein, N. A. (2021). Therapeutic Targeting of $\alpha 7$ Nicotinic Acetylcholine Receptors. *Pharmacological Reviews*, *73*(3), 1118–1149. <https://doi.org/10.1124/pharmrev.120.000097>
- Papke, R. L., Horenstein, N. A., Kulkarni, A. R., Stokes, C., Corrie, L. W., Maeng, C. Y., & Thakur, G. A. (2014). The activity of GAT107, an allosteric activator and positive modulator of $\alpha 7$ nicotinic acetylcholine receptors (nAChR), is regulated by aromatic amino acids that span the subunit interface. *Journal of Biological Chemistry*, *289*(7), 4515–4531. <https://doi.org/10.1074/jbc.M113.524603>
- Papke, R. L., Kem, W. R., Soti, F., López-Hernández, G. Y., & Horenstein, N. A. (2009). Activation and desensitization of nicotinic $\alpha 7$ -type acetylcholine receptors by benzylidene anabaseines and nicotine. *The Journal of Pharmacology and Experimental Therapeutics*, *329*(2), 791–807. <https://doi.org/10.1124/JPET.108.150151>
- Papke, R. L., & Porter Papke, J. K. (2002). Comparative pharmacology of rat and human $\alpha 7$ nAChR conducted with net charge analysis. *British Journal of Pharmacology*, *137*(1), 49–61. <https://doi.org/10.1038/sj.bjp.0704833>
- Paterson, D., & Nordberg, A. (2000). Neuronal nicotinic receptors in the human brain. *Progress in Neurobiology*, *61*(1), 75–111. [https://doi.org/10.1016/S0301-0082\(99\)00045-3](https://doi.org/10.1016/S0301-0082(99)00045-3)

- Peng, H., Ferris, R. L., Matthews, T., Hiel, H., Lopez-Albaitero, A., & Lustig, L. R. (2004). Characterization of the human nicotinic acetylcholine receptor subunit alpha (α) 9 (CHRNA9) and alpha (α) 10 (CHRNA10) in lymphocytes. *Life Sciences*, *76*(3), 263–280. <https://doi.org/10.1016/J.LFS.2004.05.031>
- Pestronk, A., Drachman, D. B., & Self, S. G. (1985). Measurement of junctional acetylcholine receptors in myasthenia gravis: clinical correlates. *Muscle & Nerve*, *8*(3), 245–251. <https://doi.org/10.1002/MUS.880080311>
- Picciotto, M. R., Caldarone, B. J., Brunzell, D. H., Zachariou, V., Stevens, T. R., & King, S. L. (2001). Neuronal nicotinic acetylcholine receptor subunit knockout mice: physiological and behavioral phenotypes and possible clinical implications. *Pharmacology & Therapeutics*, *92*(2–3), 89–108. [https://doi.org/10.1016/S0163-7258\(01\)00161-9](https://doi.org/10.1016/S0163-7258(01)00161-9)
- Picciotto, M. R., Higley, M. J., & Mineur, Y. S. (2012). Acetylcholine as a neuromodulator: cholinergic signaling shapes nervous system function and behavior. *Neuron*, *76*(1), 116–129. <https://doi.org/10.1016/J.NEURON.2012.08.036>
- Picciotto, M. R., & Kenny, P. J. (2013). Molecular mechanisms underlying behaviors related to nicotine addiction. *Cold Spring Harbor Perspectives in Medicine*, *3*(1). <https://doi.org/10.1101/cshperspect.a012112>
- Pope, J. E., & Deer, T. R. (2013). Ziconotide: A clinical update and pharmacologic review. In *Expert Opinion on Pharmacotherapy* (Vol. 14, Issue 7, pp. 957–966). Expert Opin Pharmacother. <https://doi.org/10.1517/14656566.2013.784269>
- Pucci, S., Zoli, M., Clementi, F., & Gotti, C. (2022). α 9-Containing Nicotinic Receptors in Cancer. *Frontiers in Cellular Neuroscience*, *15*. <https://doi.org/10.3389/fncel.2021.805123>
- Purohit, Y., & Grosman, C. (2006). Block of muscle nicotinic receptors by choline suggests that the activation and desensitization gates act as distinct molecular entities. *The Journal of General Physiology*, *127*(6), 703–717. <https://doi.org/10.1085/JGP.200509437>
- Quadri, M., Bagdas, D., Toma, W., Stokes, C., Horenstein, N. A., Damaj, M. I., & Papke, R. L. (2018). The Antinociceptive and Anti-Inflammatory Properties of the α 7 nAChR Weak Partial Agonist p -CF 3 N , N -diethyl- N '-phenylpiperazine. *Journal of Pharmacology and Experimental Therapeutics*, *367*(2), 203–214. <https://doi.org/10.1124/jpet.118.249904>
- Quik, M., Bordia, T., & O'Leary, K. (2007). Nicotinic receptors as CNS targets for Parkinson's disease. *Biochemical Pharmacology*, *74*(8), 1224–1234. <https://doi.org/10.1016/J.BCP.2007.06.015>
- Quik, M., & Wonnacott, S. (2011). α 6 β 2* and α 4 β 2* nicotinic acetylcholine receptors as drug targets for parkinson's disease. In *Pharmacological Reviews* (Vol. 63, Issue 4, pp. 938–966). Pharmacol Rev. <https://doi.org/10.1124/pr.110.003269>
- Rahman, M. M., Teng, J., Worrell, B. T., Noviello, C. M., Lee, M., Karlin, A., Stowell, M. H. B., & Hibbs, R. E. (2020). Structure of the Native Muscle-type Nicotinic Receptor and Inhibition by Snake Venom Toxins. *Neuron*, *106*(6), 952-962.e5. <https://doi.org/10.1016/j.neuron.2020.03.012>
- Rezende-Teixeira, P., Dusi, R. G., Jimenez, P. C., Espindola, L. S., & Costa-Lotufo, L. v. (2022). What can we learn from commercial insecticides? Efficacy, toxicity, environmental impacts, and future developments. In *Environmental Pollution* (Vol. 300, p. 118983). Environ Pollut. <https://doi.org/10.1016/j.envpol.2022.118983>
- Richter, M. C., Ludewig, S., Winschel, A., Abel, T., Bold, C., Salzburger, L. R., Klein, S., Han, K., Weyer, S. W., Fritz, A.-K., Laube, B., Wolfer, D. P., Buchholz, C. J., Korte, M., & Müller, U. C. (2018). Distinct in vivo roles of secreted APP ectodomain variants APP α and APP β

- in regulation of spine density, synaptic plasticity, and cognition. *The EMBO Journal*, 37(11). <https://doi.org/10.15252/embj.201798335>
- Romero, H. K., Christensen, S. B., di Cesare Mannelli, L., Gajewiak, J., Ramachandra, R., Elmslie, K. S., Vetter, D. E., Ghelardini, C., Iadonato, S. P., Mercado, J. L., Olivera, B. M., & McIntosh, J. M. (2017). Inhibition of $\alpha 9\alpha 10$ nicotinic acetylcholine receptors prevents chemotherapy-induced neuropathic pain. *Proceedings of the National Academy of Sciences of the United States of America*, 114(10), E1825–E1832. <https://doi.org/10.1073/PNAS.1621433114>
- Ross, G. A., Russell, E., Deng, Y., Lu, C., Harder, E. D., Abel, R., & Wang, L. (2020). Enhancing Water Sampling in Free Energy Calculations with Grand Canonical Monte Carlo. *Journal of Chemical Theory and Computation*, 16(10), 6061–6076. <https://doi.org/10.1021/acs.jctc.0c00660>
- Rossmann, A. C. (2011). The physiology of the nicotinic acetylcholine receptor and its importance in the administration of anesthesia. *AANA Journal*, 79(5), 433–440. <http://www.ncbi.nlm.nih.gov/pubmed/23256274>
- Rueter, L. E., Donnelly-Roberts, D. L., Curzon, P., Briggs, C. A., Anderson, D. J., & Bitner, R. S. (2006). A-85380: A Pharmacological Probe for the Preclinical and Clinical Investigation of the $\alpha 4\beta 2$ Neuronal Nicotinic Acetylcholine Receptor. *CNS Drug Reviews*, 12(2), 100–112. <https://doi.org/10.1111/J.1527-3458.2006.00100.X>
- Safronova, V. G., Vulpius, C. A., Astashev, M. E., Tikhonova, I. v., Serov, D. A., Jirova, E. A., Pershina, E. v., Senko, D. A., Zhmak, M. N., Kasheverov, I. E., & Tsetlin, V. I. (2021). $\alpha 9\alpha 10$ nicotinic acetylcholine receptors regulate murine bone marrow granulocyte functions. *Immunobiology*, 226(1), 152047. <https://doi.org/10.1016/J.IMBIO.2020.152047>
- Sauguet, L., Howard, R. J., Malherbe, L., Lee, U. S., Corringer, P. J., Adron Harris, R., & Delarue, M. (2013). Structural basis for potentiation by alcohols and anaesthetics in a ligand-gated ion channel. *Nature Communications* 2013 4:1, 4(1), 1–10. <https://doi.org/10.1038/ncomms2682>
- Scheffel, C., Niessen, K. v., Rappenglück, S., Wanner, K. T., Thiermann, H., Worek, F., & Seeger, T. (2018). Electrophysiological investigation of the effect of structurally different bispyridinium non-oxime compounds on human $\alpha 7$ -nicotinic acetylcholine receptor activity—An in vitro structure-activity analysis. *Toxicology Letters*, 293(September 2017), 157–166. <https://doi.org/10.1016/j.toxlet.2017.11.025>
- Schmeltz, I. (1971). Nicotine and other tobacco alkaloids. In M. Jacobson & D. G. Crosby (Eds.), *Naturally occurring insecticides* (pp. 99–136).
- Seeger, T., Eichhorn, M., Lindner, M., Niessen, K. v., Tattersall, J. E. H., Timperley, C. M., Bird, M., Green, A. C., Thiermann, H., & Worek, F. (2012). Restoration of soman-blocked neuromuscular transmission in human and rat muscle by the bispyridinium non-oxime MB327 in vitro. *Toxicology*, 294(2–3), 80–84. <https://doi.org/10.1016/j.tox.2012.02.002>
- Shao, X. M., & Feldman, J. L. (2009). Central cholinergic regulation of respiration: nicotinic receptors. *Acta Pharmacologica Sinica*, 30(6), 761. <https://doi.org/10.1038/APS.2009.88>
- Sharma, G., & Vijayaraghavan, S. (2003). Modulation of presynaptic store calcium induces release of glutamate and postsynaptic firing. *Neuron*, 38(6), 929–939. [https://doi.org/10.1016/S0896-6273\(03\)00322-2](https://doi.org/10.1016/S0896-6273(03)00322-2)
- Simmons, D. D., & Morley, B. J. (2011). Spatial and temporal expression patterns of nicotinic acetylcholine alpha 9 and alpha 10 subunits in the embryonic and early postnatal inner ear. *Neuroscience*, 194, 326–336. <https://doi.org/10.1016/J.NEUROSCIENCE.2011.08.005>

- Soliakov, L., & Wonnacott, S. (1996). Voltage-sensitive Ca²⁺ channels involved in nicotinic receptor-mediated [3H]dopamine release from rat striatal synaptosomes. *Journal of Neurochemistry*, *67*(1), 163–170. <https://doi.org/10.1046/j.1471-4159.1996.67010163.x>
- Soloway, S. B., Henry, A. C., Kollmeyer, W. D., Padgett, W. M., Powell, J. E., Roman, S. A., Tieman, C. H., Corey, R. A., & Horne, C. A. (1978). Nitromethylene Heterocycles as Insecticides. *Pesticide and Venom Neurotoxicity*, 153–158. https://doi.org/10.1007/978-1-4615-8834-4_12
- Son, L., Kryukova, E., Ziganshin, R., Andreeva, T., Kudryavtsev, D., Kasheverov, I., Tsetlin, V., & Utkin, Y. (2021). Novel Three-Finger Neurotoxins from *Naja melanoleuca* Cobra Venom Interact with GABAA and Nicotinic Acetylcholine Receptors. *Toxins 2021, Vol. 13, Page 164*, *13*(2), 164. <https://doi.org/10.3390/TOXINS13020164>
- Spitzmaul, G. F., Esandi del Carmen, M., & Bouzat, C. (1999). Amphetamine acts as a channel blocker of the acetylcholine receptor. *NeuroReport*, *10*(10), 2175–2181.
- Spurny, R., Debaveye, S., Farinha, A., Veys, K., Vos, A. M., Gossas, T., Attack, J., Bertrand, S., Bertrand, D., Danielson, U. H., Tresadern, G., & Ulens, C. (2015). Molecular blueprint of allosteric binding sites in a homologue of the agonist-binding domain of the $\alpha 7$ nicotinic acetylcholine receptor. *Proceedings of the National Academy of Sciences*, *112*(19), E2543–E2552. <https://doi.org/10.1073/pnas.1418289112>
- Stephuhn, A., Gase, K., Krock, B., Halitschke, R., & Baldwin, I. T. (2004). Nicotine's Defensive Function in Nature. *PLoS Biology*, *2*(8). <https://doi.org/10.1371/JOURNAL.PBIO.0020217>
- Stokes, C., Treinin, M., & Papke, R. L. (2015). Looking below the surface of nicotinic acetylcholine receptors. In *Trends in Pharmacological Sciences* (Vol. 36, Issue 8, pp. 514–523). NIH Public Access. <https://doi.org/10.1016/j.tips.2015.05.002>
- Sun, Y., Jia, D., Xue, M., Huang, Z., & Huang, C. (2022). Trifluoro-icaritin alleviates chronic inflammatory pain through $\alpha 7$ nAChR-mediated suppression of HMGB1/NF- κ B signaling in the spinal cord of rats. *Brain Research Bulletin*, *183*, 13–26. <https://doi.org/10.1016/J.BRAINRESBULL.2022.02.014>
- Taly, A., Corringer, P. J., Guedin, D., Lestage, P., & Changeux, J. P. (2009). Nicotinic receptors: Allosteric transitions and therapeutic targets in the nervous system. In *Nature Reviews Drug Discovery* (Vol. 8, Issue 9, pp. 733–750). Nature Publishing Group. <https://doi.org/10.1038/nrd2927>
- Tattersall, J. E. H. (1993). Ion channel blockade by oximes and recovery of diaphragm muscle from soman poisoning in vitro. *British Journal of Pharmacology*, *108*(4), 1006–1015. <https://doi.org/10.1111/j.1476-5381.1993.tb13498.x>
- Thiermann, H., Seeger, T., Gonder, S., Herkert, N., Antkowiak, B., Zilker, T., Eyer, F., & Worek, F. (2010). Assessment of neuromuscular dysfunction during poisoning by organophosphorus compounds. *Chemico-Biological Interactions*, *187*(1–3), 265–269. <https://doi.org/10.1016/J.CBI.2009.12.027>
- Thiermann, H., Worek, F., & Kehe, K. (2013). Limitations and challenges in treatment of acute chemical warfare agent poisoning. *Chemico-Biological Interactions*, *206*(3), 435–443. <https://doi.org/10.1016/j.cbi.2013.09.015>
- Timmermann, D. B., Grønlien, J. H., Kohlhaas, K. L., Nielsen, E., Dam, E., Jørgensen, T. D., Ahring, P. K., Peters, D., Holst, D., Chrsitensen, J. K., Malysz, J., Briggs, C. A., Gopalakrishnan, M., & Olsen, G. M. (2007). An allosteric modulator of the $\alpha 7$ nicotinic acetylcholine receptor possessing cognition-enhancing properties in vivo. *Journal of Pharmacology and Experimental Therapeutics*, *323*(1), 294–307. <https://doi.org/10.1124/jpet.107.120436>

- Tomizawa, M., & Casida, J. E. (2000). Imidacloprid, Thiacloprid, and Their Imine Derivatives Up-Regulate the $\alpha 4\beta 2$ Nicotinic Acetylcholine Receptor in M10 Cells. *Toxicology and Applied Pharmacology*, 169(1), 114–120. <https://doi.org/10.1006/TAAP.2000.9057>
- Tonstad, S., Arons, C., Rollema, H., Berlin, I., Hajek, P., Fagerström, K., Els, C., McRae, T., & Russ, C. (2020). Varenicline: mode of action, efficacy, safety and accumulated experience salient for clinical populations. *Current Medical Research and Opinion*, 36(5), 713–730. <https://doi.org/10.1080/03007995.2020.1729708>
- Tsetlin, V. I. (2015). Three-finger snake neurotoxins and Ly6 proteins targeting nicotinic acetylcholine receptors: Pharmacological tools and endogenous modulators. In *Trends in Pharmacological Sciences* (Vol. 36, Issue 2, pp. 109–123). Elsevier Current Trends. <https://doi.org/10.1016/j.tips.2014.11.003>
- Turner, S. R., Chad, J. E., Price, M., Timperley, C. M., Bird, M., Green, A. C., & Tattersall, J. E. H. (2011). Protection against nerve agent poisoning by a noncompetitive nicotinic antagonist. *Toxicology Letters*, 206(1), 105–111. <https://doi.org/10.1016/j.toxlet.2011.05.1035>
- Unwin, N. (2005). Refined structure of the nicotinic acetylcholine receptor at 4 Å resolution. *Journal of Molecular Biology*, 346(4), 967–989. <https://doi.org/10.1016/j.jmb.2004.12.031>
- Vallés, A. S., Garbus, I., & Barrantes, F. J. (2007). Lamotrigine is an open-channel blocker of the nicotinic acetylcholine receptor. *NeuroReport*, 18(1), 45–50. <https://doi.org/10.1097/01.WNR.0000246323.66438.94>
- van Lierop, B. J., Robinson, S. D., Kompella, S. N., Belgi, A., McArthur, J. R., Hung, A., Macrauld, C. A., Adams, D. J., Norton, R. S., & Robinson, A. J. (2013). Dicarba α -conotoxin Vc1.1 analogues with differential selectivity for nicotinic acetylcholine and GABAB receptors. *ACS Chemical Biology*, 8(8), 1815–1821. https://doi.org/10.1021/CB4002393/SUPPL_FILE/CB4002393_SI_001.PDF
- Verma, M. K., Goel, R. N., Bokare, A. M., Dandekar, M. P., Koul, S., Desai, S., Tota, S., Singh, N., Nigade, P. B., Patil, V. B., Modi, D., Mehta, M., Gundu, J., Walunj, S. S., Karche, N. P., Sinha, N., Kamboj, R. K., & Palle, V. P. (2021). LL-00066471, a novel positive allosteric modulator of $\alpha 7$ nicotinic acetylcholine receptor ameliorates cognitive and sensorimotor gating deficits in animal models: Discovery and preclinical characterization. *European Journal of Pharmacology*, 891. <https://doi.org/10.1016/j.ejphar.2020.173685>
- Vincler, M., Wittenauer, S., Parker, R., Ellison, M., Olivera, B. M., & McIntosh, J. M. (2006). Molecular mechanism for analgesia involving specific antagonism of $\alpha 9\alpha 10$ nicotinic acetylcholine receptors. *Proceedings of the National Academy of Sciences of the United States of America*, 103(47), 17880. <https://doi.org/10.1073/PNAS.0608715103>
- Vishwanath, V. A., & McIntosh, J. M. (2006). Synthesis of fluorescent analogs of α -conotoxin MII. *Bioconjugate Chemistry*, 17(6), 1612–1617. https://doi.org/10.1021/BC060163Y/SUPPL_FILE/BC060163YSI20060621_123103.PDF
- v. Uteshev, V. (2016). Allosteric Modulation of Nicotinic Acetylcholine Receptors: The Concept and Therapeutic Trends. *Current Pharmaceutical Design*, 22(14), 1986–1997. <https://doi.org/10.2174/1381612822666160201115341>
- Wang, C. K., & Craik, D. J. (2018). Designing macrocyclic disulfide-rich peptides for biotechnological applications. *Nature Chemical Biology*, 14(5), 417–427. <https://doi.org/10.1038/S41589-018-0039-Y>

- Wang, H., Li, X., Zhangsun, D., Yu, G., Su, R., & Luo, S. (2019). The $\alpha 9\alpha 10$ Nicotinic Acetylcholine Receptor Antagonist α O-Conotoxin GeXIVA[1,2] Alleviates and Reverses Chemotherapy-Induced Neuropathic Pain. *Marine Drugs* 2019, Vol. 17, Page 265, 17(5), 265. <https://doi.org/10.3390/MD17050265>
- Wang, S., & Hu, Y. (2018). $\alpha 7$ nicotinic acetylcholine receptors in lung cancer. *Oncology Letters*, 16(2), 1375. <https://doi.org/10.3892/OL.2018.8841>
- Wang, X., Xiao, H., Wang, J., Huang, Z., Peng, G., Xie, W., Bian, X., Liu, H., Shi, C., Yang, T., Li, X., Gao, J., Meng, Y., Jiang, Q., Chen, W., Hu, F., Wei, N., Wang, X., Zhang, L., ... Sun, Q. (2021). Synthesis and Biological Evaluation of Novel Triazine Derivatives as Positive Allosteric Modulators of $\alpha 7$ Nicotinic Acetylcholine Receptors. *Journal of Medicinal Chemistry*, 64(16), 12379–12396. <https://doi.org/10.1021/acs.jmedchem.1c01058>
- Wan, J., Huang, J. X., Vetter, I., Mobli, M., Lawson, J., Tae, H. S., Abraham, N., Paul, B., Cooper, M. A., Adams, D. J., Lewis, R. J., & Alewood, P. F. (2015). α -Conotoxin dendrimers have enhanced potency and selectivity for homomeric nicotinic acetylcholine receptors. *Journal of the American Chemical Society*, 137(9), 3209–3212. https://doi.org/10.1021/JACS.5B00244/SUPPL_FILE/JA5B00244_SI_001.PDF
- Wenthur, C. J., Gentry, P. R., Mathews, T. P., & Lindsley, C. W. (2014). Drugs for Allosteric Sites on Receptors. *Annual Review of Pharmacology and Toxicology*, 54, 165. <https://doi.org/10.1146/ANNUREV-PHARMTOX-010611-134525>
- Wessler, I., & Kirkpatrick, C. J. (2008). Acetylcholine beyond neurons: The non-neuronal cholinergic system in humans. In *British Journal of Pharmacology* (Vol. 154, Issue 8, pp. 1558–1571). *Br J Pharmacol*. <https://doi.org/10.1038/bjp.2008.185>
- Wilcock, G., Howe, I., Coles, H., Lilienfeld, S., Truyen, L., Zhu, Y., Bullock, R., & Kershaw, P. (2003). A long-term comparison of galantamine and donepezil in the treatment of Alzheimer's disease. *Drugs & Aging*, 20(10), 777–789. <https://doi.org/10.2165/00002512-200320100-00006>
- Wilens, T. E., & Decker, M. W. (2007). Neuronal nicotinic receptor agonists for the treatment of attention-deficit/hyperactivity disorder: focus on cognition. *Biochemical Pharmacology*, 74(8), 1212–1223. <https://doi.org/10.1016/J.BCP.2007.07.002>
- Williams, D. K., Wang, J., & Papke, R. L. (2011). Investigation of the molecular mechanism of the $\alpha 7$ nicotinic acetylcholine receptor positive allosteric modulator PNU-120596 provides evidence for two distinct desensitized states. *Molecular Pharmacology*, 80(6), 1013–1032. <https://doi.org/10.1124/mol.111.074302>
- Wilson, D. T., Bansal, P. S., Carter, D. A., Vetter, I., Nicke, A., Dutertre, S., & Daly, N. L. (2020). Characterisation of a novel α -superfamily conotoxin. *Biomedicines*, 8(5), 128. <https://doi.org/10.3390/BIOMEDICINES8050128>
- Wojas-Krawczyk, K., Krawczyk, P., Biernacka, B., Grzybek, M., Kołodziej, P., Kucharczyk, T., Mlak, R., & Milanowski, J. (2012). The polymorphism of the CHRNA5 gene and the strength of nicotine addiction in lung cancer and COPD patients. *European Journal of Cancer Prevention: The Official Journal of the European Cancer Prevention Organisation (ECP)*, 21(2), 111–117. <https://doi.org/10.1097/CEJ.0B013E32834C9B40>
- Wonnacott, S. (1997). Presynaptic nicotinic ACh receptors. *Trends in Neurosciences*, 20(2), 92–98. [https://doi.org/10.1016/S0166-2236\(96\)10073-4](https://doi.org/10.1016/S0166-2236(96)10073-4)
- Woodhull, A. M. (1973). Ionic blockage of sodium channels in nerve. *Journal of General Physiology*, 61(6), 687–708. <https://doi.org/10.1085/jgp.61.6.687>

- Worek, F., Thiermann, H., & Wille, T. (2020). Organophosphorus compounds and oximes: a critical review. *Archives of Toxicology*, *94*(7), 2275–2292. <https://doi.org/10.1007/S00204-020-02797-0>
- Wu, J., Liu, Q., Tang, P., Mikkelsen, J. D., Shen, J., Whiteaker, P., & Yakel, J. L. (2016). Heteromeric $\alpha 7\beta 2$ Nicotinic Acetylcholine Receptors in the Brain. *Trends in Pharmacological Sciences*, *37*(7), 562–574. <https://doi.org/10.1016/J.TIPS.2016.03.005>
- Wu, X., Craik, D. J., & Kaas, Q. (2021). Interactions of globular and ribbon [$\gamma 4e$]gid with $\alpha 4\beta 2$ neuronal nicotinic acetylcholine receptor. *Marine Drugs*, *19*(9), 482. <https://doi.org/10.3390/md19090482>
- Wu, Y., Wu, X., Yu, J., Zhu, X., Zhangsun, D., & Luo, S. (2014). Influence of Disulfide Connectivity on Structure and Bioactivity of α -Conotoxin TxIA. *Molecules* *2014*, Vol. 19, Pages 966–979, *19*(1), 966–979. <https://doi.org/10.3390/MOLECULES19010966>
- Xu, Y., Barrantes, F. J., Shen, J., Luo, X., Zhu, W., Chen, K., & Jiang, H. (2006). Blocking of the Nicotinic Acetylcholine Receptor Ion Channel by Chlorpromazine, a Noncompetitive Inhibitor: A Molecular Dynamics Simulation Study. *The Journal of Physical Chemistry B*, *110*(41), 20640–20648. <https://doi.org/10.1021/jp0604591>
- Yevenes, G. E., & Zeilhofer, H. U. (2011). Allosteric modulation of glycine receptors. *British Journal of Pharmacology*, *164*(2), 224. <https://doi.org/10.1111/J.1476-5381.2011.01471.X>
- Young, G. T., Zwart, R., Walker, A. S., Sher, E., & Millar, N. S. (2008). Potentiation of $\alpha 7$ nicotinic acetylcholine receptors via an allosteric transmembrane site. *Proceedings of the National Academy of Sciences of the United States of America*, *105*(38), 14686–14691. <https://doi.org/10.1073/pnas.0804372105>
- Zarkadas, E., Pebay-Peyroula, E., Thompson, M. J., Schoehn, G., Uchański, T., Steyaert, J., Chipot, C., Dehez, F., Baenziger, J. E., & Nury, H. (2022). Conformational transitions and ligand-binding to a muscle-type nicotinic acetylcholine receptor. *Neuron*, *0*(0). <https://doi.org/10.1016/j.neuron.2022.01.013>
- Zhang, L., Zhang, Y., Jiang, D., Reid, P. F., Jiang, X., Qin, Z., & Tao, J. (2012). Alpha-cobratoxin inhibits T-type calcium currents through muscarinic M4 receptor and Go-protein $\beta\gamma$ subunits-dependent protein kinase A pathway in dorsal root ganglion neurons. *Neuropharmacology*, *62*(2), 1062–1072. <https://doi.org/10.1016/J.NEUROPHARM.2011.10.017>
- Zhang, S., Zhou, Z., Gong, Q., Makielski, J. C., & January, C. T. (1999). Mechanism of Block and Identification of the Verapamil Binding Domain to HERG Potassium Channels. *Circulation Research*, *84*(9), 989–998. <https://doi.org/10.1161/01.RES.84.9.989>
- Zhang, X., Cheng, Q., Li, L., Shangguan, L., Li, C., Li, S., Huang, F., Zhang, J., & Wang, R. (2019). Supramolecular therapeutics to treat the side effects induced by a depolarizing neuromuscular blocking agent. *Theranostics*, *9*(11), 3107–3121. <https://doi.org/10.7150/THNO.34947>
- Zhao, R., Shi, P., Chen, J., Sun, S., Chen, J., Cui, J., Wu, F., Fang, G., Tian, C., Shi, J., Bierer, D., Liu, L., & Li, Y. M. (2020). Chemical synthesis and biological activity of peptides incorporating an ether bridge as a surrogate for a disulfide bond. *Chemical Science*, *11*(30), 7927–7932. <https://doi.org/10.1039/D0SC02374D>
- Zhao, Y., Liu, S., Zhou, Y., Zhang, M., Chen, H., Eric Xu, H., Sun, D., Liu, L., & Tian, C. (2021). Structural basis of human $\alpha 7$ nicotinic acetylcholine receptor activation. In *Cell Research* (Vol. 31, Issue 6, pp. 713–716). Nature Publishing Group. <https://doi.org/10.1038/s41422-021-00509-6>

- Zheng, N., Christensen, S. B., Blakely, A., Dowell, C., Purushottam, L., McIntosh, J. M., & Chou, D. H. C. (2020). Development of Conformationally Constrained α -RglA Analogues as Stable Peptide Antagonists of Human $\alpha 9\alpha 10$ Nicotinic Acetylcholine Receptors. *Journal of Medicinal Chemistry*, *63*(15), 8380–8387. <https://doi.org/10.1021/acs.jmedchem.0c00613>
- Zhong, W., Gallivan, J. P., Zhang, Y., Li, L., Lester, H. A., & Dougherty, D. A. (1998). From ab initio quantum mechanics to molecular neurobiology: A cation– π binding site in the nicotinic receptor. *Proceedings of the National Academy of Sciences*, *95*(21), 12088–12093. <https://doi.org/10.1073/PNAS.95.21.12088>
- Zia, S., Ndoye, A., Lee, T. X., Webber, R. J., & Grando, S. A. (2000). Receptor-mediated inhibition of keratinocyte migration by nicotine involves modulations of calcium influx and intracellular concentration. *The Journal of Pharmacology and Experimental Therapeutics*, *293*(3), 973–981. <http://www.ncbi.nlm.nih.gov/pubmed/10869400>
- Zimmermann, I., & Dutzler, R. (2011). Ligand Activation of the Prokaryotic Pentameric Ligand-Gated Ion Channel ELIC. *PLOS Biology*, *9*(6), e1001101. <https://doi.org/10.1371/JOURNAL.PBIO.1001101>
- Zoli, M., Pistillo, F., & Gotti, C. (2015). Diversity of native nicotinic receptor subtypes in mammalian brain. *Neuropharmacology*, *96*(PB), 302–311. <https://doi.org/10.1016/J.NEUROPHARM.2014.11.003>
- Zoli, M., Pucci, S., Vilella, A., & Gotti, C. (2018). Neuronal and Extraneuronal Nicotinic Acetylcholine Receptors. *Current Neuropharmacology*, *16*(4), 338. <https://doi.org/10.2174/1570159X15666170912110450>
- Zouridakis, M., Giastas, P., Zarkadas, E., Chroni-Tzartou, D., Bregestovski, P., & Tzartos, S. J. (2014). Crystal structures of free and antagonist-bound states of human $\alpha 9$ nicotinic receptor extracellular domain. *Nature Structural and Molecular Biology*, *21*(11), 976–980. <https://doi.org/10.1038/nsmb.2900>

4. Publication I

pp. 51 - 72

Backbone Cyclization Turns a Venom Peptide into a Stable and Equipotent Ligand at Both Muscle and Neuronal Nicotinic Receptors

Julien Giribaldi, Yves Haufe, Edward R. J. Evans, Muriel Amar, Anna Durner, Casey Schmidt, Adèle Faucherre, Hamid Moha Ou Maati, Christine Enjalbal, Jordi Molgó, Denis Servent, David T. Wilson, Norelle L. Daly, Annette Nicke, and Sébastien Dutertre*



Cite This: <https://dx.doi.org/10.1021/acs.jmedchem.0c00957>



Read Online

ACCESS |



Metrics & More

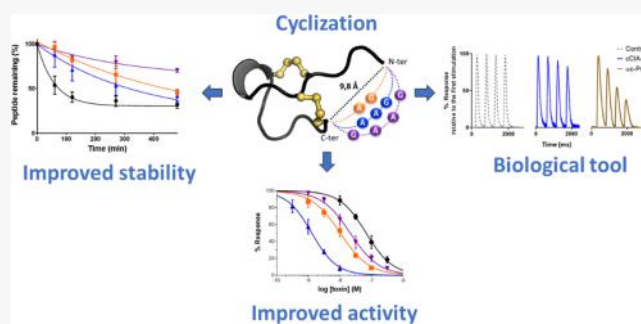


Article Recommendations



Supporting Information

ABSTRACT: Venom peptides are promising drug leads, but their therapeutic use is often limited by stability and bioavailability issues. In this study, we designed cyclic analogues of α -conotoxin CIA, a potent muscle nicotinic acetylcholine receptor (nAChR) blocker with a significantly lower affinity at the neuronal $\alpha 3\beta 2$ subtype. Remarkably, all analogues retained the low nanomolar activity of native CIA toward muscle-type nAChRs but showed greatly improved resistance to degradation in human serum and, surprisingly, displayed up to 52-fold higher potency for the $\alpha 3\beta 2$ neuronal nAChR subtype (IC_{50} 1.3 nM). Comparison of nuclear magnetic resonance-derived structures revealed some differences that might explain the gain of potency at $\alpha 3\beta 2$ nAChRs. All peptides were highly paralytic when injected into adult zebrafish and bath-applied to zebrafish larvae, suggesting barrier-crossing capabilities and efficient uptake. Finally, these cyclic CIA analogues were shown to be unique pharmacological tools to investigate the contribution of the presynaptic $\alpha 3\beta 2$ nAChR subtype to the train-of-four fade.



INTRODUCTION

Natural extracts from animals, plants, and bacteria provide one of the richest sources of bioactive peptides, some of which have entered clinical development for the treatment of human diseases such as diabetes, HIV, hepatitis, and cancer. Animal venom peptides are of particular interest, as they have been finely tuned by millions of years of prey-predator coevolution to potently and selectively target receptors involved in key physiological functions and, consequently, they are widely employed as potent pharmacological probes.¹ Cone snails are predatory marine mollusks that have evolved and radiated into more than 800 different species and nowhere is peptide diversity more apparent than within their venom.² They have developed extremely potent and fast acting neurotoxic venoms mainly composed of small peptides (10–40 residues) called conotoxins. These conotoxins are generally highly constrained by disulfide bridges (2–4 bridges), and target a wide range of receptors with key physiological functions for rapid prey immobilization and defense.^{3,4} Disulfide bridges provide conotoxins with rigid conformations, enabling a tight and specific interaction with their molecular targets, which are mainly ion channels, but also transporters and G protein-coupled receptors.^{5,6}

Members of the α -conotoxin subfamily specifically block the nicotinic acetylcholine receptors (nAChRs).^{6,7} nAChRs are ligand-gated ion channels of primary importance in the

peripheral and central nervous systems, where they intervene in a wide range of physiological and pathophysiological processes, including muscle contraction, pain sensation, nicotine addiction, and neurological disorders such as Parkinson's and Alzheimer's diseases.⁶ These receptors exist as homopentamers or heteropentamers composed of a large variety of homologous subunits. Subunits $\alpha 2$ – $\alpha 10$ and $\beta 2$ – $\beta 4$ assemble into the diverse group of neuronal nicotinic receptors, while the muscle-type nicotinic receptor exists only as adult ($\alpha 1$)₂ $\beta 1\epsilon\delta$ and fetal ($\alpha 1$)₂ $\beta 1\gamma\delta$ subunit combinations.⁸ α -Conotoxins are classified according to the number of residues within the loops formed by two conserved disulfide bridges. Interestingly, in most cases, the size of the loops seems to determine their specificity for different nAChR subtypes. Thus, 3/4 α -conotoxins target homomeric neuronal nAChRs, 3/5 α -conotoxins target muscle-type nAChRs, and 4/4, 4/6 and 4/7 α -conotoxins target different heteromeric and/or homomeric neuronal nAChRs.⁶

Received: June 8, 2020

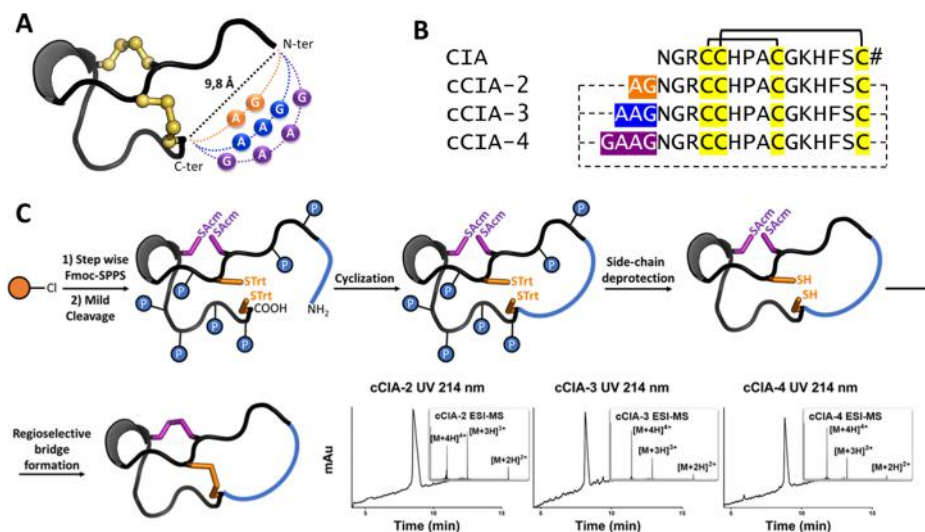


Figure 1. Sequences and chemical synthesis strategy for α -conotoxin CIA cyclic analogues (cCIAs). (A) NMR structure (backbone representation) of CIA. CIA exhibits a classical α -conotoxin fold with Cys I–Cys III and Cys II–Cys IV disulfide connectivity (represented in yellow). (B) Based on the intertermini spacing, amino acid linkers with a length between 10 and 19 Å were designed. Symbol # indicates an amidated C-terminal residue. (C) Strategy for the synthesis of three cyclic α -CIA peptides and the respective RP-HPLC/ESI-MS analysis to confirm purity >95%. The orange round circle represents a PS-chloro-(2'-chloro) trityl resin and P represents common side chain-protecting groups used in Fmoc-SPPS. RP-HPLC–UV (ACN gradient from 0 to 30% in 30 min) coupled to ESI-MS analyses revealed the presence of dominant peaks of the expected masses.

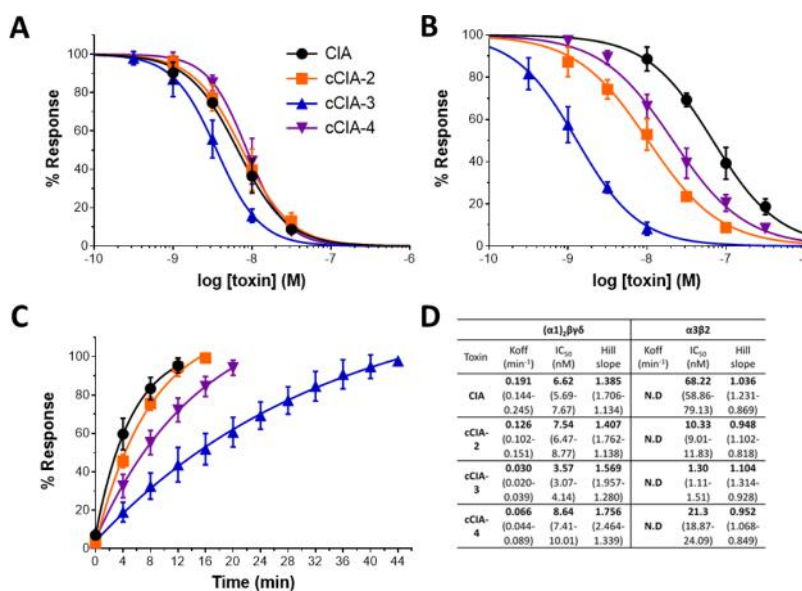


Figure 2. CIA cyclic analogues retain potency at the muscle-type nAChR and show increased affinity at $\alpha 3 \beta 2$ nAChRs. Dose–response curves of CIA and the three cyclic analogues (cCIA-2, cCIA-3, and cCIA-4) on (A) rat muscle-type and (B) neuronal $\alpha 3 \beta 2$ nAChRs. *X. laevis* oocytes expressing the indicated receptors were analyzed by two-electrode voltage-clamp at -70 mV holding potential. Responses to 2 s pulses of $100 \mu\text{M}$ ACh were recorded after 3 min preincubation with the respective toxin. (C) Recovery of muscle-type nAChRs from toxin block measured in 4 min intervals. Each point represents the mean of measurements from at least three different oocytes. Error bars represent SD. (D) Summary of inhibition and dissociation constants of the toxins. Numbers in brackets are 95% confidence intervals. N.D. = not determined.

Despite great advances in peptide synthesis and drug development, the direct utilization of conotoxins as therapeutics is limited because of their poor bioavailability, mostly because of amide bond breakdown by digestive enzymes, as well as their high polarity and molecular weight, which restrict their intestinal absorption. Thus, alternative routes of application, such as intrathecal administration, have been developed.⁹ However, head-to-tail cyclization, N-acetylation, and C-amidation are widely employed strategies to improve peptide stability through prevention of degradation by aminopeptidases and carboxypeptidases.¹⁰ Although N-acety-

lation and C-amidation are relatively easy to implement via chemical techniques, the more challenging head-to-tail cyclization is often preferred because it results in an increased permeability through biological barriers.^{11,12}

Whereas cyclization was previously shown to improve the stability of several α -conotoxins with specificity for neuronal nAChRs,^{13–17} backbone cyclization of a paralytic, muscle-type 3/5 α -conotoxin has not been reported before. Here, we describe the synthesis, pharmacological characterization, and structure determination of three cyclic analogues of the muscle-type α -conotoxin α -CIA and demonstrate their

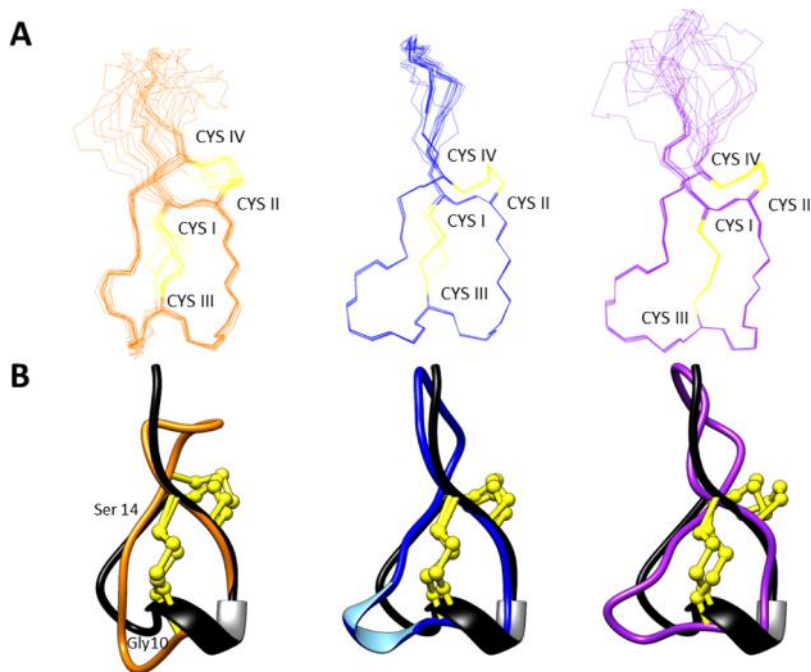


Figure 3. NMR-derived structures of the cyclic CIA analogues. (A) The 15 lowest energy structures are superimposed over the backbone atoms for residues 6–17 (cCIA-2; orange, left), 4–18 (cCIA-3, blue, middle) and 5–19 (cCIA-4, mauve, right), and the disulfide bonds are shown in yellow ball and stick representation. (B) cCIA-2 (left), cCIA-3 (middle), and cCIA-4 (right) superimposed over α -CIA backbone atoms (black) for residues 3–17 (cCIA-2), 4–18 (cCIA-3), and 5–19 (cCIA-4).

increased stability and altered subtype selectivity. In addition, we show how their unique selectivity profile can be used to study the weakening of the muscle during repetitive nerve stimulation (fading of muscle twitches during the “train-of-four” (TOF) repetitive stimulation pattern).

RESULTS

The previously described α -conotoxin CIA¹⁸ from the predation-evoked venom of *Conus catus* is a highly potent blocker of muscle-type nicotinic receptors. It has a typical 3/5 α -conotoxin disulfide framework (Cys1–Cys3; Cys2–Cys4) and displays high sequence homology with other known muscle-type conotoxins. However, contrary to other 3/5 α -conotoxins, it also shows activity at the $\alpha 3\beta 2$ neuronal subtype. Interestingly, the nuclear magnetic resonance (NMR) structure of α -CIA revealed a relatively short intertermini distance of about 10 Å that favors head-to-tail cyclization (Figure 1A). Therefore, we investigated the effect of backbone cyclization of this peptide with amino acid linkers of different lengths (Figure 1B). The objective of this modification was to produce the first proteolysis-resistant and highly potent blocker of both neuronal and muscle-type nicotinic receptors, representing a unique pharmacological tool.

Chemical Synthesis of Cyclic α -Conotoxin CIA Analogues. After anchoring of the C-terminal residue on a chloro-(2'-chloro) trityl resin, elongation of the peptide chain was performed manually using fluorenylmethoxycarbonyl (Fmoc)-based solid-phase peptide synthesis (SPPS).^{19,20} Mild cleavage conditions were used to allow the separation of the peptide from the resin without affecting the side-chain-protecting groups. The crude protected peptide was cyclized under coupling conditions.²¹ Side-chain deprotection and subsequent purification produced the cyclic peptide. Next, a regioselective folding strategy using acetamidomethyl (Acm)-

protecting groups (Cys I–Cys III) was employed to produce the disulfide bond connectivity of the native peptide.¹⁸ After final purification, the homogeneity of folded cCIA peptides was assessed by analytical reversed-phase high performance liquid chromatography (RP-HPLC)–ultra-violet (UV) coupled to electrospray ionization mass spectrometry (ESI-MS) (Figures 1C and S1).

Electrophysiology and Binding Assays. The inhibitory potencies of the cCIA peptides were investigated using the two-electrode voltage-clamp method on rat $\alpha 3\beta 2$ neuronal nAChRs subtypes and fetal rat muscle-type nAChR ($(\alpha 1)_2\beta\gamma\delta$) expressed in *Xenopus laevis* oocytes. All three cyclic analogues retained the low nanomolar (IC_{50} 4–9 nM) potency of the native toxin (IC_{50} 6.6 nM) at the fetal muscle-type nAChR (Figure 2A). Surprisingly, cyclization significantly improved the potency of CIA (IC_{50} 68.2 nM)^a at the $\alpha 3\beta 2$ subtype with up to 52-fold increase in potency for the most active analogue cCIA-3 (IC_{50} 1.3 nM, Figure 2B). Thus, α -cCIA-3 is the first highly potent blocker that displays low nanomolar IC_{50} values for both the neuronal $\alpha 3\beta 2$ subtype and the muscle-type nAChRs.

As the potency increase at the $\alpha 3\beta 2$ receptor was accompanied by a slower recovery of the receptor from the block, we next measured the dissociation of the toxin from both muscle-type and $\alpha 3\beta 2$ nAChR subtypes. Despite the similar potency of CIA and cCIA analogues on the muscle-type nAChR, the cyclic analogues displayed significantly slower off-rates with cCIA-3 having the smallest dissociation constant (K_{off}) and a wash-out time of ≈ 30 min to reach 80% recovery of ACh-induced current responses (Figures 2C and S2) at the muscle-type nAChRs. In contrast, complete dissociation from neuronal $\alpha 3\beta 2$ subtypes occurred within seconds and could not be determined with the established protocol. Therefore, the real-time receptor reactivation during a 10 s agonist application (Figures S3 and S4) was analyzed and compared to

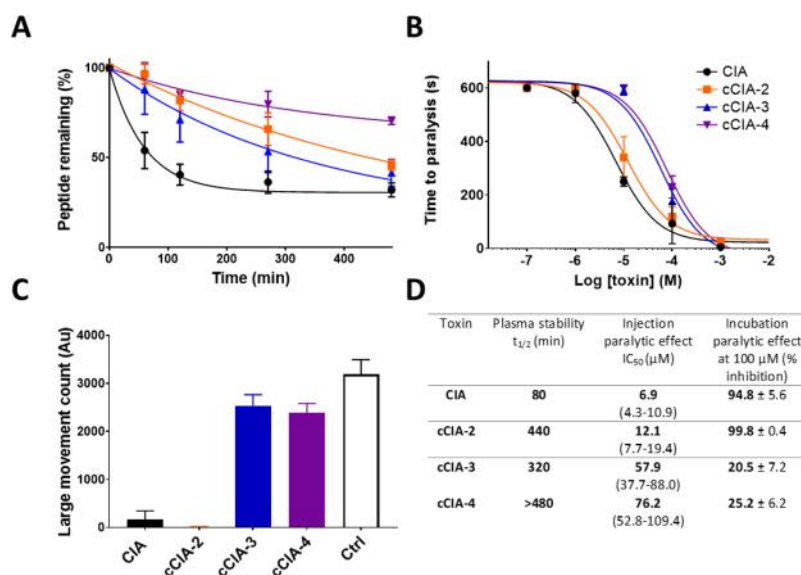


Figure 4. Serum stability of CIA and cCIA analogues and the paralytic effect of the cCIA analogues on zebrafish (*D. rerio*). (A) Stability of CIA and cCIA analogues in human serum. Positive control: linear peptide, negative control: incubation in water. Points represent the mean of one measurement performed in triplicate. Error bars represent the SD. (B) Dose–response analysis of paralysis induced by intramuscular injection of conotoxins CIA and cCIA analogues in adult zebrafish. Experiment was performed in triplicate with a negative control (water injection). Points represent the mean of the triplicate. Error bars represent the SD. (C) Large movement count over 1 h of *D. rerio* larvae movement tracking after addition of the toxins into the water at a concentration of 100 μ M. Each point represents the mean of measurements from six different larvae. Error bars represent the SD. (D) Summary of results, 95% confidence intervals are in brackets. Symbol \pm indicates the SD.

provide an estimate of the dissociation of the cCIA analogues from this receptor. Again, this revealed that cCIA-3 has the slowest dissociation rate. As many $\alpha 3\beta 2$ -selective α -conotoxins show a rather high affinity at the $\alpha 3\beta 2$ -binding site and alternative α -conotoxin-binding sites have been suggested, we wondered whether cCIA-3 may bind to an allosteric binding site at the $\alpha 3\beta 2$ receptor. However, functional competition binding experiments with α -conotoxin MII, a potent competitive antagonist at the $\alpha 3\beta 2$ subtype, showed that preincubation with 100 nM cCIA-3 inhibited binding of MII, a result consistent with a competitive binding of cCIA-3 to the orthosteric $\alpha 3\beta 2$ -binding site (Figure S5). The potency of α -cCIA-3 was further evaluated on several nAChR subtypes. Responses in the presence of 10 μ M of cCIA-3 were 80% or higher for rat $\alpha 2\beta 2$, $\alpha 2\beta 4$, $\alpha 3\beta 4$, $\alpha 4\beta 2$, $\alpha 4\beta 4$, and human $\alpha 9\alpha 10$ neuronal nAChRs, demonstrating no significant inhibitory activity (Table S1). Only weak activity was detected at the human $\alpha 7$ subtype at 10 μ M (65% of response). Remarkably, however, cCIA-3 readily blocked the $\alpha 6/\alpha 3\beta 2\beta 3$ subtype and the adult muscle nAChR with IC_{50} s of 8.64 nM and 184 pM, respectively (Figure S6A,B). The recovery of block from cCIA appears more than twice as slow for the human adult nAChR (K_{off} : 0.013 vs 0.03 min^{-1}) compared to the fetal nAChR (Figure S7).

NMR Spectroscopy. High-resolution NMR spectroscopy allowed the determination of three-dimensional structures of the CIA cyclic analogues (Figure 3A). Two-dimensional TOCSY, NOESY, COSY, and HSQC spectra were collected for all three CIA cyclic analogues and the assignments were made using standard approaches²² (Table S2). Structures were determined based on the NOE data, and angle restraints were predicted from TALOS.²³ Additional peaks are present in the cCIA-2 and cCIA-4 spectra, most likely representing alternative conformations, whereas cCIA-3 has primarily one set of peaks corresponding to a single conformation. Therefore,

the linker length appears to impact the structural stability. The dominant conformations were assigned for the peptides and a superposition of the structures with native α -CIA is shown in Figure 3B, highlighting the similarity between the cyclic analogues and the native peptide. The most striking structural deviation is within residues 10–14 of CIA, where the root mean square deviation (rmsd) values of the backbone atoms with their corresponding atoms in the cyclic analogues equate to 1.67, 4.28, and 4.10 Å for cCIA-2, cCIA-3, and cCIA-4, respectively.

Serum Stability Assay. The stability of CIA and its cyclic analogues toward enzymatic degradation was determined by incubation with human serum AB. Peptides were incubated for 8 h at 37 °C and the amount of intact peptide remaining was determined by liquid chromatography/MS analysis of aliquots taken at 0, 1, 2, 4, and 8 h postincubation. As shown in Figure 4A, the degradation kinetics of the cyclic analogues were much slower than that of CIA, especially during the first 3 h. cCIA-4 showed the highest resistance to serum degradation, with up to 70% intact peptide remaining after 8 h of incubation. In comparison, cCIA-2 and cCIA-3 have half-life values of 440 and 320 min, respectively. Finally, degradation of native α -CIA was the fastest, with a half-life of 80 min. Thus, CIA cyclization greatly improved (≥ 4 –6-fold) the resistance against enzymatic degradation, consistent with previously published data on conotoxin cyclization.^{13–17}

Zebrafish In vivo Assays. Prior to investigating a potential oral/transcutaneous uptake of CIA and its three cyclic analogues, we first performed in vivo intramuscular injections into adult zebrafish (*Danio rerio*) to evaluate the potency in this species. Intramuscular injection of α -conotoxin CIA and its three cyclic analogues produced a rapid flaccid paralysis of skeletal muscle, as evidenced by a loss of an upright posture of the fish, and ultimately complete immobilization. Paralysis induced by CIA and cCIA analogues exhibited a dose-

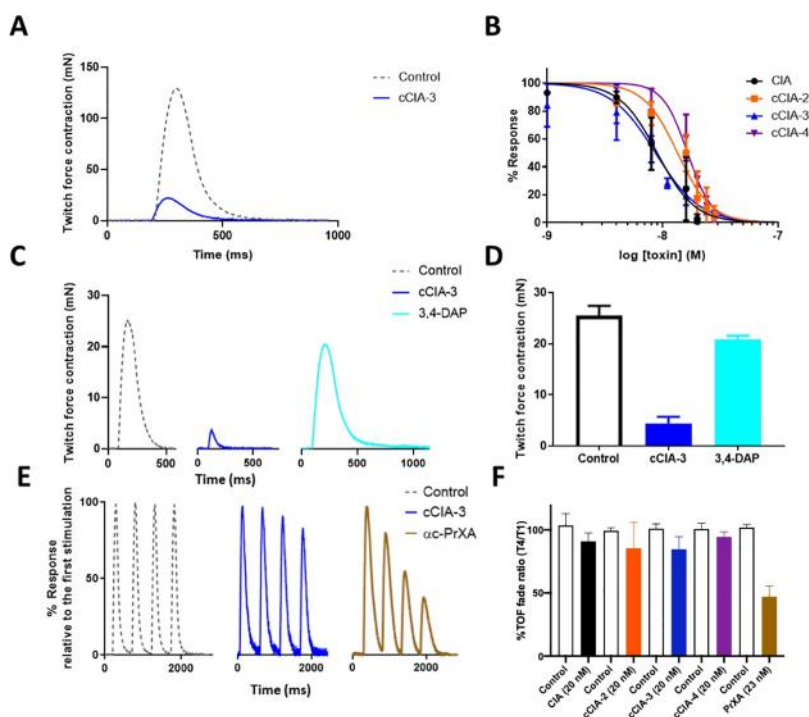


Figure 5. In vitro mouse hemidiaphragm muscle recordings and the TOF fade ratio of CIA and the cyclic analogues. (A) Typical twitch responses upon nerve stimulation (0.1 Hz) under control conditions and during the action of cCIA-3 (16 nM). (B) Concentration–response curves for CIA (IC_{50} = 8.98 nM), cCIA-2 (IC_{50} = 13.48 nM), cCIA-3 (IC_{50} = 8.70 nM), and cCIA-4 (IC_{50} = 16.47 nM). Data points represent the mean \pm SD of twitch responses from 1–9 nerve-muscle preparations, after 20–25 min toxin exposure, relative to the respective controls. (C) Isometric twitch tension recordings evoked by nerve stimulation (0.1 Hz) on the same phrenic-nerve hemidiaphragm preparation under control conditions, following 30 min incubation with 16 nM cCIA-3, and after 27 min of 10 μ M 3,4-DAP action. Note the different time course of twitch recordings between the control and after 3,4-DAP-treatment. (D) Data obtained in the same preparation and expressed as means \pm SD (n = 14). (E) Isometric tension developed during TOF nerve stimulation (2 Hz) under control conditions, and in the presence of cCIA-3 and α C-PrXA. Note the TOF fade in the presence of α C-PrXA. Signal amplitude is relative to the maximum response of each compound (F) TOF fade ratio (T4/T1) in the presence of α -CIA, cCIA analogues, and α C-PrXA. Note that a significant fade is only seen for PrXA. Control experiments are represented in white.

dependent effect, with IC_{50} values for CIA, cCIA-2, cCIA-3, and cCIA-4 of 6.88, 12.1, 57.87, and 76.22 μ M, respectively (Figure 4B). This evaluation of paralysis caused by muscle nAChR blockade led to investigation of the oral/transcutaneous toxin uptake by tracking the movement of zebrafish larvae in 100 μ M toxin for 1 h using the ZebraBox tracking system (Figure 4C). Consistent with the intramuscular injection data, native CIA and cCIA-2 induced a strong paralysis, suggesting efficient uptake of these toxins, whereas cCIA-3 and cCIA-4 were less potent (Figure 4D).

Mouse Muscle Contraction Assays. α -CIA and Analogues Block Nerve-Evoked Muscle Contraction. When applied at nanomolar concentrations to isolated phrenic-nerve hemidiaphragm muscle preparation, CIA and cCIA analogues produced a concentration- and time-dependent reduction of the isometric twitch force evoked by nerve stimulation at 0.1 Hz (Figure 5A,B).

For the most active peptide (cCIA-3), the time required to block 50% of nerve-evoked muscle contraction was 19.0 ± 6.2 min (n = 4), and a 40% recovery was obtained in 32.6 ± 1.8 min (n = 3) (data not shown), in agreement with muscle-type nAChR blockade. The effect of all peptides was reversible upon washing the preparations with an extracellular medium free of α -conotoxins. These results indicate that CIA and analogues are effective neuromuscular blockers, and are 2–3 fold more potent than the previously studied α C-PrXA, a highly specific and potent inhibitor of muscle-type nAChR.²⁴

In order to confirm that cCIA-3 acts as a competitive antagonist at the muscle-type nAChR, we determined if an increase of evoked ACh release from nerve terminals could displace cCIA-3 from its nAChR-binding site. Therefore, we used 3,4-diaminopyridine (3,4-DAP), which greatly increases quantal ACh release by reversibly blocking voltage-gated K^+ channels in motor nerve terminals,^{25–27} which is used to treat certain forms of muscle weakness.

As shown in Figure 5C, cCIA-3 (16 nM) blocked the peak amplitude of nerve-evoked contraction by approximately 85%, and this effect was 80% reversed upon addition of 3,4-DAP (10 μ M) to the medium (Figure 5C,D). Interestingly, when computing twitch tension-time integrals instead of peak amplitudes, the reversal was in the range of 96–98%. This difference in values is explained by the fact that nerve-evoked contractions exhibit a prolonged time course in the presence of 3,4-DAP (shown in a comparison of the control and 3,4-DAP traces in Figure 5C). In conclusion, these data can be explained by a mechanism in which 3,4-DAP increases acetylcholine release from nerve terminals and the increased ACh displaces the cCIA-3 analogue from the muscle endplate nAChR, and thus strongly supports our assumption that the peptide acts in a competitive manner on the muscle-type nAChR, in agreement with the described mode of action of α -conotoxins.

Train-of-Four Fade in the Presence of Conotoxins with Muscle and Dual Muscle/ α 3 β 2 Selectivity. TOF stimulation is commonly used to monitor neuromuscular transmission

when muscle relaxants are applied. A fade in muscle twitches (reduction of the twitch amplitude after repetitive nerve stimulation) is observed with nondepolarizing but not with depolarizing muscle relaxants.^{28–30} Curare-like agents (competitive inhibitors of the muscle-type nAChR) that produce a nondepolarizing neuromuscular block at the neuromuscular junction are known to display a typical TOF fade, both in vitro and in vivo.^{31–33} The TOF fade corresponds to the T4/T1 ratio, where T4 and T1 are the fourth and first twitch tensions in the same TOF stimulations. The inhibition of the presynaptic facilitatory $\alpha 3\beta 2$ nAChR autoreceptor at motor nerve terminals and the resulting inhibition of autofacilitatory ACh release have been suggested as an explanation for the TOF fade seen during a nondepolarizing neuromuscular block.^{28,29} However, this hypothesis was recently challenged by using ligands with different selectivities for pre- and postsynaptic receptors.³⁴ Therefore, because of their original dual muscular/ $\alpha 3\beta 2$ nAChRs antagonist property, it was of interest to determine whether α -CIA and the cCIA analogues were able to produce TOF fade.

Under control conditions (in the absence of peptides), no TOF fade is observed as shown by the typical recordings (Figure 5E). Remarkably, when nerve-evoked contraction was inhibited about 76% by cCIA-3, no significant TOF fade was observed either. In contrast, a marked TOF fade was observed with the highly muscle-selective α C-PrXA peptide (no inhibitory activity at $\alpha 3\beta 2$), already at approximately 45% neuromuscular block (Figure 5E). As shown in Figure 5F, TOF fadings were determined at different conotoxin concentrations. If a 50% decrease of TOF fade was measured with α C-PrXA (23 nM), no significant effect was observed at any concentrations of the α -CIA and cCIA analogues studied. Therefore, these data strongly argue against the common explanation of TOF fade, that is, the blockade of $\alpha 3\beta 2$ autoreceptors at the neuromuscular junction.

DISCUSSION AND CONCLUSIONS

Backbone cyclization has previously been reported to enhance stability and in some cases to improve the permeability of the cyclic analogue through biological membranes.^{13–17} Considering the unusual dual activity of the 3/5 α -conotoxin CIA on muscle and neuronal nAChR $\alpha 3\beta 2$ subtypes, we investigated the effect of backbone cyclization on its pharmacology and stability. During the cyclization process, a linker minimizing perturbations of the three-dimensional structure of a bioactive native toxin is highly desirable. Indeed, Clark et al. showed that an inappropriate linker can distort the structure by introducing strain to the peptide leading to a loss of bioactivity.^{13,14} Therefore, based on the intertermini spacing (9.8 Å), amino acid linkers with a length between 10 and 19 Å were chosen.

Overall conservation of the structure between CIA and its cyclic analogues was confirmed by NMR spectroscopy. Nevertheless, the linker length appeared to have a significant impact locally, particularly for residues 10–14 of CIA (Table S1). cCIA-3 displays the lowest rmsd value and, therefore, has the most well-defined structure, and shows only one predominant conformation in the NMR spectra in contrast to the other two cyclic analogues.

Consistent with the NMR data, structural conservation of the cCIA analogues compared to the native CIA led to the conservation of the bioactivity toward muscle-type nAChRs at low nanomolar concentrations. However, the significant decrease in K_{off} values suggests stronger interaction of the

cyclic analogues within one, or both, of the two orthosteric muscle nAChR-binding sites. Considering the high sequence homology of α -CIA with α -MI and α -GI, α -CIA is most likely binding at the α - δ interface.^{35,36} It has been demonstrated that the ACh-binding pocket is mostly composed of hydrophobic residues that interact with residues of the two conotoxin loops formed by the disulfide bridges. Although, the linker is outside of these cysteine loops, the lower K_{off} values of cCIA-3 and cCIA-4 might be because of stronger hydrophobic interactions arising from the additional alanine residues in the linker compared to cCIA-2. Interestingly, and in contrast to our observations at the muscle nAChRs, dissociation rates from the neuronal $\alpha 3\beta 2$ subtype were so fast that dissociation constants could not be determined with established protocols despite a strong potency increase at these subtypes. This raised the question of how exactly the native α -CIA and the cyclic analogues bind to the $\alpha 3\beta 2$ subtype. Indeed, allosteric modulators usually display very fast dissociation rates, however, functional competition binding experiments suggested a competitive binding of cCIA-3 to the orthosteric $\alpha 3\beta 2$ -binding site and we can reasonably extend this hypothesis to cCIA-2, -4 and native α -CIA toxin. Surprisingly, all of the cyclic analogues also displayed a significantly increased potency at the $\alpha 3\beta 2$ subtypes, with cCIA-3 being the most potent with a 52-fold decreased IC_{50} value compared to native α -CIA. The high rmsd value (4.28 Å) in the region of residues 13–17 of cCIA-3 (compared to the equivalent residues in CIA) might allow favorable structural changes further enhanced by the well-defined structures of cCIA-3 (0.29 Å over backbone atoms) compared to native α -CIA (0.95 Å over backbone atoms) possibly facilitating toxin binding to the receptor and explaining the higher potency of cCIA-3 at the $\alpha 3\beta 2$ nAChR subtype.

Cyclization of α -CIA leads to an improved stability toward enzymatic degradation, in agreement with the previously published data on α -conotoxin cyclization.^{13–17} cCIA-4 was the most resistant to degradation in serum, exhibiting a serum half-life of more than 8 h (70% remaining peptide), followed by cCIA-2, cCIA-3, and native CIA, which is degraded at least four times faster. Nevertheless, CIA and the cCIA analogues appear to be more readily degraded in serum than cVc1.1 and cMII, as shown in the study by Clark et al.^{13,14} Unlike Vc1.1 and MII conotoxins, CIA contains one arginine residue before the first cysteine residue, and one lysine residue in the second loop that can be cleaved by endopeptidases.

A visible paralyzing effect, resulting from the block of muscle-type nAChR, was observed when CIA or the cCIA analogues were injected intramuscularly into zebrafish. Paralysis activity of the conotoxins could also be monitored by movement tracking of zebrafish (*D. rerio*) larvae, after incubation with the toxins in the tank water. Based on the inhibition values obtained by intramuscular injection, we performed the assay at a concentration of 100 μM (higher doses would require large amounts of peptides). CIA and cCIAs showed a paralyzing effect when added into the swimming water of *D. rerio* larvae in comparison to the control, with CIA and cCIA-2 being the most potent. cCIA-3 and cCIA-4 exhibited a weaker activity, which is consistent with the intramuscular injection data. Zebrafish (*D. rerio*) might not have the required metabolic means to completely digest the native CIA and make it completely inactive.

Considering the unique capacity of α -CIA and cCIAs to block both muscle-type and neuronal $\alpha 3\beta 2$ subtype nAChRs,

they represent a novel pharmacological tool to study the contribution of the $\alpha 3\beta 2$ subtype neuromuscular transmission in the presence of neuromuscular blockers. Consistent with the electrophysiology data, CIA and its cyclic analogues block the phrenic nerve-evoked isometric twitch force in mouse hemidiaphragm muscles in the nanomolar range. The cCIA-3-induced block was reversed when increasing the quantal ACh release by 3,4-DAP, thus confirming the competitive binding evidenced by electrophysiological binding experiments.

A role of the presynaptic $\alpha 3\beta 2$ nicotinic receptor in the TOF fade phenomenon has been proposed previously.³⁴ One of the persevering theories is that presynaptic $\alpha 3\beta 2$ nicotinic receptors would increase the release of acetylcholine via a positive feedback mechanism to maintain the contraction at the same level following repeated nerve stimulation at the neuromuscular junction. Thus, the presynaptic $\alpha 3\beta 2$ inhibition could explain the attenuated release of acetylcholine leading to nerve-evoked muscle contraction fade.³⁷ This hypothesis was recently challenged by using ligands with different selectivities for pre- and postsynaptic receptors:³⁴ it was found that, in vivo experiments, the TOF fade was clearly correlated with the administration of postsynaptic muscle-type antagonist such as α -bungarotoxin or α -conotoxin GI, while the $\alpha 3\beta 2$ blocker DH β E was shown to potentiate the TOF fade. Nevertheless, DH β E is a nonselective neuronal receptor blocker, thus justifying the re-examination of the precise role of the presynaptic $\alpha 3\beta 2$ subtype here. Considering their high potency and distinct selectivities to both muscle-type and neuronal $\alpha 3\beta 2$ nAChRs, CIA and its cyclic analogues represent unique pharmacological tools to address this question. Surprisingly, neither CIA nor its cyclic analogues induced a visible TOF fade, in contrast to the muscle-specific α C-PrXA conotoxin. Hence, in contradiction to the generally accepted hypothesis that TOF fade results from a dual block of presynaptic $\alpha 3\beta 2$ and postsynaptic muscle nAChRs, our data show that dual blockade of $\alpha 3\beta 2$ and muscle-type nAChRs is able to prevent this phenomenon. Thus, the role of the $\alpha 3\beta 2$ nAChR in neuromuscular transmission needs to be studied in more detail, and the cyclic CIA analogues could provide the necessary pharmacological tools.

■ EXPERIMENTAL SECTION

Chemical Synthesis. *N,N'*-Dimethylformamide (DMF), *N,N*-diisopropylethylamine (DIPEA), acetonitrile (ACN), triisopropylsilane (TIS), trifluoroacetic acid (TFA), piperidine, and all others reagents were obtained from Sigma-Aldrich (Saint-Louis, MI, USA) or Merck (Darmstadt, Germany) and were used as supplied. Fmoc (L) amino acid derivatives and HATU were purchased from Iris Biotech (Marktredwitz, Germany). PS-2-Chlorotriyl chloride resin (100–200 mesh, 1.6 mmol/g) was purchased from Iris Biotech (Marktredwitz, Germany). The following side-chain-protecting groups were used: Asn(Trt), Cys(Trt), His(Trt), Arg(Pbf), Cys(Acm), Lys(Boc), and Ser(*t*Bu). Peptides were manually synthesized using the Fmoc-based solid-phase peptide synthesis technique on a VWR (Radnor, PA, USA) microplate shaker. All Fmoc amino acids and HATU were dissolved in DMF to reach 0.5 M. The first amino acid was coupled onto the resin for 6 h in a 1/1 (v/v) mix of DMF and dichloromethane (DCM), with a 2.5-fold excess of amino acid and 5-fold excess of DIPEA followed by the addition of methanol and further mixing for 15 min to cap any remaining reactive functionalities on the resin. The resin was washed with DMF, DCM, MeOH, and DMF. Fmoc deprotection was carried out with piperidine in DMF (1/2 v/v) twice for 3 min. Subsequent amino acids were coupled onto 0.1 mmol of prepared resin (a determined loading value of 0.73 mmol/g) twice for 10 min using an amino acid/HATU/DIPEA ratio

of 5:5:10 relative to resin loading. DMF was used for resin washing between deprotection and coupling steps. After chain assembly was complete, the terminal Fmoc group was removed and the resin was washed with DMF and DCM. Cleavage of the peptide from the resin without affecting the side-chain-protecting group was carried out in a reaction vessel and treated 10 times with 10 mL of 1% TFA in DCM (v/v) for 5 min. Eluates were collected and combined into a round-bottomed flask then DCM and TFA were removed under vacuum and cold diethyl ether was added to precipitate the peptide. The crude side-chain-protected peptide was dissolved in DMF at a concentration of 2 mM in a round-bottom flask. HATU was added to the solution to give a final concentration of 5 mM and mixed for 30 s. DIPEA was added to a final concentration of 10 mM, and the solution was stirred for 4 h at room temperature. DMF was removed under vacuum and residues were uptaken in ACN/H₂O (1/1 v/v) and freeze dried overnight. Side-chain (except acm) deprotection was carried out by adding 6.25 mL of TFA/TIS/H₂O (95/2.5/2.5 v/v/v) per 100 mg of the crude peptide and stirring the mixture for 2.5 h at room temperature. Crude peptides were purified by preparative RP-HPLC and pure fractions were combined and freeze dried. A two-step oxidation procedure was then carried out. The first disulfide bridge is formed between the free cysteine residues CysII–CysIV by dissolving the peptide at 0.2 mM in 50 mM Tris-HCl buffer adjusted to pH 8 and adding 7 equiv of 2,2'-dithiopyridine (DTP) at 10 mM in MeOH dropwise. When the reaction was complete, the reaction mixture was acidified to pH 3 and loaded onto preparative RP-HPLC and pure fractions were combined. The second disulfide bridge CysI–CysIII was formed by deprotection/oxidation of the Acm-protecting group directly on the combined pure fractions of the monobridged intermediates by treatment with 20 equiv of 10 mM iodine in H₂O/TFA/ACN (78/2/20 v/v/v). When the reaction was complete, the reaction mixture was quenched with 20 mM ascorbic acid until total discoloration of the solution, acidified, and purified by preparative RP-HPLC. The combined pure fractions were freeze dried and their purity were confirmed by LC/ESI-MS. cCIA-2,-3,-4 peptides have been obtained with 6.3, 7.5, and 5.4% yields, respectively (purity > 95%). The peptide content was estimated at 60% from dry weight.

Mass Spectrometry. Solvents used for liquid chromatography/mass spectrometry (LC/MS) were of HPLC grade. The LC/MS system consisted of a Waters (Milford, OH, USA) Alliance 2695 HPLC, coupled to a Waters Micromass ZQ spectrometer (electrospray ionization mode, ESI⁺). All the analyses were carried out using a Chromolith (Fontenay sous Bois, France) HighResolution RP-18e (4.6 × 25 mm, 15 nm to 1.15 μ m particle size, and a flow rate of 3.0 mL/min) column. A flow rate of 3 mL/min and a gradient of 0–100% B over 2.5 min for routine analyses and 0–30% B over 30 min for quality control of pure products were used. Solvent A: water/0.1% HCO₂H; solvent B: ACN/0.1% HCO₂H. UV detection was performed at 214 nm. Electrospray mass spectra were acquired at a solvent flow rate of 200 μ L/min. Nitrogen was used for both the nebulizing and drying gases. The data were obtained in a scan mode ranging from 100 to 1000 *m/z* or 250 to 1500 *m/z* to in 0.7 s intervals.

Folded peptides were characterized using a Synapt G2-S high resolution MS system (Waters Corp., Milford, MA) equipped with an ESI source. Chromatographic separation was carried out at a flow rate of 0.4 mL/min on an Acquity H-Class ultrahigh performance liquid chromatography (UPLC) system (Waters Corp., Milford, MA), equipped with a Kinetex C18 100 Å column (100 × 2.1 mm, 2.6 μ m particle size) from Phenomenex (France). The mobile phase consisted of water (solvent A) and ACN (solvent B) with both phases acidified by 0.1% (v/v) formic acid. Mass spectra were acquired in the positive ionization mode.

Preparative RP-HPLC. Preparative RP-HPLC was run on a Gilson PLC 2250 Purification system (Villiers le Bel, France) instrument using a preparative column (Waters DeltaPak C18 Radial-Pak Cartridge, 100 Å, 40 × 100 mm, 15 μ m particle size, and a flow rate of 50.0 mL/min). Solvent A was 0.1% TFA in water, and solvent B was 0.1% TFA in ACN. A gradient of 0–50% B over 50 min was used.

Electrophysiological Recordings. cDNAs encoding rats $\alpha 2$, $\alpha 3$, $\alpha 4$, $\alpha 6$, $\beta 2$, and $\beta 4$ nAChRs were provided by Jim Patrick (Baylor College of Medicine, Houston, TX, USA) and subcloned into the oocyte expression vector pNKS2. The rat $\alpha 6/\alpha 3$ Chimera^{38,39} was generated by Gibson assembly in the pNKS2 vector. Fetal rat muscle-type ($\alpha 1$, $\beta 1$, γ , and δ) subunit cDNAs in pSPOoD were provided by Veit Witzemann (MPI for Medical Research, Heidelberg, Germany). Plasmids for expression of $\alpha 7$, $\alpha 9$, $\alpha 10$, and adult muscle-type ($\alpha 1$, $\beta 1$, ϵ , and δ) nAChRs were a gift from David Adams (Illawarra Health and Medical Research Institute, Wollongong University, Australia). Synthesized human muscle subunit cDNAs (Integrated DNA Technologies (IDT) (Coralville, IA, USA) and human $\alpha 9$ and $\alpha 10$ pCMV6-XL5 constructs (OriGene (Rockville, MD, USA) were cloned in pT7TS. Human $\alpha 7$ in pMXT was provided by Prof. Jon Lindstrom (Uni. Pennsylvania, PA, USA). cRNA was synthesized from linearized plasmids with SP6 or T7 RNA polymerase using the mMessageMachine kit (Invitrogen, Thermo Fisher Scientific, USA). *X. laevis* oocytes were kindly provided by Prof. Luis Pardo (MPI of Experimental Medicine, Göttingen), injected with 50 nL aliquots of cRNA (0.5 $\mu\text{g}/\mu\text{L}$), and kept at 16 °C in filtered ND96 (96 mM NaCl, 2 mM KCl, 1 mM CaCl₂, 1 mM MgCl₂, 5 mM HEPES, and pH 7.4) containing gentamicin (5 $\mu\text{g}/\text{mL}$).

Two-electrode voltage clamp recordings were performed 1–5 days after cRNA injection at a holding potential of -70 mV. Pipettes were pulled from borosilicate glass and filled with 3 M KCl. Resistances were below 1 M Ω . Membrane currents were recorded using a Turbo Tec 05X Amplifier (npi electronic, Tamm, Germany) filtered at 200 Hz and digitized at 400 Hz. CellWorks software was used for recording. The perfusion medium was automatically switched between ND96 with or without agonist (100 μM ACh) using a custom-made magnetic valve system. A fast and reproducible solution exchange (<300 ms) for agonist application was achieved using a 50 μL funnel-shaped oocyte chamber combined with a fast solution flow (150 $\mu\text{L}/\text{s}$) fed through a custom-made manifold mounted immediately above the oocyte. ACh pulses were applied for 2 s at 4 min intervals. After each application, the cell was superfused for 54 s with agonist-free solution, and the flow was then stopped for 3 min. Immediately at the beginning of this interval, peptide (prepared in filtered ND96 containing 0.1% BSA m/v) was mixed from a 10-fold stock into the static bath when responses of three consecutive agonist applications differed by less than 10%. The use of BSA showed no change in toxin potency but produced more stable measurements at low toxin concentrations. ACh-evoked current peaks following peptide incubation were normalized to the ACh current peak before peptide exposure.

The analysis of the electrophysiological data was performed using GraphPad Prism version 8.0. Dose–response curves were fit to the data using the Hill equation: % response = bottom + (top–bottom)/(1 + 10^{-(logIC₅₀ - X) × HillSlope}) and constraints of 100 and 0% for top and bottom, respectively. Dissociation curves were fit to the data with the equation % response = (response (time 0) – plateau) × exp(-K × time) + plateau.

The functional analysis of competitive binding was performed as previously described.⁴⁰ Briefly, 2 s ACh pulses were applied in 1 min intervals until stable responses were obtained. The perfusion was then stopped for 7 min for application of cCIA-3 (after 1 min) and/or MII (after 4 min) in the static bath. As a control, ND96 was applied instead of a peptide. All peak currents were normalized to the mean of the four stable ACh-evoked peak currents before the peptide incubation.

All experiments were performed with oocytes from at least two different frogs.

NMR Spectroscopy. Lyophilized synthetic peptides (~1.5–2 mg) were resuspended in 90% H₂O:10% D₂O. 2D ¹H–¹H TOCSY, ¹H–¹H NOESY, ¹H–¹H DQF-COSY, ¹H–¹⁵N HSQC, and ¹H–¹³C HSQC spectra were acquired at 290 K using a 600 MHz AVANCE III NMR spectrometer (Bruker, Karlsruhe, Germany) equipped with a cryogenically cooled probe. All spectra were recorded with an interscan delay of 1 s. NOESY spectra were acquired with mixing times of 200–250 ms, and the TOCSY spectra were acquired with

isotropic mixing periods of 80 ms. Two-dimensional spectra were collected over 4096 data points in the f₂ dimension and 512 increments in the f₁ dimension over a spectral width of 12 ppm. Standard Bruker pulse sequences were used with an excitation sculpting scheme for solvent suppression. The two-dimensional NOESY spectra of the cCIA analogues were automatically assigned and an ensemble of structures was calculated using the program CYANA.⁴¹ Torsion-angle restraints from TALOS+ were used in the structure calculations. The final structures were visualized using Pymol (The PyMOL Molecular Graphics System, Version 2.0 Schrödinger, LLC.), MOLMOL,⁴² and UCSF Chimera.⁴³

Monitoring of the Paralysis Effect after Injection into Adult Zebrafish (*D. rerio*). Sixty three adult male and female (2–5 months) zebrafish wild-type AB were maintained under standardized conditions and experiments were conducted in accordance with the European Communities council directive 2010/63, procedures were approved by Ethical Committee for Animal Experiment of Languedoc Roussillon no 36 (reference number: 2018040911129080 #14665 v4). The AB wild-type zebrafish line has been obtained from ZIRC (Zebrafish International Resource Center, Oregon, USA; ID ZL1) and bred in-house. Toxins were diluted in Milli-Q water and 5 μL of incremental doses were injected intramuscularly into adult zebrafish with a 10 μL Neuros Syringe from Hamilton (Bonaduz, Switzerland). Each dose was repeated three times on three different fishes to determine error bars. The onset of paralysis was measured over a maximum observation time of 10 min. Paralysis was considered total when the fish went on its back. Negative control experiments were performed according to the same protocol by injecting water instead of toxins.

Monitoring of the Paralysis Effect after Incubation into Zebrafish (*D. rerio*) Larvae Swimming Water. Experiments were conducted on 5-day-old larvae of zebrafish wild-type AB. Six larvae per toxin were placed in a 96-well plate and a controlled volume of swimming water was added. Small volumes of toxin were added to reach the final desired concentration of 100 μM . Immediately after incubation, the plate was placed in the movement-tracking chamber. The movement of larvae was video captured and quantified using the ZebraBox infrared camera setup and tracking extension of the ZebraLab software system (Viewpoint Life Sciences, Canada). The integration period for movement data was set to 30 min. Each time the animal speed goes above the small/large movement threshold, the large movement counter is incremented. Negative control experiments were performed according to the same protocol by adding water instead of toxins.

In vitro Assays on Isolated Mouse Nerve-Muscle Preparations. *Animals.* Twenty eight adult (14 male and 14 female) Swiss mice (*Mus musculus*, 2–5 months of age and 23–28 g of body weight) were purchased from Janvier-Elevage (Le Genest-Saint-Isle, France). Mice were acclimatized at the CEA animal facility for at least 48 h before experiments. Live animals were treated according to the European Community guidelines for laboratory animal handling and the guidelines established by the French Council on animal care “Guide for the Care and Use of Laboratory Animals” (EEC86/609 Council Directive—Decree 2001-131). Mice were housed four- to six-wise in cages with environmental enrichment, in a room with constant temperature and a standard light cycle of 12 h light/12 h darkness and had free access to water and food. All experimental procedures on mice were approved by the Animal Ethics Committee of the CEA and by the French General Directorate for Research and Innovation (project APAFIS#2671-2015110915123958v4 authorized to E. Benoit). Male and female mice were anesthetized by isoflurane (Aerrane, Baxter S.A., Lessines, Belgium) inhalation before being euthanized by dislocation of the cervical vertebrae.

Recordings on Isolated Nerve-Muscle Preparations. In vitro assays were performed on left phrenic-nerve hemidiaphragm muscle preparations quickly removed and mounted in a silicone-lined organ bath (4 mL capacity). Preparations were bathed in a Krebs–Ringer solution of the following composition: 150 mM NaCl, 5 mM KCl, 2 mM CaCl₂, 1 mM MgCl₂, 11 mM glucose, and 5 mM HEPES (pH 7.4), continuously superfused with pure O₂ throughout the experi-

ment at a constant temperature of 22 °C, unless otherwise indicated. For nerve-evoked isometric twitch tension measurements, the phrenic nerve was usually stimulated with a suction microelectrode (adapted to the diameter of the nerve) with supramaximal current pulses of 0.25 ms duration, at a frequency of 0.1 Hz delivered by the isolation unit of a stimulator (S-44 Grass Instruments, West Warwick, RI, USA). The hemidiaphragm tendons (at the rib side) were tightly anchored onto the silicone-coated bath with stainless pins, and the other tendon (central medial tendon) was attached via an adjustable stainless-steel hook to a FT03 isometric force transducer (Grass Instruments). The resting tension was monitored for each preparation tested and adjusted with a mobile micrometer stage allowing variations of muscle length in order to obtain maximal contraction amplitude in response to motor nerve stimulation. Once maximal contraction was obtained, the resting tension was fixed, and monitored during the whole duration of the experiment. Signals from the isometric transducer were amplified, collected, and digitized with the aid of a computer equipped with an Axon Digidata-1550B A/D (interface board low-noise acquisition system plus hum silencer), using the PClamp/Axoscope 10.7 version software (Axon Instruments, Molecular Devices Inc., Sunnyvale, CA, USA).

In some experiments, a TOF stimuli was delivered to the phrenic nerve trunk at a frequency of 2 Hz for 2 s, at a train rate of 0.033 Hz. The ratio of muscle tension developed in the mouse hemidiaphragm by the fourth to the first stimulus was evaluated [$T(4)/T(1)$] at different peptide concentrations.

Statistical Analysis. Data are presented as means \pm standard deviations (SD) of n different experiments. Differences between values were tested using the parametric two-tailed Student's t -test (either paired samples for comparison within a single population or unpaired samples for comparison between two independent populations) or the Kolmogorov–Smirnov two-sample test. Differences were considered significant when $P < 0.05$.

Serum Stability Assay. Human AB serum (VWR, Fontenay-sous-Bois, France) was centrifuged at 12,000g for 10 min for the removal of the lipid component. Supernatant was taken out and incubated for 15 min at 37 °C before the assay. All peptides were tested at a final concentration of 30 μ M after dilution in serum (water for negative control). The incubation time points were 1, 2, 4, and 8 h at 37 °C. Controls and test peptides were incubated in parallel at each time point. Serum proteins were denatured by quenching with 40 μ L of 6 M urea (10 min, 4 °C), followed by the precipitation of proteins with an addition of 40 μ L of 20% trichloroacetic acid (10 min, 4 °C). These solutions were then centrifuged at 12,000g for 10 min. A volume of 100 μ L of the supernatant was taken out at each time point. Chromatographic separation was carried out at a flow rate of 0.4 mL/min on an Acquity H-Class UPLC system (Waters, Corp., Milford, MA, United States), equipped with a Kinetex C18 100A column (100 mm \times 2.1 mm, 2.6 mm particle size) from Phenomenex (France). The mobile phase consisted of water (solvent A) and ACN (solvent B) with both phases acidified by 0.1% (v/v) formic acid and the gradient was 0–80% B in 10 min. Mass spectra were acquired in the positive ionization mode. The elution time for each peptide was determined by the zero-time point. The stability at each time point was calculated as the area of the serum-treated peptide peaks on RP-HPLC at 214 nm as percentage of the area of the 0 h serum-treated peptides. Controls were an eight-residue linear peptide incubated in serum for the positive control and incubated in water for the negative control. Each experiment was performed in triplicate.

■ ASSOCIATED CONTENT

SI Supporting Information

The Supporting Information is available free of charge at <https://pubs.acs.org/doi/10.1021/acs.jmedchem.0c00957>.

Additional figures illustrating binding assays and chemical synthesis as well as a structural statistics NMR table (PDF)

■ AUTHOR INFORMATION

Corresponding Author

Sébastien Dutertre – Institut des Biomolécules Max Mousseron, Université de Montpellier, CNRS, ENSCM, 34095 Montpellier, France; orcid.org/0000-0002-2945-1484; Email: sebastien.dutertre@umontpellier.fr

Authors

Julien Giribaldi – Institut des Biomolécules Max Mousseron, Université de Montpellier, CNRS, ENSCM, 34095 Montpellier, France

Yves Haufe – Walther Straub Institute of Pharmacology and Toxicology, Faculty of Medicine, LMU Munich, 80336 Munich, Germany

Edward R. J. Evans – Centre for Molecular Therapeutics, Australian Institute of Tropical Health and Medicine, James Cook University, Cairns, Queensland 4878, Australia

Muriel Amar – Département Médicaments et Technologies pour la Santé (DMTS), Université Paris-Saclay, CEA, SIMoS, ERL CNRS 9004, F-91191 Gif sur Yvette, France

Anna Durner – Walther Straub Institute of Pharmacology and Toxicology, Faculty of Medicine, LMU Munich, 80336 Munich, Germany

Casey Schmidt – Centre for Molecular Therapeutics, Australian Institute of Tropical Health and Medicine, James Cook University, Cairns, Queensland 4878, Australia

Adèle Faucherre – Département de Physiologie, Institut de Génomique Fonctionnelle, CNRS/INSERM UMR 5203, Université de Montpellier, 34095 Montpellier, France

Hamid Moha Ou Maati – Département de Physiologie, Institut de Génomique Fonctionnelle, CNRS/INSERM UMR 5203, Université de Montpellier, 34095 Montpellier, France

Christine Enjalbal – Institut des Biomolécules Max Mousseron, Université de Montpellier, CNRS, ENSCM, 34095 Montpellier, France; orcid.org/0000-0003-4646-4583

Jordi Molgó – Département Médicaments et Technologies pour la Santé (DMTS), Université Paris-Saclay, CEA, SIMoS, ERL CNRS 9004, F-91191 Gif sur Yvette, France; orcid.org/0000-0002-0693-8994

Denis Servent – Département Médicaments et Technologies pour la Santé (DMTS), Université Paris-Saclay, CEA, SIMoS, ERL CNRS 9004, F-91191 Gif sur Yvette, France

David T. Wilson – Centre for Molecular Therapeutics, Australian Institute of Tropical Health and Medicine, James Cook University, Cairns, Queensland 4878, Australia

Norelle L. Daly – Centre for Molecular Therapeutics, Australian Institute of Tropical Health and Medicine, James Cook University, Cairns, Queensland 4878, Australia; orcid.org/0000-0002-4697-6602

Annette Nicke – Walther Straub Institute of Pharmacology and Toxicology, Faculty of Medicine, LMU Munich, 80336 Munich, Germany

Complete contact information is available at:

<https://pubs.acs.org/10.1021/acs.jmedchem.0c00957>

Author Contributions

J.G. and Y.H. contributed equally to this work. J.G. and S.D. conceived and led the study. J.G. performed peptide chemistry cyclization, stability assays, and zebrafish experiments, with input from S.D., C.E., A.F., H.M.O.M. Y.H., and A.D. carried out the electrophysiological recordings, with input from A.N. E.R.J.E., and C.S. performed the NMR experiments and analyses, with input from D.T.W. and N.L.D. M.A., and J.M.

performed in vitro assays and recordings on isolated mouse nerve-muscle preparations, with input from D.S. J.G. wrote the manuscript with input from all authors.

Notes

The authors declare no competing financial interest.

ACKNOWLEDGMENTS

This work was supported by the French Ministry of Higher Education, Research, and Innovation (PhD scholarship to J.G.), the French National Research Agency (ANR-16-CE34-0002 to S.D.), and a grant of the DFG (Research Training Group GRK2338, P01) to A.N. We thank Pranavkumar Shadamarshan for help with the oocyte recordings and Han Shen Tae and David Adams (Illawara Health and Medical Research Institute, Wollongong University, Australia) for subcloning and providing nAChR cDNAs.

ABBREVIATIONS

Acm, acetamidomethyl; ACN, acetonitrile; Boc, *tert*-butoxycarbonyl; DCM, dichloromethane; DIPEA, diisopropylethylamine; DMF, *N,N'*-dimethylformamide; DTP, 2,2'-dithiopyridine; ESI-MS, electrospray ionization mass spectrometry; Fmoc, fluorenylmethoxycarbonyl; HATU, 1[bis-(dimethylamino)methylene]-1*H*-1,2,3-triazolo[4,5-*b*]pyridinium 3-oxide hexafluorophosphate; LC/MS, liquid chromatography/mass spectrometry; MeOH, methanol; nAChR, nicotinic acetylcholine receptor; NMR, nuclear magnetic resonance; Pbf, pentamethyl-dihydrobenzofuran-5-sulfonyl; RP-HPLC, reversed-phase high performance liquid chromatography; SPPS, solid-phase peptide synthesis; *t*-Bu, *tert*-butyl; TFA, trifluoroacetic acid; TIS, triisopropylsilane; Tris, 2-amino-2-(hydroxymethyl)propane-1,3-diol; Trt, trityl; UV, ultraviolet

ADDITIONAL NOTE

“Please note that different IC₅₀ values of native CIA were found in a previous study.¹⁸ We determined that the use of BSA in the conotoxin dilutions likely reduced the nonspecific binding and resulted in higher potencies.

REFERENCES

- (1) Lewis, R. J.; Garcia, M. L. Therapeutic Potential of Venom Peptides. *Nat. Rev. Drug Discov.* **2003**, *2*, 790–802.
- (2) Puillandre, N.; Duda, T. F.; Meyer, C.; Olivera, B. M.; Bouchet, P. One, Four or 100 Genera? A New Classification of the Cone Snails. *J. Molluscan Stud.* **2015**, *81*, 1–23.
- (3) Davis, J.; Jones, A.; Lewis, R. J. Remarkable Inter- and Intra-Species Complexity of Conotoxins Revealed by LC/MS. *Peptides* **2009**, *30*, 1222–1227.
- (4) Prashanth, J. R.; Brust, A.; Jin, A.-H.; Alewood, P. F.; Dutertre, S.; Lewis, R. J. Cone Snail Venomics: From Novel Biology to Novel Therapeutics. *Future Med. Chem.* **2014**, *6*, 1659–1675.
- (5) Akondi, K. B.; Muttenthaler, M.; Dutertre, S.; Kaas, Q.; Craik, D. J.; Lewis, R. J.; Alewood, P. F. Discovery, Synthesis, and Structure-Activity Relationships of Conotoxins. *Chem. Rev.* **2014**, *114*, 5815–5847.
- (6) Giribaldi, J.; Dutertre, S. α -Conotoxins to Explore the Molecular, Physiological and Pathophysiological Functions of Neuronal Nicotinic Acetylcholine Receptors. *Neurosci. Lett.* **2018**, *679*, 24–34.
- (7) Lebbe, E.; Peigneur, S.; Wijesekara, I.; Tytgat, J. Conotoxins Targeting Nicotinic Acetylcholine Receptors: An Overview. *Mar. Drugs* **2014**, *12*, 2970–3004.

- (8) Albuquerque, E. X.; Pereira, E. F. R.; Alkondon, M.; Rogers, S. W. Mammalian Nicotinic Acetylcholine Receptors: From Structure to Function. *Physiol. Rev.* **2009**, *89*, 73–120.

- (9) Lau, J. L.; Dunn, M. K. Therapeutic Peptides: Historical Perspectives, Current Development Trends, and Future Directions. *Bioorg. Med. Chem.* **2018**, *26*, 2700–2707.

- (10) Sato, A. K.; Viswanathan, M.; Kent, R. B.; Wood, C. R. Therapeutic Peptides: Technological Advances Driving Peptides into Development. *Curr. Opin. Biotechnol.* **2006**, *17*, 638–642.

- (11) Ovadia, O.; Linde, Y.; Haskell-Luevano, C.; Dirain, M. L.; Sheynis, T.; Jelinek, R.; Gilon, C.; Hoffman, A. The Effect of Backbone Cyclization on PK/PD Properties of Bioactive Peptide-Peptoid Hybrids: The Melanocortin Agonist Paradigm. *Bioorg. Med. Chem.* **2010**, *18*, 580–589.

- (12) Wang, C. K.; Craik, D. J. Designing Macrocyclic Disulfide-Rich Peptides for Biotechnological Applications. *Nat. Chem. Biol.* **2018**, *14*, 417–427.

- (13) Clark, R. J.; Jensen, J.; Nevin, S. T.; Callaghan, B. P.; Adams, D. J.; Craik, D. J. The Engineering of an Orally Active Conotoxin for the Treatment of Neuropathic Pain. *Angew. Chem., Int. Ed.* **2010**, *49*, 6545–6548.

- (14) Clark, R. J.; Fischer, H.; Dempster, L.; Daly, N. L.; Rosengren, K. J.; Nevin, S. T.; Meunier, F. A.; Adams, D. J.; Craik, D. J. Engineering Stable Peptide Toxins by Means of Backbone Cyclization: Stabilization of the α -Conotoxin MII. *Proc. Natl. Acad. Sci. U.S.A.* **2005**, *102*, 13767–13772.

- (15) Halai, R.; Callaghan, B.; Daly, N. L.; Clark, R. J.; Adams, D. J.; Craik, D. J. Effects of Cyclization on Stability, Structure, and Activity of α -Conotoxin RgIA at the A9 α 10 Nicotinic Acetylcholine Receptor and GABA(B) Receptor. *J. Med. Chem.* **2011**, *54*, 6984–6992.

- (16) Armishaw, C. J.; Jensen, A. A.; Balle, L. D.; Scott, K. C. M.; Sørensen, L.; Strømgaard, K. Improving the Stability of α -Conotoxin Au1B Through N-to-C Cyclization: The Effect of Linker Length on Stability and Activity at Nicotinic Acetylcholine Receptors. *Antioxid. Redox Signaling* **2011**, *14*, 65–76.

- (17) Lovelace, E. S.; Armishaw, C. J.; Colgrave, M. L.; Wahlstrom, M. E.; Alewood, P. F.; Daly, N. L.; Craik, D. J. Cyclic MrIA: A Stable and Potent Cyclic Conotoxin with a Novel Topological Fold That Targets the Norepinephrine Transporter. *J. Med. Chem.* **2006**, *49*, 6561–6568.

- (18) Giribaldi, J.; Wilson, D.; Nicke, A.; El Hamdaoui, Y.; Laconde, G.; Faucherre, A.; Moha Ou Maati, H.; Daly, N.; Enjalbal, C.; Dutertre, S. Synthesis, Structure and Biological Activity of CIA and CIB, Two α -Conotoxins from the Predation-Evoked Venom of *Conus catus*. *Toxins* **2018**, *10*, 222.

- (19) Carpino, L. A.; Han, G. Y. 9-Fluorenylmethoxycarbonyl Function, a New Base-Sensitive Amino-Protecting Group. *J. Am. Chem. Soc.* **1970**, *92*, 5748–5749.

- (20) Barlos, K.; Chatzi, O.; Gatos, D.; Stavropoulos, G. 2-Chlorotriethyl Chloride Resin. Studies on Anchoring of Fmoc-Amino Acids and Peptide Cleavage. *Int. J. Pept. Protein Res.* **1991**, *37*, 513–520.

- (21) Cheneval, O.; Schroeder, C. I.; Durek, T.; Walsh, P.; Huang, Y.-H.; Liras, S.; Price, D. A.; Craik, D. J. Fmoc-Based Synthesis of Disulfide-Rich Cyclic Peptides. *J. Org. Chem.* **2014**, *79*, 5538–5544.

- (22) Wüthrich, K. *NMR of Proteins and Nucleic Acids*; The George Fisher Baker Non-Resident Lectureship in Chemistry at Cornell University; Wiley: New York, 1986.

- (23) Shen, Y.; Delaglio, F.; Cornilescu, G.; Bax, A. TALOS+: A Hybrid Method for Predicting Protein Backbone Torsion Angles from NMR Chemical Shifts. *J. Biomol. NMR* **2009**, *44*, 213–223.

- (24) Jimenez, E. C.; Olivera, B. M.; Teichert, R. W. α C-Conotoxin PrXA: A New Family of Nicotinic Acetylcholine Receptor Antagonists. *Biochemistry* **2007**, *46*, 8717–8724.

- (25) Molgó, J. Effects of Aminopyridines on Neuromuscular Transmission. *Aminopyridines and Similarly Acting Drugs: Effects on Nerves, Muscles and Synapses*; Elsevier, 1982; pp 95–116.

- (26) Molgó, J.; Lemeignan, M.; Guerrero, S. Facilitatory Effects of 4-Aminopyridine on Strontium-Mediated Evoked and Delayed Trans-

mitter Release from Motor Nerve Terminals. *Eur. J. Pharmacol.* **1982**, *84*, 1–7.

(27) Sanders, D. B.; Juel, V. C.; Harati, Y.; Smith, A. G.; Peltier, A. C.; Marburger, T.; Lou, J. S.; Pascuzzi, R. M.; Richman, D. P.; Xie, T.; Demmel, V.; Jacobus, L. R.; Aleš, K. L.; Jacobus, D. P. The Dapper Study Team. 3,4-diaminopyridine Base Effectively Treats the Weakness of Lambert-Eaton Myasthenia. *Muscle Nerve* **2018**, *57*, 561–568.

(28) Jonsson, M.; Gurley, D.; Dabrowski, M.; Larsson, O.; Johnson, E. C.; Eriksson, L. I. Distinct Pharmacologic Properties of Neuromuscular Blocking Agents on Human Neuronal Nicotinic Acetylcholine Receptors: A Possible Explanation for the Train-of-Four Fade. *Anesthesiology* **2006**, *105*, 521–533.

(29) Fagerlund, M. J.; Eriksson, L. I. Current Concepts in Neuromuscular Transmission. *Br. J. Anaesth.* **2009**, *103*, 108–114.

(30) Tajima, T.; Amaya, J.; Katayama, K.; Koizumi, T. Difference of Train-of-Four Fade Induced by Nondepolarizing Neuromuscular Blocking Drugs: A Theoretical Consideration on the Underlying Mechanisms. *J. Anesth.* **1995**, *9*, 333–337.

(31) Cheah, L. S.; Gwee, M. C. E. Train-Of-Four Fade During Neuromuscular Blockade Induced by Tubocurarine, Succinylcholine or α -Bungarotoxin in the Rat Isolated Hemidiaphragm. *Clin. Exp. Pharmacol. Physiol.* **1988**, *15*, 937–943.

(32) Robbins, R.; Donati, F.; Bevan, D. R.; Bevan, J. C. Differential Effects of Myoneural Blocking Drugs on Neuromuscular Transmission in Infants. *Br. J. Anaesth.* **1984**, *56*, 1095–1099.

(33) Baird, W. L. M.; Bowman, W. C.; Kerr, W. J. Some Actions of Org NC45 and of Edrophonium in the Anaesthetized Cat and in Man. *Br. J. Anaesth.* **1982**, *54*, 375–385.

(34) Nagashima, M.; Yasuhara, S.; Martyn, J. A. J. Train-of-Four and Tetanic Fade Are Not Always a Prejunctional Phenomenon as Evaluated by Toxins Having Highly Specific Pre- and Postjunctional Actions. *Anesth. Analg.* **2013**, *116*, 994–1000.

(35) Bren, N.; Sine, S. M. Hydrophobic Pairwise Interactions Stabilize α -Conotoxin MI in the Muscle Acetylcholine Receptor Binding Site. *J. Biol. Chem.* **2000**, *275*, 12692–12700.

(36) Ning, J.; Li, R.; Ren, J.; Zhangsun, D.; Zhu, X.; Wu, Y.; Luo, S. Alanine-Scanning Mutagenesis of α -Conotoxin GI Reveals the Residues Crucial for Activity at the Muscle Acetylcholine Receptor. *Mar. Drugs* **2018**, *16*, 507.

(37) Bowman, W. C.; Prior, C.; Marshall, I. G. Presynaptic Receptors in the Neuromuscular Junction. *Ann. N.Y. Acad. Sci.* **1990**, *604*, 69–81.

(38) Kuryatov, A.; Olale, F.; Cooper, J.; Choi, C.; Lindstrom, J. Human $\alpha 6$ AChR Subtypes: Subunit Composition, Assembly, and Pharmacological Responses. *Neuropharmacology* **2000**, *39*, 2570–2590.

(39) McIntosh, J. M.; Azam, L.; Staheli, S.; Dowell, C.; Lindstrom, J. M.; Kuryatov, A.; Garrett, J. E.; Marks, M. J.; Whiteaker, P. Analogs of α -Conotoxin MII Are Selective for $\alpha 6$ -Containing Nicotinic Acetylcholine Receptors. *Mol. Pharmacol.* **2004**, *65*, 944–952.

(40) Ellison, M.; McIntosh, J. M.; Olivera, B. M. α -Conotoxins ImI and ImII: Similar A7 Nicotinic Receptor Antagonists Act at Different Sites. *J. Biol. Chem.* **2003**, *278*, 757–764.

(41) Güntert, P. Automated NMR Structure Calculation with CYANA. *Methods Mol. Biol.* **2004**, *278*, 353–378.

(42) Koradi, R.; Billeter, M.; Wüthrich, K. MOLMOL: A Program for Display and Analysis of Macromolecular Structures. *J. Mol. Graph.* **1996**, *14*, 51–55.

(43) Pettersen, E. F.; Goddard, T. D.; Huang, C. C.; Couch, G. S.; Greenblatt, D. M.; Meng, E. C.; Ferrin, T. E. UCSF Chimera?A Visualization System for Exploratory Research and Analysis. *J. Comput. Chem.* **2004**, *25*, 1605–1612.

Supporting information

Backbone cyclization turns a venom peptide into a stable and equipotent ligand at both muscle and neuronal nicotinic receptors

Julien Giribaldi†, Yves Haufet†, Edward Evans, Muriel Amar, Anna Durner, Casey Schmidt, Adèle Faucherre, Hamid Moha Ou Maati, Christine Enjalbal, Jordi Molgó, Denis Servent, David T. Wilson, Norelle L. Daly, Annette Nicke and Sébastien Dutertre*

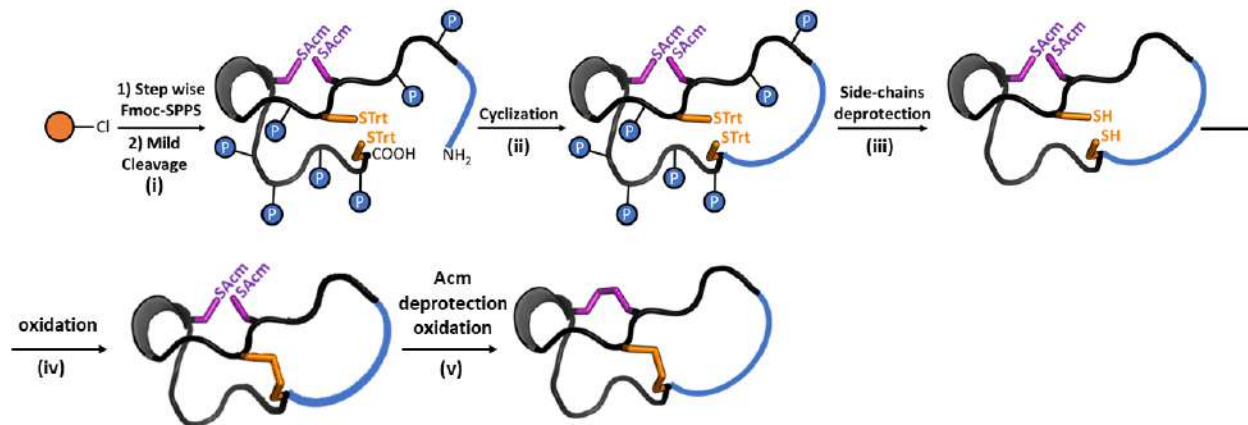
Content

Figures

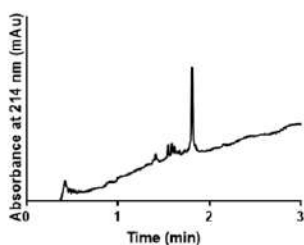
S1: Synthesis strategy of the three cyclic analogues of CIA and respective RP-HPLC-UV chromatograms and ESI/MS analyses	p 2-3
S2: Current traces of muscle-type and $\alpha 3\beta 2$ nAChR after inhibition by CIA analogues	p 4
S3: Real-time recovery of $\alpha 3\beta 2$ currents after inhibition by CIA and its cyclic derivatives	p 5
S4: Comparison of the dissociation of CIA and its cyclic derivatives from $\alpha 3\beta 2$	p 6
S5: Functional competition between cCIA-3 and MII on the $\alpha 3\beta 2$ receptor	p 7
S6: Dose response curves of α -cCIA-3 and recovery of ACh-evoked currents on $(\alpha 1)_2\beta 1\gamma\delta$, $(\alpha 1)_2\beta 1\varepsilon\delta$, $\alpha 3\beta 2$, $\alpha 6/\alpha 3\beta 2\beta 3$	p 8
S7: Recovery of fetal $((\alpha 1)_2\beta 1\gamma\delta)$ and adult $((\alpha 1)_2\beta 1\varepsilon\delta)$ muscle-type nAChRs from toxin block	p 9

Tables

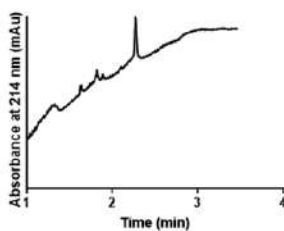
S1: Responses of additional nAChR subtypes to 10 μ M α -cCIA-3	p 10
S2: Structural statistics for the cCIA analogues	p 11



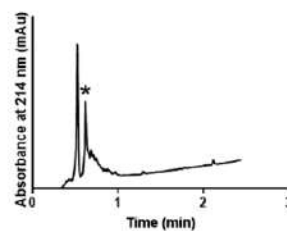
UV Chromatogram after step (i)



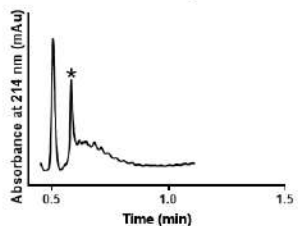
UV Chromatogram after step (ii)



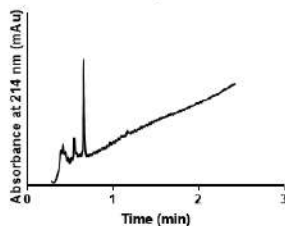
UV Chromatogram after step (iii)



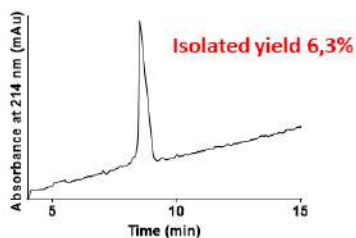
UV Chromatogram after step (vi)



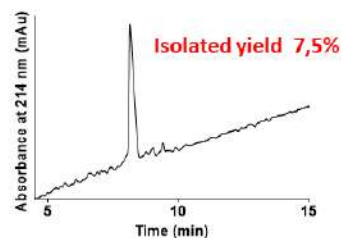
UV Chromatogram after step (v)



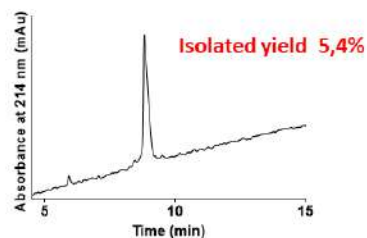
UV Chromatogram of cCIA-2



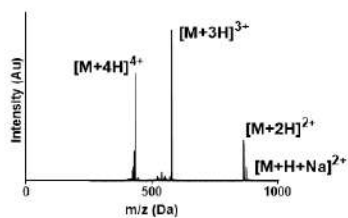
UV Chromatogram of cCIA-3



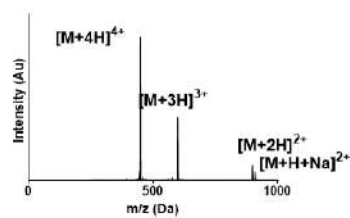
UV Chromatogram of cCIA-4



cCIA-2 ESI-MS



cCIA-3 ESI-MS



cCIA-4 ESI-MS

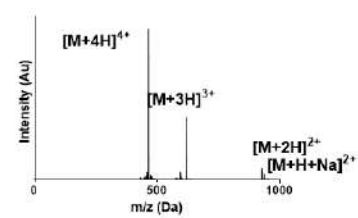


Figure S1: Synthesis strategy of the three cyclic analogues of CIA and respective RP-HPLC-UV chromatograms and ESI/MS analyses. (i) 1% TFA in DCM (v/v) 10 x 5 min (ii) HATU (2,5eq)/DIEA (5eq) 4 h (iii) TFA/TIS/H₂O (95/2.5/2.5 v/v/v) 2,5 hr (iv) Tris-HCl 50 mM buffer pH 8, DTP (7eq), 10 min (v) I₂ 10 mM (20eq) in H₂O/TFA/ACN (78/2/20 v/v/v), 10 min. The orange round circle represents a chloro-(2'-chloro) trityl resin and P represents common side chains protective groups used in Fmoc-SPPS (Solid Phase Peptide Synthesis). The asterisk indicates the peak of interest. RP-HPLC-UV (ACN gradient from 0 to 30% in 30 min) coupled to ESI-MS analyses revealed the presence of dominant peaks of the expected masses.

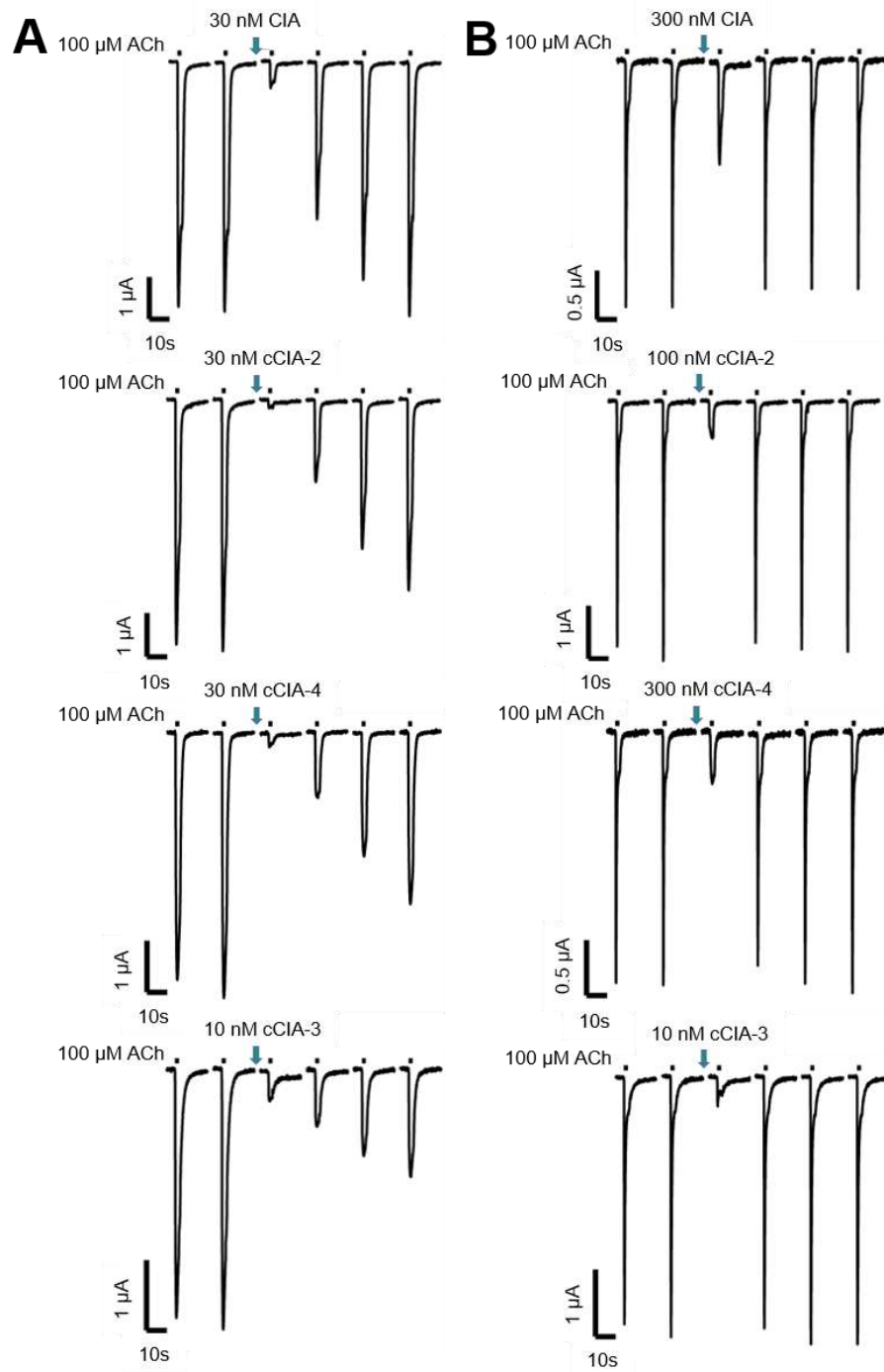


Figure S2: Recovery of ACh-induced muscle-type (A) and $\alpha 3\beta 2$ (B) nAChR currents after inhibition by CIA analogues (indicated by green arrow). 2s-pulses of ACh (100 μ M, black bar) were applied in 4 min intervals (1 min under perfusion, 3 min in a static bath). Once stable current responses were obtained, toxins were applied for 3 min in the static bath in concentrations that produced at least 80% inhibition.

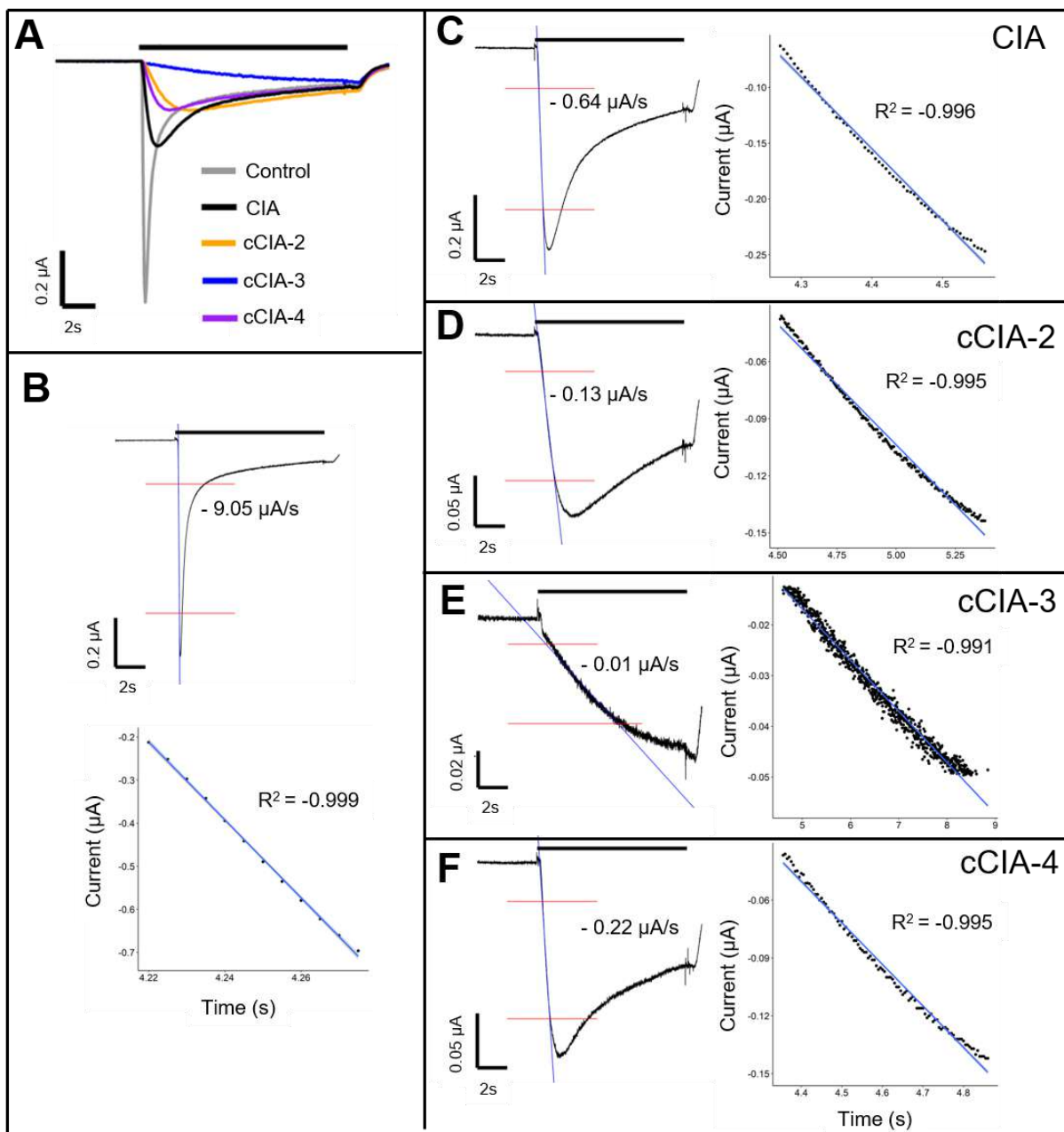


Figure S3: Real-time recovery of $\alpha\beta_2$ currents after inhibition by CIA and its cyclic derivatives. (A) Merged current responses during a 10s application of ACh (100 μM , black bar) evoked before (control) and after 3 min incubation with the indicated peptides. Note the delayed current peak due to dissociation of the peptide during the agonist application. The steepness of the rising phase of the current was used as a surrogate for the off rate. (B-F) Isolated peak traces are shown with red lines indicating the rising phases from 20% to 80% of the peak currents and a linear regression (blue line) within these borders was performed. (B) control (ND96), (C) 1 μM native CIA, (D) 1 μM cCIA-2, (E) 100 nM cCIA-3, and (F) 1 μM cCIA-4. The slope of each linear regression is written in the graph and the linear regression in the chosen borders is shown in detail with regression coefficient (R^2).

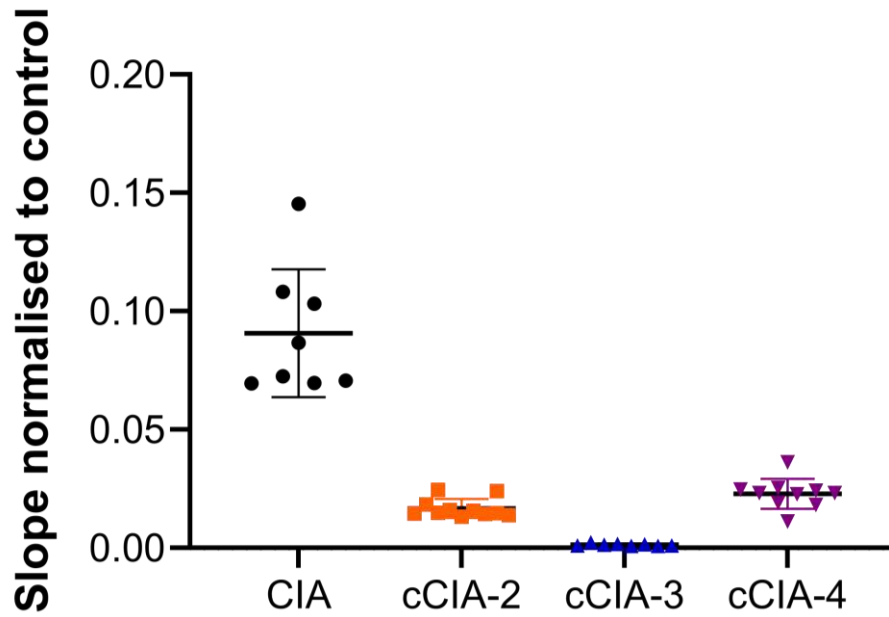


Figure S4: Comparison of the dissociation of CIA and its cyclic derivatives from $\alpha 3\beta 2$ using the slope of the rising phase of the ACh evoked current as surrogate. The slopes were determined as shown in Figure 2 and normalized to the slope of the control response before incubation with the peptide (antagonist slope / control slope). The single values are shown with the mean as straight bar and S.D., n = 8-11. Note that higher values indicate a faster dissociation.

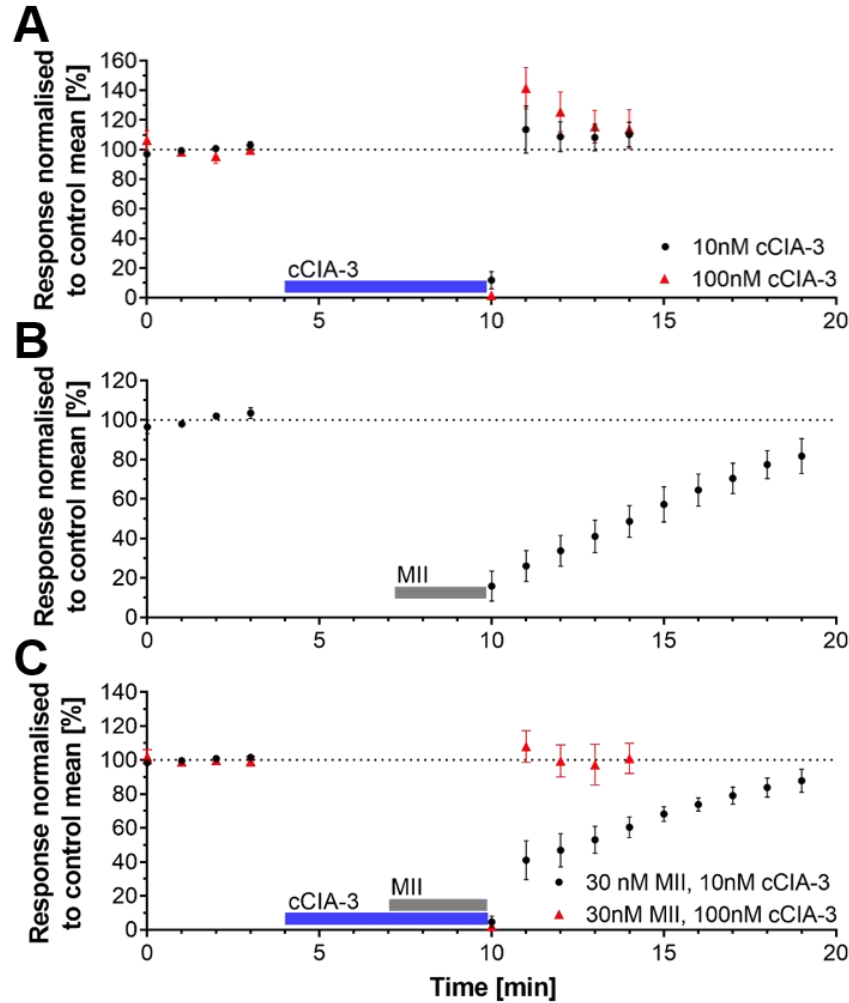


Figure S5: Functional competition between cCIA-3 and MII on the $\alpha 3\beta 2$ receptor. Responses to 2s-ACh pulses were recorded at 1-min intervals and normalized to the mean of 4 current peaks recorded prior to peptide incubation in a static bath. Three different protocols were conducted: (A) 1 min after ACh wash-out, cCIA-3 (10 or 100nM) was added to the static bath for 6 min before ACh applications were continued, (B) 4 min after ACh wash-out, MII (30 nM) was added to the static bath for 3 min before ACh applications were continued (C) cCIA-3 (10 or 100 nM) was added after 1 min and MII (30nM) was added after 3 min. ACh applications were continued after 6 min. Data are represented as MEAN \pm S.D. with $n \geq 5$.

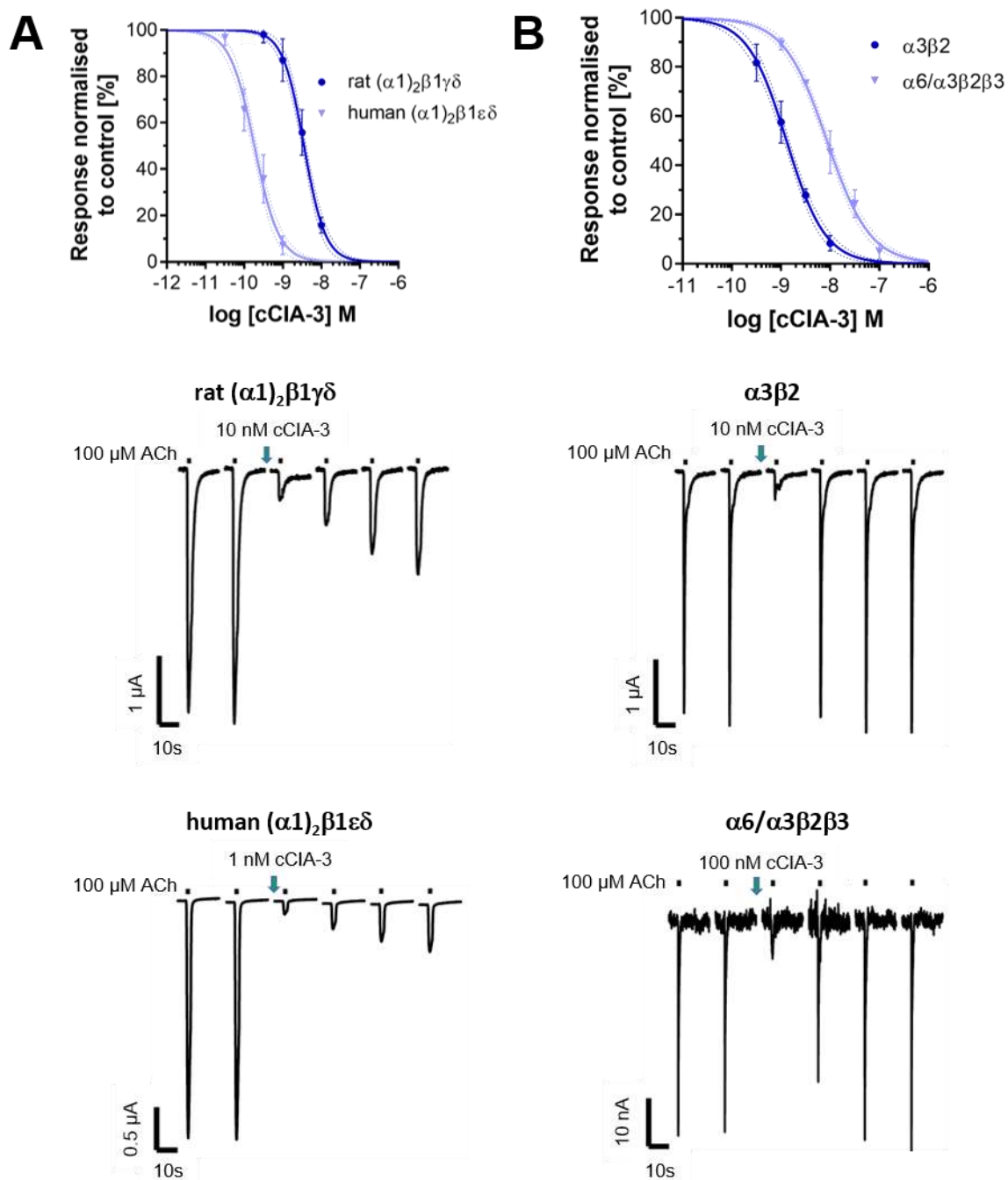


Figure S6: Dose response curves of α -cCIA-3 and recovery of ACh-evoked currents after α -cCIA-3 application. (A) Dose response curves at adult and fetal muscle type nAChRs and (B) $\alpha 3\beta 2$ and $\alpha 6/\alpha 3\beta 2\beta 3$ neuronal nAChRs. 2s-pulses of ACh (100 μ M, black bar) were applied in 4 min intervals (1 min under perfusion, 3 min in a static bath). Once stable current responses were obtained, toxins were applied for 3 min in the static bath. IC_{50} values and Hill-Slopes (in brackets) were 57 nM (-1.57) for rat $(\alpha 1)_2\beta 1\gamma\delta$, 184.5 μ M (-1.38) for human $(\alpha 1)_2\beta 1\epsilon\delta$, 1.30 nM (-1.10) for $\alpha 3\beta 2$ and 8.64 nM (-1.0) for $\alpha 6/\alpha 3\beta 2\beta 3$. Each point represents the mean of at least 3 different oocytes with S.D.

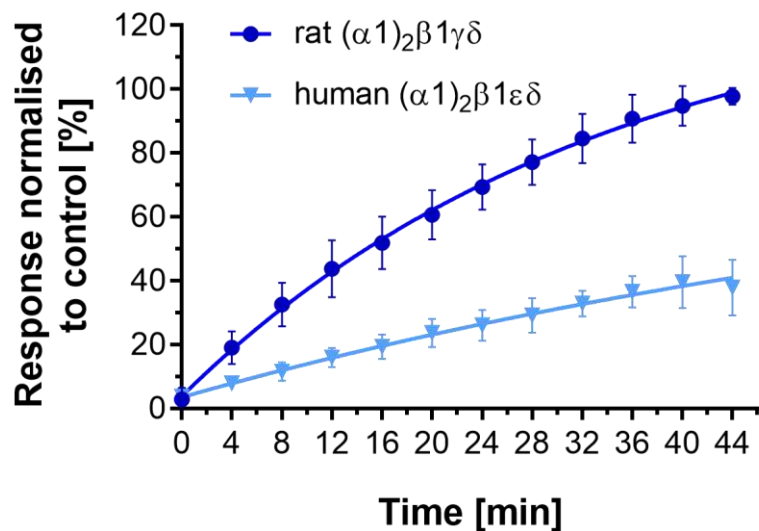


Figure S7: Recovery of fetal ($(\alpha 1)_2\beta 1\gamma\delta$) and adult($(\alpha 1)_2\beta 1\varepsilon\delta$) muscle-type nAChRs from toxin block. *X. laevis* oocytes expressing the indicated receptors were analyzed by TEVC at -70 mV. 1 nM for adult muscle type and 100 nM for fetal muscle type of α -cCIA-3 was preincubated for 3 min. Responses to 2-s pulses of 100 μ M ACh were measured in 4 min intervals. Each point represents the mean of measurements from at least 3 different oocytes, error bars represent S.D. The koff values are 0.03 min^{-1} for the rat fetal muscle type and 0.013 min^{-1} for adult muscle type nAChR.

Table S1: Normalized responses of additional nAChR subtypes to 10 μ M α -cCIA-3. In order to save peptide, and given that responses were 80% or higher, only 2 recordings were performed on two different oocytes, except for human α 7 that produced a response <80% (n=3). Unless otherwise stated, the subtypes were injected in a 1:1 subunit-ratio.

Subtype	Species	ACh [μ M]	% Response as mean \pm S.D.
α 2 β 2	rat	100	93 \pm 14%
α 2 β 4	rat	100	96 \pm 14%
α 3 β 4	rat	100	86 \pm 15%
α 4 β 2 (Ratio 5:1)	rat	100	103 \pm 16%
α 4 β 4	rat	30	92 \pm 14%
α 7	human	100	65 \pm 13%
α 9 α 10 (Ratio 5:1)	human	40	81 \pm 14%

Table S2: Structural statistics for the cCIA analogues.

Structural statistics for the cCIA ensembles			
Experimental restraints	cCIA-2	cCIA-3	cCIA-4
Interproton distance restraints	136	179	154
<i>Intraresidue</i>	36	53	49
<i>Sequential</i>	51	75	67
<i>Medium range (i-j < 5)</i>	23	33	19
<i>Long range (i-j ≥ 5)</i>	26	18	19
Dihedral-angle restraints	21	23	21
R.m.s. deviations from mean coordinate structure (Å)			
Backbone atoms (with linker)	0.91 ± 0.35	0.29 ± 0.17	1.05 ± 0.45
All heavy atoms (with linker)	1.78 ± 0.46	0.85 ± 0.24	1.59 ± 0.46
Backbone atoms (without linker)	0.72 ± 0.26	0.13 ± 0.06	0.27 ± 0.11
All heavy atoms (without linker)	1.73 ± 0.46	0.82 ± 0.22	1.17 ± 0.35
Ramachandran Statistics			
% in most favoured region	68.5%	61.10%	76.40%
% in additionally allowed region	31.5%	38.9%	23.6%

5. Publication II

pp. 74 - 84

Article

Synthesis, Structural and Pharmacological Characterizations of CIC, a Novel α -Conotoxin with an Extended N-Terminal Tail

Julien Giribaldi ¹, Yves Haufe ², Edward R. J. Evans ³, David T. Wilson ³, Norelle L. Daly ³,
Christine Enjalbal ¹, Annette Nicke ² and Sébastien Dutertre ^{1,*}

- ¹ Institut des Biomolécules Max Mousseron, UMR 5247, Université de Montpellier, CNRS, ENSCM, 34095 Montpellier, France; julien.giribaldi@umontpellier.fr (J.G.); christine.enjalbal@umontpellier.fr (C.E.)
- ² Walther Straub Institute of Pharmacology and Toxicology, Faculty of Medicine, LMU Munich, Nußbaumstraße 26, 80336 Munich, Germany; yves.haufe@lrz.uni-muenchen.de (Y.H.); annette.nicke@lrz.uni-muenchen.de (A.N.)
- ³ Centre for Molecular Therapeutics, Australian Institute of Tropical Health and Medicine, James Cook University, Cairns, QLD 4878, Australia; edwardrobertjonathan.evans@my.jcu.edu.au (E.R.J.E.); david.wilson4@jcu.edu.au (D.T.W.); norelle.daly@jcu.edu.au (N.L.D.)
- * Correspondence: sebastien.dutertre@umontpellier.fr

Abstract: Cone snails are venomous marine predators that rely on fast-acting venom to subdue their prey and defend against aggressors. The conotoxins produced in the venom gland are small disulfide-rich peptides with high affinity and selectivity for their pharmacological targets. A dominant group comprises α -conotoxins, targeting nicotinic acetylcholine receptors. Here, we report on the synthesis, structure determination and biological activity of a novel α -conotoxin, CIC, found in the predatory venom of the piscivorous species *Conus catus* and its truncated mutant Δ -CIC. CIC is a 4/7 α -conotoxin with an unusual extended N-terminal tail. High-resolution NMR spectroscopy shows a major influence of the N-terminal tail on the apparent rigidity of the three-dimensional structure of CIC compared to the more flexible Δ -CIC. Surprisingly, this effect on the structure does not alter the biological activity, since both peptides selectively inhibit $\alpha 3\beta 2$ and $\alpha 6/\alpha 3\beta 2\beta 3$ nAChRs with almost identical sub- to low micromolar inhibition constants. Our results suggest that the N-terminal part of α -conotoxins can accommodate chemical modifications without affecting their pharmacology.

Keywords: conotoxin; peptide synthesis; NMR structure; electrophysiology; nicotinic acetylcholine receptors



Citation: Giribaldi, J.; Haufe, Y.; Evans, E.R.J.; Wilson, D.T.; Daly, N.L.; Enjalbal, C.; Nicke, A.; Dutertre, S. Synthesis, Structural and Pharmacological Characterizations of CIC, a Novel α -Conotoxin with an Extended N-Terminal Tail. *Mar. Drugs* **2021**, *19*, 141. <https://doi.org/10.3390/md19030141>

Academic Editor:
Orazio Tagliatela-Scafati

Received: 29 January 2021
Accepted: 25 February 2021
Published: 2 March 2021

Publisher's Note: MDPI stays neutral with regard to jurisdictional claims in published maps and institutional affiliations.



Copyright: © 2021 by the authors. Licensee MDPI, Basel, Switzerland. This article is an open access article distributed under the terms and conditions of the Creative Commons Attribution (CC BY) license (<https://creativecommons.org/licenses/by/4.0/>).

1. Introduction

Conotoxins are short peptides (8 to 32 residues) highly constrained by disulfide bridges (1 to 4 disulfide bonds) found in predatory marine cone snail venoms [1]. Cone snails have evolved into more than 800 different species [2]; their fast-acting venom is composed of 100–200 different conotoxins and has been tailored for predation and defense purposes [3]. There is relatively low overlap between the toxins present within different cone snail species [4], and it is estimated that cone snail venoms may overall contain at least 70,000 mostly neuroactive peptides, of which less than 0.1% have currently been pharmacologically characterized [5]. Moreover, their small size, structural stability and target specificity are valuable assets that make them important pharmacological probes or even drug leads [6]. Based on their conserved signal sequence, conotoxins are grouped into various gene superfamilies and further classified according to their cysteine frameworks and their biological activity [5].

Members of the α -subfamily specifically target neuronal and muscle-type nicotinic acetylcholine receptors (nAChRs) [1]. In addition, a pattern is emerging based on the number of amino acids between the cysteine residues: 3/5 α -conotoxins are most likely to target muscle-type nAChRs, while 4/7 α -conotoxins target $\alpha 7$ and/or $\alpha 3\beta 2^*$ neuronal nAChRs [7]. However, in most α -conotoxins, the number of residues outside the cysteine

loops is usually limited to one or two amino acids (Figure 1A). Based on Conoserver data [8,9], α -conotoxin GID is the only described 4/7 α -conotoxin showing a significant N-terminal extension (>2 residues) and is a potent blocker of $\alpha 3\beta 2$ and $\alpha 7$ (low nanomolar IC_{50}) nAChRs, but also shows a significant and noteworthy inhibition of $\alpha 4\beta 2$ nAChR subtypes (IC_{50} 152 nM), which appear to be “ α -conotoxin-resistant” receptors [1,10]. Considering the important role of $\alpha 4$ and $\beta 2$ subunits in addiction, pain and cognition, which has been revealed by knockout studies [11], $\alpha 4\beta 2$ nAChR-selective ligands would be very valuable pharmacological tools. Interestingly, deletion of the N-terminal sequence of GID (Δ -1-4) leads to loss of activity at the $\alpha 4\beta 2$ subtype but has no effect on the IC_{50} value at $\alpha 3\beta 2$ and $\alpha 7$ subtypes (but affects the dissociation rate at these receptors). These findings suggest that the N-terminal residues are important for both selectivity and affinity [10]. However, despite these effects, the N-terminal tail of GID appears to be disordered in solution.

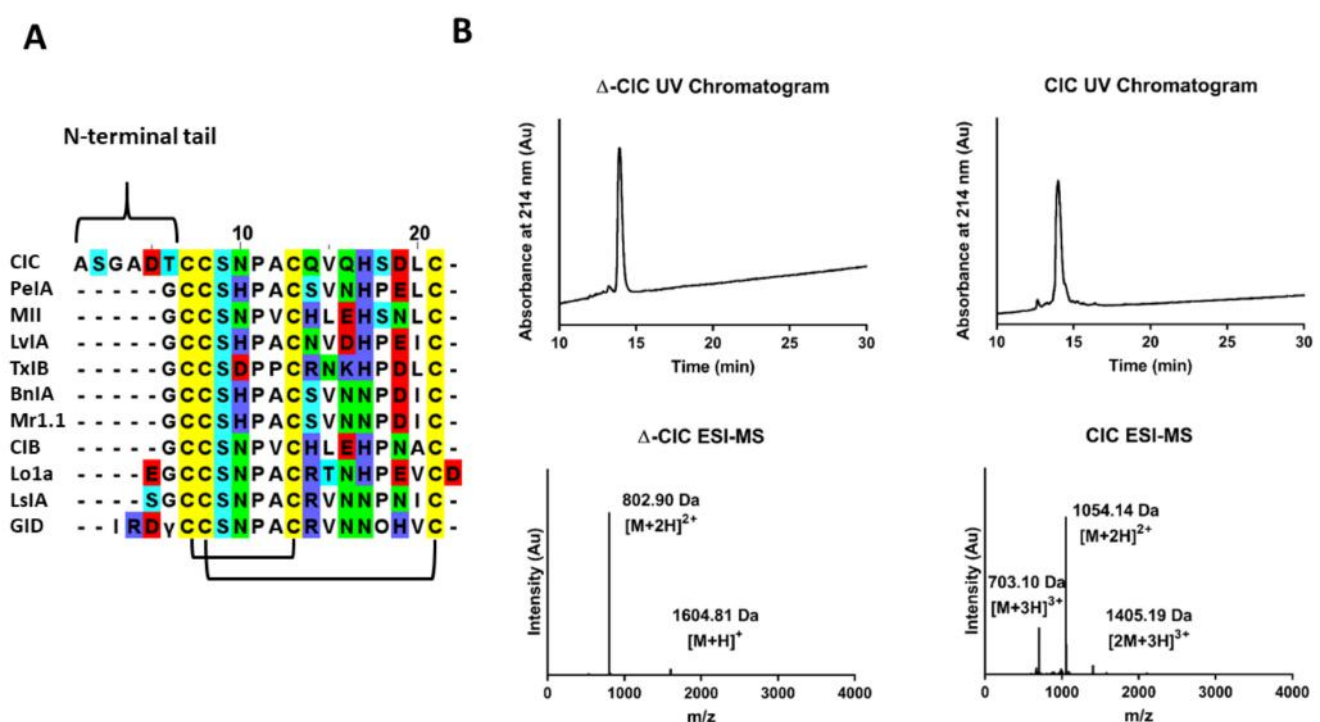


Figure 1. CIC alignment, UV chromatograms and ESI-MS analyses of synthetic peptides. (A). Alignment of CIC conotoxin with others closely related 4/7 α -conotoxins. The γ symbol indicates a carboxyglutamate residue, and O as a capital letter indicates a hydroxyproline residue. GID and CIC conotoxins are the only ones to display an N-terminal tail comprising more than two residues. The globular disulfide connectivity Cys I-III, Cys II-IV is represented. (B). RP-HPLC/ESI-MS analyses of synthetic Δ -CIC and CIC. ACN gradient was from 0 to 30% over 30 min. Reported mass values correspond to the average masses.

Here, we describe a new α -conotoxin, CIC, which was previously found in the proteo-transcriptomic study of *Conus catus* and identified as a component of the predation-evoked venom [12]. The native CIC has never been isolated from the venom and tested nor its sequence chemically synthesized. CIC shows high sequence similarity to PeIA and MII α -conotoxins, both potent antagonists of $\alpha 3\beta 2$ nAChR subtypes with IC_{50} values in the low nanomolar range [13,14]. However, unlike every other characterized 4/7 α -conotoxins, CIC displays an extended N-terminal tail comprising six residues. Therefore, the aim of this study was to investigate the role of this unusual N-terminal part on the three-dimensional structure and on the pharmacological activity. To this end, native CIC conotoxin, as well as a deletion variant with no N-terminal tail (Ala1-Thr6 removed) named Δ -CIC, were synthesized and both pharmacologically and structurally characterized.

2. Results

2.1. Chemical Synthesis of CIC and Δ -CIC

CIC and Δ -CIC were synthesized manually using Fmoc-SPPS after anchoring of the first C-terminal residue on a chloro-(2'-chloro) trityl resin. Considering its sequence homology to other 4/7 α -conotoxins (Figure 1A), which all display the canonical globular disulfide bond connectivity CysI-CysIII, CysII-CysIV, linear peptides were folded using a regioselective folding strategy to obtain the globular isomer. Briefly, the first disulfide bridge (CysII-CysIV) is formed by oxidation of the free cysteine residues in an aqueous basic buffer assisted by DTP (2,2'-Dithiopyridine), and the second disulfide bond (CysI-CysIII) is formed by deprotection/oxidation of the AcM protecting groups [15]. The homogeneity of folded toxins was assessed by analytical RP-HPLC coupled to ESI-MS (Figure 1B). ESI-MS(+) confirmed a monoisotopic mass of 1602.90 g/mol (calculated 1602.59 g/mol) for Δ -CIC and 2106.27 g/mol (calculated 2106.29 g/mol) for CIC. Overall, 7.7 mg (yield 3.1% from resin loading) and 9.9 mg (yield 3.2% from resin loading) of pure (>95% based on LC/ESI-MS) Δ -CIC and CIC were obtained, respectively.

2.2. Electrophysiology of CIC and Δ -CIC on Neuronal nAChRs

α -conotoxins PeIA [13] and MII [14], which are closely related (based on the primary structure, Figure 1A) to CIC, are potent inhibitors of α 3 β 2 nAChRs subtypes, while the N-terminally extended GID conotoxin inhibits α 3 β 2, α 7 and α 4 β 2 nAChR subtypes (Table 1). The latter is also inhibited to a limited extent by MII. Because of these similarities, the antagonistic potency of CIC and Δ -CIC was firstly investigated using two-electrode voltage-clamp analysis on α 3 β 2, α 7, and α 4 β 2 rat nAChRs subtypes. Whereas no inhibition was detected at the α 7 and α 4 β 2 subtypes, CIC and Δ -CIC inhibited the rat α 3 β 2 neuronal nAChR subtype with rather high IC₅₀ values of 3.51 μ M and 4.56 μ M, respectively. At the closely related α 6/ α 3 β 2 β 3 subtype, CIC and Δ -CIC showed IC₅₀ values of 0.94 μ M and 1.00 μ M, respectively (Figure 2, Table 1). Considering that these values are approximately 1000-fold higher than those of the similar (based on sequence) α -conotoxin MII, we assumed major structural differences and also tested CIC and Δ -CIC on additional rat nAChRs such as α 4 β 4, α 3 β 4, α 2 β 2, α 2 β 4 and (α 1)2 β 1 δ γ subtypes as well as human α 9 α 10 subtype. It is noteworthy that no inhibition was detected at concentrations up to 10 μ M on any of the additional nAChRs tested. In summary, despite some similarity to potent conotoxins, both CIC and Δ -CIC showed weak or no inhibition at common mammalian nAChR combinations (with no difference in dissociation behavior), and the quasi-identical values of inhibition constant between CIC and Δ -CIC at α 3 β 2-containing nAChRs suggest that there is no major influence of the N-terminal tail on their affinity.

Table 1. IC₅₀ values of the conotoxins discussed in the text on the different nAChR subtypes. N.D means not determined.

nAChR Subtypes	Toxin (IC ₅₀)			
	CIC	Δ -CIC	MI I	GID
α 3 β 2	3.51 μ M	4.56 μ M	3.7 nM	3.1 nM
α 6/ α 3 β 2 β 3	1.03 μ M	1.08 μ M	390 pM	N.D
α 7	>10 μ M	>10 μ M	200 nM (56% inhibition)	4.5 nM
α 4 β 2	>10 μ M	>10 μ M	200 nM (30% inhibition)	152 nM
α 4 β 4	>10 μ M	>10 μ M	200 nM (4% inhibition)	>5 μ M
α 3 β 4	>10 μ M	>10 μ M	200 nM (15% inhibition)	>5 μ M
α 2 β 2	>10 μ M	>10 μ M	200 nM (20% inhibition)	N.D
α 2 β 4	>10 μ M	>10 μ M	200 nM (4% inhibition)	N.D
(α 1)2 β 1 δ γ	>10 μ M	>10 μ M	200 nM (11% inhibition)	N.D
α 9 α 10	>10 μ M	>10 μ M	>1 μ M	N.D
References	This work	This work	[14,16–18]	[10]

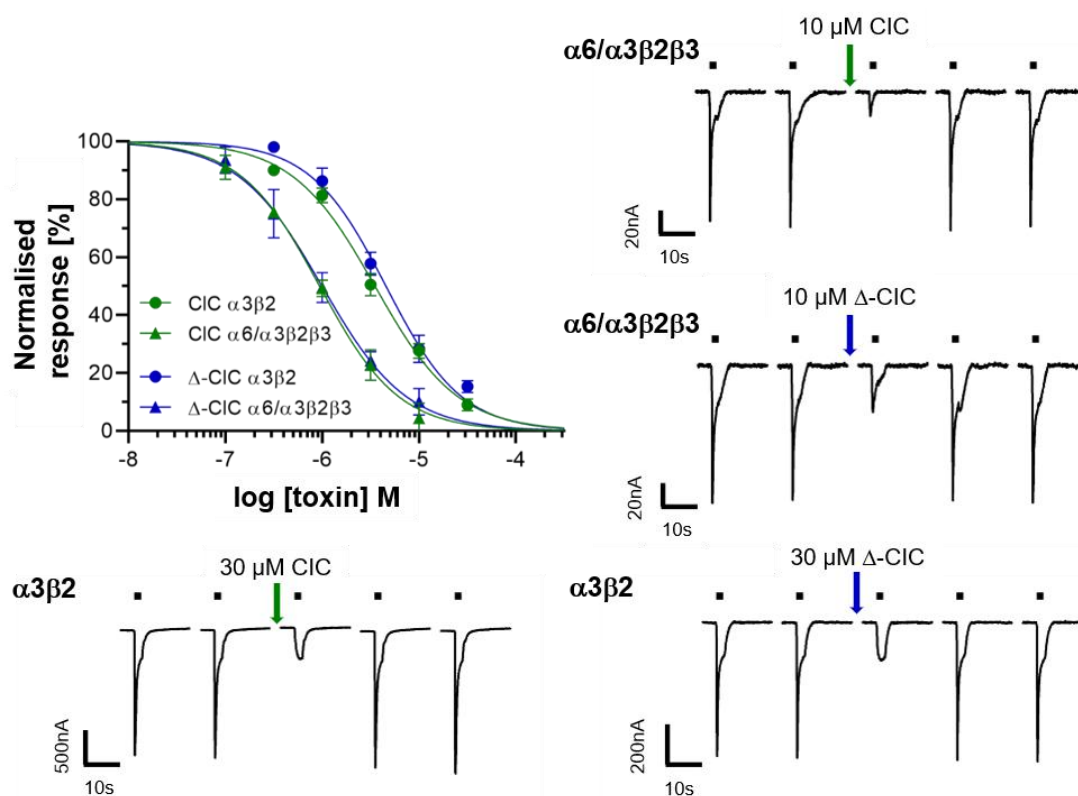


Figure 2. Dose–response curves and representative current traces of CIC and Δ -CIC on rat $\alpha 3\beta 2$ and $\alpha 6/\alpha 3\beta 2\beta 3$ nAChR subtypes expressed in *Xenopus laevis* oocytes. 2-Electrode voltage-clamp experiments were performed at -70 mV. Responses to 2-s pulses of $100 \mu\text{M}$ ACh (indicated by a black bar) were recorded after a 3-min preincubation with the indicated peptides. Each point represents the mean of measurements from at least 3 different oocytes. Error bars represent S.D. No effects were observed on $\alpha 7$, $\alpha 4\beta 2$, $\alpha 4\beta 4$, $\alpha 3\beta 4$, $\alpha 2\beta 2$, $\alpha 2\beta 4$ and $(\alpha 1)_2\beta 1\delta\gamma$ rat subtypes as well as human $\alpha 9\alpha 10$ subtype at concentrations up to $10 \mu\text{M}$.

2.3. Three-Dimensional Structure Determination of CIC and Δ -CIC

High-resolution NMR spectroscopy allowed the determination of the three-dimensional structures of both CIC and Δ -CIC (Figure 3). The structure statistics are given in Table 2. The calculated structures of CIC are well-defined with an RMSD value over backbone atoms, excluding the N-terminal tail, of $0.29 \pm 0.16 \text{ \AA}$ (residues 7–21). CIC exhibits two 3^{10} helices from residues Thr6 to Ser9 and Pro11 to Gln16. Interestingly the N-terminal tail displays a relatively well-defined structure. However, Δ -CIC lacks the first helix and has only one 3^{10} helix from residues Pro5 to Val9, suggesting that the N-terminal tail plays a role in inducing the first helix. Counterintuitively, the calculated structures of Δ -CIC are less defined and display a higher RMSD value ($2.06 \pm 0.73 \text{ \AA}$, over backbone atoms) than CIC, which indicates a stabilizing role of the N-terminal tail. Moreover, the lack of the N-terminal tail in Δ -CIC appears to change the overall structure, with the C-terminal region (Ser18–Cys21) in a different orientation with respect to the helix.

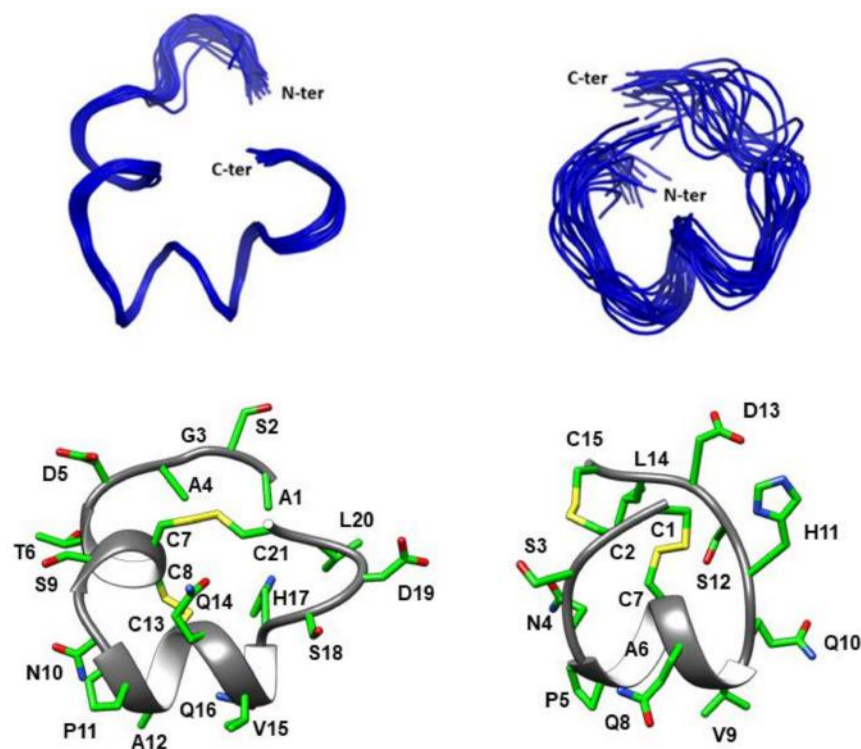


Figure 3. Three-dimensional structures of CIC and Δ -CIC. The backbones are shown in ribbon format and the side-chains in stick format. Top panels. Superposed backbone atoms (ribbon representation) for the 20 lowest-energy NMR structures for CIC (left) and Δ -CIC (right). Lower panels. Ribbon and stick representation of the lowest energy state for CIC (left) and Δ -CIC (right).

Table 2. Structural statistics for CIC and Δ -CIC.

Experimental Restraints	CIC	Δ -CIC
Interproton distance restraints	230	88
<i>Intraresidue</i>	64	36
<i>Sequential</i>	75	45
<i>Medium range</i> ($i - j < 5$)	79	7
<i>Long range</i> ($i - j \geq 5$)	12	0
Dihedral-angle restraints	30	15
R.m.s. deviations from the mean coordinate structure (Å)		
Backbone atoms	0.79 \pm 0.3	2.06 \pm 0.73
All heavy atoms	1.11 \pm 0.22	2.97 \pm 0.69
Ramachandran statistics		
% in most favoured region	82.6%	62.2%
% in additionally allowed region	17.4%	33.7%

3. Discussion

α -conotoxin CIC has been previously found in a proteo-transcriptomic study of the predation-evoked venom of *Conus catus* [12]. Since this toxin exhibited a typical α -conotoxin cysteine pattern -CC-C-C [5] along with an unusual N-terminal extended tail, we decided to investigate the influence of the N-terminal tail on the three-dimensional structure and on the pharmacological properties of the toxin. To this end, we synthesized the globular form (CysI-CysIII, CysII-CysIV) of the α -conotoxin CIC as well as a mutant variant named Δ -CIC in which the first six residues (Ala1-Thr6) were removed. Considering that the other known bioactive 4/7 α -conotoxins [5] mainly display the “native” globular fold, a regioselective folding strategy was applied.

So far, α -GID [10] is the only described 4/7 α -conotoxin with an extended N-terminal tail. α -GID was isolated using assay-directed fractionation of *Conus geographus* crude venom and is a potent blocker of $\alpha 3\beta 2$, $\alpha 7$ (low nanomolar IC_{50} , Table 1) and $\alpha 4\beta 2$ nAChR subtypes (IC_{50} 152 nM, Table 1). It is noteworthy that the deletion of the N-terminal sequence of GID (Δ -1-4) leads to a significant loss of potency at the $\alpha 4\beta 2$ subtype [10]. However, unlike α -GID, α -CIC showed no inhibition of $\alpha 4\beta 2$ nAChR subtypes at concentrations up to 10 μ M. Moreover, the structure of the N-terminal tail of CIC was found to be well-defined, which is in contrast to the disordered N-terminal tail of conotoxin GID [10] (Figure 4A).

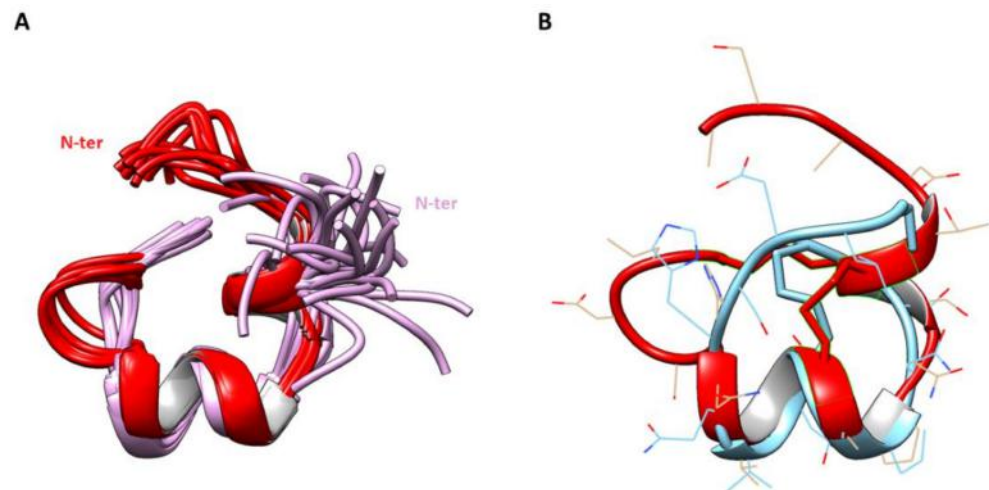


Figure 4. Superposition of CIC with GID and Δ -CIC. (A). Superimposition of the 20 lowest energy states of CIC (red) and GID (PDB: 1MTQ, mauve) over backbone atoms of residues Cys7-Cys21 (CIC numbering). Only the backbones are represented in ribbon format. (B). Superposition of the lowest energy state of CIC (red) and Δ -CIC (blue) over backbone atoms of residues Cys7-Cys21 (CIC numbering). The backbones are shown in ribbon format and the side-chains in stick format.

In addition to its N-terminal tail, α -CIC displays high sequence similarity to α -conotoxin MII, including the conservation of some critical residues (Figure 1A) that have been described to be responsible for its low nanomolar activity at $\alpha 3\beta 2^*$ and $\alpha 7$ nAChRs [14,16,19]. Everhart et al. [18] performed an Ala-scan of α -conotoxin MII and showed that Asn5, Pro6 and His12 play a major role in α -conotoxin binding, probably via Asn5 and His12 electrostatic interactions with $\beta 2E61$ and $\beta 2D169$, as suggested by molecular modeling. Despite displaying all the sequence features required for the inhibitory potency and high sequence similarity with α -conotoxin MII, CIC and Δ -CIC were found to be ~ 1000 -fold less potent at $\alpha 3\beta 2$ and $\alpha 6/\alpha 3\beta 2\beta 3$ nAChRs than MII (Table 1). This potency drop most likely arises from slight structural differences between MII and CIC/ Δ -CIC that weaken and/or prevent the critical interactions between the toxin and the nAChRs. To further assess the potency and selectivity profile of CIC and Δ -CIC, we have tested them at other common nAChR subunit combinations such as rat $\alpha 4\beta 4$, $\alpha 3\beta 4$, $\alpha 2\beta 2$, $\alpha 2\beta 4$ and $(\alpha 1)2\beta 1\delta\gamma$ subtypes as well as the human $\alpha 9\alpha 10$ subtype. Interestingly, no inhibition was detected at any of these receptors at concentrations up to 10 μ M, highlighting the high selectivity profile of CIC and Δ -CIC for $\alpha 3\beta 2$ and $\alpha 6/\alpha 3\beta 2\beta 3$ nAChRs. Moreover, our result suggests that there is no influence of the N-terminal tail on the activity at $\alpha 3\beta 2$ and $\alpha 6/\alpha 3\beta 2\beta 3$ nAChRs since CIC and Δ -CIC display quasi-similar inhibition constants (Table 1, Figure 2). Thus, we suggest that the N-terminal tail could serve as a chemical platform for bioconjugation and that CIC bioconjugates could be developed into valuable pharmacological tools to probe $\alpha 3\beta 2^*$ nAChRs.

While the N-terminal tail has no influence on CIC potency, it clearly plays two major roles at the structural level: (i) decrease of flexibility and (ii) stabilization of secondary structure. Indeed, Figure 3 clearly shows that the NMR structure of Δ -CIC is less defined

than that of CIC, as highlighted by the RMSD values (Table 2). Moreover, the N-terminal tail is associated with an additional 3^{10} helix from residues Thr6 to Ser9, which contains the first two cysteine residues. This result suggests that the N-terminal tail of CIC plays a major role in the stabilization of the global structure. Additionally, the superposition of CIC and Δ -CIC reveals a major structural deviation of Δ -CIC (compared to CIC) in the C-terminal region (Figure 4B). Whereas the calculated RMSD value is 0.88 Å from residues Cys7 to Gln14 (CIC numbering), this value greatly increases to 6.29 Å from residues Cys7 to Cys21, i.e., when the C-terminal region is included. Interestingly, the C-terminal region is not only less structured but is in a different orientation compared to CIC, which could be attributed to the absence of the additional first helix (residues Thr6-Ser9), forcing the CysII-CysIV bridge into a different position compared to the CIC conotoxin.

Overall, the role of the N-terminal tail in α -conotoxins remains poorly understood. During the writing of this article, a new conotoxin, P1168, was identified in the transcriptome of *Conus planorbis*, which shows an unusual 4/8 loop framework. P1168 also displays an extended N-terminal tail comprising five amino acids but did not show inhibitory potency on a range of nAChRs, Ca^{2+} and Na^{+} channels [20]. It cannot be excluded that these N-terminally extended conotoxins (P1168 and CIC) target a different class of receptors or that they are designed to be effective on cone snail prey receptors, which likely display structural differences to mammalian receptors.

4. Materials and Methods

4.1. Abbreviations

ACh, Acetylcholine; AcM, acetamidomethyl; ACN, acetonitrile; Boc, tert-butoxycarbonyl; DCM, dichloromethane; DIPEA, diisopropylethylamine; DMF, N,N'-dimethylformamide; DTP, 2,2'-dithiopyridine; ESI-MS, electrospray ionization mass spectrometry; Fmoc, fluorenylmethoxycarbonyl; HATU, 1[Bis(dimethylamino)methylene]-1H-1,2,3-triazolo[4,5-b]pyridinium 3-oxid hexafluorophosphate; LC/MS, liquid chromatography/mass spectrometry; MeOH, methanol; nAChR, nicotinic acetylcholine receptor; NMR, nuclear magnetic resonance; Pbf, pentamethyl-dihydrobenzofuran-5-sulfonyl; RP-HPLC, reversed-phase high performance liquid chromatography; SPPS, solid-phase peptide synthesis; t-Bu, tert-butyl; TFA, trifluoroacetic acid; TIS, triisopropylsilane; Tris, 2-Amino-2-(hydroxymethyl)propane-1,3-diol; Trt, trityl; UV, ultra-violet.

4.2. Chemical Synthesis

DMF, DIPEA, ACN, TIS, TFA, piperidine and all other reagents were obtained from Sigma-Aldrich (Saint-Louis, MI, USA) or Merck (Darmstadt, Germany) and were used as supplied. Fmoc (L) amino acid derivatives and HATU were purchased from Iris Biotech (Marktredwitz, Germany). PS-2-Chlorotriyl chloride resin (100-200 mesh, 1.6 mmol/g) was purchased from Iris Biotech (Marktredwitz, Germany). The following side-chain protecting groups were used: Trt for Asn, II-IV Cys, His and Gln; tBu for Ser, Thr and Asp; and AcM for I-III Cys. Peptides were manually synthesized using the Fmoc-based solid-phase peptide synthesis technique as already described elsewhere [15]. All Fmoc amino acids and HATU were dissolved in DMF to reach 0.5 M. The first amino acid was coupled onto the resin for 6 h in a 1/1 (v/v) mix of DMF and DCM, with a 2.5-fold excess of amino acid and 5-fold excess of DIPEA followed by addition of methanol and further mixing for 15 min to cap any remaining reactive functionalities on the resin. The resin was washed with DMF, DCM, MeOH, and DMF. Fmoc deprotection was carried out with piperidine in DMF (1/2 v/v) twice for 3 min. Subsequent amino acids were coupled onto 0.1 mmol of prepared resin (determined loading value 0.73 mmol/g) twice for 10 min using an amino acid/HATU/DIPEA ratio of 5:5:10 relative to resin loading. DMF was used for resin washing between deprotection and coupling steps. After chain assembly was complete, the terminal Fmoc group was removed and the resin washed with DMF and DCM. Side-chain (except AcM) deprotection and cleavage from the resin was carried out by adding 10 mL of TFA/TIS/ H_2O (95/2.5/2.5 v/v/v) and stirring the mixture for

2.5 h at room temperature. Crude peptides were purified by preparative RP-HPLC and pure fractions were combined and freeze-dried. A two-step oxidation procedure was then carried out. The first disulfide bridge was formed between the free cysteine residues CysII-CysIV by dissolving the peptide at 0.2 mM in 50 mM Tris-HCl buffer adjusted to pH 8 and adding dropwise 7 equivalents of DTP at 10 mM in MeOH. When the reaction was complete, the reaction mixture was acidified to pH 3 and loaded onto preparative RP-HPLC and pure fractions were combined. The second disulfide bridge (CysI-CysIII) was formed by deprotection/oxidation of the Acm protecting group directly on the combined pure fractions of the mono-bridged intermediates by treatment with 20 equivalents of 10 mM iodine in H₂O/TFA/ACN (78/2/20 *v/v/v*). When the reaction was complete, the reaction mixture was quenched with 20 mM ascorbic acid until total discoloration of the solution, acidified and purified by preparative RP-HPLC. The combined pure fractions were freeze-dried, and their purity was confirmed by LC/ESI-MS. CIC and Δ -CIC peptides were obtained with 3.2 and 3.1% yields (from resin loading), respectively (purity >95% estimated from LC/ESI-MS). The peptide content was estimated (from amino acid analysis) at 60% from dry weight.

4.3. Mass Spectrometry

4.3.1. Solvents Used for LC/MS Were of HPLC Grade

Intermediate peptides were characterized using an LC/MS system consisting of an Alliance 2695 HPLC coupled to a ZQ mass spectrometer (Waters, Corp., Milford, MA, USA) fitted with an electrospray ionization source operated in the positive mode (ESI+) and a quadrupole mass analyzer. All the analyses were carried out using a Chromolith (Fontenay sous Bois, France) HighResolution RP-18e (4.6 × 25 mm, 15 nm pore, 1.15 μ m particle size, flow rate 3.0 mL/min) column. A flow rate of 3 mL/min and a gradient of 0–100% B over 2.5 min for routine analyses and 0–30% B over 30 min for quality control of pure products were used. Eluent A was water/0.1% HCO₂H, and eluent B consisted of acetonitrile/0.1% HCO₂H. UV detection was performed at 214 nm. Electrospray mass spectra were acquired at a solvent flow rate of 200 μ L/min. Nitrogen was used for both the nebulizing and drying gas. The data were obtained in a scan mode ranging from 100 to 1000 *m/z* or 250 to 1500 *m/z* in 0.7 s intervals.

Folded peptides were characterized using a Synapt G2-S high-resolution MS system (Waters, Corp., Milford, MA, USA) equipped with an ESI source and a hybrid Q-TOF mass analyzer configuration. Chromatographic separation was carried out at a flow rate of 0.4 mL/min on an Acquity H-Class ultrahigh performance liquid chromatography (UPLC) system (Waters, Corp., Milford, MA, USA) equipped with a Kinetex C18 100 Å column (100 mm × 2.1 mm, 2.6 μ m particle size) from Phenomenex (France). The mobile phase consisted of water (solvent A) and ACN (solvent B) with both phases acidified by 0.1% (*v/v*) formic acid. Mass spectra were acquired in the positive ionization mode.

4.3.2. Preparative RP-HPLC

Preparative RP-HPLC was run on a Gilson PLC 2250 Purification system (Villiers le Bel, France) instrument using a preparative column (Waters DeltaPak C18 Radial-Pak Cartridge, 100 Å, 40 × 100 mm, 15 μ m particle size, flow rate 50.0 mL/min). Buffer A was 0.1% TFA in water, and buffer B was 0.1% TFA in acetonitrile.

4.4. Electrophysiology

Functional experiments were performed as described previously [15]. Briefly, plasmids encoding the respective nAChR subunits (rat α 2, α 3, α 4, α 6, β 2, β 4 nAChRs provided by Jim Patrick (Baylor College of Medicine, Houston, TX, USA) and subcloned in pNKS2; rat α 1, β 1, γ , δ in pSPOoD provided by Veit Witzemann (MPI for Medical Research, Heidelberg, Germany); human α 9 and α 10 in pT7TS provided by David Adams (Illawara Health and Medical Research Institute, Wollongong University, Wollongong, Australia); α 6/ α 3 chimera generated in pNKS [15,16,21] were linearized and cRNA synthesized using

the mMessageMachine kit (Invitrogen, ThermoFisher Scientific, Waltham, MA, USA). Fifty nanoliters of cRNA (0.1–0.5 $\mu\text{g}/\mu\text{L}$) was injected per oocyte (EcoCyte Bioscience (Dortmund, Germany) or a gift from Prof. Luis Pardo (MPI of Experimental Medicine, Göttingen, Germany) with a subunit ratio of 1:1 for $\alpha 3\beta 2$, $\alpha 3\beta 4$, $\alpha 2\beta 2$, $\alpha 2\beta 4$, $\alpha 4\beta 4$, 5:1 for $\alpha 4\beta 2$, 3:1 for $\alpha 9\beta 10$ and 1:1:1 for $\alpha 6/ \alpha 3\beta 2\beta 3$. Oocytes were stored at 16 °C in sterile-filtered ND96 containing 5 $\mu\text{g}/\text{ml}$ gentamicin.

After 1–4 days, two-electrode voltage clamp recordings were performed at -70 mV with a Turbo Tec 05X Amplifier (npi electronic, Tamm, Germany) and CellWorks software. Electrode resistances were less than 1 M Ω , and currents were filtered at 200 Hz and digitized at 400 Hz. The recording solution (ND115 for $\alpha 9\beta 10$, ND96 in all other cases) with or without ACh was automatically applied via a custom-made magnetic valve system combined with a manifold mounted closely above the oocyte, thus allowing a fast (<300 ms) and reproducible solution exchange. Toxins were applied manually in the 50- μl measuring chamber and preincubated for 3 min. Agonist pulses (2s) were applied in 4-min intervals. Current responses were normalized to control responses before toxin application. GraphPad Prism (version 9.0) was used for data analysis, and a four-parameter logistic fit (Hill-fit) with plateaus constrained to 100% and 0% was used to generate dose–response curves. Oocytes from at least two frogs were used for each experiment.

4.5. NMR Structure Determination

NMR spectra were acquired using a Bruker 600 MHz AVANCE III NMR spectrometer (Bruker, Karlsruhe, Germany) equipped with a cryoprobe. Lyophilized synthetic peptides (~1.5–2 mg) were dissolved in 90% H₂O/10% D₂O, and 2D ¹H-¹H TOCSY, ¹H-¹H NOESY, ¹H-¹H DQF-COSY, ¹H-¹⁵N HSQC, and ¹H-¹³C HSQC spectra were recorded using standard Bruker pulse sequences with excitation sculpting for solvent suppression. All spectra were acquired at 290 K with an interscan delay of 1 s. A mixing time of 200–250 ms was used when acquiring NOESY spectra, and isotropic mixing periods of 80 ms for TOCSY spectra. Spectra were processed using Topspin v3.6.1 (Bruker, Billerica, MA, USA) and assigned manually in CcpNmr V2 [22]. An ensemble of structures was calculated using CYANA [23] including torsion-angle restraints generated by TALOS+ [24]. Final structures were visualized using MOLMOL [25] PyMol (The PyMOL Molecular Graphics System, Version 2.0 Schrödinger, LLC., New York, NY, USA) and UCSF Chimera 4.1 [26].

Author Contributions: Conceptualization, J.G. and S.D.; methodology, J.G., Y.H., D.T.W. and N.L.D.; data acquisition, J.G., Y.H. and E.R.J.E.; validation, D.T.W., N.L.D., A.N. and S.D.; formal analysis and data curation, J.G., Y.H., E.R.J.E., N.L.D. and D.T.W.; writing—original draft preparation, J.G.; writing—review and editing, all authors; supervision, D.T.W., N.L.D., A.N., C.E. and S.D. All authors have read and agreed to the published version of the manuscript.

Funding: This work received financial support from the French Ministry of Higher Education, Research and Innovation (PhD scholarship to J.G.) and a grant from the German Research Foundation (DFG, Research Training Group GRK 2338, P01) to A.N. The James Cook University NMR facility was partially funded by the Australian Research Council (LE160100218). This project was supported by an AITHM Capacity Building Grant (D.W.). The Northcote Trust supports E.R.J.E. with a Northcote Graduate Scholarship.

Data Availability Statement: The structures presented in this paper have all been deposited in the Protein Data Bank (PDB) and Biological Magnetic Resonance Bank (BMRB) with the following codes: CIC (PDB: 7LQR) and (BMRB: 30859); Δ -CIC (PDB: 7LQS) and (BMRB: 30860). All remaining data are contained within the article.

Acknowledgments: We thank Fiona Mandausch and Pranavkumar Shadamarsan for assistance and Han Shen Tae and David Adams (Illawarra Health and Medical Research Institute, Wollongong University, Australia) for providing nAChR cDNAs.

Conflicts of Interest: The authors declare no conflict of interest.

References

1. Giribaldi, J.; Dutertre, S. α -Conotoxins to explore the molecular, physiological and pathophysiological functions of neuronal nicotinic acetylcholine receptors. *Neurosci. Lett.* **2018**, *679*, 24–34. [[CrossRef](#)]
2. Puillandre, N.; Duda, T.F.; Meyer, C.P.; Olivera, B.M.; Bouchet, P. One, four or 100 genera? A new classification of the cone snails. *J. Molluscan Stud.* **2015**, *81*, 1–23. [[CrossRef](#)] [[PubMed](#)]
3. Dutertre, S.; Jin, A.-H.; Vetter, I.; Hamilton, B.; Sunagar, K.; Laverigne, V.; Dutertre, V.; Fry, B.G.; Antunes, A.; Venter, D.J.; et al. Evolution of separate predation- and defence-evoked venoms in carnivorous cone snails. *Nat. Commun.* **2014**, *5*, 3521. [[CrossRef](#)] [[PubMed](#)]
4. Davis, J.; Jones, A.; Lewis, R.J. Remarkable inter- and intra-species complexity of conotoxins revealed by LC/MS. *Peptides* **2009**, *30*, 1222–1227. [[CrossRef](#)] [[PubMed](#)]
5. Akondi, K.B.; Muttenthaler, M.; Dutertre, S.; Kaas, Q.; Craik, D.J.; Lewis, R.J.; Alewood, P.F. Discovery, Synthesis, and Structure–Activity Relationships of Conotoxins. *Chem. Rev.* **2014**, *114*, 5815–5847. [[CrossRef](#)] [[PubMed](#)]
6. Lewis, R.J.; Garcia, M.L. Therapeutic potential of venom peptides. *Nat. Rev. Drug Discov.* **2003**, *2*, 790–802. [[CrossRef](#)] [[PubMed](#)]
7. El Hamdaoui, Y.; Wu, X.; Clark, R.J.; Giribaldi, J.; Anangi, R.; Craik, D.J.; King, G.F.; Dutertre, S.; Kaas, Q.; Herzig, V.; et al. Periplasmic Expression of 4/7 α -Conotoxin TxIA Analogs in *E. coli* Favors Ribbon Isomer Formation—Suggestion of a Binding Mode at the $\alpha 7$ nAChR. *Front. Pharmacol.* **2019**, *10*, 577. [[CrossRef](#)]
8. Kaas, Q.; Westermann, J.-C.; Halai, R.; Wang, C.K.L.; Craik, D.J. ConoServer, a database for conopeptide sequences and structures. *Bioinformatics* **2008**, *24*, 445–446. [[CrossRef](#)]
9. Kaas, Q.; Yu, R.; Jin, A.-H.; Dutertre, S.; Craik, D.J. ConoServer: Updated content, knowledge, and discovery tools in the conopeptide database. *Nucleic Acids Res.* **2011**, *40*, D325–D330. [[CrossRef](#)]
10. Nicke, A.; Loughnan, M.L.; Millard, E.L.; Alewood, P.F.; Adams, D.J.; Daly, N.L.; Craik, D.J.; Lewis, R.J. Isolation, Structure, and Activity of GID, a Novel $\alpha 4/7$ -Conotoxin with an Extended N-terminal Sequence. *J. Biol. Chem.* **2003**, *278*, 3137–3144. [[CrossRef](#)] [[PubMed](#)]
11. Cordero-Erausquin, M.; Marubio, L.M.; Klink, R.; Changeux, J.-P. Nicotinic receptor function: New perspectives from knockout mice. *Trends Pharmacol. Sci.* **2000**, *21*, 211–217. [[CrossRef](#)]
12. Himaya, S.W.A.; Jin, A.-H.; Dutertre, S.; Giacomotto, J.; Mohialdeen, H.; Vetter, I.; Alewood, P.F.; Lewis, R.J. Comparative Venomics Reveals the Complex Prey Capture Strategy of the Piscivorous Cone Snail *Conus catus*. *J. Proteome Res.* **2015**, *14*, 4372–4381. [[CrossRef](#)] [[PubMed](#)]
13. McIntosh, J.M.; Plazas, P.V.; Watkins, M.; Gomez-Casati, M.E.; Olivera, B.M.; Elgoyhen, A.B. A Novel α -Conotoxin, PeIA, Cloned from *Conus pergrandis*, Discriminates between Rat $\alpha 9\alpha 10$ and $\alpha 7$ Nicotinic Cholinergic Receptors. *J. Biol. Chem.* **2005**, *280*, 30107–30112. [[CrossRef](#)] [[PubMed](#)]
14. Cartier, G.E.; Yoshikami, D.; Gray, W.R.; Luo, S.; Olivera, B.M.; McIntosh, J.M. A New α -Conotoxin Which Targets $\alpha 3\beta 2$ Nicotinic Acetylcholine Receptors. *J. Biol. Chem.* **1996**, *271*, 7522–7528. [[CrossRef](#)]
15. Giribaldi, J.; Wilson, D.; Nicke, A.; El Hamdaoui, Y.; Laconde, G.; Faucherre, A.; Moha, O.; Maati, H.; Daly, N.; Enjalbal, C.; et al. Synthesis, Structure and Biological Activity of CIA and CIB, Two α -Conotoxins from the Predation-Evoked Venom of *Conus catus*. *Toxins* **2018**, *10*, 222. [[CrossRef](#)]
16. McIntosh, J.M.; Azam, L.; Staheli, S.; Dowell, C.; Lindstrom, J.M.; Kuryatov, A.; Garrett, J.E.; Marks, M.J.; Whiteaker, P. Analogs of α -Conotoxin MII Are Selective for $\alpha 6$ -Containing Nicotinic Acetylcholine Receptors. *Mol. Pharmacol.* **2004**, *65*, 944–952. [[CrossRef](#)] [[PubMed](#)]
17. Klimis, H.; Adams, D.J.; Callaghan, B.; Nevin, S.; Alewood, P.F.; Vaughan, C.W.; Mozar, C.A.; Christie, M.J. A novel mechanism of inhibition of high-voltage activated calcium channels by α -conotoxins contributes to relief of nerve injury-induced neuropathic pain. *Pain* **2011**, *152*, 259–266. [[CrossRef](#)]
18. Everhart, D.; Cartier, G.E.; Malhotra, A.; Gomes, A.V.; McIntosh, J.M.; Luetje, C.W. Determinants of Potency on α -Conotoxin MII, a Peptide Antagonist of Neuronal Nicotinic Receptors. *Biochemistry* **2004**, *43*, 2732–2737. [[CrossRef](#)] [[PubMed](#)]
19. Dutertre, S.; Nicke, A.; Lewis, R.J. $\beta 2$ Subunit Contribution to 4/7 α -Conotoxin Binding to the Nicotinic Acetylcholine Receptor. *J. Biol. Chem.* **2005**, *280*, 30460–30468. [[CrossRef](#)] [[PubMed](#)]
20. Wilson, D.T.; Bansal, P.S.; Carter, D.A.; Vetter, I.; Nicke, A.; Dutertre, S.; Daly, N.L. Characterisation of a Novel A-Superfamily Conotoxin. *Biomedicines* **2020**, *8*, 128. [[CrossRef](#)]
21. Kuryatov, A.; Olale, F.; Cooper, J.; Choi, C.; Lindström, J. Human $\alpha 6$ AChR subtypes: Subunit composition, assembly, and pharmacological responses. *Neuropharmacology* **2000**, *39*, 2570–2590. [[CrossRef](#)]
22. Skinner, S.P.; Fogh, R.H.; Boucher, W.; Ragan, T.J.; Mureddu, L.G.; Vuister, G.W. CcpNmr AnalysisAssign: A flexible platform for integrated NMR analysis. *J. Biomol. NMR* **2016**, *66*, 111–124. [[CrossRef](#)] [[PubMed](#)]
23. Güntert, P. Automated NMR Structure Calculation with CYANA. In *Protein NMR Techniques*; Humana Press: Totowa, NJ, USA, 2004; pp. 353–378.

24. Shen, Y.; Delaglio, F.; Cornilescu, G.; Bax, A. TALOS+: A hybrid method for predicting protein backbone torsion angles from NMR chemical shifts. *J. Biomol. NMR* **2009**, *44*, 213–223. [[CrossRef](#)] [[PubMed](#)]
25. Koradi, R.; Billeter, M.; Wüthrich, K. MOLMOL: A program for display and analysis of macromolecular structures. *J. Mol. Graph.* **1996**, *14*, 51–55. [[CrossRef](#)]
26. Pettersen, E.F.; Goddard, T.D.; Huang, C.C.; Couch, G.S.; Greenblatt, D.M.; Meng, E.C.; Ferrin, T.E. UCSF Chimera? A visualization system for exploratory research and analysis. *J. Comput. Chem.* **2004**, *25*, 1605–1612. [[CrossRef](#)] [[PubMed](#)]

6. Supplementary A: Publication III

pp. 86 - 97



Interaction of $\alpha 9\alpha 10$ Nicotinic Receptors With Peptides and Proteins From Animal Venoms

Victor Tsetlin¹, Yves Haufe², Valentina Safronova³, Dmitriy Serov³, PranavKumar Shadamarshan², Lina Son¹, Irina Shelukhina¹, Denis Kudryavtsev¹, Elena Kryukova¹, Igor Kasheverov¹, Annette Nicke² and Yuri Utkin^{1*}

¹ Department of Molecular Neuroimmune Signaling, Shemyakin-Ovchinnikov Institute of Bioorganic Chemistry, Russian Academy of Sciences, Moscow, Russia, ² Faculty of Medicine, Walther Straub Institute of Pharmacology and Toxicology, Ludwig-Maximilians-Universität München, Munich, Germany, ³ Laboratory of Cellular Neurobiology, Institute of Cell Biophysics, Russian Academy of Sciences, Pushchino, Russia

OPEN ACCESS

Edited by:

Veronika Grau,
University of Giessen, Germany

Reviewed by:

Katrin Richter,
University of Giessen, Germany
Arik J. Hone,
The University of Utah, United States

*Correspondence:

Yuri Utkin
utkin@ibch.ru;
yutkin@yandex.ru

Specialty section:

This article was submitted to
Cellular Neurophysiology,
a section of the journal
Frontiers in Cellular Neuroscience

Received: 27 August 2021

Accepted: 15 November 2021

Published: 23 December 2021

Citation:

Tsetlin V, Haufe Y, Safronova V, Serov D, Shadamarshan P, Son L, Shelukhina I, Kudryavtsev D, Kryukova E, Kasheverov I, Nicke A and Utkin Y (2021) Interaction of $\alpha 9\alpha 10$ Nicotinic Receptors With Peptides and Proteins From Animal Venoms. *Front. Cell. Neurosci.* 15:765541. doi: 10.3389/fncel.2021.765541

Unlike most neuronal nicotinic acetylcholine receptor (nAChR) subunits, $\alpha 7$, $\alpha 9$, and $\alpha 10$ subunits are able to form functional homo- or heteromeric receptors without any β subunits. While the $\alpha 7$ subtype is widely distributed in the mammalian brain and several peripheral tissues, $\alpha 9$ and $\alpha 9\alpha 10$ nAChRs are mainly found in the cochlea and immune cells. α -Conotoxins that specifically block the $\alpha 9\alpha 10$ receptor showed anti-nociceptive and anti-hyperalgesic effects in animal models. Hence, this subtype is considered a drug target for analgesics. In contrast to the $\alpha 9\alpha 10$ -selective α -conotoxins, the three-finger toxin α -bungarotoxin inhibits muscle-type and $\alpha 7$ nAChRs in addition to $\alpha 9\alpha 10$ nAChRs. However, the selectivity of α -neurotoxins at the $\alpha 9\alpha 10$ subtype was less intensively investigated. Here, we compared the potencies of α -conotoxins and α -neurotoxins at the human $\alpha 9\alpha 10$ nAChR by two-electrode voltage clamp analysis upon expression in *Xenopus* oocytes. In addition, we analyzed effects of several $\alpha 9\alpha 10$ -selective α -conotoxins on mouse granulocytes from bone marrow to identify possible physiological functions of the $\alpha 9\alpha 10$ nAChR subtype in these cells. The α -conotoxin-induced IL-10 release was measured upon LPS-stimulation. We found that α -conotoxins RglA, PelA, and Vc1.1 enhance the IL-10 expression in granulocytes which might explain the known anti-inflammatory and associated analgesic activities of $\alpha 9\alpha 10$ -selective α -conotoxins. Furthermore, we show that two long-chain α -neurotoxins from the cobra *Naja melanoleuca* venom that were earlier shown to bind to muscle-type and $\alpha 7$ nAChRs, also inhibit the $\alpha 9\alpha 10$ subtype at nanomolar concentrations with one of them showing a significantly slower dissociation from this receptor than α -bungarotoxin.

Keywords: nicotinic acetylcholine receptor, $\alpha 9\alpha 10$ subtype, *Xenopus laevis* oocytes, α -neurotoxin, α -conotoxin, granulocytes, interleukin-10, inflammation

INTRODUCTION

Nicotinic acetylcholine receptors (nAChRs) consisting of $\alpha 9$ subunits were originally discovered in the hair cells of the inner ear (Elgoyhen et al., 1994) and were found to be involved in hearing. Later, the accessory $\alpha 10$ subunit was identified (Elgoyhen et al., 2001) and both homomeric $\alpha 9$ and heteromeric $\alpha 9\alpha 10$ assemblies were found to form functional nAChRs receptors. The

$\alpha 9\alpha 10$ nAChR is distinguished from other members of the nAChR family by its sensitivity to several ligands of muscarinic AChRs and agonists of other Cys-loop receptors, such as type A γ -aminobutyric acid (GABA_A), glycine, and 5-hydroxytryptamine type 3 (5-HT₃) receptors (Rothlin et al., 1999). Moreover, typical nAChR agonists (nicotine and epibatidine) act as antagonists at $\alpha 9$ (Verbitsky et al., 2000) and $\alpha 9\alpha 10$ receptors (Moglie et al., 2021).

$\alpha 9\alpha 10$ nAChRs have also been found in a number of immune cells (Peng et al., 2004; Galvis et al., 2006; Grau et al., 2019) where they have been involved in the modulation of pain signals and regulation of inflammatory processes (McIntosh et al., 2009; Grau et al., 2019). Together with a proposed role in cancer development (Sun et al., 2020a) this makes them promising targets for drug development with an emphasis on inhibitory ligands.

Well-recognized tools in nAChR research are snake venom α -neurotoxins which are classified into short-chain and long-chain ones (Barber et al., 2013). Short-chain α -neurotoxins comprising 60–62 amino acids residues and four disulfide bridges inhibit muscle-type nAChRs with high selectivity. Long-chain α -neurotoxins containing 66–75 amino acid residues and five disulfide bridges additionally block $\alpha 7$ nAChRs and, moreover, also inhibit $\alpha 9\alpha 10$ nAChRs (Elgoyhen et al., 2001; Chandna et al., 2019) and thus must be considered rather non-selective. In contrast, α -conotoxins, small neurotoxic peptides from venomous *Conus* marine mollusks, are much more selective. They not only allow to distinguish the muscle-type nAChRs from the neuronal ones, but provide markers for individual neuronal subtypes (Ellison et al., 2006; Vincler et al., 2006; Dutertre et al., 2017; Ho et al., 2020). In particular, the naturally occurring α -conotoxins Vc1.1 and RgIA as well as the α O-conotoxin GeXIVA (and their derivatives) show high affinity for $\alpha 9\alpha 10$ nAChRs and have been investigated in models of neuropathic pain (Luo et al., 2015; Huynh et al., 2020; Sun et al., 2020b).

At the Shemyakin-Ovchinnikov Institute of Bioorganic Chemistry in collaborations with several other laboratories, snake-venom α -neurotoxins, and peptides, as well as synthetic α -conotoxins are applied to investigate the structure and function of nAChRs, with a focus on the muscle-type and $\alpha 7$ nAChRs (Tsetlin, 2015; Dutertre et al., 2017; Tsetlin et al., 2021). We have recently published the synthesis of oligoarginine inhibitors of the $\alpha 9\alpha 10$ nAChRs (Lebedev et al., 2019), and analyzed the interaction of α O-conotoxin GeXIVA with the acetylcholine-binding protein (AChBP) and with the soluble ligand-binding domain (LBD) of the $\alpha 9$ subunit (Kryukova et al., 2018). In collaboration with crystallographers from Hellenic Pasteur Institute (Athens, Greece), we contributed to the determination of the X-ray structure of α -conotoxin RgIA in complex with the LBD of the $\alpha 9$ subunit (Zouridakis et al., 2019). We further found that α -conotoxins RgIA and Vc1.1 influence cytosolic Ca²⁺ concentration, cell adhesion, and generation of reactive oxygen species in murine bone marrow granulocytes (Safronova et al., 2021). In this special issue on the $\alpha 9\alpha 10$ nAChR subtype, we will briefly discuss these findings and (1) report the selectivity and potency of novel α -neurotoxins from *Naja melanoleuca* snake venom at human $\alpha 9\alpha 10$ nAChRs and (2) present new data

showing that $\alpha 9\alpha 10$ -selective α -conotoxins potentiate release of the anti-inflammatory cytokine interleukin-10 (IL-10) from murine granulocytes.

MATERIALS AND METHODS

Materials

Percoll, trypan blue, lipopolysaccharide from *E. coli* O55:B51 were purchased from Sigma-Aldrich (St. Louis, United States). PE-anti-mouse Ly-6G/Ly-6C antibody, RB6-8C5 clone was from BioLegend (San-Diego, United States). DMEM, fetal bovine serum (FBS), L-glutamine, penicillin, streptomycin, amphotericin B were from Gibco (United States). Nicotine bitartrate and acetylcholine chloride (ACh) were purchased from Sigma-Aldrich (St. Louis, United States). Chemicals for oocyte buffers and electrophysiology were purchased from Carl Roth (Karlsruhe, Germany), except for BAPTA-AM [1,2-bis(o-Aminophenoxy)ethane-N,N,N',N'-tetraacetic Acid Tetra(acetoxymethyl) Ester] which was purchased from Calbiochem (Merck KGaA, Darmstadt, Germany).

The synthesis of α -conotoxins MII, RgIA, and Vc1.1 was described in Safronova et al. (2021), GeXIVA and PeIA in Kryukova et al. (2018). α -Neurotoxins were isolated from snake venoms: long-chain Tx-NM2 and Tx-NM3-1 from *N. melanoleuca* venom (Son et al., 2021); long-chain neurotoxin I (NT I) and short-chain neurotoxin II (NT II) from *N. oxiana* and α -bungarotoxin (α -Btx) from *Bungarus multicinctus* (Kudryavtsev et al., 2015); non-conventional WTX and long-chain α -cobratoxin (α -Ctx) from *N. kaouthia* (Utkin et al., 2001; Osipov et al., 2008, respectively). Peptide neurotoxin azemiopsin (AZE) was synthesized as described (Utkin et al., 2012).

Nicotinic Acetylcholine Receptor, cDNAs, RNA Preparation, and Oocyte Injection

The human $\alpha 3$ (GenBank: U62432.1), $\alpha 4$ (GenBank: L35901.1, with silent base exchanges to reduce GC content), $\beta 2$ (GenBank: X53179.1), and $\beta 4$ (GenBank: U48861.1) nAChR subunits were synthesized (FragmentGene service, Genewiz) and cloned into the pNKS2 vector (Gloor et al., 1995) by Gibson assembly. cDNAs of human $\alpha 7$ in pMXT and $\alpha 9$ and $\alpha 10$ in pT7TS vectors were a gift from David Adams (Illawara Health and Medical Research Institute, Wollongong University, Australia). cRNA was synthesized from linearized plasmids using the SP6 mMessageMachine kit (Invitrogen, Thermo Fisher Scientific, United States). *Xenopus laevis* females were obtained from Nasco (Fort Atkinson, WI, United States) and kept at the core facility animal models (CAM) of the biomedical center (BMC) of LMU Munich, Germany (Az:4.3.2-5682/LMU/BMC/CAM) in accordance with the EU Animal Welfare Act. To obtain oocytes, frogs were killed with an overdose of MS222. Death was confirmed by cardiac puncture/exsanguination. Oocytes were extracted and injected with 50-nl aliquots of cRNA (0.75 μ g/ μ l, $\alpha 9\alpha 10$ in 3:1 subunit ratio, all other cRNAs with 0.5 μ g/ μ l and the indicated α : β ratios), and kept at 16°C in sterile-filtered ND96 (96 mM NaCl, 2 mM KCl, 1 mM CaCl₂, 1 mM MgCl₂, 5 mM HEPES, pH 7.4) containing 5 μ g/ml gentamicin.

Electrophysiological Recordings and Data Analysis

Two-electrode voltage clamp (TEVC) recordings were performed 3 days after cRNA injection at a holding potential of -70 mV. $\alpha 9\alpha 10$ -expressing oocytes were incubated for 2–4 h in 30–100 mM BAPTA prior to recordings to obtain stable current responses. Pipettes (resistances < 1 M Ω) were pulled from borosilicate glass and filled with 3 M KCl. Membrane currents were recorded with a Turbo Tec 05X amplifier (npi electronic, Tamm, Germany), filtered at 200 Hz, and digitized at 400 Hz using CellWorks software. For $\alpha 9\alpha 10$ recordings, the perfusion medium was automatically switched between ND115 recording solution (115 mM NaCl, 2.5 mM KCl, 1.8 mM CaCl₂, 10 mM HEPES, pH 7.4) with or without agonist (40 μ M ACh) using a custom-made magnetic valve system as described in Giribaldi et al. (2020). Briefly, ACh pulses were applied for 2 s at 4-min intervals. After each agonist application, cells were superfused for 54 s with ND115, followed by a 3 min interval with no perfusion during which the toxin was mixed from a 10-fold stock into the static bath. Toxins were applied when responses to three consecutive agonist applications differed by less than 10%. ACh-evoked responses following toxin incubation were normalized to the ACh responses before toxin exposure. Data were analyzed with GraphPad Prism version 9 (GraphPad Prism, RRID: SCR_002798). Dose-response curves were fit to the data using the Hill equation: % response = Bottom + (Top-Bottom)/[1 + 10^{-(LogIC₅₀-X) × Hill Slope}] and constraints of 100 and 0% for Top and Bottom, respectively. Dissociation curves were fit to the data with the equation: % response = [response (time 0) – plateau] × exp(-K × time) + plateau. Recordings for all other subtypes were performed in ND96 recording solution (96 mM NaCl, 2 mM KCl, 1 mM CaCl₂, 1 mM MgCl₂, 5 mM HEPES, pH 7.4) using the same protocol. BAPTA-AM was not well tolerated by the oocytes and a baseline correction was applied to compensate for baseline shifts in repetitive measurements. Recordings were denoised using a 20 Hz Gaussian lowpass filter. All measurements were performed with oocytes from at least two different frogs.

Animals

BALB/c male mice (21–23 g of weight) were obtained from the Branch “Stolbovaya” of the Scientific Biomedical Technology Centre of the Federal Medico-Biological Agency (Moscow region, Russia). The ethical protocol No. 2019/5 based on the Manual for Working with Laboratory Animals No. 57 (30.12.2011) of the Institute of Cell Biophysics of the Russian Academy of Sciences (Pushchino, Russia) was applied for all manipulations with animals.

Granulocyte Isolation

Polymorphonuclear neutrophilic granulocytes (PMNs) were isolated from murine bone marrow using the previously described method (Safronova et al., 2021). Shortly, a cell suspension was obtained after washing out murine femur, tibia, and humerus with cold RPMI-1640 medium and layered on a Percoll gradient (78, 62.5, and 55% in PBS). After centrifugation

(1,500 × g, 35 min, 4°C), cells were collected between the 78 and 62.5% layers and washed thrice with RPMI-1640 medium. PMNs accounted for nearly 90% of the isolated cell population as estimated by expression of granulocyte maturity marker Gr-1 using the PE-anti-mouse Ly-6G/Ly-6C antibody (RB6-8C5 clone) for FACS analysis (EPICS XL-MCL, Beckman Coulter, United States). The cell survival was 98% as determined by trypan blue staining. PMNs were used in the experiment after 1 h resting at 4°C.

Enzyme-Linked Immunosorbent Assay for IL-10

In each well of a 48-well plate, 600 μ l of culture medium (DMEM, 10% FBS, 2 mM L-glutamine, 100 units/ml penicillin, 100 μ g/ml streptomycin, and 250 ng/ml amphotericin B) were added. 1.2×10^6 cells were added in each well and incubated for 20 min at 37°C in a CO₂-incubator (Sanyo, Japan). After cell adhesion, LPS from *E. coli* (O55:B5, 10 ng/ml final concentration) was added or not (control) followed by 30 min incubation at 37°C. Then 100 μ M nicotine or one of the α -conotoxins (200 nM MII, 10 nM RgIA, 25 nM Vc1.1, 10 nM PeIA, or 10 nM GeXIVA) were added to the LPS-treated cells and cells were incubated for 23 h. The total volume of each sample was 612 μ l. All incubations were carried out in a CO₂-incubator (5% CO₂, 37°C, 100% humidity). Afterward, the supernatants from each well were collected into individual reaction tubes (Eppendorf, Germany) and centrifuged (2,000 × g, 10 min, 4°C). Measurement of IL-10 concentrations was carried out using a mouse IL-10 ELISA kit (ab108870, Abcam, United Kingdom) according to the manufacturer’s protocol for which the minimum detectable dose of IL-10 is typically ~ 14 pg/ml. Optical density of the samples was measured with an Infinity F50 microplate photometer (Tecan, Grödig, Austria). IL-10 concentrations were calculated using the calibration curve in the range of 7–125 pg/ml obtained with the provided IL-10 standards.

Statistical Analysis for Granulocyte Assay

Experiments were performed in duplicates on the cells from 9 to 12 animals. MATLAB software (MATHWORK INC., United States) was used for data analysis. The Kruskal-Wallis One Way Analysis of Variance on Ranks was used for multiple comparisons. Further the Mann-Whitney Rank Sum Test was applied to reveal significant differences between “LPS” and “LPS + any nAChR ligand” groups based on the fact that measurement of each sample was carried out independently. The average values and SEM were calculated for each of the experimental data.

RESULTS

Testing Effects of α -Conotoxins on IL-10 Release From Mouse Granulocytes

mRNA for the $\alpha 9$ nAChR subunit was previously detected in BM-PMNs (St-Pierre et al., 2016) and recently confirmed

by us (Safronova et al., 2021). In addition, we identified for the first time mRNA of the $\alpha 10$ subunit in these cells (Safronova et al., 2021). In support of a functional role of the $\alpha 9$ and/or $\alpha 9\alpha 10$ nAChRs in BM-PMNs, we showed that α -conotoxins RgIA and Vc1.1 induced Ca^{2+} transients, enhanced cell adhesiveness and decreased production of reactive oxygen species in these cells (Safronova et al., 2021). To further investigate the physiological roles of $\alpha 9\alpha 10$ nAChRs and a possible involvement in inflammation, we investigated in the present study the influence of the specific $\alpha 9/\alpha 10$ antagonists on IL-10 release by LPS-stimulated BM-PMNs, an *in vitro* model of inflammation.

As seen in **Figure 1**, nicotine (100 μ M) application in addition to LPS did not change the release of IL-10 and addition of 200 nM α -conotoxin MII (employed as a control for $\alpha 3^*$, $\alpha 6^*$, and $\alpha 7$ nAChRs) did not influence significantly the IL-10 level. These results indicate that MII-sensitive $\alpha 3^*$, $\alpha 6^*$, and $\alpha 7$ nAChR subtypes are not involved in IL-10 release. Interestingly, application of α -conotoxin RgIA (10 nM) resulted in nearly threefold increased IL-10 release, while it increased almost 6 times in the presence of α -conotoxins Vc1.1 (25 nM) or PeIA (10 nM). Application of α -conotoxin GeXIVA (10 nM) showed a tendency to increase the cytokine IL-10 release, but a statistically significant effect was not achieved. Although the minimum detectable concentration of IL-10 for the Abcam kit is typically ~ 14 pg/ml, using our standard calibration curve we detected as low IL-10 concentration as 7 pg/ml. This kit was also used before for the measurement of fairly low IL-10 concentrations: 5–20 pg/ml (Khezri et al., 2019), 10–13 pg/ml (Zhang et al., 2019; Ai

et al., 2020), and 10–38 pg/ml (Monga et al., 2019). It should be mentioned that the concentrations of IL-10 detected in the presence of α -conotoxins Vc1.1 and PeIA (**Figure 1**) exceeded the minimum detectable concentration of the Abcam kit. The concentrations for α -conotoxins RgIA, GeXIVA, PeIA, and Vc1.1 were chosen around their IC_{50} values at the $\alpha 9\alpha 10$ nAChR (McIntosh et al., 2005; Vincler et al., 2006; Ellison et al., 2008; Luo et al., 2015). Together, the results suggest that $\alpha 9$ -containing nAChRs, that may be activated by endogenous ACh secreted by cells into the culture media, prevent IL-10 release.

IL-10 induces analgesic and anti-inflammatory activity (Saadane et al., 2005; da Silva et al., 2015). The increased IL-10 production in our experiments therefore provides a possible mechanism how α -conotoxins (RgIA, Vc1.1, and PeIA) *via* blockade of $\alpha 9$ and/or $\alpha 9\alpha 10$ nAChRs could exert protective effects against pain and progression of inflammation.

Potencies of Snake Venom Neurotoxins at the Human $\alpha 9\alpha 10$ Nicotinic Acetylcholine Receptor

As mentioned above, $\alpha 9\alpha 10$ nAChRs show unusual pharmacological properties in comparison to other nAChRs and represent potential drug targets. The snake venom toxins α -Btx and α -Ctx have been shown to inhibit rat $\alpha 9$ nAChRs (Elgoyhen et al., 1994) and human $\alpha 9\alpha 10$ (Chandna et al., 2019) in addition to $\alpha 7$ and muscle type receptors. To further evaluate the potential of snake venom toxins as $\alpha 9\alpha 10$ ligands, we compared the potency and subtype selectivity of the long-chain α -neurotoxins

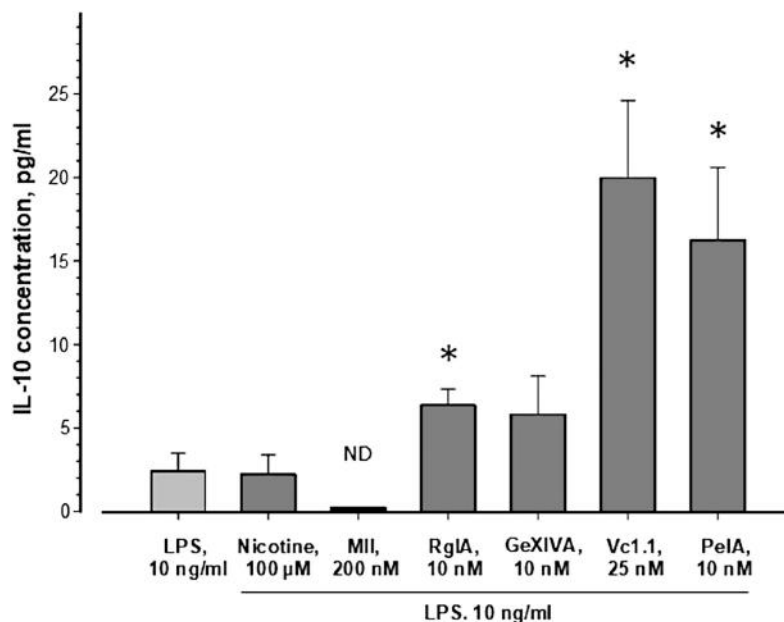


FIGURE 1 | Influence of nAChR ligands on the release of IL-10 from murine bone marrow granulocytes. Cells were incubated in a medium containing 10 ng/ml lipopolysaccharide from *E. coli* without or with nicotine or α -conotoxins, as indicated. IL-10 concentrations were measured in supernatants after 23 h of cell incubation using a mouse IL-10 ELISA kit (ab108870, Abcam, United Kingdom). The average values \pm SEM of 9–12 independent measurements, each performed in duplicates, are shown. The Kruskal-Wallis One Way Analysis of Variance on Ranks and the Mann-Whitney Rank Sum Test were used. ND, not detectable; * $p < 0.05$ compared to the cells treated with LPS only.

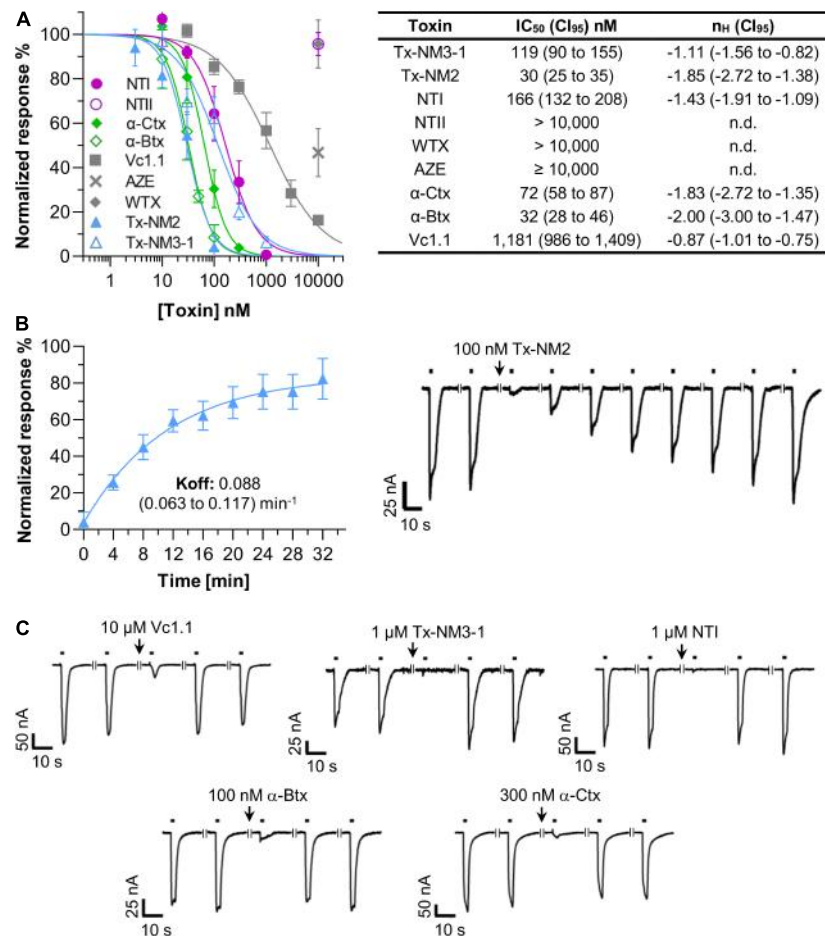


FIGURE 2 | Potencies of snake toxins at the *Xenopus laevis* oocyte-expressed human $\alpha 9\alpha 10$ nicotinic acetylcholine receptor (nAChR). **(A)** Dose-Response curves and half-maximal inhibitory concentrations (IC₅₀) values of the indicated toxins. Responses to 2 s pulses of 40 μ M acetylcholine (ACh) were measured at a potential of -70 mV. Toxins were pre-incubated for 3 min in a static bath. nH: Hill-slope. 95% confidence intervals (Cl₉₅) are given in parenthesis. Note that the high values of the Hill coefficients suggest that a 3 min pre-incubation with the toxins is insufficient for complete binding and IC₅₀ values might therefore be underestimated (compare **Supplementary Figure 1**). However, for practical reasons (decreasing stability of oocytes in the static bath, need of large toxin amounts in case of superfusion), all measurements were performed after 3 min pre-incubation. **(B)** Recovery of $\alpha 9\alpha 10$ current responses after a block induced by 100 nM Tx-NM2. Representative current traces are shown. Black bars indicate application of 40 μ M ACh. Interruptions in the traces indicate a 4 min interval. **(C)** Representative current traces showing the fast dissociation of the indicated toxins from the $\alpha 9\alpha 10$ nAChR. Recording conditions are as in **(B)**. Each point represents the mean of 3–5 measurements from different oocytes of least two different frogs. Error bars represent the standard deviation (S.D.).

Tx-NM2, Tx-NM3-1, NT I, the short-chain α -neurotoxin NT II, the non-conventional neurotoxin WTX, and the linear peptide AZE on the human $\alpha 9\alpha 10$ nAChRs expressed in *X. laevis* oocytes.

All experiments were performed with an injected $\alpha 9:\alpha 10$ cRNA ratio of 3:1 as this resulted in most robust current responses. To validate our recordings conditions, we first used α -conotoxin Vc1.1 as a positive control. **Figure 2A** shows that the ACh-activated currents were efficiently inhibited by α -conotoxin Vc1.1 with an IC₅₀ value of 1.18 μ M, very similar to previously described values (Yu et al., 2013, 2018).

Using the same protocol, we next determined the IC₅₀ values of the snake toxins at the $\alpha 9\alpha 10$ nAChR subtype. **Figure 2A** shows that the long-chain α -neurotoxins from *N. melanoleuca* (Tx-NM2 and Tx-NM3) inhibited this receptor with potencies close to those of α -Btx (IC₅₀ 32 nM) and α -Ctx (72 nM).

Interestingly, the most potent toxin Tx-NM2 (IC₅₀ 30 nM) needed 30 min to fully dissociate from the receptor (**Figure 2B**). In contrast, all other toxins tested in this study, including α -Btx and α -Ctx, allowed full recovery of the ACh responses within 4 min (**Figure 2C**).

A somewhat weaker potency was found for the long-chain α -neurotoxin NT I from the *N. oxiana* venom (IC₅₀ 166 nM, **Figure 2**). In contrast, the short-chain α -neurotoxin NT II from this species failed to inhibit the $\alpha 9\alpha 10$ nAChR at concentrations up to 10 μ M. All short-chain α -neurotoxins including NT II were previously found to lack affinity to the $\alpha 7$ nAChR but their possible effect at the $\alpha 9\alpha 10$ nAChR was not analyzed before. The non-conventional neurotoxin WTX from *Naja kaouthia*, which at micromolar concentrations binds to both the muscle-type and $\alpha 7$ nAChRs (Utkin et al., 2001), also did not affect $\alpha 9\alpha 10$ currents.

TABLE 1 | Normalized responses of human nAChR subtypes to the indicated acetylcholine (ACh) concentration after 3 min pre-incubation with 1 μ M of the indicated toxins.

ACh conc.	$\alpha 4\beta 2$ (5:1)	$\alpha 3\beta 2$ (1:1)	$\alpha 2\beta 2$ (1:1)	$\alpha 7$	$(\alpha 1)2\beta 1\epsilon\delta$ (2:1:1:1)
	100 μ M	100 μ M	100 μ M	100 μ M	30 μ M
Tx-NM3-1	80 \pm 6%	67 \pm 6%	96 \pm 2%	2 \pm 2%**	1 \pm 1%*
Tx-NM2	84 \pm 9%	68 \pm 7%	99 \pm 2%	2 \pm 2%**	1 \pm 1%*
WTX	99 \pm 1%	101 \pm 2%	95 \pm 4%	99 \pm 2%	100 \pm 7%
NT I	101 \pm 1%	101 \pm 1%	94 \pm 2%	2 \pm 2%**	2 \pm 3%**
NT II	99 \pm 2%	101 \pm 1%	96 \pm 3%	91 \pm 4%	0 \pm 0%*
AZE	100 \pm 1%	101 \pm 1%	98 \pm 3%	101 \pm 2%	13 \pm 10%

Three recordings were performed on different oocytes from at least two frogs. Mean values with standard deviation (S.D.) are shown. The injected mRNA ratio is given in parenthesis for each nAChR subtype.

* Indicates a slow off-rate of the toxin, ** indicates no off-rate of toxin within 10 min. High potency is highlighted in bold.

AZE (Utkin et al., 2012), a linear peptide from the venom of *Azemiops feae* viper showed only a weak inhibition of about 40% at a concentration of 10 μ M (Figure 2).

To estimate the nAChR subtype selectivities of the above toxins, we next measured their ability to inhibit human $\alpha 7$, $\alpha 2\beta 2$, $\alpha 3\beta 2$, $\alpha 4\beta 2$, and muscle-type nAChRs at 1 μ M concentration. As seen in Table 1, none of the toxins inhibited neuronal $\alpha 2\beta 2$, $\alpha 3\beta 2$, or $\alpha 4\beta 2$ nAChR subtypes. Similar to α -Btx and α -Ctx, the toxins Tx-NM3-1, Tx-NM2, and NT-I, while being most effective against the $\alpha 9\alpha 10$ nAChRs, were also potent inhibitors of $\alpha 7$ and muscle-type receptors, indicating similar binding motives for long-chain α -neurotoxins in these subtypes. The short chain α -neurotoxin NT II and the linear peptide AZE selectively inhibited the muscle-type receptor, as previously reported (Utkin et al., 2001, 2012).

In conclusion, although Tx-NM2 is not selective for the $\alpha 9\alpha 10$ nAChR, it has the highest affinity for this subtype and is the only venom-derived toxin that shows a slow dissociation from this receptor.

DISCUSSION

Research at the Shemyakin-Ovchinnikov Institute originally concentrated on muscle-type and $\alpha 7$ nAChRs but recently focused also on $\alpha 9\alpha 10$ subtypes and their interactions with α -conotoxins and three-finger proteins, namely α -neurotoxins and human proteins of the Ly6 family (see review Tsetlin et al., 2021).

Structural Studies on Nicotinic Acetylcholine Receptors in Complex With Toxins

While cryo-electron microscopy structures of the *T. marmorata* nAChR (Unwin and Fujiyoshi, 2012) and the X-ray structure of the $\alpha 4\beta 2$ nAChR (Morales-Perez et al., 2016) are known, the number of nAChR structures in complexes with peptide and protein neurotoxins is limited. Advances in cryo-EM

only recently revealed the structures of the *Torpedo* nAChR (Rahman et al., 2020) and the human $\alpha 7$ nAChR in complex with α -Btx (Noviello et al., 2021). Previously, binding modes of α -neurotoxins or α -conotoxins were based on the X-ray analysis of their complexes with the AChBP, a versatile surrogate of the LBD of nicotinic and other Cys-loop receptors. Our laboratories participated in the structure determination of AChBP in complex with α -conotoxins specific for the $\alpha 7$ (PnIA analog and ImI), $\alpha 3\beta 2$ (LvIA), and $\alpha 3\beta 4$ (GIC) receptors (Celie et al., 2005; Ulens et al., 2006; Lin et al., 2016; Zhu et al., 2020). Recently the combination of alanine scanning, site-directed mutagenesis, computer modeling, and X-ray crystallography of the AChBP in complex with α -conotoxin LvIA and its synthetic analogs, identified several residues in the $\beta 2$ subunit that confer LvIA specificity for the $\alpha 3\beta 2$ nAChR (Zhu et al., 2020). In collaboration with Greek crystallographers, who earlier demonstrated the similarity between the α -Btx structures in complexes with AChBP and the heterologously expressed $\alpha 9$ LBD (Zouridakis et al., 2014), the first X-ray structure of α -conotoxin RgIA in complex with the $\alpha 9$ LBD was solved and, based on computer modeling, a model for RgIA binding at the $\alpha 9$ - $\alpha 10$ interface was proposed (Zouridakis et al., 2019).

Most α -conotoxins bind at the orthosteric ligand binding sites in different nAChRs subtypes. Because of the high homology of such sites in all nAChR subtypes, drugs that bind at more diverse allosteric sites would have a higher chance to act in a subtype-selective way (Wang and Lindstrom, 2018). In this respect, α O-conotoxin GeXIVA with analgesic activity (Wang et al., 2019) is of interest. In TEVC experiments it inhibited the rat $\alpha 9\alpha 10$ nAChR at nanomolar concentrations (Luo et al., 2015) by binding exclusively to an allosteric site, thus opening up a strategy for subtype-selective targeting. However, competition with radioactive α -Btx revealed that α O-conotoxin GeXIVA also binds with a lower affinity (at micromolar concentrations) to the orthosteric sites in the monomeric $\alpha 9$ LBD and in the pentameric *Aplysia californica* AChBP (Kryukova et al., 2018).

Toxins as Tools for Functional Studies

Due to their high subtype selectivity, α -conotoxins might provide a basis for the development of novel drugs. Most interesting are α -conotoxin RgIA, α O-conotoxin GeXIVA, and their derivatives, which have analgesic properties and target $\alpha 9\alpha 10$ nAChRs (Wang et al., 2019; Huynh et al., 2020). The anticancer activity of several nAChR subtype selective α -conotoxins was also tested (Terpinskaya et al., 2015, 2020). The application of α -conotoxins PnIA, RgIA, ArIB[V11L,V16D], or MIII together with either baicalein or indomethacin to Ehrlich carcinoma enhanced the antitumor activity several-fold (Osipov et al., 2020). However, while baicalein exerted antiproliferative and cytotoxic effects also on C6 glioma cells, α -Ctx and α -conotoxin RgIA on the contrary promoted proliferation of these cells (Terpinskaya et al., 2021). Thus, further research is required to elucidate the role of nAChRs in different tumor cell lines and environments.

α -Conotoxins are not only convenient tools for structure-function studies on heterologously expressed nAChRs, but also

for characterization of their physiological roles in native tissues. Here, we extended a previous study on the involvement of $\alpha 9\alpha 10$ nAChRs in mouse granulocyte functions and found that α -conotoxins (RgIA, Vc1.1 and PeIA) significantly increased the release of IL-10 (see **Figure 1**), which is known to produce analgesic and anti-inflammatory effects (Saadane et al., 2005; da Silva et al., 2015). We suggest that $\alpha 9$ -containing nAChRs activated by endogenous ACh may prevent IL-10 release. Similarly, the inhibition of hybridoma cell proliferation by α -Ctx or WTX has been explained by prior action of endogenously released ACh (Skok et al., 2003). There is also evidence in the literature that non-neuronal ACh released by immune cells regulates immune functions *via* nAChRs (Mashimo et al., 2021) and ACh synthesis was demonstrated in granulocytes (Neumann et al., 2007). Although there are no data showing that $\alpha 9\alpha 10$ nAChRs in murine bone marrow granulocytes are constitutively active, we have previously shown effects of $\alpha 9\alpha 10$ antagonists, RgIA and Vc1.1 in the absence of agonists, on functions of murine bone marrow granulocytes (Safronova et al., 2021). Similar results were obtained by other groups for the action of different nAChR antagonists on immune cells (Razani-Boroujerdi et al., 2007; Zazueta-Favela et al., 2019). Together with previous findings (Safronova et al., 2016, 2021; Serov et al., 2021), this supports the participation of the $\alpha 9$ and/or $\alpha 9\alpha 10$ nAChR in the anti-inflammatory processes and might help to explain the analgesic action of compounds inhibiting this receptor.

Subtype-Selectivity of Snake Toxins

It was earlier shown that α -Btx and α -Ctx can inhibit distinct subtypes of ionotropic GABA_A receptors (McCann et al., 2006; Hannan et al., 2015; Kudryavtsev et al., 2015) and similar properties were found for the recently isolated *N. melanoleuca* long-chain α -neurotoxins (Son et al., 2021). However, *N. melanoleuca* Tx-NM2, in contrast to α -Btx and α -Ctx, distinguishes the two ACh binding sites in the *Torpedo* receptor (Son et al., 2021). Here we checked if the *N. melanoleuca* toxins can also interact with the $\alpha 9\alpha 10$ nAChRs and whether their binding to this nAChR subtype would differ from that of α -Btx and α -Ctx.

As seen in **Figure 2A**, both *N. melanoleuca* toxins inhibit the $\alpha 9\alpha 10$ nAChRs with IC₅₀ values of 30 nM (Tx-NM2) and 119 nM (Tx-NM3-1), the first one being slightly more potent than α -Btx or α -Ctx. We also tested the ability of a series of toxins from other venoms to interact with the $\alpha 9\alpha 10$ nAChRs. A relatively high affinity (166 nM) was detected for the NT I, a long-chain α -neurotoxin from *N. oxiana*. No activity was detected for short-chain NT II, which is not surprising since short-chain α -neurotoxins are known to bind also very weakly to the $\alpha 7$ nAChR. No strong inhibition was found with non-conventional toxin WTX as well. Analysis of the linear peptide AZE that does not contain disulfide bonds was interesting because it was earlier shown to inhibit the muscle-type nAChR (Utkin et al., 2012) and because other linear peptides, oligoarginines, inhibit various nAChR subtypes including the $\alpha 9\alpha 10$ nAChRs quite potently (Lebedev et al., 2019). However, no efficient inhibition by AZE was detected at the $\alpha 9\alpha 10$ nAChR (**Figure 2A** and **Table 1**).

Thus, Tx-NM2 appears most promising for $\alpha 9\alpha 10$ nAChR research. It has the highest affinity and dissociates significantly slower from this receptor than all other toxins tested in this study. However, Tx-NM2 was also the most active against the earlier tested nAChR and GABA_A receptor subtypes (Son et al., 2021). Nevertheless, it is the first described snake toxin that shows such high affinity at the human $\alpha 9\alpha 10$ receptor and provides a valuable basis to elucidate critical determinants for $\alpha 9\alpha 10$ selectivity and for the development of $\alpha 9\alpha 10$ nAChR labels.

DATA AVAILABILITY STATEMENT

The original contributions presented in the study are included in the article/**Supplementary Material**, further inquiries can be directed to the corresponding author/s.

ETHICS STATEMENT

The animal study was reviewed and approved by the Commission for the Rules for the Treatment of Animals [The protocol No. 2019/5] of the Institute of Cell Biophysics of the Russian Academy of Sciences (Pushchino, Russia).

AUTHOR CONTRIBUTIONS

VT planned the project, wrote the first draft and together with AN, IS, YH, and YU finalized the manuscript. DK, EK, and LS contributed to the essential materials. DS, YH, PS, and VS performed the experiments. AN, YH, IK, and VS analyzed and interpreted the data. YU, VT, VS, and AN led the project. VT, YU, AN, VS, and IK contributed to the funding acquisition. All authors contributed to, reviewed and approved the manuscript.

FUNDING

This work was supported by the DFG [Research Training Group GRK2338, P01 (AN)], Russian Foundation for Basic Research (RFBR) grant 20-04-00761 (IK), and Russian Science Foundation (RSF) grant 21-14-00316 (isolation of snake toxins).

ACKNOWLEDGMENTS

We thank Han Shen Tae and David Adams (Illawara Health and Medical Research Institute, Wollongong University, Australia) for providing $\alpha 9\alpha 10$ nAChR cDNAs and Monika Haberland for preparing oocytes.

SUPPLEMENTARY MATERIAL

The Supplementary Material for this article can be found online at: <https://www.frontiersin.org/articles/10.3389/fncel.2021.765541/full#supplementary-material>

REFERENCES

- Ai, L., Luo, W., Yuan, P., Liu, L., and Zhou, Y. (2020). Liver macrophages mediate effects of downhill running and caloric restriction on nonalcoholic fatty liver disease of high fat diet-fed mice. *Life Sci.* 256:117978. doi: 10.1016/j.lfs.2020.117978
- Barber, C. M., Isbister, G. K., and Hodgson, W. C. (2013). Alpha neurotoxins. *Toxicol.* 66, 47–58. doi: 10.1016/j.toxicol.2013.01.019
- Celie, P. H. N., Kasheverov, I. E., Mordvintsev, D. Y., Hogg, R. C., van Nierop, P., van Elk, R., et al. (2005). Crystal structure of nicotinic acetylcholine receptor homolog AChBP in complex with an alpha-conotoxin PnIA variant. *Nat. Struct. Mol. Biol.* 12, 582–588. doi: 10.1038/nsmb951
- Chandna, R., Tae, H. S., Seymour, V. A. L., Chathrath, S., Adams, D. J., and Kini, R. M. (2019). Drysdalin, an antagonist of nicotinic acetylcholine receptors highlights the importance of functional rather than structural conservation of amino acid residues. *FASEB Bioadv.* 1, 115–131. doi: 10.1096/fba.1027
- da Silva, M. D., Bobinski, F., Sato, K. L., Kolker, S. J., Sluka, K. A., and Santos, A. R. S. (2015). IL-10 Cytokine Released from M2 Macrophages Is Crucial for Analgesic and Anti-inflammatory Effects of Acupuncture in a Model of Inflammatory Muscle Pain. *Mol. Neurobiol.* 51, 19–31. doi: 10.1007/s12035-014-8790-x
- Dutertre, S., Nicke, A., and Tsetlin, V. I. (2017). Nicotinic acetylcholine receptor inhibitors derived from snake and snail venoms. *Neuropharmacology* 127, 196–223. doi: 10.1016/j.neuropharm.2017.06.011
- Elgoyhen, A. B., Johnson, D. S., Boulter, J., Vetter, D. E., and Heinemann, S. (1994). $\alpha 9$: An acetylcholine receptor with novel pharmacological properties expressed in rat cochlear hair cells. *Cell* 79, 705–715. doi: 10.1016/0092-8674(94)90555-X
- Elgoyhen, A. B., Vetter, D. E., Katz, E., Rothlin, C. V., Heinemann, S. F., and Boulter, J. (2001). $\alpha 10$: A determinant of nicotinic cholinergic receptor function in mammalian vestibular and cochlear mechanosensory hair cells. *Proc. Natl. Acad. Sci. U. S. A.* 98, 3501–3506. doi: 10.1073/pnas.051622798
- Ellison, M., Feng, Z. P., Park, A. J., Zhang, X., Olivera, B. M., McIntosh, J. M., et al. (2008). Alpha-RgIA, a novel conotoxin that blocks the alpha9alpha10 nAChR: structure and identification of key receptor-binding residues. *J. Mol. Biol.* 377, 1216–1227. doi: 10.1016/j.jmb.2008.01.082
- Ellison, M., Haberlandt, C., Gomez-Casati, M. E., Watkins, M., Elgoyhen, A. B., McIntosh, J. M., et al. (2006). Alpha-RgIA: a novel conotoxin that specifically and potently blocks the alpha9alpha10 nAChR. *Biochemistry* 45, 1511–1515. doi: 10.1021/bi0520129
- Galvis, G., Lips, K. S., and Kummer, W. (2006). Expression of nicotinic acetylcholine receptors on murine alveolar macrophages. *J. Mol. Neurosci.* 30, 107–108. doi: 10.1385/JMN:30:1:107
- Giribaldi, J., Haufe, Y., Evans, E. R. J., Amar, M., Durner, A., Schmidt, C., et al. (2020). Backbone cyclization turns a venom peptide into a stable and equipotent ligand at both muscle and neuronal nicotinic receptors. *J. Med. Chem.* 63, 12682–12692. doi: 10.1021/acs.jmedchem.0c00957
- Gloor, S., Pongs, O., and Schmalzing, G. (1995). A vector for the synthesis of cRNAs encoding Myc epitope-tagged proteins in *Xenopus laevis* oocytes. *Gene* 160, 213–217. doi: 10.1016/0378-1119(95)00226-v
- Grau, V., Richter, K., Hone, A. J., and McIntosh, J. M. (2019). Conopeptides [V11L;V16D]Arib and RGIA4: Powerful tools for the identification of novel nicotinic acetylcholine receptors in monocytes. *Front. Pharmacol.* 9:1499. doi: 10.3389/fphar.2018.01499
- Hannan, S., Mortensen, M., and Smart, T. G. (2015). Snake neurotoxin α -bungarotoxin is an antagonist at native GABA_A receptors. *Neuropharmacology* 93, 28–40. doi: 10.1016/j.neuropharm.2015.01.001
- Ho, T. N. T., Abraham, N., and Lewis, R. J. (2020). Structure-function of neuronal nicotinic acetylcholine receptor inhibitors derived from natural toxins. *Front. Neurosci.* 14:1209. doi: 10.3389/fnins.2020.609005
- Huynh, P. N., Giuvelis, D., Christensen, S., Tucker, K. L., and McIntosh, J. M. (2020). RgIA4 accelerates recovery from paclitaxel-induced neuropathic pain in rats. *Mar. Drugs* 18:12. doi: 10.3390/md18010012
- Khezri, K., Farahpour, M. R., and Mounesi Rad, S. (2019). Accelerated infected wound healing by topical application of encapsulated Rosemary essential oil into nanostructured lipid carriers. *Artif. Cells Nanomed. Biotechnol.* 47, 980–988. doi: 10.1080/21691401.2019.1582539
- Kryukova, E. V., Ivanov, I. A., Lebedev, D. S., Spirova, E. N., Egorova, N. S., Zouridakis, M., et al. (2018). Orthosteric and/or Allosteric Binding of α -Conotoxins to Nicotinic Acetylcholine Receptors and Their Models. *Mar. Drugs* 16:460. doi: 10.3390/md16120460
- Kudryavtsev, D. S., Shelukhina, I. V., Son, L. V., Ojomoko, L. O., Kryukova, E. V., Lyukmanova, E. N., et al. (2015). Neurotoxins from snake venoms and α -conotoxin ImI inhibit functionally active Ionotropic γ -aminobutyric acid (GABA) receptors. *J. Biol. Chem.* 290, 22747–22758. doi: 10.1074/jbc.M115.648824
- Lebedev, D. S., Kryukova, E. V., Ivanov, I. A., Egorova, N. S., Timofeev, N. D., Spirova, E. N., et al. (2019). Oligoarginine peptides, a new family of nicotinic acetylcholine receptor inhibitors. *Mol. Pharmacol.* 96, 664–673. doi: 10.1124/mol.119.117713
- Lin, B., Xu, M., Zhu, X., Wu, Y., Liu, X., Zhangsun, D., et al. (2016). From crystal structure of α -conotoxin GIC in complex with Ac-AChBP to molecular determinants of its high selectivity for $\alpha 3\beta 2$ nAChR. *Sci. Rep.* 6, 1–10. doi: 10.1038/srep22349
- Luo, S., Zhangsun, D., Harvey, P. J., Kaas, Q., Wu, Y., Zhu, X., et al. (2015). Cloning, synthesis, and characterization of αO -conotoxin GeXIVA, a potent $\alpha 9\alpha 10$ nicotinic acetylcholine receptor antagonist. *Proc. Natl. Acad. Sci. U. S. A.* 112, E4026–E4035. doi: 10.1073/pnas.1503617112
- Mashimo, M., Moriwaki, Y., Misawa, H., Kawashima, K., and Fujii, T. (2021). Regulation of immune functions by non-neuronal acetylcholine (ACh) via muscarinic and nicotinic ACh receptors. *Int. J. Mol. Sci.* 22:6818. doi: 10.3390/ijms22136818
- McCann, C. M., Bracamontes, J., Steinbach, J. H., and Sanes, J. R. (2006). The cholinergic antagonist alpha-bungarotoxin also binds and blocks a subset of GABA receptors. *Proc. Natl. Acad. Sci. U. S. A.* 103, 5149–5154. doi: 10.1073/pnas.0600847103
- McIntosh, J. M., Absalom, N., Chebib, M., Elgoyhen, A. B., and Vincler, M. (2009). Alpha9 nicotinic acetylcholine receptors and the treatment of pain. *Biochem. Pharmacol.* 78, 693–702. doi: 10.1016/j.bcp.2009.05.020
- McIntosh, J. M., Plazas, P. V., Watkins, M., Gomez-Casati, M. E., Olivera, B. M., and Elgoyhen, A. B. (2005). A novel alpha-conotoxin, PeIA, cloned from *Conus pergrandis*, discriminates between rat alpha9alpha10 and alpha7 nicotinic cholinergic receptors. *J. Biol. Chem.* 280, 30107–30112. doi: 10.1074/jbc.M504102200
- Moglie, M. J., Marcovich, I., Corradi, J., Carpaneto Freixas, A. E., Gallino, S., Plazas, P. V., et al. (2021). Loss of choline agonism in the inner ear hair cell nicotinic acetylcholine receptor linked to the $\alpha 10$ subunit. *Front. Mol. Neurosci.* 14:5. doi: 10.3389/fnmol.2021.639720
- Monga, S., Nagler, R., Amara, R., Weizman, A., and Gavish, M. (2019). Inhibitory effects of the two novel TSP0 ligands 2-Cl-MGV-1 and MGV-1 on LPS-induced microglial activation. *Cells* 8:486. doi: 10.3390/cells8050486
- Morales-Perez, C. L., Noviello, C. M., and Hibbs, R. E. (2016). X-ray structure of the human $\alpha 4\beta 2$ nicotinic receptor. *Nature* 538, 411–415. doi: 10.1038/nature19785
- Neumann, S., Razen, M., Habermehl, P., Meyer, C. U., Zepp, F., Kirkpatrick, C. J., et al. (2007). The non-neuronal cholinergic system in peripheral blood cells: effects of nicotinic and muscarinic receptor antagonists on phagocytosis, respiratory burst and migration. *Life Sci.* 80, 2361–2364. doi: 10.1016/j.lfs.2007.01.010
- Noviello, C. M., Gharpure, A., Mukhtasimova, N., Cabuco, R., Baxter, L., Borek, D., et al. (2021). Structure and gating mechanism of the $\alpha 7$ nicotinic acetylcholine receptor. *Cell* 184, 2121–2134. doi: 10.1016/j.cell.2021.02.049
- Osipov, A. V., Kasheverov, I. E., Makarova, Y. V., Starkov, V. G., Vorontsova, O. V., Ziganshin, R., et al. (2008). Naturally occurring disulfide-bound dimers of three-fingered toxins: a paradigm for biological activity diversification. *J. Biol. Chem.* 283, 14571–14580. doi: 10.1074/jbc.M802085200
- Osipov, A. V., Terpinskaya, T. I., Yanchanka, T., Balashevich, T., Zhmak, M. N., Tsetlin, V. I., et al. (2020). α -Conotoxins enhance both the *in vivo* suppression of Ehrlich carcinoma growth and *in vitro* reduction in cell viability elicited by

- cyclooxygenase and lipoxygenase inhibitors. *Mar. Drugs* 18:193. doi: 10.3390/md18040193
- Peng, H., Ferris, R. L., Matthews, T., Hiel, H., Lopez-Albaitero, A., and Lustig, L. R. (2004). Characterization of the human nicotinic acetylcholine receptor subunit alpha (alpha) 9 (CHRNA9) and alpha (alpha) 10 (CHRNA10) in lymphocytes. *Life Sci.* 76, 263–280. doi: 10.1016/j.lfs.2004.05.031
- Rahman, M. M., Teng, J., Worrell, B. T., Noviello, C. M., Lee, M., Karlin, A., et al. (2020). Structure of the native muscle-type nicotinic receptor and inhibition by snake venom toxins. *Neuron* 106, 952.e–962.e. doi: 10.1016/j.neuron.2020.03.012
- Razani-Boroujerdi, S., Boyd, R. T., Dávila-García, M. I., Nandi, J. S., Mishra, N. C., Singh, S. P., et al. (2007). T cells express alpha7-nicotinic acetylcholine receptor subunits that require a functional TCR and leukocyte-specific protein tyrosine kinase for nicotine-induced Ca²⁺ response. *J. Immunol.* 179, 2889–2898. doi: 10.4049/jimmunol.179.5.2889
- Rothlin, C. V., Katz, E., Verbitsky, M., and Elgoyhen, A. B. (1999). The $\alpha 9$ nicotinic acetylcholine receptor shares pharmacological properties with type A γ -aminobutyric acid, glycine, and type 3 serotonin receptors. *Mol. Pharmacol.* 55, 248–254. doi: 10.1124/mol.55.2.248
- Saadane, A., Soltys, J., and Berger, M. (2005). Role of IL-10 deficiency in excessive nuclear factor- κ B activation and lung inflammation in cystic fibrosis transmembrane conductance regulator knockout mice. *J. Allergy Clin. Immunol.* 115, 405–411. doi: 10.1016/j.jaci.2004.10.044
- Safronova, V. G., Vulfius, C. A., Astashev, M. E., Tikhonova, I. V., Serov, D. A., Jirova, E. A., et al. (2021). $\alpha 9\alpha 10$ nicotinic acetylcholine receptors regulate murine bone marrow granulocyte functions. *Immunobiology* 226:152047. doi: 10.1016/j.imbio.2020.152047
- Safronova, V. G., Vulfius, C. A., Shelukhina, I. V., Mal'tseva, V. N., Berezhnov, A. V., Fedotova, E. I., et al. (2016). Nicotinic receptor involvement in regulation of functions of mouse neutrophils from inflammatory site. *Immunobiology* 221, 761–772. doi: 10.1016/j.imbio.2016.01.016
- Serov, D., Tikhonova, I., Safronova, V., and Astashev, M. (2021). Calcium activity in response to nAChR ligands in murine bone marrow granulocytes with different Gr-1 expression. *Cell. Biol. Int.* 45, 1533–1545. doi: 10.1002/cbin.11593
- Skok, M. V., Kalashnik, E. N., Koval, L. N., Tsetlin, V. I., Utkin, Y. N., Changeux, J. P., et al. (2003). Functional nicotinic acetylcholine receptors are expressed in B lymphocyte-derived cell lines. *Mol. Pharmacol.* 64, 885–889. doi: 10.1124/mol.64.4.885
- Son, L., Kryukova, E., Ziganshin, R., Andreeva, T., Kudryavtsev, D., Kasheverov, I., et al. (2021). Novel three-finger neurotoxins from *Naja melanoleuca* cobra venom interact with GABAA and nicotinic acetylcholine receptors. *Toxins* 13:164. doi: 10.3390/toxins13020164
- St-Pierre, S., Jiang, W., Roy, P., Champigny, C., LeBlanc, E., Morley, B. J., et al. (2016). Nicotinic acetylcholine receptors modulate bone marrow-derived pro-inflammatory monocyte production and survival. *PLoS One* 11:e0150230. doi: 10.1371/journal.pone.0150230
- Sun, Z., Bao, J., Zhangsun, M., Dongs, S., Zhangsun, D., and Luo, S. (2020a). AO-conotoxin GexIVa inhibits the growth of breast cancer cells via interaction with $\alpha 9$ nicotine acetylcholine receptors. *Mar. Drugs* 18:195. doi: 10.3390/md18040195
- Sun, Z., Zhangsun, M., Dong, S., Liu, Y., Qian, J., Zhangsun, D., et al. (2020b). Differential expression of nicotine acetylcholine receptors associates with human breast cancer and mediates antitumor activity of α O-conotoxin gexiva. *Mar. Drugs* 18:61. doi: 10.3390/md18010061
- Terpinskaya, T. I., Osipov, A. V., Balashevich, T. V., Yanchanka, T. L., Tamashionik, E. A., Tsetlin, V. I., et al. (2020). Blockers of nicotinic acetylcholine receptors delay tumor growth and increase antitumor activity of mouse splenocytes. *Dokl. Biochem. Biophys.* 491, 89–92. doi: 10.1134/S1607672920020143
- Terpinskaya, T. I., Osipov, A. V., Kryukova, E. V., Kudryavtsev, D. S., Kopylova, N. V., Yanchanka, T. L., et al. (2021). α -Conotoxins and α -cobratoxin promote, while lipoxygenase and cyclooxygenase inhibitors suppress the proliferation of glioma C6 cells. *Mar. Drugs* 19:118. doi: 10.3390/md19020118
- Terpinskaya, T. I., Osipov, A. V., Kuznetsova, T. E., Ryzhkovskaya, E. L., Ulaschik, V. S., Ivanov, I. A., et al. (2015). α -Conotoxins revealed different roles of nicotinic cholinergic receptor subtypes in oncogenesis of Ehrlich tumor and in the associated inflammation. *Dokl. Biochem. Biophys.* 463, 216–219. doi: 10.1134/S1607672915040055
- Tsetlin, V. I. (2015). Three-finger snake neurotoxins and Ly6 proteins targeting nicotinic acetylcholine receptors: pharmacological tools and endogenous modulators. *Trends Pharmacol. Sci.* 36, 109–123. doi: 10.1016/j.tips.2014.11.003
- Tsetlin, V. I., Kasheverov, I. E., and Utkin, Y. N. (2021). Three-finger proteins from snakes and humans acting on nicotinic receptors: Old and new. *J. Neurochem.* 158, 1223–1235. doi: 10.1111/jnc.15123
- Ulen, C., Hogg, R. C., Celie, P. H., Bertrand, D., Tsetlin, V., Smit, A. B., et al. (2006). Structural determinants of selective alpha-conotoxin binding to a nicotinic acetylcholine receptor homolog AChBP. *Proc. Natl. Acad. Sci. U S A.* 103, 3615–3620. doi: 10.1073/pnas.0507889103
- Unwin, N., and Fujiyoshi, Y. (2012). Gating movement of acetylcholine receptor caught by plunge-freezing. *J. Mol. Biol.* 422, 617–634. doi: 10.1016/j.jmb.2012.07.010
- Utkin, Y. N., Kukhtina, V. V., Kryukova, E. V., Chiodini, F., Bertrand, D., Methfessel, C., et al. (2001). “Weak toxin” from *Naja kaouthia* is a nontoxic antagonist of $\alpha 7$ and muscle-type nicotinic acetylcholine receptors. *J. Biol. Chem.* 276, 15810–15815. doi: 10.1074/jbc.M100788200
- Utkin, Y. N., Weise, C., Kasheverov, I. E., Andreeva, T. V., Kryukova, E. V., Zhmak, M. N., et al. (2012). Azemiopsin from *Azemiops feae* viper venom, a novel polypeptide ligand of nicotinic acetylcholine receptor. *J. Biol. Chem.* 287, 27079–27086. doi: 10.1074/jbc.M112.363051
- Verbitsky, M., Rothlin, C. V., Katz, E., and Belén Elgoyhen, A. (2000). Mixed nicotinic-muscarinic properties of the $\alpha 9$ nicotinic cholinergic receptor. *Neuropharmacology* 39, 2515–2524. doi: 10.1016/S0028-3908(00)00124-6
- Vinclair, M., Wittenauer, S., Parker, R., Ellison, M., Olivera, B. M., and McIntosh, J. M. (2006). Molecular mechanism for analgesia involving specific antagonism of alpha9alpha10 nicotinic acetylcholine receptors. *Proc. Natl. Acad. Sci. U S A.* 103, 17880–17884. doi: 10.1073/pnas.0608715103
- Wang, H., Li, X., Zhangsun, D., Yu, G., Su, R., and Luo, S. (2019). The $\alpha 9\alpha 10$ nicotinic acetylcholine receptor antagonist α -conotoxin GexXIVA[1,2] alleviates and reverses chemotherapy-induced neuropathic pain. *Mar. Drugs* 17:265. doi: 10.3390/md17050265
- Wang, J., and Lindstrom, J. (2018). Orthosteric and allosteric potentiation of heteromeric neuronal nicotinic acetylcholine receptors. *Br. J. Pharmacol.* 175, 1805–1821. doi: 10.1111/bph.13745
- Yu, R., Kompella, S. N., Adams, D. J., Craik, D. J., and Kaas, Q. (2013). Determination of the α -conotoxin Vc1.1 binding site on the $\alpha 9\alpha 10$ nicotinic acetylcholine receptor. *J. Med. Chem.* 56, 3557–3567. doi: 10.1021/jm400041h
- Yu, R., Tae, H. S., Tabassum, N., Shi, J., Jiang, T., and Adams, D. J. (2018). Molecular determinants conferring the stoichiometric-dependent activity of α -conotoxins at the human $\alpha 9\alpha 10$ nicotinic acetylcholine receptor subtype. *J. Med. Chem.* 61, 4628–4634. doi: 10.1021/acs.jmedchem.8b00115
- Zazueta-Favela, D., Donis-Maturano, L., Licea-Navarro, A. F., Bernáldez-Sarabia, J., Dan, K. W. L., Cota-Arce, J. M., et al. (2019). Marine peptides as immunomodulators: *Californiconus californicus*-derived synthetic conotoxins induce IL-10 production by regulatory T cells (CD4⁺ Foxp3⁺). *Immunopharmacol. Immunotoxicol.* 1, 463–468. doi: 10.1080/08923973.2019.1641114
- Zhang, C. W., Wu, X., Liu, D., Zhou, W., Tan, W., Fang, Y. X., et al. (2019). Long non-coding RNA PVT1 knockdown suppresses fibroblast-like synovocyte inflammation and induces apoptosis in rheumatoid arthritis through demethylation of *sirt6*. *J. Biol. Eng.* 13:60. doi: 10.1186/s13036-019-0184-1
- Zhu, X., Pan, S., Xu, M., Zhang, L., Yu, J., Yu, J., et al. (2020). High selectivity of an α -conotoxin LvIA analogue for $\alpha 3\beta 2$ nicotinic acetylcholine receptors is mediated by $\beta 2$ functionally important residues. *J. Med. Chem.* 63, 13656–13668. doi: 10.1021/acs.jmedchem.0c00975
- Zouridakis, M., Giastas, P., Zarkadas, E., Chroni-Tzartou, D., Bregestovski, P., and Tzartos, S. J. (2014). Crystal structures of free and antagonist-bound states of human $\alpha 9$ nicotinic receptor extracellular domain. *Nat. Struct. Mol. Biol.* 21, 976–980. doi: 10.1038/nsmb.2900

Zouridakis, M., Papakyriakou, A., Ivanov, I. A., Kasheverov, I. E., Tsetlin, V., Tzartos, S., et al. (2019). Crystal structure of the monomeric extracellular domain of $\alpha 9$ nicotinic receptor subunit in complex with α -conotoxin RgIA: molecular dynamics insights into RgIA binding to $\alpha 9\alpha 10$ nicotinic receptors. *Front. Pharmacol.* 10:474. doi: 10.3389/fphar.2019.00474

Conflict of Interest: The authors declare that the research was conducted in the absence of any commercial or financial relationships that could be construed as a potential conflict of interest.

Publisher's Note: All claims expressed in this article are solely those of the authors and do not necessarily represent those of their affiliated organizations, or those of

the publisher, the editors and the reviewers. Any product that may be evaluated in this article, or claim that may be made by its manufacturer, is not guaranteed or endorsed by the publisher.

Copyright © 2021 Tsetlin, Haufe, Safronova, Serov, Shadamarshan, Son, Shelukhina, Kudryavtsev, Kryukova, Kasheverov, Nicke and Utkin. This is an open-access article distributed under the terms of the Creative Commons Attribution License (CC BY). The use, distribution or reproduction in other forums is permitted, provided the original author(s) and the copyright owner(s) are credited and that the original publication in this journal is cited, in accordance with accepted academic practice. No use, distribution or reproduction is permitted which does not comply with these terms.

Supporting information

Interaction of $\alpha 9\alpha 10$ nicotinic receptors with peptides and proteins from animal venoms

Victor Tsetlin¹, Yves Haufe², Valentina Safronova³, Dmitriy Serov³, Pranavkumar Shadarmarshan², Lina Son¹, Irina Shelukhina¹, Denis Kudryavtsev¹, Elena Kryukova¹, Igor Kasheverov¹, Annette Nicke², Yuri Utkin^{1*}

¹Department of Molecular Neuroimmune Signaling, Shemyakin-Ovchinnikov Institute of Bioorganic Chemistry, Russian Academy of Sciences, Moscow, Russia

²Walther Straub Institute of Pharmacology and Toxicology, Faculty of Medicine, LMU Munich, Munich, Germany

³Institute of Cell Biophysics, Russian Academy of Sciences, Pushchino, Russia.

*** Correspondence:**

Yuri Utkin

utkin@ibch.ru; yutkin@yandex.ru

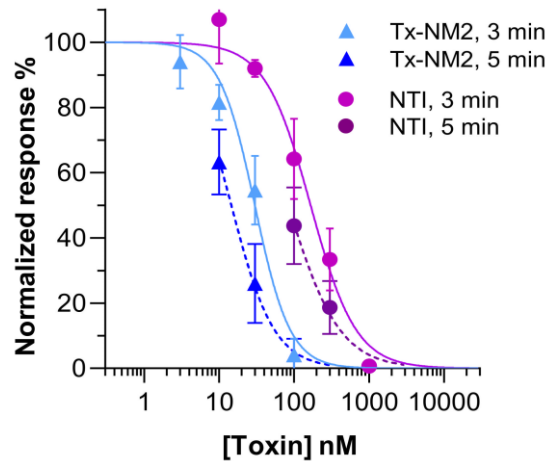


Figure S1: Influence of antagonist incubation time on Hill slopes of dose inhibition response curves. Human $\alpha 9\alpha 10$ nicotinic acetylcholine receptor (nAChR) was expressed in *Xenopus laevis* oocytes. Oocytes were clamped at -70 mV and activated by 2 s pulses of 40 μ M acetylcholine (ACh). Estimated effect of a longer pre-incubation time on the dose inhibition curves of Tx-NM2 and NTI. The solid lines represent dose inhibition curves obtained with a three min pre-incubation time (as presented in Fig. 2A). The dashed lines show a trend towards lower IC_{50} and Hill slope values with longer (five min) pre-incubation time. Note that only two concentrations per toxin were measured. It can be expected that even longer preincubation times than five min would be required to reach equilibrium binding at low toxin concentrations and the effect of longer preincubation time increases with lower toxin concentrations and would result in a Hill coefficient closer to -1. Mean values with standard deviation are shown. Estimated IC_{50} values/ Hill slopes for 5 min pre-incubation of Tx-NM2 and NTI are 15 nM/-1.52, and 83 nM/-1.26, respectively. Note that the estimated IC_{50} values are in the same order of magnitude for both toxins. $n = 3-5$ different oocytes for each concentration.

7. Supplementary B: Publication IV

pp. 99 - 120



Acute effects of the imidacloprid metabolite desnitro-imidacloprid on human nACh receptors relevant for neuronal signaling

Dominik Loser^{1,2} · Karin Grillberger³ · Maria G. Hinojosa⁴ · Jonathan Blum² · Yves Haufe⁵ · Timm Danker¹ · Ylva Johansson⁴ · Clemens Möller⁶ · Annette Nicke⁵ · Susanne H. Bennekou⁷ · Iain Gardner⁸ · Caroline Bauch⁹ · Paul Walker⁹ · Anna Forsby⁴ · Gerhard F. Ecker³ · Udo Kraushaar¹ · Marcel Leist²

Received: 8 June 2021 / Accepted: 20 September 2021
© The Author(s) 2021

Abstract

Several neonicotinoids have recently been shown to activate the nicotinic acetylcholine receptor (nAChR) on human neurons. Moreover, imidacloprid (IMI) and other members of this pesticide family form a set of diverse metabolites within crops. Among these, desnitro-imidacloprid (DN-IMI) is of special toxicological interest, as there is evidence (i) for human dietary exposure to this metabolite, (ii) and that DN-IMI is a strong trigger of mammalian nicotinic responses. We set out here to quantify responses of human nAChRs to DN-IMI and an alternative metabolite, IMI-olefin. To evaluate toxicological hazards, these data were then compared to those of IMI and nicotine. Ca^{2+} -imaging experiments on human neurons showed that DN-IMI exhibits an agonistic effect on nAChRs at sub-micromolar concentrations (equipotent with nicotine) while IMI-olefin activated the receptors less potently (in a similar range as IMI). Direct experimental data on the interaction with defined receptor subtypes were obtained by heterologous expression of various human nAChR subtypes in *Xenopus laevis* oocytes and measurement of the transmembrane currents evoked by exposure to putative ligands. DN-IMI acted on the physiologically important human nAChR subtypes $\alpha 7$, $\alpha 3\beta 4$, and $\alpha 4\beta 2$ (high-sensitivity variant) with similar potency as nicotine. IMI and IMI-olefin were confirmed as nAChR agonists, although with 2–3 orders of magnitude lower potency. Molecular docking studies, using receptor models for the $\alpha 7$ and $\alpha 4\beta 2$ nAChR subtypes supported an activity of DN-IMI similar to that of nicotine. In summary, these data suggest that DN-IMI functionally affects human neurons similar to the well-established neurotoxicant nicotine by triggering $\alpha 7$ and several non- $\alpha 7$ nAChRs.

Keywords Live-cell calcium imaging · Pesticide metabolism · Nicotine · Developmental neurotoxicity · Molecular docking · Oocyte recording

Udo Kraushaar and Marcel Leist contributed equally.

✉ Marcel Leist
marcel.leist@uni-konstanz.de

¹ NMI Natural and Medical Sciences Institute at the University of Tübingen, 72770 Reutlingen, Germany

² In Vitro Toxicology and Biomedicine, Department Inaugurated by the Doerenkamp-Zbinden Foundation, University of Konstanz, 78457 Konstanz, Germany

³ Department of Pharmaceutical Chemistry, University of Vienna, Vienna, Austria

⁴ Department of Biochemistry and Biophysics, Stockholm University, 106 91 Stockholm, Sweden

⁵ Walther Straub Institute of Pharmacology and Toxicology, Faculty of Medicine, LMU Munich, 80336 Munich, Germany

⁶ Life Sciences Faculty, Albstadt-Sigmaringen University, 72488 Sigmaringen, Germany

⁷ Technical University of Denmark, Kongens Lyngby, Denmark

⁸ CERTARA UK Limited, Simcyp Division, Level 2-Acero, 1 Concourse Way, Sheffield S1 2BJ, UK

⁹ Cyprotex Discovery Ltd, No. 24 Mereside, Alderley Park, Cheshire SK10 4TG, UK

Abbreviations

ACh	Acetylcholine
AUC	Area under the curve
BMC	Benchmark concentration
$[Ca^{2+}]_i$	Intracellular free Ca^{2+} concentration
cAMP	N6,2'-O-Dibutyryl 3',5'-cyclic adenosine monophosphate
DN-IMI	Desnitro-imidacloprid
DNT	Developmental neurotoxicity
DMSO	Dimethyl sulfoxide
EC ₂₅	Quarter maximal effective concentration
IMI	Imidacloprid
IMI-olefin	Imidacloprid-olefin
LD ₅₀	Median lethal dose
Mec	Mecamylamine
MIE	Molecular initiating event
MLA	Methyllycaconitine
nAChR	Nicotinic acetylcholine receptor
pEC ₂₅	Negative logarithm of the quarter maximal effective concentration
pEC ₅₀	Negative logarithm of the half-maximal effective concentration
pIC ₅₀	Negative logarithm of the half-maximal inhibitory concentration
PBTK	Physiology-based toxicokinetic
PLO	Poly-L-ornithine
PNU	PNU-120596
Tubo	Tubocurarine

Introduction

The toxicological assessment of many pesticides is complicated by the fact that there is not only exposure to the original substances, but also to their many metabolites formed in the environment. This also applies to the neonicotinoids, a class of insecticides with long persistence within crops (Simon-Delso et al. 2015; Craddock et al. 2019; Thompson et al. 2020). They comprise, e.g., imidacloprid (IMI), acetamiprid, clothianidin, and thiacloprid. With a global market turnover of > 1 billion € (Jeschke et al. 2011; Sparks and Nauen 2015), this group of compounds has dominated many pesticide application domains and thus has led to widespread human exposure (Klarich et al. 2017; Craddock et al. 2019; Thompson et al. 2020). The neonicotinoids had a worldwide market share of the insecticide sales of around 25% in 2014–2018 (Bass et al. 2015; Casida 2018; Sparks et al. 2020). IMI accounted for around one-third of neonicotinoid use (Bass et al. 2015). In the US, the use of IMI for crop protection was estimated to be roughly around 1000 tons per year from 2011 to 2014 (Douglas and Tooker 2015; Craddock et al. 2019; US Geological Survey 2021). The insecticidal mode of action is based on the over-activation of the

nicotinic acetylcholine receptor (nAChR) of the target species. This activity has been assumed to be relatively specific for the insect nervous system (Brown et al. 2006; Tan et al. 2007), as neonicotinoids have been developed to exhibit a higher affinity for insect nAChRs compared to vertebrate paralogs (Tomizawa et al. 2000; Tomizawa and Casida 2005; Casida 2018). However, some studies suggest adverse effects of neonicotinoids on mammals (Abou-Donia et al. 2008; Duzguner and Erdogan 2012; Burke et al. 2018; Berheim et al. 2019). A broad toxicological debate has been triggered by the observation that acetamiprid and IMI activated the nAChRs on neonatal rat neurons in the low μ M range (Kimura-Kuroda et al. 2012). The relevance of this finding for human toxicology is further supported by a recent study using cultured human neurons. Clear nAChR signaling and also pronounced receptor desensitization were demonstrated for several neonicotinoids at concentrations that may be reached by dietary or accidental exposure (Loser et al. 2021a).

Food products intended for human consumption have high detection rates for IMI (Chen et al. 2014; Craddock et al. 2019; Thompson et al. 2020). In addition, several metabolites are found. The transformation of the parent compounds can arise via abiotic (photolysis, hydrolysis, and chlorination) or biological (microbial, fungal, and plant) processes (Simon-Delso et al. 2015; Thompson et al. 2020). One important metabolic step is the reduction of the nitro group of IMI to form aminoguanidine derivatives or derivatives that entirely lack the nitro group (e.g., DN-IMI) (Ford and Casida 2006). Besides cytochrome P450 enzymes, especially aldehyde oxidase seems to play an important role in this biotransformation (Schulz-Jander and Casida 2002; Schulz-Jander et al. 2002; Dick et al. 2005; Swenson and Casida 2013; Simon-Delso et al. 2015; Vardavas et al. 2018).

Imidacloprid-olefin (IMI-olefin) has been detected in honey (Codling et al. 2016; Thompson et al. 2020), and DN-IMI is a major IMI degradation product in the environment (Anon 2006; Koshlukova 2006). The latter metabolite is produced abiotically by photodegradation (17% of all IMI), but also biotically as the dominant bacterial metabolite, and as a major metabolite in many plants (Anon 2006; Koshlukova 2006). It has, e.g., been found in drinking water (Klarich Wong et al. 2019; Wan et al. 2020) and it has been reported to be formed in diverse foods such as apples, tomatoes, eggplants, and potatoes, where it accounted for around 10–30% of IMI degradation products. It reached concentrations in the 10–30 μ g/kg range in apples and potatoes and up to 300 μ g/kg in fodder corn (Anon 2006). The outdoor use of IMI has been banned in Europe in 2018 (European Commission 2018), due to unacceptable toxicity risks for bees (European Food Safety Authority [EFSA] 2016), and in 2020 the approval of IMI expired (European Commission 2020). However, exposure via the diet still occurs via imported food

commodities, and until now, several EU countries still grant temporary exemptions and notify the EU of these emergency authorizations (<https://ec.europa.eu/food/plant/pesticides/eu-pesticides-database/ppp/pppeas/screen/home>). The current dietary risk assessment on IMI in Europe covers the exposure to the parent compound IMI and its metabolites. However, there is no specific residue definition for DN-IMI (European Food Safety Authority [EFSA] et al. 2019). This means that it is assumed that the toxicological potency is similar to the parent compound.

DN-IMI has also been detected in mice exposed to IMI. This suggests that it can also be produced within mammals by endogenous metabolism (Ford and Casida 2006; Swenson and Casida 2013). This is consistent with findings of DN-IMI and IMI-olefin in human urine samples analyzed in a recent biomonitoring study (Wang et al. 2020).

The previous knowledge of IMI metabolism shows that a shift in the bioactivity spectrum can occur. For instance, the metabolite DN-IMI has a strongly reduced potency on insect nAChRs, but in turn an increased affinity for mammalian nAChRs (Liu et al. 1993; Chao and Casida 1997; Tomizawa et al. 2000). This is in line with studies in mice that suggested a higher toxicity of DN-IMI, compared to its parent compound IMI (Chao and Casida 1997; Tomizawa et al. 2000). Furthermore, binding assays using mammalian nAChRs have shown that DN-IMI has an affinity similar to the high-affinity ligand nicotine (Tomizawa and Casida 1999; D'Amour and Casida 1999; Tomizawa et al. 2000). Nicotine is a well-known neurotoxicant and developmental neurotoxicant for vertebrates, including man (Levin et al. 1993; Slikker Jr et al. 2005; LeSage et al. 2006; Grandjean and Landrigan 2006; Dwyer et al. 2009; Slotkin et al. 2016; Zahedi et al. 2019). Therefore, IMI metabolites mimicking the activity profile of nicotine on human receptors are of high toxicological concern.

The activation of ionotropic receptors like nAChRs on neurons leads to a depolarization of the cell membrane, and thereby, activates voltage-dependent Ca^{2+} channels. The transient influx of Ca^{2+} into the cell increases the intracellular free Ca^{2+} concentration ($[\text{Ca}^{2+}]_i$), which can be measured by Ca^{2+} -imaging in neuronal cell cultures (Leist and Nico-tera 1998; Sirenko et al. 2019; Grunwald et al. 2019; Loser et al. 2021b). This method is based on the quantifications of fluorescence signals of calcium-sensitive dyes introduced into the cells, and it is amenable to high-throughput formats (Sirenko et al. 2019; Karreman et al. 2020; Brüll et al. 2020; Loser et al. 2021b). Alternatively, xenobiotic effects on individual nAChR subtypes may be measured directly by the recording of the transmembrane currents in *Xenopus laevis* oocytes that heterologously express human receptors of interest. The basis of this method is the injection of mRNA coding for human neurotransmitter receptor subunits into the cells. It is well known that this experimental system has a

high efficiency for protein translation and functional insertion of the respective receptors in the cell membrane. The large size of the oocytes allows the current flow through the cell membrane (triggered by agonists) to be measured by two sharp microelectrodes placed inside the cell. The test method obtains its specificity from the strong heterologous expression of the respective receptor. (Bermudez and Moroni 2006; Moroni et al. 2006; Jonsson et al. 2006; Carbone et al. 2009; Mineur et al. 2009; Mazzaferro et al. 2011; Harpsøe et al. 2011; Li et al. 2011; Benallegue et al. 2013).

The human neuronal precursor cell line LUHMES and the neuroblastoma cell line SH-SY5Y can be differentiated into post-mitotic neurons (Lopes et al. 2010; Scholz et al. 2011), and they are often used as a model system to investigate adverse effects on human neurons (Tomizawa and Casida 1999; Gustafsson et al. 2010; Krug et al. 2013, 2014; Zhang et al. 2014; Ring et al. 2015; Lohren et al. 2015; Attoff et al. 2016, 2020; Smirnova et al. 2016; Harris et al. 2017; Tong et al. 2017; Witt et al. 2017; Delp et al. 2018a, b, 2019; Brüll et al. 2020). The utility of these cell models for functional neurotoxicity testing has been demonstrated for agents that affect voltage-dependent sodium channels or ionotropic receptors (Loser et al. 2021a, b). Both cell types express functional nAChRs and have been used in Ca^{2+} -imaging assays to study the effects of several neonicotinoids (Loser et al. 2021a).

In this study, we explored whether DN-IMI possesses a potential neurotoxicity or developmental neurotoxicity hazard, by acting on nAChRs of human neurons. The IMI metabolite was chosen for this study, as it may be directly ingested by food. However, it is also relevant as it may be generated in individuals exposed to IMI. We compared the signaling effects of DN-IMI on LUHMES neurons and SH-SY5Y to that of IMI and nicotine. To determine differences in nAChR subtype selectivity of the compounds, we further investigated the agonist activity of these compounds on human $\alpha 4\beta 2$, $\alpha 7$, and $\alpha 3\beta 4$ nAChR subtypes, expressed in *Xenopus laevis* oocytes, and we developed a molecular docking approach explaining these findings. To gather background information on the persistence and distribution of DN-IMI in man, a toxicokinetic model was implemented and parameterized by metabolism data from human hepatocytes. The broad data set of this study was used for a preliminary risk assessment of DN-IMI.

Materials and methods

Materials and chemicals

An overview of experimental tool compounds and toxicants is given in Table S1. Consumables are indicated in the specific methods paragraphs. Chemical structures of

imidacloprid (IMI) (<https://pubchem.ncbi.nlm.nih.gov/compound/86287518#section=2D-Structure>), desnitroimidacloprid (DN-IMI) (<https://pubchem.ncbi.nlm.nih.gov/compound/10130527#section=2D-Structure>) and imidacloprid-olefin (IMI-olefin) (<https://pubchem.ncbi.nlm.nih.gov/compound/14626249#section=2D-Structure>) were obtained from PubChem and visualized in ChemDraw JS (version 19.0.0-CDJS-19.0.x.9 + da9bec968, PerkinElmer).

LUHMES cell culture

The cultivation of the LUHMES cells was performed as described earlier (Scholz et al. 2011; Krug et al. 2013; Schildknecht et al. 2013). In brief, LUHMES cells were cultured in standard cell culture flasks (Sarstedt) that were pre-coated with 50 µg/ml poly-L-ornithine (PLO) and 1 µg/ml fibronectin (Sigma Aldrich) in H₂O overnight at 37 °C. The cells were maintained in proliferation medium containing advanced DMEM/F12 (Gibco) with 2 mM L-glutamine (Sigma Aldrich), 1 × N2-supplement (Gibco), and 40 ng/ml recombinant human basic fibroblast growth factor (FGF-2, R&D Systems). The cells were kept at 37 °C and 5% CO₂ and passaged three times a week when the culture reached a confluency of 75–90%. Cells were used until passage 18. For differentiation, cells were cultured in differentiation medium consisting of advanced DMEM/F12 (Gibco) supplemented with 2 mM L-glutamine (Sigma Aldrich), 1 × N2-supplement (Gibco), 1 mM N₆,2'-O-dibutyryl 3',5'-cyclic adenosine monophosphate (cAMP) (Sigma Aldrich), 1 µg/ml tetracycline (Sigma Aldrich) and 2 ng/ml recombinant human glial cell-derived neurotrophic factor (GDNF, R&D Systems).

For Ca²⁺-imaging, the cells were pre-differentiated for 48 h in cell culture flasks, detached and plated at a density of 20,000 cells and 30,000 cells per well on 0.1% PEI-coated 384-well and 96-well plates (Greiner Bio-One), respectively, for the Ca²⁺-imaging. The cells were further differentiated for another 7 days. 50% of the medium was exchanged every 2–3 days.

Cell culture of SH-SY5Y cells

SH-SY5Y cells were cultured as previously described (Attoff et al. 2016). Briefly, they were cultured in MEM supplemented with 10% fetal bovine serum (Gibco, 31330095), 1% non-essential amino acid solution (Gibco, 11140035), 2 mM L-glutamine (Gibco, 25030024), 100 µg/ml streptomycin, and 100 U/ml penicillin (Gibco, 15140122). For maintenance culture, SH-SY5Y cells were seeded at 27,000 cells/cm² in 75 cm² cell culture flasks (Corning). The cells were passaged once a week using TrypLE Express Enzyme (Gibco). SH-SY5Y cells were differentiated into a neuronal-like phenotype by exchanging the maintenance medium with differentiation medium consisting of DMEM/F12 (Gibco,

31330095) supplemented with 1 mM L-glutamine (Gibco, 25030024), 100 µg streptomycin/mL, 100 U penicillin/mL, 1 × N2-supplement (Gibco, 17502048) and 1 µM all-trans retinoic acid (RA, Sigma, R2625) 24 h after seeding. The cells were incubated in 100% humidity at 37 °C in air with 5% CO₂.

LUHMES Ca²⁺-imaging

Ca²⁺-imaging was performed using HT Functional Drug Screening System FDSS/µCELL (Hamamatsu Photonics) at nominal 37 °C. The FDSS/µCell system enables the indirect recording of changes of [Ca²⁺]_i via a Ca²⁺-sensitive fluorescent dye. The fluorescence signal of a complete 384-well plate is acquired at once with a high-speed and high-sensitivity digital ImagEM X2 EM-CCD camera (Electron Multiplying Charge-Coupled Device, Hamamatsu Photonics), but with limited spatial resolution. Therefore, the software only determines the mean fluorescence signal of each well rather than of individual cells. For compound application, the integrated dispenser head with 384 pipette tips was used, which can add the test compound to all wells simultaneously. Cells were preincubated with Cal-520 AM (AAT Bioquest) at a concentration of 1 µM for 1 h at 37 °C. For recording, the medium was exchanged by a buffer solution containing [mM]: 135 NaCl, 5 KCl, 0.2 MgCl₂, 2.5 CaCl₂, 10 HEPES, and 10 D-glucose, pH 7.4. Test compound application was executed after obtaining a 1.5 min baseline recording. Where applicable, a second application was executed 4.5 min after the first application. The total recording never exceeded 8 min.

For Ca²⁺-imaging experiments with a higher resolution on the single-cell level, the Cell Observer (Carl Zeiss Microscopy) was used. The Ca²⁺-sensitive dye, the cell handling before the experiment, and the buffer were the same as described above for the experiments with the high-throughput FDSS/µCELL system. The recordings were performed with 2 × 2 binning and a 42 ms exposure time. The compounds were applied after a baseline recording of at least 10 s.

Ca²⁺ measurements in SH-SY5Y

To measure acute changes in the average [Ca²⁺]_i of a population, SH-SY5Y cells were examined in the 96-well plate fluorescence reader FlexStation II (Molecular Devices) using the fluorophore Fura-2AM. SH-SY5Y (35,000 cells/well; 109,375 cells/cm²) were seeded in maintenance culture medium in black 96-well plates with clear bottom (Corning, #3603). 24 h after seeding, maintenance medium was replaced with differentiation medium. After 72 h of differentiation, Fura-2AM dissolved in DMSO and diluted in KRH buffer (125 mM NaCl, 5 mM KCl, 1.2 mM MgSO₄, 1.2 mM

KH₂PO₄, 2.0 mM CaCl₂, 6.0 mM D-glucose, and 25 mM HEPES (free acid), pH adjusted to 7.4 by 1.0 M NaOH) were added to the medium to a final concentration of 4 μM (Gustafsson et al. 2010). The plates were incubated for 30 min at 37 °C before cells were washed once with 200 μl KRH buffer. 90 μl of KRH buffer without or with 10 μM PNU-120596 (PNU) and/or 125 μM mecamylamine (Mec) and/or test chemicals in different concentrations for antagonist experiments were added to the Fura-2AM-loaded cells. The plate was again incubated for 20 min to allow full hydrolysis of the AM group before the experiment. The fluorescence was assessed at 37 °C in the fluorescence plate reader (FlexStation II; Molecular Devices) at two different excitation wavelengths, 340 nm for Ca²⁺-bound Fura-2 and 380 nm for free Fura-2, and at 510 nm emission, every 3.1 s using bottom read settings. After 26–29 s of initial baseline recording of the fluorescence intensity, 10 μl of the compound dilution (10 times higher than the final concentration to the cells) was transferred automatically by the FlexStation II (“Flex mode”) to the cell plate wells (five wells per concentration) and the fluorescence intensity was monitored for another 150 s. The ratio of fluorescence intensity at 340/380 nm was determined and the mean values from the baseline recording before the addition of test compounds was set to zero. The acute change in the Ca²⁺ influx after the addition of the compounds was quantified as the area under the curve (AUC) using the SoftMax Pro 4.8 software (Molecular Devices). All test compounds were dissolved in DMSO. Compounds were diluted in KRH buffer in 1:3 series, with 100 μM as the highest concentration. As a negative control, 0.1% DMSO in KRH buffer was used. Nicotine (11 μM) and KCl (30 mM) in KRH were used as positive controls. The Ca²⁺ influx induced by DN-IMI was normalized to the response triggered by nicotine (11 μM) or KCl (30 mM).

Oocyte recordings

The human α3 (GenBank: U62432.1), α4 (GenBank: L35901.1, silent base exchanges to reduce GC content), β2 (GenBank: X53179.1), and β4 (GenBank: U48861.1) nAChR subunits were synthesized using FragmentGene service by Genewiz company and subsequently cloned in the pNKS2 vector (Gloor et al. 1995) using Gibson Assembly. The human α7 nAChR subunit was cloned in the pCDNA3.1 vector.

For the generation of the mRNA for injection, the plasmid DNAs of α3, α4, β2, and β4 were linearized with the NotI restriction endonuclease (New England Biolabs) and the plasmid DNA of α7 was linearized with the XbaI restriction endonuclease (New England Biolabs). The mRNAs of α3, α4, β2, and β4 were generated by in vitro transcription using the mMACHINE mMACHINE SP6 Transcription Kit (Invitrogen). For the generation of α7 mRNA, the mMACHINE

mMACHINE T7 Transcription Kit (Invitrogen) was used. For the separation of the DNA and mRNA, a phenol–chloroform extraction (Chomczynski and Sacchi 2006) was performed. The mRNA was then obtained by ethanol precipitation from the aqueous phase; for quantification, the BioPhotometer (Eppendorf) was used.

The recordings of human α7, α3β4, α4β2, and α4β4 nAChRs expressed in *Xenopus laevis* oocytes (EcoCyte Bioscience) were performed in two-electrode voltage-clamp mode using the Roboocyte2 system and the corresponding software (version 1.4.1; Multi Channel Systems MCS). Prior to the recordings, the oocytes were maintained at 19 °C in modified Barth’s solution containing [mM]: 88 NaCl, 1 KCl, 0.33 Ca(NO₃)₂, 0.82 MgSO₄, 2.4 NaHCO₃, 0.41 CaCl₂, 5 Tris, 100 U/ml penicillin, 100 μg/ml streptomycin, pH 7.4.

To express human α7 nAChR, we injected 50 nl of mRNA solution (30 ng mRNA) per oocyte, using the Roboinject and the corresponding software (version 1.2.1; Multi Channel Systems MCS). The subunits of the heteromeric human α3β4 nAChRs and high-sensitivity (HS) (α4)₂(β2)₃ combination were injected in a ratio of 1:10 (α:β subunit) with an mRNA amount of 0.33 ng of α3 and 3.33 ng of β4 for α3β4, and 3 ng of α4 and 30 ng of β2 for α4β2. The mRNA for the subunits of the low-sensitivity (LS) (α4)₃(β2)₂ stoichiometry was injected in a ratio of 10:1 (α:β subunit) with 10 ng of α4 and 1 ng of β2. The subunits of the α4β4 nAChR subtype were injected in a ratio of 1:1 with 3.33 ng of α4 and 3.33 ng of β4. After mRNA injection, the oocytes were maintained for 3–6 days before recordings were performed. The experiments were executed in a ND96 buffer solution containing [mM]: 96 NaCl, 2 KCl, 1 MgCl₂, 1.8 CaCl₂, 5 HEPES, pH 7.4. The oocyte membrane potential was kept at –50 mV in all recordings. In experiments with α7, the compounds were applied for 5 s followed by a 60 s wash period. At the end of each recording, a reference application of 1 mM nicotine was performed. In experiments with heteromeric nAChRs, the compound was applied for 3 s, followed by a washout of 10 s, and an application of acetylcholine (ACh) for 1 s, which was followed by a washout of 60 s. The recordings for α3β4, α4β2 (HS), α4β2 (LS) and α4β4 were performed with 200 μM, 3 μM, 100 μM and 100 μM ACh, respectively. ACh was applied as an additional reference for run-down detection and positive control. Therefore, ACh was applied four times before the addition of the first compound concentration and after the application of each compound concentration. After the measurement of all compound concentrations, the last application was a reference exposure to nicotine with 1 mM for α3β4, 10 μM for α4β2 (HS), 100 μM for α4β2 (LS) and 100 μM for α4β4. The reference response triggered by nicotine was used for the normalization of the compound effects.

For the antagonist experiments, DN-IMI was applied for 3 s after a 5 s baseline period. The application of DN-IMI

was followed by a wash period of 70 s. At first, four control recordings were performed, followed by three recordings in the presence of each of the three antagonist concentrations in ascending order. Finally, three recordings were executed during the washout. DN-IMI was applied at 1 μM in recordings with $\alpha 4\beta 2$ (HS) and at 30 μM in recordings with $\alpha 3\beta 4$ and $\alpha 7$.

Physiologically based toxicokinetic modeling

A physiology-based toxicokinetic (PBTK) model for DN-IMI was established in the Simcyp Simulator V20 (Certara) using a previously published approach (Albrecht et al. 2019). Due to the lack of published human metabolism and exposure data for DN-IMI, an analog approach was used to inform the PBTK model using a compound, in our case atenolol, with known human pharmacokinetics and similar physicochemical properties. The input parameters for DN-IMI and atenolol are given in Table S8 and further details are found in Fig. S10.

Data analysis

For the high-throughput Ca^{2+} -imaging data obtained in LUHMES cells, an offset correction using the FDSS software (version 3.2) was performed. Afterward, the data were exported and further analyzed with scripts written in R (version 3.6.3) (R Core Team 2020). The concentration–response curves were fitted using a log-logistic model described by Ritz et al. (2015), utilizing the R package *drc* with its function *drm()* and *LL2.2()* with the following equation: $f(x) = d / [1 + \exp(b(\log(x) - \tilde{e}))]$ (Ritz et al. 2015). The logarithm of the half-maximal effective concentration ($\log\text{EC}_{50}$) between 0 and the upper limit (d), which was set to 1, is represented by \tilde{e} , x denotes the concentration, and b stands for the slope parameter (Ritz et al. 2015). In cases with normalizations to responses induced by other compounds, the function *LL2.3()* was used with a variable upper limit (d ; Ritz et al. 2015). The same equation was used to determine the half-maximal inhibitory concentration ($\log\text{IC}_{50}$). Then the $\log\text{EC}_{50}$ and $\log\text{IC}_{50}$ values were converted into the pIC_{50} and pEC_{50} values, which are the negative logarithms to base 10.

Concentration–effect responses in the SH-SY5Y $[\text{Ca}^{2+}]_i$, were analyzed by the GraphPad Prism8.0 software using the four-parameter sigmoidal curve fit settings and the concentrations giving 50% increase in $[\text{Ca}^{2+}]_i$ in relation to the nicotine response were estimated.

The single-cell Ca^{2+} -imaging recordings were exported and analyzed in Fiji ImageJ (version 1.52i) to get the average fluorescence signal of each cell. These signals were further analyzed in R, where a threshold detection was performed to detect responding cells. For this, the offset was corrected by subtracting the mean of 20–65% of the fluorescence signal

of the pre-application period from the recording, to be robust against spontaneous activity. The threshold was defined as mean + 3 * SD of the negative control recordings, during the detection phase of 6.5 s during the application.

The baseline correction of voltage-clamp oocyte recordings was performed with the Roboocyte2 + software (version 1.4.3; Multi Channel Systems MCS, Germany). The maximal current influx and further analysis were executed in scripts written in R. In the antagonist experiments with oocytes, the maximal inward current was determined for the last response of each period (control, three antagonist concentrations, and washout).

The following R packages were utilized for data handling: *cowplot* (Wilke 2019), *dplyr* (Wickham et al. 2020), *drc* (Ritz et al. 2015), *ephy2* (Danker 2018), *ggplot2* (Wickham 2016), *htmlwidgets* (Vaidyanathan et al. 2019), *lemon* (Edwards 2019), *magick* (Ooms 2020), *magrittr* (Bache and Wickham 2014), *matrixStats* (Bengtsson 2020), *modelr* (Wickham 2020), *multcomp* (Hothorn et al. 2008), *plotrix* (Lemon 2006), *proto* (Grothendieck et al. 2016), and *tidyverse* (Wickham et al. 2019).

Unless mentioned differently, values are presented as means \pm SEM. Experiments were usually performed with at least three technical replicates per condition. Detailed data on pEC_{50} , pIC_{50} , and numbers of experimental repetitions are given in supplementary tables. Unless mentioned differently, statistical significance was defined as $P < 0.05$ and was determined by one-way ANOVA with Dunnett's post hoc test as indicated. To determine benchmark concentrations (BMC), and their upper and lower 95% confidence intervals (BMCL, BMCU), the BMC online software of UKN was used (Krebs et al. 2020).

Results and discussion

Activation, inhibition, and desensitization of nAChRs functionally expressed in LUHMES and SH-SY5Y cells

Activation of nAChRs on LUHMES cells by DN-IMI

LUHMES neurons express functional $\alpha 7$ and non- $\alpha 7$ nAChRs, and they have proven useful for the characterization of different neonicotinoids like IMI by high-throughput Ca^{2+} -imaging (Loser et al. 2021a). We used this system here for the functional characterization of the two IMI metabolites DN-IMI and IMI-olefin (Fig. 1A). Both metabolites produced clear signals (Fig. 1B, C). A quantification of $[\text{Ca}^{2+}]_i$ responses yielded a pEC_{50} of 6.6 for DN-IMI (Fig. 1D). DN-IMI appeared at least as potent as ACh and nicotine (pEC_{50} values of ~ 6.0 in LUHMES neurons) (Loser

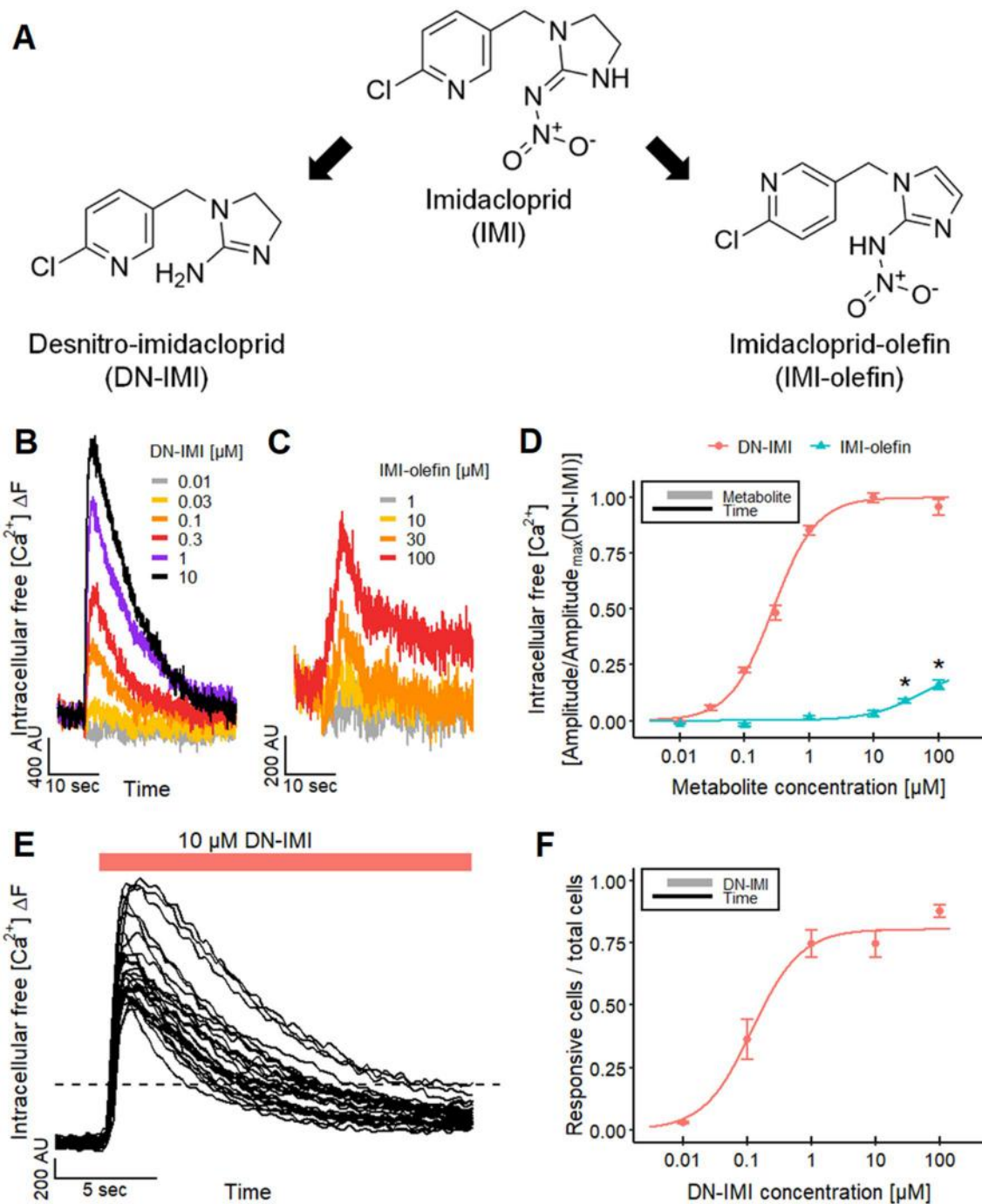


Fig. 1 Effect of desnitro-imidacloprid (DN-IMI) and imidacloprid-olefin (IMI-olefin) on LUHMES neurons. **A** Chemical structures of imidacloprid (IMI) and its two metabolites desnitro-imidacloprid (DN-IMI) and imidacloprid-olefin (IMI-olefin). **B–F** LUHMES neurons were differentiated for 9 days before they were loaded with an $[Ca^{2+}]_i$ indicator dye and used for Ca^{2+} -imaging. **B, C** The cells cultivated in 384-well plates were exposed to various concentrations of DN-IMI and IMI-olefin, and exemplary recordings of the fluorescence signal from a whole well are shown. **D** The fluorescence data (peak amplitude) of multiple experiments were quantified and normalized to the maximal response stimulated by DN-IMI (means \pm SEM are displayed). The significance of the responses triggered by IMI-olefin was determined between control recordings and

the responses evoked by IMI-olefin (*: $p < 0.05$). For DN-IMI, a sigmoid curve was fitted to the data, and a pEC_{50} value of 6.6 ± 0.03 was obtained as a potency estimate. Note the treatment scheme (upper left corner), illustrating the experimental design. **E, F** LUHMES cultures in 96-well plates were used to image the $[Ca^{2+}]_i$ responses of single cells with a fluorescent microscope. Regions of interest were assigned for all individual cell bodies in the image section. **E** Ca^{2+} -imaging traces of the responses of individual cell bodies are shown after exposure to DN-IMI (10 μM). **F** The percentage of cells that responded with a clear fluorescence increase (= rise in $[Ca^{2+}]_i$) to different concentrations of DN-IMI was determined. Note the treatment scheme (upper left corner), illustrating the experimental design. Detailed data on n numbers are listed in Tables S6

et al. 2021a). These signaling data are in line with published binding data that suggest a similar affinity of DN-IMI and nicotine for mammalian nAChRs (Tomizawa and Casida 1999; D'Amour and Casida 1999; Tomizawa et al. 2000).

For IMI-olefin, the pEC_{50} was not reached within the measurement range ($\leq 100 \mu\text{M}$), but a significant response (around 15% of the maximal response to DN-IMI) was found at 30–100 μM . Thus, the potency of IMI-olefin was similar to that of its parent compound IMI (Loser et al. 2021a). Our observations on signaling potency are consistent with the literature data for differences in binding affinity to mammalian nAChRs (Chao and Casida 1997; Tomizawa and Casida 1999; D'Amour and Casida 1999; Tomizawa et al. 2000).

The data on DN-IMI were confirmed by a different analytical method. Instead of the whole-culture-based high-throughput $[Ca^{2+}]_i$ assay, we used traditional time-lapse fluorescence microscopy to quantify responses of individual cells (Fig. 1E). We found here a percentage of responsive cells of ~80%. This population was similar in size to that measured in a previous study, using nicotine as a stimulus (Loser et al. 2021a). The quantification of single-cell responses confirmed the sub-micromolar potency of DN-IMI and suggested that the majority of all cells responded functionally to the IMI metabolite (Fig. 1F).

Activation of $\alpha 7$ and non- $\alpha 7$ nAChRs on LUHMES and SH-SY5Y cells by DN-IMI

There is a large variety of nAChR subtypes with distinct functions in the nervous system. To get initial information, we examined whether the human $\alpha 7$ nAChR is affected by DN-IMI. This Ca^{2+} permeable receptor is widely distributed in the central nervous system and involved in the modulation of neurotransmitter release (McGehee et al. 1995; Gray et al. 1996; Alkondon et al. 1999; Gotti et al. 2006; Zoli et al. 2015). We utilized PNU-120596 (PNU), a selective positive allosteric modulator of the $\alpha 7$ nAChR, to slow down the $\alpha 7$ nAChR inactivation and enable thereby the detection of the $\alpha 7$ nAChR-mediated response in Ca^{2+} -imaging (Hurst et al. 2005; Dickinson et al. 2007; Ng et al. 2007; Grønlien et al. 2007; Papke et al. 2009; Williams et al. 2011; Chatzidaki et al. 2015; Larsen et al. 2019). The response of LUHMES neurons to DN-IMI was strongly enhanced and prolonged in the presence of PNU (Fig. 2A). A quantification at multiple DN-IMI concentrations showed that this effect is less pronounced at sub-maximal receptor stimulation (Fig. 2B). The maximal amplitude triggered by DN-IMI was increased by PNU by around 40%. This strongly suggests the activation of $\alpha 7$ nAChRs. These data are fully in line with findings showing the enhancement of neonicotinoid effects by PNU in LUHMES neurons (Loser et al. 2021a). The activation of non- $\alpha 7$ nAChRs at low concentrations of DN-IMI

(0.03–0.3 μM) is most likely the reason for an absence of PNU enhancement in the low concentration range.

To further support these findings, we examined the effect of DN-IMI on a second human cell system. SH-SY5Y neuroblastoma cells predominantly express the $\alpha 7$ nAChR subtype, together with $\alpha 3$ -containing receptors (Loser et al. 2021a). Therefore, they show little response to neonicotinoids or nicotine in the absence of PNU, and also DN-IMI only triggered small responses reaching about 44% of the maximal response obtained in the presence of PNU (Fig. 2C). In this experimental setup (presence of PNU), DN-IMI led to a strong, concentration-dependent $[Ca^{2+}]_i$ response with half-maximal responses at about 0.3 μM , a peak at ~3 μM , and declining responses at even higher concentrations (Fig. 2C). The maximal response triggered by DN-IMI was roughly similar to the one evoked by nicotine. The strong signal increase in the presence of PNU is in line with our results for LUHMES.

We also examined the effect of IMI-olefin in the absence and presence of PNU on $[Ca^{2+}]_i$ of LUHMES neurons (Fig. S1A), and we observed a strong enhancement of the signal. This allowed for the determination of a pEC_{50} (5.5 in the presence of PNU) (Fig. S1B). The significant increase of the responses indicates the activation of human $\alpha 7$ nAChRs by IMI-olefin, but with a significantly lower potency compared to DN-IMI.

Inhibition of DN-IMI-evoked responses of LUHMES and SH-SY5Y cells by nAChR antagonists

We used a pharmacological approach to verify that the signaling ($[Ca^{2+}]_i$) effect of DN-IMI is mediated exclusively by nAChRs. For this purpose, LUHMES cells were pretreated with several well-known nAChR antagonists. Tubocurarine (Tubo) (Jonsson et al. 2006) antagonized the responses evoked by DN-IMI with a pIC_{50} of 5.9 (Fig. 3A, C). Tubo completely blocked the response at 100 μM , indicating that the entire DN-IMI-evoked Ca^{2+} -signaling was mediated by nAChRs. The obtained pIC_{50} value is comparable to the values determined for several nAChR agonists in experiments with LUHMES (Loser et al. 2021a).

To further substantiate this finding, we utilized the non-competitive nAChR antagonist mecamlamine (Mec) (Papke et al. 2008; Capelli et al. 2011). It blocked the DN-IMI-induced response in LUHMES neurons with a pIC_{50} of 6.8 (Fig. 3B, C), which is in line with the literature data of 6.6 for human $\alpha 3\beta 2$ nAChRs (Chavez-Noriega et al. 2000). We also used Mec in the SH-SY5Y cultures, and the $[Ca^{2+}]_i$ responses induced by DN-IMI were strongly blocked (Fig. 2D). This confirmed that also in this cell model, DN-IMI signaling was strictly dependent on nAChRs.

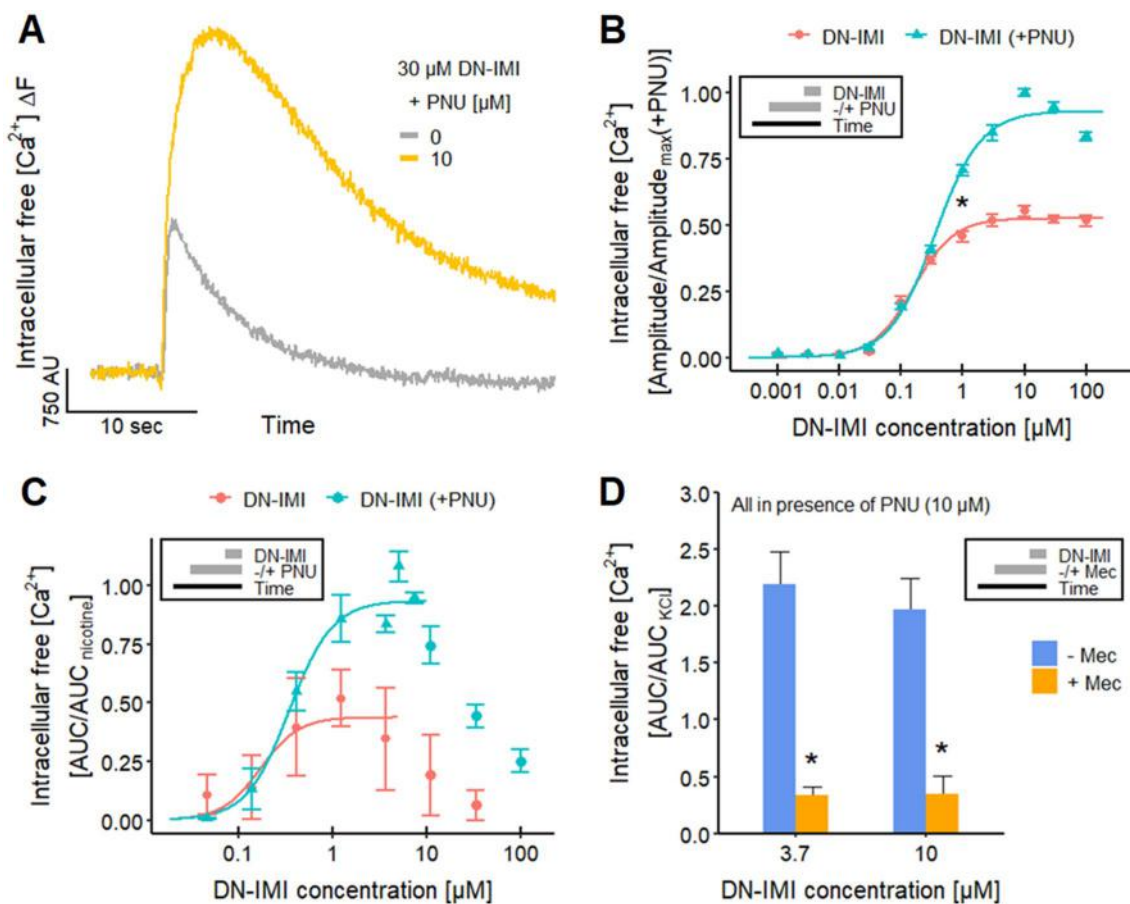


Fig. 2 Activation of human $\alpha 7$ nAChRs on LUHMES and SH-SY5Y cells by DN-IMI. **A**, **B** LUHMES neurons differentiated in 384-well plates were exposed to various concentrations of DN-IMI in the absence and presence of PNU-120596 (PNU, 10 μ M), a selective positive allosteric modulator of $\alpha 7$ nAChRs. **A** Representative recordings of the Ca^{2+} -imaging fluorescence signal from a whole well are shown. **B** The fluorescence data (peak amplitude) of multiple experiments were quantified and normalized to the maximal response triggered by DN-IMI in the presence of PNU (means \pm SEM are displayed). After sigmoidal curve fitting, the relative half maximum (turning point) was determined: they were on a $-\log(\text{M})$ scale: 6.8 ± 0.04 in the absence of PNU and 6.5 ± 0.03 in the presence of PNU. The upper asymptote was at 53% of the maximal response (found in all experiments at all conditions) in the absence of PNU and at 93% in the presence of PNU. The significance of the difference between the effects of DN-IMI (1 μ M) in the absence and pres-

ence of PNU was evaluated (*: $p < 0.05$). Detailed data on n numbers are found in Table S6. **C**, **D** SH-SY5Y cells were used for automated $[\text{Ca}^{2+}]_i$ monitoring, with the area under the curve (AUC) of the fluorescence intensity as assay endpoint. Data were normalized to a reference signal (10 μ M nicotine in **C**, 30 mM KCl in **D**). All data are from multiple experiments and are displayed as means \pm SEM. **C** Data were obtained for multiple concentrations of DN-IMI in the absence and presence of PNU, and the ascending arms of the curves were fitted for concentrations $< 10 \mu\text{M}$. The sigmoidal curve fit yielded relative pEC_{50} s of 6.8 ± 0.36 in the absence of PNU (estimated maximum at ~ 0.44 , $n=5$) and 6.5 ± 0.07 (0.3 μM , estimated maximum at ~ 0.93 , $n=4$) in the presence of PNU. **D** The $[\text{Ca}^{2+}]_i$ response of SH-SY5Y cells triggered by DN-IMI [in the presence of PNU (10 μM)] was measured in the absence and presence of the nAChR antagonist mecamylamine (Mec, 125 μM) ($n=5$); *: $p < 0.05$. Note the treatment schemes, illustrating the experimental design

To further investigate the agonism of DN-IMI on nAChRs on LUHMES, we researched the effect of the antagonist methyllycaconitine (MLA), which is highly potent (low nM range) on $\alpha 7$ nAChRs compared to other nAChR subtypes (Puchacz et al. 1994; Gopalakrishnan et al. 1995; Palma et al. 1996; Buisson et al. 1996; Capelli et al. 2011). MLA inhibited the response to DN-IMI with a pIC_{50} of 6.8 (Fig. 3D, F), which is comparable to the value obtained for nicotine with LUHMES (Loser et al. 2021a). The pIC_{50} is similar to the literature data

for human $\alpha 4\beta 2$ and $\alpha 6$ -containing ($\alpha 6/3\beta 2\beta 3$) nAChRs (Capelli et al. 2011). This (relatively low) potency of MLA in LUHMES indicates the involvement of non- $\alpha 7$ nAChRs in the $[\text{Ca}^{2+}]_i$ response evoked by DN-IMI.

Finally, we applied the nAChR antagonist MG 624 (Gotti et al. 2000; Capelli et al. 2011) on LUHMES neurons. The resulting pIC_{50} of 6.8 (Fig. 3E, F) is comparable to the pIC_{50} of nicotine obtained with LUHMES neurons (Loser et al. 2021a) and previously reported data for $\alpha 4\beta 2$, $\alpha 3\beta 4$, $\alpha 7$, and $\alpha 1\beta 1\delta \epsilon$ nAChRs (Capelli et al. 2011).

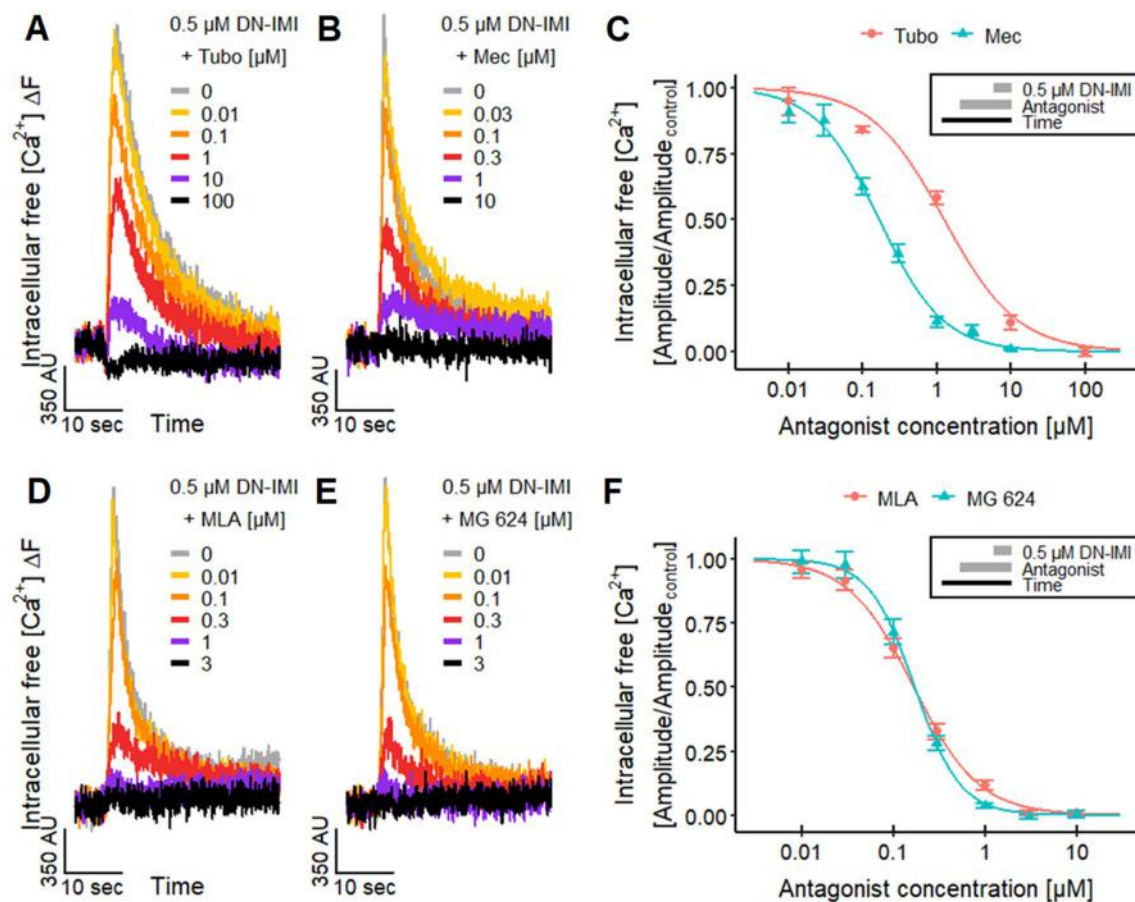


Fig. 3 Inhibition of DN-IMI signaling by nAChR antagonists. LUHMES neurons differentiated in 384-well plates were pretreated with various concentrations of nAChR antagonists before DN-IMI (0.5 μM) was applied in Ca²⁺-imaging experiments. **A, B** Exemplary recordings of the fluorescence signal from a whole well are shown for the effects of **A** tubocurarine (Tubo) and **B** mecamylamine (Mec) on the responses evoked by DN-IMI. **C** The fluorescence data (peak amplitude) of multiple experiments were quantified and normalized to control recordings (means ± SEM are displayed). After curve fitting, pIC₅₀ values of 5.9 ± 0.05 for Tubo and 6.8 ± 0.03 for Mec were determined for their inhibitory effects on DN-IMI-induced [Ca²⁺]_i responses. Note the treatment scheme (upper right corner), illustrating the experimental design. **D, E** Exemplary recordings of the fluorescence signal from a whole well are shown for the effects of **D** MLA and **E** MG 624 on the [Ca²⁺]_i responses evoked by DN-IMI. **F** The fluorescence data (peak amplitude) of multiple experiments were quantified and normalized to control recordings (means ± SEM are displayed). After curve fitting, pIC₅₀ values of 6.8 ± 0.03 for MLA and 6.8 ± 0.03 for MG 624 were determined. Note the treatment scheme (upper right corner), illustrating the experimental design. Detailed data on n numbers are found in Table S6

In summary, the antagonist data demonstrate the activation of nAChRs by DN-IMI and indicate the involvement of different nAChR subtypes.

Desensitization of cholinergic responses of LUHMES and SH-SY5Y cells by DN-IMI

An important feature of nAChRs is desensitization. This is the inactivation of the receptor during agonist exposure or upon closely timed repeated agonist applications. Thus, even in the presence of an agonist, the receptor can stop the signaling and may not be activated again within a certain period after an initial stimulation (Fenster et al. 1997; Quick and Lester 2002; Paradiso and Steinbach 2003; Lester 2004; Rollema et al. 2010; Marks et al. 2010; Capelli

et al. 2011; Papke et al. 2011; Campling et al. 2013; Eaton et al. 2014; Arias et al. 2015; Rollema and Hurst 2018). The desensitization of a receptor is typically caused by an agonist concentration that activates the receptor, but it can also occur at low concentrations that are not sufficient to activate it (Fenster et al. 1997; Paradiso and Steinbach 2003; Lester 2004; Rollema et al. 2010; Capelli et al. 2011; Arias et al. 2015; Rollema and Hurst 2018). As our previous results indicate an agonistic effect of both IMI metabolites, we investigated whether they would also desensitize the nAChRs on LUHMES neurons. In these experiments, the metabolites were pre-applied at various concentrations and then the response of LUHMES neurons was triggered by the exposure to nicotine and measured by Ca²⁺-imaging. The pretreatment led to a pronounced reduction of the

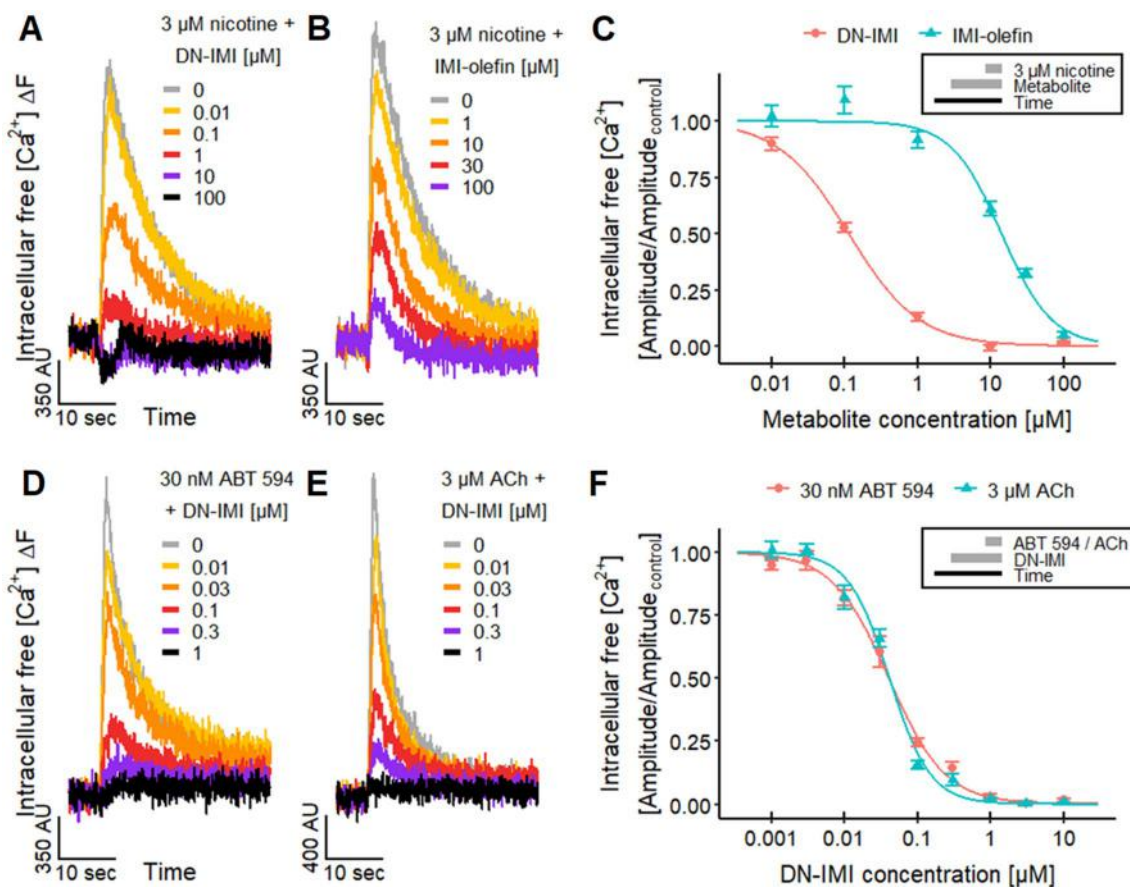


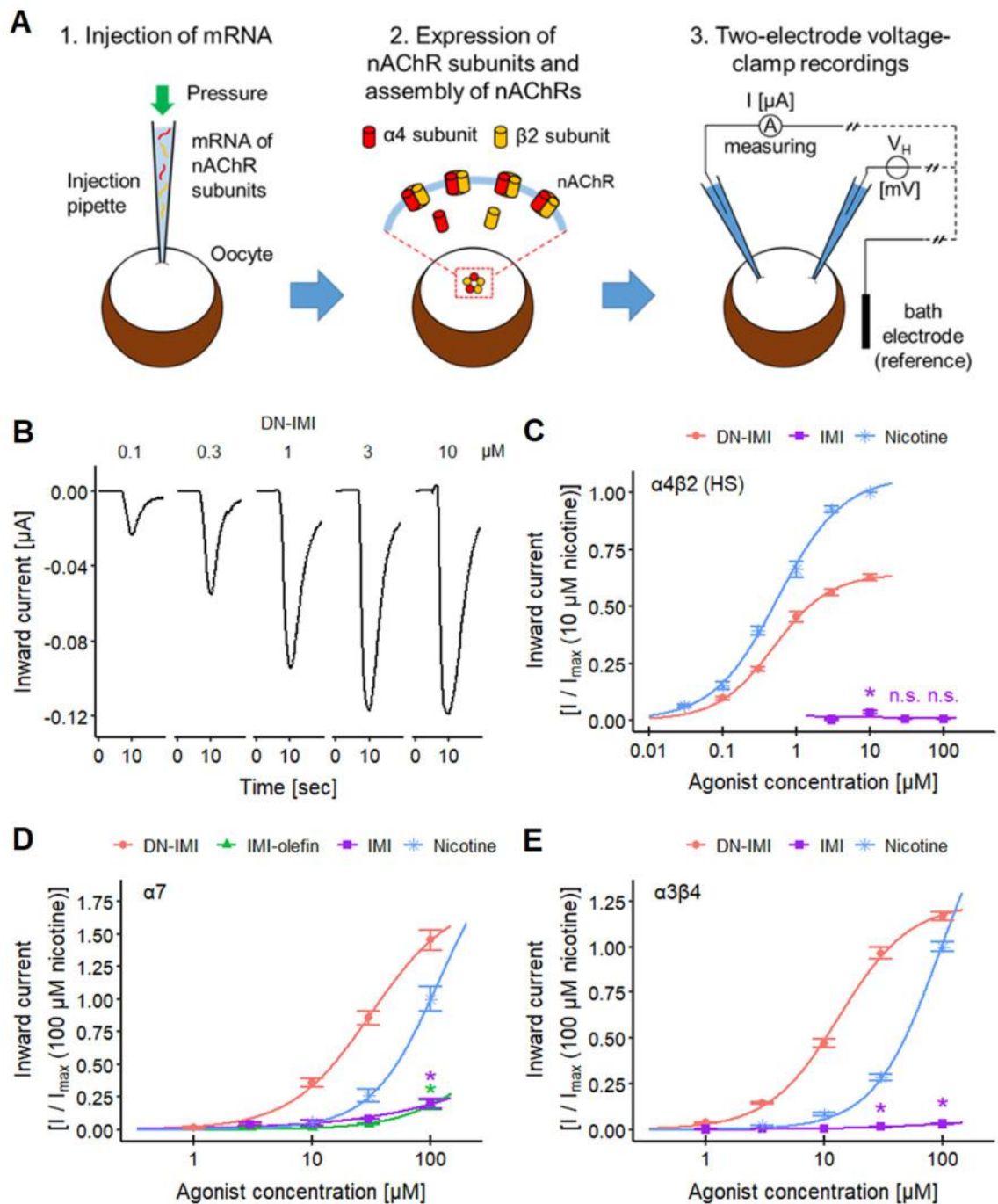
Fig. 4 Desensitizing effects of DN-IMI and IMI-olefin on nAChRs. LUHMES neurons differentiated in 384-well plates were pretreated with various concentrations of DN-IMI or IMI-olefin for 4.5 min before different nAChR agonists were applied and $[Ca^{2+}]_i$ signals were recorded. **A, B** Exemplary traces of the fluorescence signal from a whole well are shown for the desensitizing effects of different concentrations of **A** DN-IMI and **B** IMI-olefin on the $[Ca^{2+}]_i$ responses evoked by nicotine. **C** The fluorescence data (peak amplitude of 3 μ M nicotine) of multiple experiments were quantified and normalized to control recordings (means \pm SEM are displayed). After curve fitting, pIC_{50} values of 6.9 ± 0.03 for DN-IMI and 4.9 ± 0.03 for IMI-

olefin were determined. Note the treatment scheme (upper right corner), illustrating the experimental design. **D, E** Exemplary traces of the fluorescence signal are shown for the effects of DN-IMI on the responses evoked by **D** 30 nM ABT 594 and **E** 3 μ M ACh. **F** The fluorescence data (peak amplitude of the agonist stimulus) of multiple experiments were quantified and normalized to control recordings (means \pm SEM are displayed). After curve fitting, pIC_{50} values of 7.4 ± 0.03 (ABT 594) and 7.4 ± 0.03 (ACh) were determined. Note the treatment scheme (upper right corner), illustrating the experimental design. Detailed data on n numbers are found in Table S6

nicotinic signaling (Fig. 4A, B). The corresponding concentration–response curves yielded pIC_{50} values of 6.9 for DN-IMI and 4.9 for IMI-olefin (Fig. 4C). The pIC_{50} of IMI-olefin is comparable to the effects of its parent compound IMI and other neonicotinoids (Loser et al. 2021a). The pIC_{50} of DN-IMI is comparable to pIC_{50} values reported for the desensitizing effect of nicotine on human $\alpha 4\beta 2$, $\alpha 4\beta 4$, and $\alpha 3\beta 4$ nAChRs (Fenster et al. 1997; Lester 2004; Capelli et al. 2011). Thus, DN-IMI was more potent than several neonicotinoids (pIC_{50} s of ~ 5.4) (Loser et al. 2021a) and IMI-olefin at attenuating the response evoked by nicotine. For confirmation of the desensitization in a different cell model, we used SH-SY5Y cells. In addition, here, pretreatment with DN-IMI reduced/abolished the response to nicotine in the submicromolar range. This effect was clearly more potent

than the desensitization observed by IMI and another neonicotinoid pesticide, acetamiprid (Fig. S2). Thus, desensitization by neonicotinoids was confirmed in a second cell model, and the particularly high potency of DN-IMI was reproduced.

To confirm that the desensitizing effect was not specific for nicotine stimulation, we used the endogenous nAChR agonist ACh and the selective non- $\alpha 7$ nAChR agonist ABT 594 for stimulation (Donnelly-Roberts et al. 1998; Michelmore et al. 2002) (Fig. 4D, E). Here, we observed pIC_{50} values of ~ 7.4 for the desensitization (Fig. 4F). This high potency is in agreement with other observations that desensitization of nAChR can occur at lower concentrations than required for activation (Fenster et al. 1997; Paradiso and Steinbach 2003; Lester 2004; Rollema et al.



2010; Capelli et al. 2011; Arias et al. 2015; Rollema and Hurst 2018). The large difference in potency of DN-IMI and its parent compound IMI and other neonicotinoids is consistent with the literature data for potency differences in binding assays with mammalian nAChRs (Chao and Casida 1997; Tomizawa and Casida 1999; D'Amour and Casida 1999; Tomizawa et al. 2000).

In summary, DN-IMI desensitized nAChRs in the nM range, and this may be of toxicological significance, as nAChR signaling plays an important role in the central

nervous system (Alkondon et al. 1999; Champtiaux et al. 2003; Levin et al. 2006; Gotti et al. 2006; Zoli et al. 2015).

Activation of human $\alpha 4\beta 2$, $\alpha 7$, and $\alpha 3\beta 4$ nAChRs by DN-IMI

To verify an agonistic effect of DN-IMI on the physiologically important neuronal nAChR subtypes $\alpha 4\beta 2$, $\alpha 7$, and $\alpha 3\beta 4$, we expressed each of them in *Xenopus laevis* oocytes and performed two-electrode voltage-clamp recordings (Fig. 5A).

Fig. 5 Effects of DN-IMI on human nAChR subtypes heterologously expressed by *Xenopus laevis* oocytes. **A** The basic principle of the experiments with human nAChRs heterologously expressed by *Xenopus laevis* oocytes is presented. (1) The genetic information (mRNA) of the respective nAChR subunits, in this example $\alpha 4$ (red) and $\beta 2$ (orange), is injected at the desired ratio [here: 1 ($\alpha 4$):10 ($\beta 2$)] into the oocytes. (2) The oocytes are incubated for a few days to allow protein expression and membrane integration as functional nAChRs. (3) The experiments were performed in two-electrode voltage-clamp recording mode. The agonist-evoked inward current through the nAChRs was measured by the current electrode, while the membrane potential of the oocyte was kept constant ($V_H = -50$ mV) by a regulated voltage electrode and its reference electrode in the bath solution. **B** Increasing concentrations of DN-IMI were added to the bath solution, with washout phases between the recordings. Exemplary inward currents through human $\alpha 4\beta 2$ (HS) nAChRs are shown. Note that an excess of $\beta 2$ subunits was used here to generate pentameric receptors with two α subunits (designated here as high-sensitivity (HS) variant, compared to receptors with > 2 α subunits). **C** The inward current data (amplitude) of human $\alpha 4\beta 2$ (HS) nAChRs heterologously expressed by *Xenopus laevis* oocytes of multiple experiments were quantified (means \pm SEM are displayed). After curve fitting, relative pEC₅₀ values (curve inflection point) of 6.3 ± 0.04 (estimated maximum amplitude at 64% of nicotine's) for DN-IMI and 6.3 ± 0.04 for nicotine were determined. The significance of the responses triggered by IMI was evaluated between the lowest concentration (3 μ M) and the other concentrations (*: $p < 0.05$; n.s., not significant). The inward current amplitudes were normalized to the response induced by nicotine (10 μ M). Exemplary current traces of DN-IMI and nicotine are shown in Fig. S3C and S3D, respectively. **D** The inward current data (amplitude) of human $\alpha 7$ nAChRs heterologously expressed by *Xenopus laevis* oocytes of multiple experiments were quantified (means \pm SEM are displayed), and after curve fitting relative pEC₅₀ values of 4.5 ± 0.09 (estimated maximum of 83%) for DN-IMI and 3.9 ± 0.04 for nicotine were obtained. The significance of the responses triggered by IMI-olefin and IMI was evaluated between the lowest concentration (3 μ M) and the other concentrations (*: $p < 0.05$). The current amplitudes were normalized to the response induced by nicotine (100 μ M). Exemplary current traces of DN-IMI, IMI-olefin, and nicotine and the complete concentration–response curve for nicotine are shown in Fig. S5. **E** The inward current data (amplitude) of human $\alpha 3\beta 4$ nAChRs heterologously expressed by *Xenopus laevis* oocytes of multiple experiments were quantified (means \pm SEM are displayed), and after curve fitting relative pEC₅₀ values of 4.9 ± 0.03 for DN-IMI and 4.0 ± 0.01 for nicotine were determined. The significance of the responses triggered by IMI was determined between the lowest concentration (1 μ M) and the other concentrations (*: $p < 0.05$). The current amplitudes were normalized to the response induced by nicotine (100 μ M). Exemplary current traces of DN-IMI, IMI, and the complete concentration–response curve for nicotine are shown in Fig. S6C–F. Detailed data on n numbers are found in Table S6

First, we focused our experiments on the $\alpha 4\beta 2$ receptor, which can assemble in two different stoichiometries. The high-sensitivity (HS) variant (two $\alpha 4$ subunits and three $\beta 2$ subunits) has been reported to have a pEC₅₀(ACh) of ~ 5.7 in the *Xenopus laevis* oocyte expression system, while the low-sensitivity variant (three $\alpha 4$ subunits and two $\beta 2$ subunits) had a pEC₅₀(ACh) of ~ 4.1 (Bermudez and Moroni 2006; Moroni et al. 2006; Jonsson et al. 2006; Carbone et al. 2009; Mineur et al. 2009; Mazzaferro et al. 2011; Harpsøe et al. 2011; Li et al. 2011; Benallegue et al.

2013). In our system, we found for the $\alpha 4\beta 2$ (HS) receptor a pEC₅₀(ACh) of ~ 5.7 (Fig. S3A, B). For nicotine, we found a pEC₅₀ of 6.3, in line with the literature data (Moroni et al. 2006). DN-IMI yielded a relative pEC₅₀ of 6.3 (Fig. 5B, C). The data show a high potency for this nAChR subtype; our data suggest that DN-IMI has a similar potency but slightly lower efficacy (64% of full stimulation) than nicotine (Fig. S3C, D). Its parent compound IMI did not trigger a concentration-dependent activation of the receptor in the tested concentration range (≤ 100 μ M). For control purposes, we applied DN-IMI (30 μ M) to *Xenopus laevis* oocytes without additional receptor expression (injection of water without mRNA). In this experimental setup, we did not detect any current responses ($n = 5$, data not shown). These findings show that DN-IMI only triggered inward currents via the activation of the heterologously expressed human nAChRs. This was further confirmed by antagonist experiments, where the response of the human $\alpha 4\beta 2$ (HS) receptor to DN-IMI was concentration-dependently and reversibly blocked by the non-competitive nAChR antagonist Mec (Fig. S4).

To verify an agonistic effect of DN-IMI and IMI-olefin on human $\alpha 7$ nAChRs, we expressed this nAChR subtype in *Xenopus laevis* oocytes and performed two-electrode voltage-clamp recordings (Figs. 5D and S5). DN-IMI had a relative pEC₅₀ of 4.5 with a lower efficacy than nicotine (Figs. 5D and S5A, D). Compared to nicotine, DN-IMI thus showed a slightly higher potency and a partial agonistic effect (estimated maximum at $\sim 81\%$ of the maximal response to nicotine) on human $\alpha 7$ nAChRs, well in line with our Ca²⁺-imaging data (Fig. 2B, C). IMI-olefin and its parent compound IMI also stimulated significant inward currents but with a lower potency and efficacy than DN-IMI (Figs. 5D and S5B, D). The results for IMI match our previous findings with LUHMES and SH-SY5Y neurons (Loser et al. 2021a). The application of nicotine yielded a pEC₅₀ of 3.9 (Figs. 5D and S5C, D), which is comparable to the literature data (Briggs et al. 1995). As an internal consistency check, we performed antagonist experiments, where the DN-IMI-triggered response of the human $\alpha 7$ nAChR was concentration-dependently and reversibly blocked by the selective $\alpha 7$ receptor antagonist MLA (Fig. S4).

As a third approach, we investigated the effects of DN-IMI on human $\alpha 3\beta 4$ nAChRs expressed by *Xenopus laevis* oocytes. The application of nicotine and ACh resulted in pEC₅₀s of 4.0 and 3.8 (Figs. 5E and S6A, B, D), respectively, which are both comparable to the literature data (Wang et al. 1996; Nelson et al. 2001; Jonsson et al. 2006). The addition of DN-IMI to oocytes expressing human $\alpha 3\beta 4$ nAChR yielded a relative pEC₅₀ of 4.9 (Figs. 5E and S6C, D). IMI evoked small but significant inward currents in a concentration-dependent manner (Figs. 5E and S6D–F). Responses of the human $\alpha 3\beta 4$ nAChR triggered by DN-IMI

were concentration-dependently and reversibly blocked by the nAChR antagonist Tubo (Fig. S4).

For the further characterization of DN-IMI on individual receptors, we investigated the effects of DN-IMI and IMI on the low-sensitivity variant of $\alpha 4\beta 2$ (LS) and on $\alpha 4\beta 4$ nAChRs. DN-IMI yielded pEC_{50} s of 5.3 for $\alpha 4\beta 2$ (LS) and 5.5 for $\alpha 4\beta 4$ (Fig. S7). IMI did not trigger a concentration-dependent activation of these two nAChR subtypes in the tested concentration range ($\leq 100 \mu\text{M}$).

Having obtained data on nicotine and DN-IMI for nAChR subtypes, we used them for a comparison of their potencies. For this purpose, we determined the absolute EC_{25} values (Fig. 6A). These data suggest that DN-IMI and nicotine were about equipotent on the $\alpha 4\beta 2$ (HS) nAChR (less than half a log-step difference). On the other receptors, DN-IMI appeared slightly more potent than nicotine (about 0.6 log-steps). To understand differences between experimental systems or possibly to predict toxicological consequences for brain areas with different receptor expression patterns, it was interesting to compare apparent (functional) receptor affinities: this showed that both ligands were more potent on the $\alpha 4\beta 2$ (HS) nAChR than on other subtypes (> 1 log-step for DN-IMI; > 2 log-steps for nicotine), while there was no difference between, e.g., $\alpha 7$ and $\alpha 3\beta 4$ (Fig. 6B). This might explain mixed responses, e.g., on LUHMES cultures that express all these receptor types, and it provides an explanation for differences between, e.g., SH-SY5Y cells and LUHMES (the former cells predominantly express $\alpha 7$ receptors but also $\alpha 3$ -containing receptors (Loser et al. 2021a)).

In summary, the metabolite DN-IMI exhibits significantly higher potency and efficacy on the human nAChR subtypes

than its parent compound IMI. We performed extensive molecular docking studies of nicotine, IMI, DN-IMI, and IMI-olefin to further substantiate the experimental findings from oocytes and to provide a molecular explanation. The modeling results suggest a positioning of DN-IMI similar to that of nicotine at the binding sites of two nAChR subtypes. In contrast, IMI and IMI-olefin tend to adopt inverted and less favorable binding poses (Figs. S8 and S9). The docking studies thus provide a potential explanation for the lower signaling potency of these two compounds compared to DN-IMI.

Exposure considerations and in vitro-to-in vivo comparisons

While the above approaches inform on potential hazards by DN-IMI, the interpretation of the data and their use for risk assessment requires some understanding of concentrations to be reached in human tissues/body fluids. Due to the lack of more direct human data, we built a physiology-based toxicokinetic (PBTK) model to predict the plasma concentrations of DN-IMI. Because of the limited availability of human metabolism and exposure data for DN-IMI, the model construction was based on data from atenolol, a compound with similar physicochemical properties, and with well-known human pharmacokinetics. As DN-IMI-specific parametrization of the model, we used metabolic turnover data from human primary hepatocytes and physicochemical properties of DN-IMI as predictors for passive membrane permeability and protein binding (Table S8). As input (oral exposure), we used 0.016 mg DN-IMI/kg body weight. This

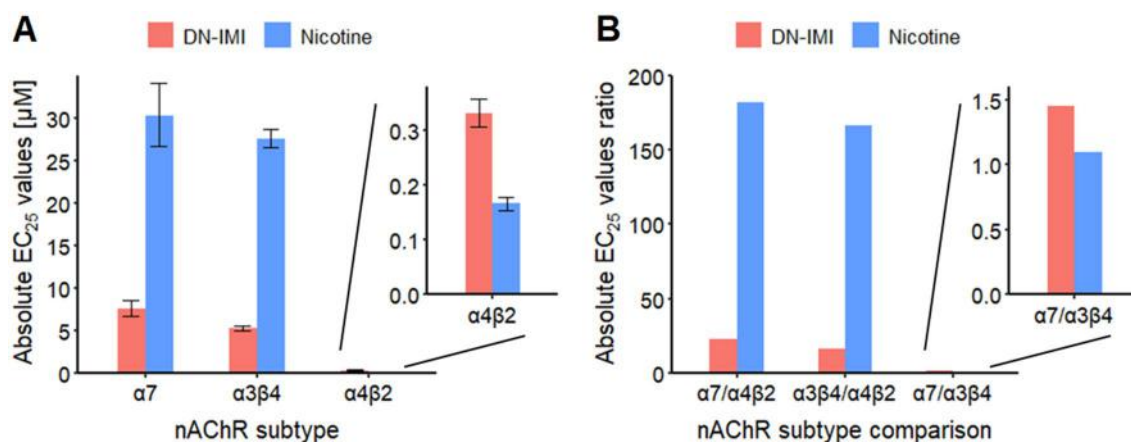


Fig. 6 Comparative display of agonist potencies at nAChRs. Oocyte recordings were performed, and data for nicotine and DN-IMI stimulations are normalized as in Fig. 5. From the curve-fitted concentration–response data, EC_{25} values were determined. **A** The absolute EC_{25} values are shown for the effects on $\alpha 7$ (7.6 μM by DN-IMI and 30.2 μM by nicotine), $\alpha 3\beta 4$ (5.2 μM by DN-IMI and 27.5 μM by nicotine), and $\alpha 4\beta 2$ (HS) (0.33 μM for DN-IMI and 0.17 μM for

nicotine) nAChRs. Note that the latter data set is shown as insert, because of the altered y-axis. **B** The ratios of the absolute EC_{25} values between the nAChR subtypes $\alpha 7$, $\alpha 3\beta 4$, and $\alpha 4\beta 2$ (HS) are displayed for the effects of DN-IMI and nicotine. HS=high-sensitivity variant of the receptor (two $\alpha 4$ subunits per receptor); note the different y-axis of the insert

amount corresponds to 10% of the value used earlier for IMI PBTK modeling (Loser et al. 2021a). Our rationale was that DN-IMI can reach about 10% of the IMI content in fruits, vegetables, and cereals (see the introduction for reference).

Under these conditions, the model predicted average plasma concentrations of around 50 nM and peak concentrations in a subfraction of the human population of at least 100 nM (Fig. S10A). The plasma concentrations predicted for atenolol from our PBTK model were in good agreement with measured data found in the literature (Fig. S10B). We see this as an indication of a good predictive capacity of our model. As the central nervous system is a main target tissue of DN-IMI, we also predicted brain concentrations. They were even slightly higher than the plasma concentrations (Fig. S10C). It is likely that the free diffusion of the compound through the blood–brain barrier also predicts a free distribution into the fetus. It is, therefore, reasonable to assume that also fetal brains would be exposed to DN-IMI at concentrations up to the three-digit nM range.

BMC modeling of our $[Ca^{2+}]_i$ signaling and single nAChR data showed 20% response (in different systems) at about 100–300 nM of DN-IMI (Tables S9 and S10). Such concentrations are close to the ones reachable in some subjects by dietary exposure. While such concentrations may not be reached for the average of the population, the gap between realistic internal exposure levels and the minimal effect concentration is less than tenfold. This marginal safety buffer is eliminated, if receptor desensitization is considered as an effect parameter: the BMC for this endpoint was at ~17 nM (Table S11, for a 20% effect). Such concentrations may be reached by the consumption of food derived from crops treated with IMI. Notably, the desensitizing effect may be equally problematic for normal brain function and neuronal development, as the direct activation of the nAChRs.

To conclude these preliminary risk assessment considerations, it is important to consider that exposure to DN-IMI may also occur through the metabolism of IMI after it has been ingested. From rodent experiments, it is clear that DN-IMI is generated after exposure to IMI, and that the endogenous metabolite DN-IMI distributes to the brain (Chao and Casida 1997; Ford and Casida 2006). In addition, goat data suggest that IMI is converted to DN-IMI (about 25% of the IMI dose recovered in the liver) (Anon 2006). In rabbits, DN-IMI was excreted in the urine after exposure to IMI (Vardavas et al. 2018), and this agrees well with human biomonitoring data that identified high (several fold higher than IMI) levels of DN-IMI in urine (Wang et al. 2020).

If one assumes that 10% of ingested IMI is converted to DN-IMI, then the endogenously formed metabolite may reach levels of a similar magnitude as those generated from direct ingestion of the metabolite (assuming that the intake of IMI is 10 times higher than that of DN-IMI (input parameter of our PBTK model, based on food consumption

data)). Therefore, a mixed exposure to IMI, DN-IMI, but also other metabolites, either produced endogenously (see PBTK model) or exogenously (see introduction), seems to be realistic and may lead to the summation of their adverse effects on the organism.

Even though such considerations of potential internal exposure are consistent with the literature data, they need to be considered as very preliminary. There is still considerable uncertainty on the human metabolism. It is not known which percentage of IMI is metabolized to DN-IMI within the liver and whether other tissues also contribute to the metabolism. The situation is complex, as several competing enzymes may oxidize or reduce IMI. Besides cytochrome P450 enzymes, there is evidence for the contribution of cytosolic aldehyde oxidases (Dick et al. 2005; Swenson and Casida 2013; Vardavas et al. 2018). These enzymes show high species variation in their expression and activity (Dick et al. 2005; Pryde et al. 2010). Considering that humans express relatively high levels of aldehyde oxidase, data from animals cannot be easily translated to humans, and experiments are ongoing to better quantify IMI metabolism by different cell compartments.

Conclusions and outlook

The present study shows that the IMI metabolite DN-IMI potently (at sub-micromolar concentrations) affects human nAChRs. This was found both in neuronal cultures and in defined individual receptor subtypes expressed in *Xenopus laevis* oocytes. The evidence from all systems clearly indicates a much higher potency of DN-IMI relative to its parent compound IMI. The comparative data show that the desnitro metabolite is equipotent to nicotine, while another IMI metabolite, IMI-olefin, rather was equipotent to IMI. The study on DN-IMI showcases the role of metabolism for human neurotoxicology, as it demonstrates that a particular metabolite can be several orders of magnitude more potent as a neuronal signaling disrupter (desensitization) than its parent compound. This may have consequences for the risk assessment of the parent compound and for the need of additional data on metabolite generation in the environment and in man. Our preliminary modeling suggests that bioactive, potentially toxic DN-IMI concentrations may be reached by nutritional exposure in the normal (not professionally exposed) population.

Median lethal dose (LD₅₀) studies with mice showed that DN-IMI (LD₅₀: 6–24 mg/kg) is more toxic than its parent compound IMI (LD₅₀: 35–50 mg/kg) (Chao and Casida 1997; Tomizawa et al. 2000, 2001) and IMI-olefin (no lethality at the highest tested dose of 50 mg/kg) (Chao and Casida 1997). Little information is available on more subtle forms of neurotoxicity, and to our knowledge, no data are available on the potential developmental neurotoxicity of DN-IMI.

The latter is important, considering that nicotine is an established developmental neurotoxicant (Levin et al. 1993; LeSage et al. 2006; Aschner et al. 2017). The former is relevant, as different nAChR subtypes are present on, e.g., dopaminergic neurons and play an important role in the modulation of the electrical activity and neurotransmitter release (Rapier et al. 1988; Grady et al. 1992; Quik and Kulak 2002; Mameli-Engvall et al. 2006; Quik and Wonnacott 2011; de Kloet et al. 2015). Thus, substance-induced disturbances of nicotinic signaling can have an impact on the functioning, plasticity, and development of the nervous system (Wheeler and Cooper 2004; Welsby et al. 2006; Slotkin et al. 2006; Ziviani et al. 2011; Lozada et al. 2012; de Kloet et al. 2015; Romoli et al. 2019).

Several studies reported that the binding affinity of DN-IMI to mammalian or chicken nAChRs was similar to the affinity of nicotine and clearly higher than the one of its parent compound IMI (Chao and Casida 1997; Tomizawa and Casida 1999, 2000; D'Amour and Casida 1999; Tomizawa et al. 2000). Our functional data using a physiological signaling response in human neurons are in line with these observations. DN-IMI triggered $[Ca^{2+}]_i$ responses at concentrations ≥ 100 nM, i.e., it was at least two orders of magnitude more potent than its parent compound (Loser et al. 2021a). These findings were further supported by oocyte recordings, which showed an agonistic effect of DN-IMI on human $\alpha 7$ and several non- $\alpha 7$ nAChRs. DN-IMI activated $\alpha 4\beta 2$ (HS) receptors at 20-fold lower concentrations than $\alpha 7$ and $\alpha 3\beta 4$ nAChRs. This potency difference on $\alpha 7$ and $\alpha 3\beta 4$ vs $\alpha 4\beta 2$ (HS) is also seen for nicotine. Such relative receptor preferences may be responsible for a selective toxicity on certain brain regions or neuronal functions, and future studies should also include assays on non-neuronal nAChR.

In desensitization experiments with LUHMES, the pretreatment with DN-IMI inhibited the subsequent activation of the nAChRs at concentrations ≥ 10 nM (BMR10, Table S11), which is ~ 70 times more potent compared to the effects of IMI (Loser et al. 2021a). The more potent desensitization effect of DN-IMI in comparison with IMI was confirmed in SH-SY5Y neurons (Fig. S2). After prolonged agonist exposure, nicotinic receptors desensitize by adopting a high-affinity and agonist-bound, non-conducting conformation (Nemecz et al. 2016; Morales-Perez et al. 2016). This may adversely affect normal neuronal function and neurodevelopment.

For adverse outcome pathways (AOPs), it is important to understand the molecular initiating events (MIEs) both for parent compounds and also for the relevant metabolites formed (Leist et al. 2017). Until now, few such cases have been fully resolved, as the focus in neurotoxicology has either been on toxicants acting independent of metabolism, e.g., rotenone or vinca alkaloids (Delp et al. 2018b,

2021), or on compounds that act by a single toxic metabolite, without any effect of the parent, such as methylphenylpyridinium (Schildknecht et al. 2015; Terron et al. 2018) or methylmercury (Aschner et al. 2017). In many other cases, the target is little defined (e.g., for solvents or acrylamide). In this context, mechanistic studies on neonicotinoids and their metabolites should eventually provide an explanation for different potencies and activity spectra of all metabolites on various nAChRs. While we provide here evidence for the stimulation of nAChRs and on the attenuation of signaling (by desensitization) as MIEs, it is not possible to predict the most relevant adverse outcome. The reason for this is that nicotinic receptors are widespread throughout the central nervous systems and they are crucial for a large panel of higher order nervous system functions (Levin et al. 2006; Gotti et al. 2006; Zoli et al. 2015; Terry and Callahan 2019).

Concerning the understanding of the MIE, we used molecular docking studies to provide a rationale for the experimental findings. The availability of several X-ray structures with co-crystallized neonicotinoids has facilitated the establishment of a robust docking model (Ihara et al. 2008, 2014; Loser et al. 2021a). In the present work, we focused on the overlap of the pesticide N-heteroaromatic ring with the pyridine ring of nicotine. The comparison with published studies showed good accuracy of our model. Structural alignments of these complexes and docking studies at human nAChRs demonstrate that the electronegative moiety in IMI can contribute to a flip of the imidazolidine ring in the binding pocket. We demonstrate here that this is less likely to happen with DN-IMI. This feature may explain its higher affinity/potency. Our binding hypothesis is supported by ranking via different docking scores, binding free energy approximates, and comparisons of nicotinoids and neonicotinoids bound to homologous proteins. This gives a rationale for the functional differences of neonicotinoids and nicotine that were reported for cell experiments with LUHMES and SH-SY5Y cells (Loser et al. 2021a). These studies are still mainly qualitative, and their applicability domain is most likely narrow (applying only to the compounds of this study). However, our approach forms the basis for the development of a more powerful and refined model in the future. Eventually, this might then be able to quantitatively predict MIEs for the dozens of neonicotinoid metabolites found in food. Such a model might distinguish, e.g., high- vs. low-affinity ligands or discriminate between agonists and antagonists.

Further research is also needed to elucidate whether the signaling disturbances revealed here have lasting effects on neuronal function. It has been reported that other nAChR agonists (including nicotine) may affect nervous system plasticity and development (Levin et al. 1993; Wheeler

and Cooper 2004; Welsby et al. 2006; Slotkin et al. 2006; Ziviani et al. 2011; Lozada et al. 2012; Romoli et al. 2019). Epidemiological studies are quite scarce, but some general developmental/neurological effects have been reported for neonicotinoids used in agriculture or anti-tick sprays (Cimino et al. 2017).

Some other compounds that evoke disturbances of neuronal network activity without causing structural changes have been reported to induce developmental neurotoxicity (DNT). Examples are 3,4-methylenedioxyamphetamine (MDMA, ecstasy), heroin, or nicotine (Levin et al. 1993; Slikker Jr et al. 2005; LeSage et al. 2006; Dwyer et al. 2009; Slotkin et al. 2016; Aschner et al. 2017). Moreover, compounds for example methylmercury and lead can have severe effects on the developing brain, although they have a low neurotoxicity for adults (Grandjean and Landrigan 2014). These examples make it conceivable that neonicotinoids and their metabolites such as DN-IMI may exhibit a DNT risk. However, a transfer of knowledge from one compound (e.g., nicotine) to others (e.g., DN-IMI) holds the risk of uncertainties (Rovida et al. 2020). Therefore, further mechanistic studies are needed to address the difficult question of a DNT hazard of DN-IMI and other neonicotinoid metabolites like a descyano metabolite of thiacloprid, which has also been reported to exhibit a higher affinity for mammalian and chicken nAChRs than its parent compound (Tomizawa and Casida 2000; Tomizawa et al. 2000).

Supplementary Information The online version contains supplementary material available at <https://doi.org/10.1007/s00204-021-03168-z>.

Acknowledgements This work was supported by the Land Berlin (LTB-P769), the InViTe PhD program and the 3Rs Center of the Baden-Wuerttemberg Ministry for Science, Research and Art (MWK Baden-Wuerttemberg), EFSA, the DK-EPA (MST-667-00205), the Swedish Research Council (VR-2018-03269), the University of Konstanz and Stockholm University. It has received funding from the European Union's ERASMUS+ program, the DFG (Research Training Group GRK 2338, P01), and the Horizon 2020 research and innovation program under grant agreements no. 681002 (EU-ToxRisk), no. 964537 (RISK-HUNT3R), no. 964518 (ToxFree) and no. 825759 (ENDpoiNTs). This work received financial support from the State Ministry of Baden-Wuerttemberg for Economic Affairs, Labour and Tourism.

Author contributions DL: conceived or designed the study, performed research, analyzed data, and wrote the paper. KG and JB: performed research, analyzed data, and wrote the paper. MH, YJ, CB, and PW: performed research and analyzed data. YH, GE, AN, TD, CM, and IG: contributed new methods or models. AF, SB, UK, and ML: conceived of or designed the study and wrote the paper.

Funding Open Access funding enabled and organized by Projekt DEAL.

Declarations

Conflict of interest The authors declare no conflict of interest.

Open Access This article is licensed under a Creative Commons Attribution 4.0 International License, which permits use, sharing, adaptation, distribution and reproduction in any medium or format, as long as you give appropriate credit to the original author(s) and the source, provide a link to the Creative Commons licence, and indicate if changes were made. The images or other third party material in this article are included in the article's Creative Commons licence, unless indicated otherwise in a credit line to the material. If material is not included in the article's Creative Commons licence and your intended use is not permitted by statutory regulation or exceeds the permitted use, you will need to obtain permission directly from the copyright holder. To view a copy of this licence, visit <http://creativecommons.org/licenses/by/4.0/>.

References

- Abou-Donia MB, Goldstein LB, Bullman S et al (2008) Imidacloprid induces neurobehavioral deficits and increases expression of glial fibrillary acidic protein in the motor cortex and hippocampus in offspring rats following in utero exposure. *J Toxicol Environ Health A* 71:119–130. <https://doi.org/10.1080/15287390701613140>
- Albrecht W, Kappenberg F, Brecklinghaus T et al (2019) Prediction of human drug-induced liver injury (DILI) in relation to oral doses and blood concentrations. *Arch Toxicol* 93:1609–1637. <https://doi.org/10.1007/s00204-019-02492-9>
- Alkondon M, Pereira EFR, Eisenberg HM, Albuquerque EX (1999) Choline and selective antagonists identify two subtypes of nicotinic acetylcholine receptors that modulate GABA release from CA1 interneurons in rat hippocampal slices. *J Neurosci* 19:2693–2705. <https://doi.org/10.1523/JNEUROSCI.19-07-02693.1999>
- Anon (2006) Draft Assessment Report (DAR)—public version—initial risk assessment provided by the rapporteur Member State Germany for the existing active substance imidacloprid. Vol. 3, Annex B, p. B.7
- Arias HR, Feuerbach D, Targowska-Duda K et al (2015) Pharmacological and molecular studies on the interaction of varenicline with different nicotinic acetylcholine receptor subtypes. Potential mechanism underlying partial agonism at human $\alpha 4\beta 2$ and $\alpha 3\beta 4$ subtypes. *Biochim Biophys Acta BBA Biomembr* 1848:731–741. <https://doi.org/10.1016/j.bbmem.2014.11.003>
- Aschner M, Ceccatelli S, Daneshian M et al (2017) Reference compounds for alternative test methods to indicate developmental neurotoxicity (DNT) potential of chemicals: example lists and criteria for their selection and use. *Altex* 34:49–74. <https://doi.org/10.14573/altex.1604201>
- Attoff K, Kertika D, Lundqvist J et al (2016) Acrylamide affects proliferation and differentiation of the neural progenitor cell line C17.2 and the neuroblastoma cell line SH-SY5Y. *Toxicol Vitro* 35:100–111. <https://doi.org/10.1016/j.tiv.2016.05.014>
- Attoff K, Johansson Y, Cediell-Ulloa A et al (2020) Acrylamide alters CREB and retinoic acid signalling pathways during differentiation of the human neuroblastoma SH-SY5Y cell line. *Sci Rep* 10:16714. <https://doi.org/10.1038/s41598-020-73698-6>
- Bache SM, Wickham H (2014) magrittr: a forward-pipe operator for R. R package version 1.5. <https://CRAN.R-project.org/package=magrittr>

- Bass C, Denholm I, Williamson MS, Nauen R (2015) The global status of insect resistance to neonicotinoid insecticides. *Pestic Biochem Physiol* 121:78–87. <https://doi.org/10.1016/j.pestbp.2015.04.004>
- Benallegue N, Mazzaferro S, Alcaino C, Bermudez I (2013) The additional ACh binding site at the $\alpha 4(+)/\alpha 4(-)$ interface of the ($\alpha 4\beta 2$) $\alpha 4$ nicotinic ACh receptor contributes to desensitization. *Br J Pharmacol* 170:304–316. <https://doi.org/10.1111/bph.12268>
- Bengtsson H (2020) matrixStats: functions that apply to rows and columns of matrices (and to vectors). R package version 0.56.0. <https://CRAN.R-project.org/package=matrixStats>
- Berheim EH, Jenks JA, Lundgren JG et al (2019) Effects of neonicotinoid insecticides on physiology and reproductive characteristics of captive female and fawn white-tailed deer. *Sci Rep* 9:4534. <https://doi.org/10.1038/s41598-019-40994-9>
- Bermudez I, Moroni M (2006) Phosphorylation and function of $\alpha 4\beta 2$ receptor. *J Mol Neurosci* 30:97–98. <https://doi.org/10.1385/JMN:30:1:97>
- Briggs CA, McKenna DG, Piattina-Kaplan M (1995) Human $\alpha 7$ nicotinic acetylcholine receptor responses to novel ligands. *Neuropharmacology* 34:583–590. [https://doi.org/10.1016/0028-3908\(95\)00028-5](https://doi.org/10.1016/0028-3908(95)00028-5)
- Brown LA, Ihara M, Buckingham SD et al (2006) Neonicotinoid insecticides display partial and super agonist actions on native insect nicotinic acetylcholine receptors. *J Neurochem* 99:608–615. <https://doi.org/10.1111/j.1471-4159.2006.04084.x>
- Brüll M, Spreng A-S, Gutbier S et al (2020) Incorporation of stem cell-derived astrocytes into neuronal organoids to allow neuro-glial interactions in toxicological studies. *ALTEX Altern Anim Exp* 37:409–428. <https://doi.org/10.14573/altex.1911111>
- Buisson B, Gopalakrishnan M, Arneric SP et al (1996) Human $\alpha 4\beta 2$ neuronal nicotinic acetylcholine receptor in HEK 293 cells: a patch-clamp study. *J Neurosci* 16:7880–7891. <https://doi.org/10.1523/JNEUROSCI.16-24-07880.1996>
- Burke AP, Niibori Y, Terayama H et al (2018) Mammalian susceptibility to a neonicotinoid insecticide after fetal and early postnatal exposure. *Sci Rep* 8:16639. <https://doi.org/10.1038/s41598-018-35129-5>
- Campling BG, Kuryatov A, Lindstrom J (2013) Acute activation, desensitization and smoldering activation of human acetylcholine receptors. *PLoS ONE* 8:e79653. <https://doi.org/10.1371/journal.pone.0079653>
- Capelli AM, Castelletti L, Chen YH et al (2011) Stable expression and functional characterization of a human nicotinic acetylcholine receptor with $\alpha 6\beta 2$ properties: discovery of selective antagonists. *Br J Pharmacol* 163:313–329. <https://doi.org/10.1111/j.1476-5381.2011.01213.x>
- Carbone A-L, Moroni M, Groot-Kormelink P-J, Bermudez I (2009) Pentameric concatenated (a4)2(b2)3 and (a4)3(b2)2 nicotinic acetylcholine receptors: subunit arrangement determines functional expression. *Br J Pharmacol* 156:970–981. <https://doi.org/10.1111/j.1476-5381.2008.00104.x>
- Casida JE (2018) Neonicotinoids and other insect nicotinic receptor competitive modulators: progress and prospects. *Annu Rev Entomol* 63:125–144. <https://doi.org/10.1146/annurev-ento-020117-043042>
- Champiaux N, Gotti C, Cordero-Erausquin M et al (2003) Subunit composition of functional nicotinic receptors in dopaminergic neurons investigated with knock-out mice. *J Neurosci* 23:7820–7829. <https://doi.org/10.1523/JNEUROSCI.23-21-07820.2003>
- Chao SL, Casida JE (1997) Interaction of imidacloprid metabolites and analogs with the nicotinic acetylcholine receptor of mouse brain in relation to toxicity. *Pestic Biochem Physiol* 58:77–88. <https://doi.org/10.1006/pest.1997.2284>
- Chatzidakis A, Fouillet A, Li J et al (2015) Pharmacological characterization of nicotinic acetylcholine receptors expressed in human iPSC-derived neurons. *PLoS ONE*. <https://doi.org/10.1371/journal.pone.0125116>
- Chavez-Noriega LE, Gillespie A, Stauderman KA et al (2000) Characterization of the recombinant human neuronal nicotinic acetylcholine receptors $\alpha 3\beta 2$ and $\alpha 4\beta 2$ stably expressed in HEK293 cells. *Neuropharmacology* 39:2543–2560. [https://doi.org/10.1016/S0028-3908\(00\)00134-9](https://doi.org/10.1016/S0028-3908(00)00134-9)
- Chen M, Tao L, McLean J, Lu C (2014) Quantitative analysis of neonicotinoid insecticide residues in foods: implication for dietary exposures. *J Agric Food Chem* 62:6082–6090. <https://doi.org/10.1021/jf501397m>
- Chomczynski P, Sacchi N (2006) The single-step method of RNA isolation by acid guanidinium thiocyanate–phenol–chloroform extraction: twenty-something years on. *Nat Protoc* 1:581–585. <https://doi.org/10.1038/nprot.2006.83>
- Cimino AM, Boyles AL, Thayer KA, Perry MJ (2017) Effects of neonicotinoid pesticide exposure on human health: a systematic review. *Environ Health Perspect* 125:155–162. <https://doi.org/10.1289/EHP515>
- Codling G, Al Naggar Y, Giesy JP, Robertson AJ (2016) Concentrations of neonicotinoid insecticides in honey, pollen and honey bees (*Apis mellifera* L.) in central Saskatchewan, Canada. *Chemosphere* 144:2321–2328. <https://doi.org/10.1016/j.chemosphere.2015.10.135>
- Craddock HA, Huang D, Turner PC et al (2019) Trends in neonicotinoid pesticide residues in food and water in the United States, 1999–2015. *Environ Health* 18:7. <https://doi.org/10.1186/s12940-018-0441-7>
- D'Amour KA, Casida JE (1999) Desnitroimidacloprid and nicotine binding site in rat recombinant $\alpha 4\beta 2$ neuronal nicotinic acetylcholine receptor. *Pestic Biochem Physiol* 64:55–61. <https://doi.org/10.1006/pest.1999.2409>
- Danker T (2018) ephys2: read, analyze and plot HEKA patchmaster files. R package version 0.12.0. <https://github.com/tdanker/ephs2>
- de Kloet SF, Mansvelter HD, De Vries TJ (2015) Cholinergic modulation of dopamine pathways through nicotinic acetylcholine receptors. *Biochem Pharmacol* 97:425–438. <https://doi.org/10.1016/j.bcp.2015.07.014>
- Delp J, Gutbier S, Cerff M et al (2018a) Stage-specific metabolic features of differentiating neurons: implications for toxicant sensitivity. *Toxicol Appl Pharmacol* 354:64–80. <https://doi.org/10.1016/j.taap.2017.12.013>
- Delp J, Gutbier S, Klima S et al (2018b) A high-throughput approach to identify specific neurotoxicants/developmental toxicants in human neuronal cell function assays. *Altex* 35:235–253. <https://doi.org/10.14573/altex.1712182>
- Delp J, Funke M, Rudolf F et al (2019) Development of a neurotoxicity assay that is tuned to detect mitochondrial toxicants. *Arch Toxicol* 93:1585–1608. <https://doi.org/10.1007/s00204-019-02473-y>
- Delp J, Cediél-Ulloa A, Suciú I et al (2021) Neurotoxicity and underlying cellular changes of 21 mitochondrial respiratory chain inhibitors. *Arch Toxicol* 95:591–615. <https://doi.org/10.1007/s00204-020-02970-5>
- Dick RA, Kanne DB, Casida JE (2005) Identification of aldehyde oxidase as the neonicotinoid nitroreductase. *Chem Res Toxicol* 18:317–323. <https://doi.org/10.1021/tx049737i>
- Dickinson JA, Hanrott KE, Mok MHS et al (2007) Differential coupling of $\alpha 7$ and non- $\alpha 7$ nicotinic acetylcholine receptors to calcium-induced calcium release and voltage-operated calcium channels in PC12 cells. *J Neurochem* 100:1089–1096. <https://doi.org/10.1111/j.1471-4159.2006.04273.x>
- Donnelly-Roberts DL, Puttfarcken PS, Kuntzweiler TA et al (1998) ABT-594 [(R)-5-(2-Azetidinylmethoxy)-2-Chloropyridine]: a novel, orally effective analgesic acting via neuronal nicotinic

- acetylcholine receptors: I. Vitro Charact J Pharmacol Exp Ther 285:777–786
- Douglas MR, Tooker JF (2015) Large-scale deployment of seed treatments has driven rapid increase in use of neonicotinoid insecticides and preemptive pest management in US. *Field Crops Environ Sci Technol* 49:5088–5097. <https://doi.org/10.1021/es506141g>
- Duzguner V, Erdogan S (2012) Chronic exposure to imidacloprid induces inflammation and oxidative stress in the liver and central nervous system of rats. *Pestic Biochem Physiol* 104:58–64. <https://doi.org/10.1016/j.pestbp.2012.06.011>
- Dwyer JB, McQuown SC, Leslie FM (2009) The dynamic effects of nicotine on the developing brain. *Pharmacol Ther* 122:125–139. <https://doi.org/10.1016/j.pharmthera.2009.02.003>
- Eaton JB, Lucero LM, Stratton H et al (2014) The unique $\alpha 4(+)(-)\alpha 4$ agonist binding site in $(\alpha 4)3(\beta 2)$ subtype nicotinic acetylcholine receptors permits differential agonist desensitization pharmacology versus the $(\alpha 4)2(\beta 2)3$ subtype. *J Pharmacol Exp Ther* 348:46–58. <https://doi.org/10.1124/jpet.113.208389>
- Edwards SM (2019) lemon: Freshing up your “ggplot2” Plots. R package version 0.4.3. <https://CRAN.R-project.org/package=lemon>
- European Commission (2018) Commission Implementing Regulation (EU) 2018/783 of 29 May 2018 amending Implementing Regulation (EU) No 540/2011 as regards the conditions of approval of the active substance imidacloprid (Text with EEA relevance.) http://data.europa.eu/eli/reg_impl/2018/783/oj/eng. Accessed 3 Aug 2021
- European Commission (2020) Commission Implementing Regulation (EU) 2020/1643 of 5 November 2020 amending Implementing Regulation (EU) No 540/2011 as regards the approval periods of the active substances calcium phosphide, denatonium benzoate, haloxypop-P, imidacloprid, pencycuron and zeta-cypermethrin (Text with EEA relevance) http://data.europa.eu/eli/reg_impl/2020/1643/oj. Accessed 3 Aug 2021
- European Food Safety Authority (EFSA) (2016) Peer review of the pesticide risk assessment for the active substance imidacloprid in light of confirmatory data submitted. *EFSA J* 14:4607. <https://doi.org/10.2903/j.efsa.2016.4607>
- European Food Safety Authority (EFSA), Abdourahime H, Anastasiadou M et al (2019) Review of the existing maximum residue levels for imidacloprid according to article 12 of regulation (EC) No 396/2005. *EFSA J* 17:e05570. <https://doi.org/10.2903/j.efsa.2019.5570>
- Fenster CP, Rains MF, Noerager B et al (1997) Influence of subunit composition on desensitization of neuronal acetylcholine receptors at low concentrations of nicotine. *J Neurosci* 17:5747–5759. <https://doi.org/10.1523/JNEUROSCI.17-15-05747.1997>
- Ford KA, Casida JE (2006) Chloropyridinyl neonicotinoid insecticides: diverse molecular substituents contribute to facile metabolism in mice. *Chem Res Toxicol* 19:944–951. <https://doi.org/10.1021/tx0600696>
- Gloor S, Pongs O, Schmalzing G (1995) A vector for the synthesis of cRNAs encoding Myc epitope-tagged proteins in *Xenopus laevis* oocytes. *Gene* 160:213–217. [https://doi.org/10.1016/0378-1119\(95\)00226-v](https://doi.org/10.1016/0378-1119(95)00226-v)
- Gopalakrishnan M, Buisson B, Touma E et al (1995) Stable expression and pharmacological properties of the human $\alpha 7$ nicotinic acetylcholine receptor. *Eur J Pharmacol Mol Pharmacol* 290:237–246. [https://doi.org/10.1016/0922-4106\(95\)00083-6](https://doi.org/10.1016/0922-4106(95)00083-6)
- Gotti C, Carbonnelle E, Moretti M et al (2000) Drugs selective for nicotinic receptor subtypes: a real possibility or a dream? *Behav Brain Res* 113:183–192. [https://doi.org/10.1016/S0166-4328\(00\)00212-6](https://doi.org/10.1016/S0166-4328(00)00212-6)
- Gotti C, Zoli M, Clementi F (2006) Brain nicotinic acetylcholine receptors: native subtypes and their relevance. *Trends Pharmacol Sci* 27:482–491. <https://doi.org/10.1016/j.tips.2006.07.004>
- Grady S, Marks MJ, Wonnacott S, Collins AC (1992) Characterization of nicotinic receptor-mediated [3 H]dopamine release from synaptosomes prepared from mouse striatum. *J Neurochem* 59:848–856. <https://doi.org/10.1111/j.1471-4159.1992.tb08322.x>
- Grandjean P, Landrigan P (2006) Developmental neurotoxicity of industrial chemicals. *Lancet* 368:2167–2178. [https://doi.org/10.1016/S0140-6736\(06\)69665-7](https://doi.org/10.1016/S0140-6736(06)69665-7)
- Grandjean P, Landrigan PJ (2014) Neurobehavioural effects of developmental toxicity. *Lancet Neurol* 13:330–338. [https://doi.org/10.1016/S1474-4422\(13\)70278-3](https://doi.org/10.1016/S1474-4422(13)70278-3)
- Gray R, Rajan AS, Radcliffe KA et al (1996) Hippocampal synaptic transmission enhanced by low concentrations of nicotine. *Nature* 383:713–716. <https://doi.org/10.1038/383713a0>
- Grønlien JH, Håkerud M, Ween H et al (2007) Distinct profiles of $\alpha 7$ nAChR positive allosteric modulation revealed by structurally diverse chemotypes. *Mol Pharmacol* 72:715–724. <https://doi.org/10.1124/mol.107.035410>
- Grothendieck G, Kates L, Petzoldt T (2016) proto: prototype object-based programming. R package version 1.0.0. <https://CRAN.R-project.org/package=proto>
- Grunwald L-M, Stock R, Haag K et al (2019) Comparative characterization of human induced pluripotent stem cells (hiPSC) derived from patients with schizophrenia and autism. *Transl Psychiatry* 9:179. <https://doi.org/10.1038/s41398-019-0517-3>
- Gustafsson H, Runesson J, Lundqvist J et al (2010) Neurofunctional endpoints assessed in human neuroblastoma SH-SY5Y cells for estimation of acute systemic toxicity. *Toxicol Appl Pharmacol* 245:191–202. <https://doi.org/10.1016/j.taap.2010.02.018>
- Harpsoe K, Ahring PK, Christensen JK et al (2011) Unraveling the high- and low-sensitivity agonist responses of nicotinic acetylcholine receptors. *J Neurosci* 31:10759–10766. <https://doi.org/10.1523/JNEUROSCI.1509-11.2011>
- Harris G, Hogberg H, Hartung T, Smirnova L (2017) 3D differentiation of LUHMES cell line to study recovery and delayed neurotoxic effects. *Curr Protoc Toxicol*. <https://doi.org/10.1002/cptx.29>
- Hothorn T, Bretz F, Westfall P (2008) Simultaneous inference in general parametric models. *Biom J* 50:346–363. <https://doi.org/10.1002/bimj.200810425>
- Hurst RS, Hajós M, Raggenbass M et al (2005) A novel positive allosteric modulator of the $\alpha 7$ neuronal nicotinic acetylcholine receptor. In vitro and in vivo characterization. *J Neurosci* 25:4396–4405. <https://doi.org/10.1523/JNEUROSCI.5269-04.2005>
- Ihara M, Okajima T, Yamashita A et al (2008) Crystal structures of *Lymnaea stagnalis* AChBP in complex with neonicotinoid insecticides imidacloprid and clothianidin. *Invert Neurosci* 8:71–81. <https://doi.org/10.1007/s10158-008-0069-3>
- Ihara M, Okajima T, Yamashita A et al (2014) Studies on an acetylcholine binding protein identify a basic residue in loop G on the $\beta 1$ strand as a new structural determinant of neonicotinoid actions. *Mol Pharmacol* 86:736–746. <https://doi.org/10.1124/mol.114.094698>
- Jeschke P, Nauen R, Schindler M, Elbert A (2011) Overview of the status and global strategy for neonicotinoids. *J Agric Food Chem* 59:2897–2908. <https://doi.org/10.1021/jf101303g>
- Jonsson M, Gurley D, Dabrowski M et al (2006) Distinct pharmacologic properties of neuromuscular blocking agents on human neuronal nicotinic acetylcholine receptors: a possible explanation for the train-of-four fade. *Anesthesiology* 105:521–533
- Karreman C, Kliema S, Holzer A-K, Leist M (2020) CaFFEE: a program for evaluating time courses of Ca $^{2+}$ dependent signal changes of complex cells loaded with fluorescent indicator dyes. *Altern Anim Exp ALTEX* 37:332–336. <https://doi.org/10.14573/altex.2003191>

- Kimura-Kuroda J, Komuta Y, Kuroda Y et al (2012) Nicotine-like effects of the neonicotinoid insecticides acetamiprid and imidacloprid on cerebellar neurons from neonatal rats. *PLoS ONE* 7:e32432. <https://doi.org/10.1371/journal.pone.0032432>
- Klarich KL, Pflug NC, DeWald EM et al (2017) Occurrence of neonicotinoid insecticides in finished drinking water and fate during drinking water treatment. *Environ Sci Technol Lett* 4:168–173. <https://doi.org/10.1021/acs.estlett.7b00081>
- Klarich Wong KL, Webb DT, Nagorzanski MR et al (2019) Chlorinated byproducts of neonicotinoids and their metabolites: an unrecognized human exposure potential? *Environ Sci Technol Lett* 6:98–105. <https://doi.org/10.1021/acs.estlett.8b00706>
- Koshlukova SE (2006) Imidacloprid risk characterization document: dietary and drinking water exposure. Department of Pesticide Regulation, California Environmental Protection Agency. <https://www.cdpr.ca.gov/docs/risk/rcd/imidacloprid.pdf>. Accessed 17 May 2021
- Krebs A, Nyffeler J, Karreman C et al (2020) Determination of benchmark concentrations and their statistical uncertainty for cytotoxicity test data and functional in vitro assays. *ALTEX Altern Anim Exp* 37:155–163. <https://doi.org/10.14573/altex.1912021>
- Krug AK, Balmer NV, Matt F et al (2013) Evaluation of a human neurite growth assay as specific screen for developmental neurotoxicants. *Arch Toxicol* 87:2215–2231. <https://doi.org/10.1007/s00204-013-1072-y>
- Krug AK, Gutbier S, Zhao L et al (2014) Transcriptional and metabolic adaptation of human neurons to the mitochondrial toxicant MPP+. *Cell Death Dis* 5:e1222–e1222. <https://doi.org/10.1038/cddis.2014.166>
- Larsen HM, Hansen SK, Mikkelsen JD et al (2019) Alpha7 nicotinic acetylcholine receptors and neural network synaptic transmission in human induced pluripotent stem cell-derived neurons. *Stem Cell Res* 41:101642. <https://doi.org/10.1016/j.scr.2019.101642>
- Leist M, Nicotera P (1998) Calcium and neuronal death. *Reviews of physiology biochemistry and pharmacology*, vol 132. Springer, Berlin, pp 79–125
- Leist M, Ghallab A, Graepel R et al (2017) Adverse outcome pathways: opportunities, limitations and open questions. *Arch Toxicol* 91:3477–3505. <https://doi.org/10.1007/s00204-017-2045-3>
- Lemon J (2006) Plotrix: a package in the red light district of R. *R-News* 6:8–12
- LeSage MG, Gustaf E, Dufek MB, Pentel PR (2006) Effects of maternal intravenous nicotine administration on locomotor behavior in pre-weanling rats. *Pharmacol Biochem Behav* 85:575–583. <https://doi.org/10.1016/j.pbb.2006.10.012>
- Lester RAJ (2004) Activation and desensitization of heteromeric neuronal nicotinic receptors: implications for non-synaptic transmission. *Bioorganic Med Chem Lett* 14:1897–1900. <https://doi.org/10.1016/j.bmcl.2004.02.081>
- Levin ED, Briggs SJ, Christopher NC, Rose JE (1993) Prenatal nicotine exposure and cognitive performance in rats. *Neurotoxicol Teratol* 15:251–260. [https://doi.org/10.1016/0892-0362\(93\)90006-A](https://doi.org/10.1016/0892-0362(93)90006-A)
- Levin ED, McClernon FJ, Rezvani AH (2006) Nicotinic effects on cognitive function: behavioral characterization, pharmacological specification, and anatomic localization. *Psychopharmacology* 184:523–539. <https://doi.org/10.1007/s00213-005-0164-7>
- Li P, Ann J, Akk G (2011) Activation and modulation of human $\alpha 4 \beta 2$ nicotinic acetylcholine receptors by the neonicotinoids clothianidin and imidacloprid. *J Neurosci Res* 89:1295–1301. <https://doi.org/10.1002/jnr.22644>
- Liu MY, Lanford J, Casida JE (1993) Relevance of [3H]imidacloprid binding site in house fly head acetylcholine receptor to insecticidal activity of 2-nitromethylene- and 2-nitroimino-imidazolidines. *Pestic Biochem Physiol* 46:200–206. <https://doi.org/10.1006/pest.1993.1051>
- Lohren H, Blagojevic L, Fitkau R et al (2015) Toxicity of organic and inorganic mercury species in differentiated human neurons and human astrocytes. *J Trace Elem Med Biol* 32:200–208. <https://doi.org/10.1016/j.jtemb.2015.06.008>
- Lopes FM, Schröder R, da Júnior MLCF et al (2010) Comparison between proliferative and neuron-like SH-SY5Y cells as an in vitro model for Parkinson disease studies. *Brain Res* 1337:85–94. <https://doi.org/10.1016/j.brainres.2010.03.102>
- Loser D, Hinojosa MG, Blum J et al (2021a) Functional alterations by a subgroup of neonicotinoid pesticides in human dopaminergic neurons. *Arch Toxicol* 95:2081–2107. <https://doi.org/10.1007/s00204-021-03031-1>
- Loser D, Schaefer J, Danker T et al (2021b) Human neuronal signaling and communication assays to assess functional neurotoxicity. *Arch Toxicol* 95:229–252. <https://doi.org/10.1007/s00204-020-02956-3>
- Lozada AF, Wang X, Gounko NV et al (2012) Glutamatergic synapse formation is promoted by $\alpha 7$ -containing nicotinic acetylcholine receptors. *J Neurosci* 32:7651–7661. <https://doi.org/10.1523/JNEUROSCI.6246-11.2012>
- Mameli-Engvall M, Evvard A, Pons S et al (2006) Hierarchical control of dopamine neuron-firing patterns by nicotinic receptors. *Neuron* 50:911–921. <https://doi.org/10.1016/j.neuron.2006.05.007>
- Marks MJ, Meinerz NM, Brown RWB, Collins AC (2010) 86Rb+ efflux mediated by $\alpha 4 \beta 2^*$ -nicotinic acetylcholine receptors with high and low-sensitivity to stimulation by acetylcholine display similar agonist-induced desensitization. *Biochem Pharmacol* 80:1238–1251. <https://doi.org/10.1016/j.bcp.2010.06.040>
- Mazzaferro S, Benallegue N, Carbone A et al (2011) Additional acetylcholine (ACh) binding site at $\alpha 4 / \alpha 4$ interface of $(\alpha 4 \beta 2) 2 \alpha 4$ nicotinic receptor influences agonist sensitivity. *J Biol Chem* 286:31043–31054. <https://doi.org/10.1074/jbc.M111.262014>
- McGehee DS, Heath MJ, Gelber S et al (1995) Nicotine enhancement of fast excitatory synaptic transmission in CNS by presynaptic receptors. *Science* 269:1692–1696. <https://doi.org/10.1126/science.7569895>
- Michelmore S, Croskery K, Nozulak J et al (2002) Study of the calcium dynamics of the human $\alpha 4 \beta 2$, $\alpha 3 \beta 4$ and $\alpha 1 \beta 1 \gamma \delta$ nicotinic acetylcholine receptors. *Naunyn Schmiedeberg's Arch Pharmacol* 366:235–245. <https://doi.org/10.1007/s00210-002-0589-z>
- Mineur YS, Eibl C, Young G et al (2009) Cytisine-based nicotinic partial agonists as novel antidepressant compounds. *J Pharmacol Exp Ther* 329:377–386. <https://doi.org/10.1124/jpet.108.149609>
- Morales-Perez CL, Noviello CM, Hibbs RE (2016) X-ray structure of the human $\alpha 4 \beta 2$ nicotinic receptor. *Nature* 538:411–415. <https://doi.org/10.1038/nature19785>
- Moroni M, Zwart R, Sher E et al (2006) $\alpha 4 \beta 2$ Nicotinic receptors with high and low acetylcholine sensitivity: pharmacology, stoichiometry, and sensitivity to long-term exposure to nicotine. *Mol Pharmacol* 70:755–768. <https://doi.org/10.1124/mol.106.023044>
- Nelson ME, Wang F, Kuryatov A et al (2001) Functional properties of human nicotinic achrs expressed by Imr-32 neuroblastoma cells resemble those of $\alpha 3 \beta 4$ achrs expressed in permanently transfected hek cells. *J Gen Physiol* 118:563–582. <https://doi.org/10.1085/jgp.118.5.563>
- Nemecz Á, Prevost MS, Menny A, Corringer P-J (2016) Emerging molecular mechanisms of signal transduction in pentameric ligand-gated ion channels. *Neuron* 90:452–470. <https://doi.org/10.1016/j.neuron.2016.03.032>
- Ng HJ, Whittemore ER, Tran MB et al (2007) Nootropic $\alpha 7$ nicotinic receptor allosteric modulator derived from GABAA receptor modulators. *Proc Natl Acad Sci* 104:8059–8064. <https://doi.org/10.1073/pnas.0701321104>

- Ooms J (2020) magick: Advanced graphics and image-processing in R. R package version 2.3. <https://CRAN.R-project.org/package=magick>
- Palma E, Bertrand S, Binzoni T, Bertrand D (1996) Neuronal nicotinic alpha 7 receptor expressed in *Xenopus oocytes* presents five putative binding sites for methyllycaconitine. *J Physiol* 491:151–161. <https://doi.org/10.1113/jphysiol.1996.sp021203>
- Papke RL, Dvoskin LP, Crooks PA et al (2008) Extending the analysis of nicotinic receptor antagonists with the study of $\alpha 6$ nicotinic receptor subunit chimeras. *Neuropharmacology* 54:1189–1200. <https://doi.org/10.1016/j.neuropharm.2008.03.010>
- Papke RL, Kem WR, Soti F et al (2009) Activation and desensitization of nicotinic $\alpha 7$ -type acetylcholine receptors by benzylidene anabaseines and nicotine. *J Pharmacol Exp Ther* 329:791–807. <https://doi.org/10.1124/jpet.108.150151>
- Papke RL, Trocmé-Thibierge C, Guendisch D et al (2011) Electrophysiological perspectives on the therapeutic use of nicotinic acetylcholine receptor partial agonists. *J Pharmacol Exp Ther* 337:367–379. <https://doi.org/10.1124/jpet.110.177485>
- Paradiso KG, Steinbach JH (2003) Nicotine is highly effective at producing desensitization of Rat $\alpha 4\beta 2$ neuronal nicotinic receptors. *J Physiol* 553:857–871. <https://doi.org/10.1113/jphysiol.2003.053447>
- Pryde DC, Dalvie D, Hu Q et al (2010) Aldehyde oxidase: an enzyme of emerging importance in drug discovery. *J Med Chem* 53:8441–8460. <https://doi.org/10.1021/jm100888d>
- Puchacz E, Buisson B, Bertrand D, Lukas RJ (1994) Functional expression of nicotinic acetylcholine receptors containing rat $\alpha 7$ subunits in human SH-SY5Y neuroblastoma cells. *FEBS Lett* 354:155–159. [https://doi.org/10.1016/0014-5793\(94\)01108-7](https://doi.org/10.1016/0014-5793(94)01108-7)
- Quick MW, Lester RAJ (2002) Desensitization of neuronal nicotinic receptors. *J Neurobiol* 53:457–478. <https://doi.org/10.1002/neu.10109>
- Quik M, Kulak JM (2002) Nicotine and nicotinic receptors; relevance to parkinson's disease. *Neurotoxicology* 23:581–594. [https://doi.org/10.1016/S0161-813X\(02\)00036-0](https://doi.org/10.1016/S0161-813X(02)00036-0)
- Quik M, Wonnacott S (2011) $\alpha 6\beta 2^*$ and $\alpha 4\beta 2^*$ Nicotinic acetylcholine receptors as drug targets for parkinson's disease. *Pharmacol Rev* 63:938–966. <https://doi.org/10.1124/pr.110.003269>
- R Core Team (2020) R: a language and environment for statistical computing. R Foundation for Statistical Computing, Vienna, Austria. <https://www.R-project.org>
- Rapier C, Lunt GG, Wonnacott S (1988) Stereoselective nicotine-induced release of dopamine from striatal synaptosomes: concentration dependence and repetitive stimulation. *J Neurochem* 50:1123–1130. <https://doi.org/10.1111/j.1471-4159.1988.tb10582.x>
- Ring A, Strom BO, Turner SR et al (2015) Bispyridinium compounds inhibit both muscle and neuronal nicotinic acetylcholine receptors in human cell lines. *PLoS ONE* 10:e0135811. <https://doi.org/10.1371/journal.pone.0135811>
- Ritz C, Baty F, Streibig JC, Gerhard D (2015) Dose-response analysis using r. *PLoS ONE* 10:e0146021. <https://doi.org/10.1371/journal.pone.0146021>
- Rollema H, Hurst RS (2018) The contribution of agonist and antagonist activities of $\alpha 4\beta 2^*$ nAChR ligands to smoking cessation efficacy: a quantitative analysis of literature data. *Psychopharmacology* 235:2479–2505. <https://doi.org/10.1007/s00213-018-4921-9>
- Rollema H, Shrikhande A, Ward KM et al (2010) Pre-clinical properties of the $\alpha 4\beta 2$ nicotinic acetylcholine receptor partial agonists varenicline, cytisine and dianicline translate to clinical efficacy for nicotine dependence. *Br J Pharmacol* 160:334–345. <https://doi.org/10.1111/j.1476-5381.2010.00682.x>
- Romoli B, Lozada AF, Sandoval IM et al (2019) Neonatal nicotine exposure primes midbrain neurons to a dopaminergic phenotype and increases adult drug consumption. *Biol Psychiatry* 86:344–355. <https://doi.org/10.1016/j.biopsych.2019.04.019>
- Rovida C, Barton-Maclaren T, Benfenati E et al (2020) Internationalization of read-across as a validated new approach method (NAM) for regulatory toxicology. *ALTEX Altern Anim Exp* 37:579–606. <https://doi.org/10.14573/altex.1912181>
- Schildknecht S, Karreman C, Pörtl D et al (2013) Generation of genetically-modified human differentiated cells for toxicological tests and the study of neurodegenerative diseases. *ALTEX Altern Anim Exp* 30:427–444. <https://doi.org/10.14573/altex.2013.4.427>
- Schildknecht S, Pape R, Meiser J et al (2015) Preferential extracellular generation of the active parkinsonian toxin MPP+ by transporter-independent export of the intermediate MPDP+. *Antioxid Redox Signal* 23:1001–1016. <https://doi.org/10.1089/ars.2015.6297>
- Scholz D, Pörtl D, Genewsky A et al (2011) Rapid, complete and large-scale generation of post-mitotic neurons from the human LUHMES cell line. *J Neurochem* 119:957–971. <https://doi.org/10.1111/j.1471-4159.2011.07255.x>
- Schulz-Jander DA, Casida JE (2002) Imidacloprid insecticide metabolism: human cytochrome P450 isozymes differ in selectivity for imidazolidine oxidation versus nitroimine reduction. *Toxicol Lett* 132:65–70. [https://doi.org/10.1016/S0378-4274\(02\)00068-1](https://doi.org/10.1016/S0378-4274(02)00068-1)
- Schulz-Jander DA, Leimkuehler WM, Casida JE (2002) Neonicotinoid insecticides: reduction and cleavage of imidacloprid nitroimine substituent by liver microsomal and cytosolic enzymes. *Chem Res Toxicol* 15:1158–1165. <https://doi.org/10.1021/tx0200360>
- Simon-Delso N, Amaral-Rogers V, Belzunces LP et al (2015) Systemic insecticides (neonicotinoids and fipronil): trends, uses, mode of action and metabolites. *Environ Sci Pollut Res* 22:5–34. <https://doi.org/10.1007/s11356-014-3470-y>
- Sirenko O, Parham F, Dea S et al (2019) Functional and mechanistic neurotoxicity profiling using human iPSC-derived neural 3D cultures. *Toxicol Sci* 167:58–76. <https://doi.org/10.1093/toxsci/kfy218>
- Slikker W Jr, Xu ZA, Levin ED, Slotkin TA (2005) Mode of action: disruption of brain cell replication, second messenger, and neurotransmitter systems during development leading to cognitive dysfunction—developmental neurotoxicity of nicotine. *Crit Rev Toxicol* 35:703–711. <https://doi.org/10.1080/10408440591007421>
- Slotkin TA, Tate CA, Cousins MM, Seidler FJ (2006) Prenatal nicotine exposure alters the responses to subsequent nicotine administration and withdrawal in adolescence: serotonin receptors and cell signaling. *Neuropsychopharmacology* 31:2462–2475. <https://doi.org/10.1038/sj.npp.1300988>
- Slotkin TA, Skavicus S, Card J et al (2016) Diverse neurotoxicants target the differentiation of embryonic neural stem cells into neuronal and glial phenotypes. *Toxicology* 372:42–51. <https://doi.org/10.1016/j.tox.2016.10.015>
- Smirnova L, Harris G, Delp J et al (2016) A LUHMES 3D dopaminergic neuronal model for neurotoxicity testing allowing long-term exposure and cellular resilience analysis. *Arch Toxicol* 90:2725–2743. <https://doi.org/10.1007/s00204-015-1637-z>
- Sparks TC, Nauen R (2015) IRAC: mode of action classification and insecticide resistance management. *Pestic Biochem Physiol* 121:122–128. <https://doi.org/10.1016/j.pestbp.2014.11.014>
- Sparks TC, Crossthwaite AJ, Nauen R et al (2020) Insecticides, biologics and nematicides: Updates to IRAC's mode of action classification—a tool for resistance management. *Pestic Biochem Physiol* 167:104587. <https://doi.org/10.1016/j.pestbp.2020.104587>
- Swenson TL, Casida JE (2013) Aldehyde oxidase importance in vivo in xenobiotic metabolism: imidacloprid nitroreduction in mice. *Toxicol Sci* 133:22–28. <https://doi.org/10.1093/toxsci/kft066>

- Tan J, Galligan JJ, Hollingworth RM (2007) Agonist actions of neonicotinoids on nicotinic acetylcholine receptors expressed by cockroach neurons. *Neurotoxicology* 28:829–842. <https://doi.org/10.1016/j.neuro.2007.04.002>
- Terron A, Bal-Price A, Paini A et al (2018) An adverse outcome pathway for parkinsonian motor deficits associated with mitochondrial complex I inhibition. *Arch Toxicol* 92:41–82. <https://doi.org/10.1007/s00204-017-2133-4>
- Terry AV, Callahan PM (2019) Nicotinic acetylcholine receptor ligands, cognitive function, and preclinical approaches to drug discovery. *Nicotine Tob Res* 21:383–394. <https://doi.org/10.1093/ntr/nty166>
- Thompson DA, Lehmler H-J, Kolpin DW et al (2020) A critical review on the potential impacts of neonicotinoid insecticide use: current knowledge of environmental fate, toxicity, and implications for human health. *Environ Sci Process Impacts*. <https://doi.org/10.1039/C9EM00586B>
- Tomizawa M, Casida JE (1999) Minor structural changes in nicotinic insecticides confer differential subtype selectivity for mammalian nicotinic acetylcholine receptors. *Br J Pharmacol* 127:115–122. <https://doi.org/10.1038/sj.bjp.0702526>
- Tomizawa M, Casida JE (2000) Imidacloprid, thiacloprid, and their imine derivatives up-regulate the $\alpha 4\beta 2$ nicotinic acetylcholine receptor in M10 cells. *Toxicol Appl Pharmacol* 169:114–120. <https://doi.org/10.1006/taap.2000.9057>
- Tomizawa M, Casida JE (2005) NEONICOTINOID INSECTICIDE TOXICOLOGY: mechanisms of selective action. *Annu Rev Pharmacol Toxicol* 45:247–268. <https://doi.org/10.1146/annurev.pharmtox.45.120403.095930>
- Tomizawa M, Lee DL, Casida JE (2000) Neonicotinoid insecticides: molecular features conferring selectivity for insect versus mammalian nicotinic receptors. *J Agric Food Chem* 48:6016–6024. <https://doi.org/10.1021/jf000873c>
- Tomizawa M, Cowan A, Casida JE (2001) Analgesic and toxic effects of neonicotinoid insecticides in mice. *Toxicol Appl Pharmacol* 177:77–83. <https://doi.org/10.1006/taap.2001.9292>
- Tong Z-B, Hogberg H, Kuo D et al (2017) Characterization of three human cell line models for high-throughput neuronal cytotoxicity screening: Neurotoxicity models. *J Appl Toxicol* 37:167–180. <https://doi.org/10.1002/jat.3334>
- U.S. Geological Survey (2021) Pesticide national synthesis project, estimated annual agricultural pesticide use, pesticide use maps: US Department of the Interior. <https://water.usgs.gov/nawqa/pnsp/usage/maps/>. Accessed 3 Aug 2021
- Vaidyanathan R, Xie Y, Allaire J, et al (2019) htmlwidgets: HTML widgets for R. R package version 1.5.1. <https://CRAN.R-project.org/package=htmlwidgets>
- Vardavas AI, Ozcagli E, Fragkiadaki P et al (2018) The metabolism of imidacloprid by aldehyde oxidase contributes to its clastogenic effect in New Zealand rabbits. *Mutat Res Toxicol Environ Mutagen* 829–830:26–32. <https://doi.org/10.1016/j.mrgentox.2018.03.002>
- Wan Y, Han Q, Wang Y, He Z (2020) Five degradates of imidacloprid in source water, treated water, and tap water in Wuhan, central China. *Sci Total Environ* 741:140227. <https://doi.org/10.1016/j.scitotenv.2020.140227>
- Wang F, Gerzanich V, Wells GB et al (1996) Assembly of human neuronal nicotinic receptor $\alpha 5$ subunits with $\alpha 3$, $\beta 2$, and $\beta 4$ subunits. *J Biol Chem* 271:17656–17665. <https://doi.org/10.1074/jbc.271.30.17656>
- Wang A, Mahai G, Wan Y et al (2020) Assessment of imidacloprid related exposure using imidacloprid-olefin and desnitro-imidacloprid: neonicotinoid insecticides in human urine in Wuhan, China. *Environ Int* 141:105785. <https://doi.org/10.1016/j.envint.2020.105785>
- Welsby P, Rowan M, Anwyl R (2006) Nicotinic receptor-mediated enhancement of long-term potentiation involves activation of metabotropic glutamate receptors and ryanodine-sensitive calcium stores in the dentate gyrus. *Eur J Neurosci* 24:3109–3118. <https://doi.org/10.1111/j.1460-9568.2006.05187.x>
- Wheeler DG, Cooper E (2004) Weak synaptic activity induces ongoing signaling to the nucleus that is enhanced by BDNF and suppressed by low-levels of nicotine. *Mol Cell Neurosci* 26:50–62. <https://doi.org/10.1016/j.mcn.2003.12.016>
- Wickham H (2016) ggplot2: elegant graphics for data analysis. Springer, New York
- Wickham H (2020) modelr: modelling functions that work with the pipe. R package version 0.1.6. <https://CRAN.R-project.org/package=modelr>
- Wickham H, Averick M, Bryan J et al (2019) Welcome to the Tidyverse. *J Open Source Softw* 4:1686. <https://doi.org/10.21105/joss.01686>
- Wickham H, François R, Henry L, Müller K (2020) dplyr: A grammar of data manipulation. R package version 0.8.5. <https://CRAN.R-project.org/package=dplyr>
- Wilke CO (2019) cowplot: Streamlined plot theme and plot annotations for “ggplot2”. R package version 1.0.0. <https://CRAN.R-project.org/package=cowplot>
- Williams DK, Wang J, Papke RL (2011) Investigation of the molecular mechanism of the $\alpha 7$ nicotinic acetylcholine receptor positive allosteric modulator PNU-120596 provides evidence for two distinct desensitized states. *Mol Pharmacol* 80:1013–1032. <https://doi.org/10.1124/mol.111.074302>
- Witt B, Meyer S, Ebert F et al (2017) Toxicity of two classes of arsenolipids and their water-soluble metabolites in human differentiated neurons. *Arch Toxicol* 91:3121–3134. <https://doi.org/10.1007/s00204-017-1933-x>
- Zahedi A, Phandthong R, Chaili A et al (2019) Mitochondrial stress response in neural stem cells exposed to electronic cigarettes. *iScience* 16:250–269. <https://doi.org/10.1016/j.isci.2019.05.034>
- Zhang X, Yin M, Zhang M (2014) Cell-based assays for Parkinson’s disease using differentiated human LUHMES cells. *Acta Pharmacol Sin* 35:945–956. <https://doi.org/10.1038/aps.2014.36>
- Ziviani E, Lippi G, Bano D et al (2011) Ryanodine receptor-2 upregulation and nicotine-mediated plasticity. *EMBO J* 30:194–204. <https://doi.org/10.1038/emboj.2010.279>
- Zoli M, Pistillo F, Gotti C (2015) Diversity of native nicotinic receptor subtypes in mammalian brain. *Neuropharmacology* 96:302–311. <https://doi.org/10.1016/j.neuropharm.2014.11.003>

Publisher's Note Springer Nature remains neutral with regard to jurisdictional claims in published maps and institutional affiliations.

8. Supplementary C: Publication V (unpublished manuscript)

Symmetrical bispyridinium compounds act as open channel blockers of cation-selective ion channels

Yves Haufe¹, Dominik Loser², Karin V. Niessen³, Thomas Seeger³, Timm Danker², Annette Nicke^{1*}

¹ Walther Straub Institute of Pharmacology and Toxicology, Faculty of Medicine, LMU Munich, Munich, Germany

² NMI Natural and Medical Sciences Institute at the University of Tübingen, 72770 Reutlingen, Germany.

³ Bundeswehr Institute of Pharmacology and Toxicology, Neuherbergstr. 11, 80937 Munich, Germany.

*** Correspondence:**

Annette Nicke, annette.nicke@lrz.uni-muenchen.de

Keywords: nicotinic acetylcholine receptor, organophosphate poisoning, *Xenopus laevis* oocytes, bispyridinium, two-electrode voltage clamp, molecular docking, open channel block, allosteric modulator

Abstract

Background and Purpose: Current treatments against organophosphate poisoning (OPP) do not address effects mediated by nicotinic acetylcholine receptors (nAChR). Non-oxime bispyridinium compounds (BPCs) were shown to promote acetylcholine esterase-independent recovery of organophosphate-induced muscle block although the exact molecular mechanism is unclear.

Experimental Approach: Here, we used two-electrode voltage clamp analysis of $\alpha 7$ and muscle type nAChRs expressed in *Xenopus laevis* oocytes in combination with mutagenesis and molecular docking analysis to determine the potency of a series of 9 BPCs and their molecular mode of action.

Key Results: All investigated BPCs blocked human $\alpha 7$ and/or muscle-type nAChRs with IC₅₀-values down to the high nM range. Further analysis of the two most potent analogues revealed a non-competitive, voltage-dependent inhibition. Co-application with PNU-120596 and generation of receptor chimeras excluded a direct interaction with the positive allosteric binding site and binding to the extracellular domain of the $\alpha 7$ nAChR. Molecular docking localized the BPCs binding area to the outer channel vestibule at the transition from extracellular to transmembrane domain and increased van der Waals volume of BPCs correlates with stronger inhibition. Investigation of other cation-selective channels suggest a rather unspecific inhibition of pentameric cation channels by BPCs.

Conclusion and Implications: The described data indicate that the investigated BPCs act as channel blockers of cation-selective ion-channels with a selectivity for $\alpha 7$ and muscle-type nAChRs. The BPC analogue PTM0022 is the most potent BPC described so far at the muscle nAChR. The potential of channel blocker as treatment for OPP requires further investigation.

1. Introduction

Since the development of the first organophosphorus compounds (OPC) in 1850, poisoning with OPCs (OPP) either by exposure to pesticides (e.g. paraquat, fenamiphos) or by nerve agents (e.g. soman, tabun, VX, novichok), still represents a serious condition with insufficient treatment options and, in case of recovery, possible long term impairment (Buckley *et al.*, 2004; John *et al.*, 2018; Franca *et al.*, 2019; Alozi and Rawas-Qalaji, 2020; Haslam *et al.*, 2021; Maksimović *et al.*, 2021). The primary effect of OPCs is an irreversible block of the enzyme acetylcholine esterase (AChE) resulting in the accumulation of acetylcholine and overstimulation of both nicotinic (nAChR) and muscarinic (mAChR) acetylcholine receptors in the CNS and PNS, the so-called cholinergic syndrome. Initial muscle fasciculations mediated by nAChR overstimulation at the neuromuscular junction lead eventually to receptor desensitization with subsequent depolarization block and muscle paralysis (Aldridge and Reiner, 1972). Respiratory failure is the most common cause of death (Thiermann, Worek and Kehe, 2013). The standard therapy comprises the mAChR antagonist atropine, AChE reactivating pyridinium oximes, and symptomatic treatments such as benzodiazepines and ventilation (Thiermann, Worek and Kehe, 2013). However, treatment regimens showed only limited improvements in the last decades and the survival rate still depends mainly on the lag time until treatment (Muley *et al.*, 2014; Banday *et al.*, 2015; Amin *et al.*, 2018). In particular, the usage of oximes is limited, because of their short therapeutic window due to the fast formation of covalently linked OP-AChE complexes (so-called “aging”). Efficiency of the two available oximes critically depends on the OPC and the respective oxime and its dosage are decided case-dependently (Worek, Thiermann and Wille, 2020; Stigler *et al.*, 2021). A major therapeutic gap exists regarding the nAChR-mediated effects such as respiratory failure, and ventilation might be required for weeks (Thiermann, Worek and Kehe, 2013). While the prevalent acute effects of OPCs are mediated by muscle paralysis and the cholinergic syndrome, neurotoxicity and effects such as polyneuropathy, neurodegeneration, and memory impairment are also associated with acute or chronic exposure of OPCs, indicating a possible involvement of neuronal nAChRs (Hung *et al.*, 2015; Sánchez-Santed, Colomina and Herrero Hernández, 2016; Jokanović, 2018; Dassanayake *et al.*, 2021; de Roos *et al.*, 2021). To close the therapeutic gap, additional nAChR-targeting strategies are urgently required. The non-oxime bispyridinium compounds (BPCs) were derived from oximes and have shown beneficial effects in *in vitro* experiments with mammalian muscle preparations (Tattersall, 1993; Turner *et al.*, 2011; Seeger *et al.*, 2012) and in animal experiments (Turner *et al.*, 2011; Kassa *et al.*, 2020). However, their mode of action is controversial and several are currently discussed: an action as open channel blockers (OCB) of muscle nAChRs (Alkondon and Albuquerque, 1989; Tattersall, 1993) was supposed to prevent receptor activation and subsequent desensitization and, more recently, actions on the orthosteric site (Niessen *et al.* 2018) with participation of a close allosteric pocket (Epstein *et al.* 2021). Another study suggests that BPCs act as positive allosteric modulators (PAMS, Scheffel *et al.*, 2018b) and promote resensitization of the neuronal $\alpha 7$ nAChR (Scheffel *et al.* 2018a).

The nAChRs are members of the cys-loop receptor superfamily of pentameric ligand-gated ion channels (pLGICs), which also includes cationic serotonin (5HT₃) and anionic glycine and γ -amino butyric acid neurotransmitter receptors. The muscle-type nAChR is composed of $\alpha 1$, $\beta 1$, γ (fetal) or ϵ (adult) and δ subunits while the highly diverse group of neuronal nAChRs is generally formed by heteromeric assemblies between α -subunits ($\alpha 2$ -10) and β -subunits ($\beta 2$ -4) but can also form as homomeric or only- α complexes (in case of $\alpha 7$ and $\alpha 9$, Dani, 2015; Changeux, 2018). While PAMs of the GABA receptors like barbiturates and benzodiazepines represent important drugs, this concept has been less exploited in the case of other pLGICs. One of the best studied nAChR subtypes in regard to allosteric modulation is the $\alpha 7$ nAChR and most of the PAMs described for nAChRs act exclusively on this receptor (Papke and Horenstein, 2021). Since PAMs are compounds that in the presence of an orthosteric agonist prevent desensitization and/or promote resensitization of $\alpha 7$ receptors (Hurst *et al.*, 2005; Williams, Wang and Papke, 2011), identification of a PAMs that modulate muscle-type nAChRs represents a promising approach to counteract OPP.

In this study, we therefore set out to characterize the activity, pharmacological mode of action, and the binding area of selected symmetrical C3-linker BPCs at the human $\alpha 7$ and muscle-type

nAChRs. Our data show that BPCs can act as open channel blockers at different nAChR subtypes but interestingly also block other cation-selective ion channels including 5HT3A and P2X7. Using mutated and chimeric receptors in combination with computational docking analysis, we further identified a possible binding area in the upper part of the $\alpha 7$ channel pore. In summary, this study does not support a specific PAM action of BPCs at nAChRs but suggests that the previously observed effects in models of OPP result from a rather unspecific open channel block and might also involve other cation channels.

2. Materials and Methods

2.1 Materials

NaCl, KCl, CaCl₂, HEPES, MgCl₂, Serotonin hydrochloride were supplied by Carl Roth, Germany. Acetylcholine, QX-314, methyllycaconitine (MLA) were obtained from Sigma-Aldrich, Merck Eurolabs, Germany. PNU-120596 was obtained from Tocris Bioscience, USA. All chemicals were purchased in highest purity available.

Bispyridinium compounds were synthesized by Sebastian Rappenglück (Department of Pharmacy–Center for Drug Research, Ludwig-Maximilians-Universität München, Germany) (Scheffel et al. 2018) and kindly provided by Thomas Seeger and Karin Niessen.

Stock solutions were prepared in ND96 (see section 2.2) or in case of PNU-120596 in DMSO and kept as aliquots at -20° until usage.

2.2 Frogs and oocyte preparation

Xenopus laevis females were obtained from Nasco (Fort Atkinson, WI, USA) and kept at the core facility animal models (CAM) of the biomedical center (BMC) at the LMU Munich (Az:4.3.2-5682/LMU/BMC/CAM) in accordance with the EU Animal Welfare Act. To obtain oocytes, frogs were anaesthetized with MS222, killed by decapitation and ovary was surgically extracted. Alternatively, oocytes were provided by Prof. Luis Pardo (Max-Planck-Institute for Multidisciplinary Sciences, Göttingen) or Ecocyte Bioscience (Castrop-Rauxel, Germany). Ovaries were dissociated in 2mg/ml Collagense NB 4G proved Grade (Nordmark Pharma GmbH) in ND96 (96 mM NaCl, 2 mM KCl, 1 mM CaCl₂, 1 mM MgCl₂, 5 mM HEPES, and pH 7.4) defolliculated in Ca²⁺-free ND96, sorted and kept at 16 °C in filtered ND96 supplemented with 5 µg/ml gentamicin.

2.3 cDNAs, cloning, mutagenesis and cRNA synthesis

cDNA for human adult muscle-type nAChR subunits $\alpha 1$, $\beta 1$, ϵ and δ in pT7TS vector and the human $\alpha 7$ subunit in pMXT vector (originally from Jon Lindstrom, Uni. Pennsylvania, PA, USA) were a gift from Prof. David Adams (Illawara Health and Medical Research Institute, Wollongong University, Australia). cDNAs of human $\alpha 4$ (L35901.1, with silent base exchanges to reduce GC content) and $\beta 2$ (X53179.1) nAChR subunits, mouse 5HT3A (M74425.1), human NA-CHO/TMEM35A (NM_021637.3), human RIC3 (AY326435), and a short fragment carrying P236 insertion and E237A and V251T point mutations (Galzi et al., 1992) were synthesized (Genewiz, Azenta Life Science, USA) and cloned into the pNKS2 vector (Gloor, Pongs and Schmalzing, 1995) by Gibson assembly (Gibson et al., 2009) using Q5 Polymerase and reagents from New England Biolabs (USA). Receptor chimeras and point mutations were created by Gibson Assembly or site-directed mutagenesis (KLD Enzyme Mix, New England Biolabs (USA)). Oligonucleotides were from metabion international AG, Germany. All constructs were confirmed by sequencing of the whole cDNA (Eurofines Genomics, Germany). Details of the chimeras and point mutations are given in Supplementary table S1. Plasmids were linearized using NotI (pNKS2), BamHI (pMXT), or XbaI (pT7TS) from New England Biolabs (USA) and cRNA was synthesized using the mMessageMachine kit (Invitrogen, Thermo Fisher Scientific, USA).

Rat Nav1.4 in pcDNA3.1 (Uniprot: P13390; (Trimmer *et al.*, 1989)) was kindly provided by Stefan Heinemann, University of Jena. Human P2X7 was used as described in (T. Pournara *et al.*, 2020).

2.4 Electrophysiological recordings

Xenopus laevis oocytes were injected with 50 nl aliquots of cRNA (500 ng/ μ l). α 7 SDT cRNA was co-injected with NACHO cRNA (ratio 1:1). Reduced cRNA concentrations were injected for α 7, (α 1) β 1 ϵ δ (2:1:1:1 subunit ratio), and 5HT3A (100 ng/ μ l), 5HT3A AEI (20 ng/ μ l) and α 7^{4TM} 5HT3A (4 ng/ μ l). 23 nl of Nav 1.4 cDNA (150 ng/ μ l) were injected into the nucleus (Bataillé, Helser and Fried, 1990).

1–5 days after injection, two-electrode voltage clamp recordings were performed in ND96 at a holding potential of -70 mV if not otherwise stated. P2X7 measurements were performed at -60 mV in ORI (90 mM NaCl, 1 mM KCl, 1 mM CaCl₂, 1 mM MgCl₂, 5 mM HEPES, and pH 7.4) and ATP was applied in ORII (90 mM NaCl, 1 mM KCl, 2 mM MgCl₂, 5 mM HEPES, and pH 7.4). Microelectrodes were pulled from borosilicate glass, filled with 3 M KCl, and had resistances between 0.3 - 1 M Ω . Membrane currents were recorded using a Turbo Tec 05X Amplifier (npi electronic, Tamm, Germany), filtered at 200 Hz, and digitized at 400 Hz using CellWorks software (npi electronic, Tamm, Germany). The voltage-gated sodium channel Nav 1.4 was held at a membrane potential of -80 mV and activated by a 50 ms pulses of -10 mV, preceded by a 50 ms pulse of -120 mV. Currents were filtered at 3 kHz and digitized at a sampling frequency of 10 kHz. Solutions were automatically applied with a VC3-8xP valve system (ALA scientific instruments, USA) and perfusion speed was regulated by air pressure using an PR-10 analog pressure regulator (ALA scientific instruments, USA). Oocytes were placed in a 200 μ l Teflon bath (Automate Scientific, USA) and solution were applied via 1 mm diameter Teflon tubings and a Teflon micro-manifold to minimize ligand binding to surfaces. Oocytes were continuously perfused at 20 μ l/s and ligand-containing solutions were applied at \sim 250 μ l/s. All measurements were performed with oocytes from at least two different frogs.

2.5 Recording protocols

To determine agonist dose response relations, stable current responses were established by application of 5 s pulses of a reference concentration (generally 300 μ M ACh, 30 μ M ACh for muscle-type nAChR, and 10 μ M ACh for α 7^{Anion} and α 7^{Anion} E258R) in 2 min intervals. Then, increasing ACh concentrations and reference concentrations were applied alternatingly. In case of low test concentrations this was followed by an additional 2 s pulse of reference concentration to maintain equal fractions of desensitized channels. Each test concentration was normalized to the mean of the preceding and following reference concentrations. To investigate competitive antagonist binding, agonist solutions were supplemented with a constant concentration of antagonist and responses were normalized to the reference concentration without antagonist.

To determine antagonist dose response curves, 7 s pulses of a fixed agonist concentration (generally 100 μ M ACh, 30 μ M for muscle-type nAChR, and 5 μ M 5HT for 5HT3A) were applied in intervals of 2 min and 20 s without perfusion. When stable current responses were established, oocytes were perfused for 2 min with buffer and then the antagonist was perfused for 3 s and preincubated for 17 s in a static bath before co-application of agonist and antagonist. Current responses in the presence of antagonist were normalized to the last agonist response before antagonist application.

In the case of PNU-120596/antagonist co-application, responses to ACh (100 μ M) were stabilized at 2 min intervals (with perfusion) and then 10 μ M PNU-120596 were co-applied with agonist and followed by a 9 s-antagonist application after another 5 s.

To investigate α 7 resensitization by different ligands stable current responses were established with pulses of 100 μ M ACh at 2 min intervals. Then one 5 s pulse of 1 mM ACh was applied and

solution flow was stopped for 1 min followed by 5 s perfusion with buffer and another 5s pulse of 1 mM ACh (control response without additional ligand). In case of additional ligand application, PTM0022 or PNU-120596 were applied 10 s after application of 1 mM ACh. Note that PNU-120596 was continuously perfused to avoid stability issues of recordings. Control experiments and ligand applications were performed on the same oocyte with a 5 min interval of buffer perfusion.

2.6 Data analysis and visualization of electrophysiological recordings

CellWorks recordings were imported into Clampfit 11 (Molecular Devices, pClamp, RRID:SCR_011323), baseline corrected and analyzed. In case of small currents, recordings were digitally low-pass filtered at 20 Hz to eliminate the noise. Because of the fast desensitization of the $\alpha 7$ nAChR the area under the curve (AUC)/ net current (Meyer *et al.*, 1998) were used for data analysis (instead of current amplitudes) to minimize effects of perfusion speed. The dose-response analysis was performed using GraphPad Prism version 9 (RRID:SCR_002798). Dose-response curves were fit to the data using the inbuilt Hill equation $normalized\ response = \frac{bottom + (top - bottom)}{1 + \frac{IC_{50}^{n_H}}{c}}$ for antagonists and $normalized\ response = \frac{bottom + c^{n_H} \cdot (top - bottom)}{c^{n_H} + EC_{50}^{n_H}}$ for agonists with n_H = Hill slope, c = concentration (μM) and $bottom$ and top constraint to 0 and 1, respectively.

Current traces were visualized with R (R Project for Statistical Computing, RRID:SCR_001905) using the following packages: dplyr (RRID:SCR_016708), tidyr (RRID:SCR_017102) and ggplot2 (RRID:SCR_014601). In the case of averaged current traces, recordings of the currents prior to antagonist exposure (control) and with antagonist (test) of five oocytes were combined. Each current trace was first baseline corrected and then all data points of the test current were normalized to the peak current of its respective control current. Then the mean and the standard deviation of each time point of the five normalized test currents was calculated. Note that, due to this normalization absolute current values cannot be shown.

2.7 Molecular docking and sequence alignment

3D-structures of PTM0022, MB327 and QX-314 were generated with MarvinSketch 21.3 (ChemAxon, RRID:SCR_004111) and saved as *pdb* files. Cryo-EM structures of the bungarotoxin-bound resting, PNU-120596 mediated, epibatidine-bound open, and epibatidine-bound desensitized states of human $\alpha 7$ nAChR were obtained from the Protein Data Bank (PDB, RRID:SCR_012820) (PDB IDs: 7KOO, 7KOX and 7KOQ, respectively, Noviello *et al.*, 2021). Receptor structures were cleared of glycosylation, ligands and potential water molecules using PyMol (RRID:SCR_000305, Schrödinger), receptors and ligands prepared with AutoDockTools 1.5.7 (Morris *et al.*, 2009). Hydrogen atoms (merged non-polar hydrogens) were added and the Boltzmann and Gasteiger Charges (Gasteiger and Marsili, 1978) computed. The ligands were kept flexible with 6, 8 and 7 rotatable bonds for MB327, PTM0022 and QX-314, respectively. 3D grids of the non-covalent interactions between the prepared ligand and receptor states, as well as electrostatic potentials and desolvation free energies were mapped with AutoGrid4 (RRID:SCR_015982). In a virtual screening approach two grids (XxYxZ, spacing 0.375 Å), one covering the transition area between the extracellular and transmembrane domains with 90x90x70 Å and one covering the whole channel pore with 60x60x126 Å (see supplementary figure 1) were used to mainly cover binding pockets accessible from within the channel pore. The molecular docking was performed with autodock4 (RRID:SCR_012746) (Huey *et al.*, 2007) using the Lamarckian genetic algorithm (LGA) with 50 GA runs, a population size of 200 and 2,500,000 maximum numbers of evaluations (remaining parameters with default settings). The resulting 50 possible confirmations per grid were ranked by the lowest binding energy (see supplementary table 2 to 4, supplementary figure 1). For confirmations with the lowest binding energy, the interacting amino acid residues of the receptor were analyzed employing Protein-Ligand Interaction

Profiler (PLIP, (Adasme *et al.*, 2021)) and a final docking was performed using a grid of 60x60x60 Å around these identified amino acid residues with 10 GA runs, a population size of 300 and 25,000,000 maximum numbers of evaluations. The interacting amino acid residues were analyzed with PLIP and visualized with PyMol. The surface representation of hydrophobic interactions was done running the YRB script by (Hagemans *et al.*, 2015) and Inkscape (RRID:SCR_014479). When PNU-120596 is shown in 7KOX then after alignment with 7EKT (using PyMol) of the more recently published cryo-EM structure of all three states of the human $\alpha 7$ nAChR but with PNU-120596 (Zhao *et al.*, 2021, PDB IDs: 7EKI, 7EKT, 7EKP). Sequence alignments were performed with Jalview (RRID:SCR_006459) using the muscle algorithm (Edgar, 2004) with default settings. The canonical amino acid sequences were taken from the uniprot database (Universal Protein Resource, RRID:SCR_002380).

2.8 Correlation analysis

Physicochemical properties of the BPCs used in this study were calculated using chemicalize service by ChemAxon (RRID:SCR_004111). The correlation analysis was done using R and the ggplot2 based ggcorrmat function of the ggstatsplot package. The physicochemical properties were correlated with the log-transformed IC_{50} (pIC_{50}) values from 2.4.2. The correlation analysis used the person correlation and Holmes-corrected significance analysis with $\alpha=0.05$.

3. Results

3.1 Symmetrical bispyridinium compounds block nAChR currents with micromolar potency

The symmetrical bispyridinium compound MB327 (Turner *et al.*, 2011) was found to show reactivation of muscle contractility in an organ model of OPP (Seeger *et al.*, 2012) and to act as PAM on the $\alpha 7$ nAChR (Scheffel *et al.*, 2018b). It therefore served as a lead structure for the design and synthesis of several derivatives with altered side chains (Rappenglück *et al.*, 2018) of which eight derivatives were tested here. To directly determine their action on nAChRs, we first expressed the homomeric $\alpha 7$ and the heteromeric $(\alpha 1)_2\beta 1\epsilon\delta$ muscle nAChR subtypes in *Xenopus laevis* oocytes and estimated the effects of BPC exposure (preincubation and co-application with agonist) on ACh-activated currents by two-electrode voltage clamp (TEVC, **Figure 1**). Unexpectedly, none of the compounds showed a PAM-like action but most compounds either blocked both receptors or didn't show any activity in the tested concentrations. Dose-response analysis at the $\alpha 7$ nAChR revealed IC_{50} values in the high nanomolar to micromolar range for all compounds, except for PTM0008 and PTM0009, which had no effect in the tested concentration range (**Figure 1B**). The lead compound, MB327, showed intermediate potency with an IC_{50} value of 3.5 μM . PTM0022 and PTM0015 had up to 17-fold higher potency with IC_{50} values of 0.20 μM and 0.49 μM , respectively. At the muscle-type nAChR, IC_{50} values for most of the BPCs, including MB327, were above 10 μM and therefore not determined. Again, PTM0022 and PTM0015 showed the highest potency with IC_{50} values just below and around 1 μM , respectively. Therefore, the lead compound MB327 and PTM0022 were selected for further analysis. To test whether they act as competitive antagonists at the ACh binding site (orthosteric site), we next determined ACh dose-response curves at constant BPCs concentrations ranging from 300 nM to 3 μM (**Figure 1C**). These revealed that the BPC-induced block at both nAChR subtypes is insurmountable by increasing agonist concentrations, indicating a non-competitive binding mode.

3.2 BPCs do not interact directly with the allosteric PNU-120596 binding site of the $\alpha 7$ nAChR

Recent data showed that MB327 and derivatives caused similar effects as the widely used PAM PNU-120596 at the CHO cell-expressed $\alpha 7$ receptor (Scheffel *et al.*, 2018b). Because it has been shown that minor changes in the receptor and environment can alter the effect of allosteric modulators dramatically, we next investigated if the inhibitory effects observed in this study could be caused by a negative allosteric mechanism (Smelt *et al.*, 2018) via the PNU-120596 binding site. To this aim, we used the $\alpha 7$ PAM binding site mutant M253L to test if the BPCs bind to the same transmembrane site as PNU-120596 and other allosteric modulators (**Figure 2**). As shown before, PNU-120596 strongly delays $\alpha 7$ desensitization and increases the current amplitude (Hurst *et al.*, 2005) while the M253L point mutation reduced the potentiating effect of PNU-120596 more than 11-fold (Young *et al.*, 2008) (**Figure 2A**). Interestingly, the antagonistic potency of MB327 increased fourfold on this mutation, whereas the DRC of PTM0022 had only a slightly steeper hill coefficient (**Figure 2B** and **Table 3**). This suggests that the mutation had a selective effect on MB327 binding and/or its allosteric efficiency. To further test the possibility of a shared allosteric binding site with PNU-120596, we investigated the binding kinetics of the selected BPCs by co-application with PNU-120596, making use of the prolonged open state of the $\alpha 7$ (**Figure 2C**). As a control, we used QX-314, a lidocaine derivative that is one of the best-characterized open channel blockers for some nAChRs (Neher and Steinbach, 1978; Pascual and Karlin, 1998; Papke, Horenstein and Placzek, 2001). All compounds were applied in concentrations that in the absence of PNU-120596 resulted in 70-90% block of the receptor. Surprisingly, PTM0022 showed a fast on-set and almost complete block of the PNU-120596-potentiated $\alpha 7$ current and a fast recovery of this current upon washout. Likewise, MB327 showed a quickly reversible inhibition, although to a much smaller extent. Unexpectedly, the open channel blocker QX-314, was unable to block at all. The fast effect of the BPCs and the obvious lack of a direct interaction between BPC and PNU-120596 binding can be explained by either a distinct allosteric binding site with a dominant effect or, more likely, a channel block as mode of action.

3.3 BPCs act as channel blockers

Channel blockers are non-competitive antagonists that prevent ion flux by physically occluding the channel pore. In case of open channel blockers they are characterised by their use-dependency meaning that their effect increases with prolonged opening until their binding equilibrium is reached. In addition, they generally show voltage-dependent inhibition and most of them carry a permanent charge (Heidmann and Changeux, 1986; Buisson and Bertrand, 1998; Hille, 2001). Since BPCs are charged, we next tested the voltage-dependency of their inhibition by comparing their potency at $\alpha 7$ nAChR-expressing oocytes clamped at -50 mV and -100 mV (**Figure 3**). Methyllycaconitine (MLA, 3 nM), an uncharged $\alpha 7$ -selective competitive antagonist was employed as negative control and did not show an altered response at -100 mV compared to -50 mV (**Figure 3A**). In contrast, the positive control QX-314 (10 μ M) showed a significant decline in ACh (100 μ M)-evoked responses from 61% to 23%. Likewise, MB327 and PTM0022 showed a significantly stronger reduction of $\alpha 7$ responses at -100 mV. Notably, the voltage-dependence of the inhibition was even more pronounced at the muscle-type nAChR. These data support a channel block as mode of action of BPCs.

3.4 Ion channel mutants and chimeras support BPC binding within the transmembrane domain

In order to act as channel blocker, the BPCs must bind within the channel pore. To further test our hypothesis, we generated $\alpha 7/5HT3$ receptor chimeras. Chimeras between these receptors have previously been generated and essential gating mechanisms were shown to be preserved (Eiselé *et al.*, 1993). We first determined the potency differences of PTM0022 (1 μ M), MB327 (10

μM) and the positive control QX-314 (30 μM) at the $\alpha 7$ nAChR and the 5HT3A serotonin receptors. All compounds produced a significantly stronger block of the $\alpha 7$ nAChR (mean responses of $\alpha 7$ vs 5HT3A respectively, for PTM0022: 9.3% vs 59.7%, MB327: 36.3% vs 90.2%, QX-314: 9.6% vs 90.0%) (**Figure 4**). We then systematically exchanged domains of the $\alpha 7$ nAChR with those of the 5HT3A receptor, and *vice versa* (see **Supplementary Table S1**), and tested to which extend the chimera was inhibited. On the $\alpha 7$ -5HT3A chimera with the $\alpha 7$ extracellular domain (ECD, ($\alpha 7^{\text{V201-5HT3A}}$, (Eiselé *et al.*, 1993)) all compounds behaved similar as on the WT 5HT3A receptor, excluding a binding area within the $\alpha 7$ ECD. The additional introduction of the intracellular domain (ICD) of the $\alpha 7$ into the 5HT3A ($\alpha 7^{\text{TM5HT3A}}$) likewise did not result in a substantial potency increase of PTM0022 or QX-314. MB327, however, showed significantly increased potency on this chimera, indicating an influence of the ICD on the binding of some of the compounds. Additional chimeras did not result in functional receptors (see **Supplementary Table S1**).

Blocking of nAChRs by high concentrations of the cationic agonist ACh have been observed and were attributed to an open channel block due to its cation-conducting properties (Sine and Steinbach, 1984; Zwart and Vijverberg, 1998). To explore the possibility that the cationic BPCs also interact with negative residues in the entrance of the channel pore, we generated a previously characterized $\alpha 7$ triple mutant (P236 insertion, E237A, V251T, Galzi *et al.*, 1992) here called $\alpha 7^{\text{Anion}}$, that functions as an anion channel and should not attract cations into the pore. Neither QX-314 nor MB327 were able to inhibit this mutant with the used concentrations. In contrast, inhibition by 1 μM PTM0022 was significantly reduced but not eliminated. Substitution of an additional negatively charged residue contributing to the anionic ring at the upper part of the pore by a positively charged residues (E258R) completely abolished the inhibition by PTM0022.

3.5 Molecular docking identifies a high affinity of BPCs to binding pockets in the upper part of the $\alpha 7$ channel pore

To narrow down the possible binding area, an unbiased molecular docking-based screening approach was employed based on the recently published cryo-EM structures for all three distinct states of the $\alpha 7$ nAChR (Noviello *et al.*, 2021). Since no evidence for binding in the ECD was found, this domain was excluded from the screening. Two grids were used for the molecular docking, one spanning the entire inner pore and the other one spanning the upper part of the pore and the junction to the ECD (**Supplementary figure S1**). The conformations with the highest binding affinities (**Supplementary table S2, S3 and S4**) for each grid showed preferential binding of all compounds in the upper part of the channel pore in all three states. While the possible binding sites of the BPCs are more concentrated in both grids, QX-314 binding sites in the upper channel pore are more spread and orientated towards the ECD. In a follow-up docking approach, we focused on the conformations with the highest binding energies in each grid and state in order to identify the most relevant interacting amino acid residues (results shown in **Table 4**). For all three compounds, lowest binding affinities were found for the resting state of the receptor. For PTM0022 the calculated binding affinities were 4.01 μM , 376.7 nM, and 41.4 nM in resting, open and desensitized state, respectively. For MB327 comparably lower affinities of 10.49 μM , 22.6 μM , 327.8 nM were calculated for resting, open, and desensitized state, respectively. Remarkably, for both BPCs the affinity differences between the poorly bound resting state and the strongly bound desensitized state were about 70 - 100-fold while MB327 displayed the weakest binding affinity for the open state. For QX-314, on the other hand, only small differences in binding affinities were found between the different $\alpha 7$ receptor states with the highest affinity for the open state. Interestingly, and in agreement with our experimental data described above, all three compounds bind in the docking simulations to hydrophobic patches (yellow parts of the surface representation, **Figure 5**) around the first channel ring of positively charged glutamate residues (E258, E20', 'indicates channel lining residue) and position in different orientations, depending on the state of the $\alpha 7$ (**Figure 5**).

3.6 Mutagenesis supports a PTM0022 binding area in the upper part of the $\alpha 7$ channel pore

Because of the high potency on both $\alpha 7$ and muscle-type nAChRs, PTM0022 was used to experimentally confirm essential interacting amino acid residues identified in the docking simulations (**Table 4**). Based on a sequence alignment between 5HT3A and $\alpha 7$ nAChR (**Supplementary figure S3**), residues of the identified PTM0022 positions in the $\alpha 7$ nAChR were exchanged with the corresponding residues of the 5HT3A receptor and *vice versa*. As seen in **Figure 6A**, an exchange of the three amino acids, one at the negative ring at position E258D and the two neighboring residues A257S and I259T (orange frame in **supplementary figure S3**) reduces the potency of 1 μ M PTM0022 already significantly. This was further reduced by an additional Y210F exchange ($\alpha 7$ 257-259SDT, Y210F), resulting in responses similar to those at the 5HT3A receptor. The corresponding substitutions in the 5HT3A receptor (SDT into AEI) did, however, not reconstitute $\alpha 7$ -like properties, suggesting that in addition to the charged patch, a favorable channel geometry is required. We also did not see a change in inhibition when substituting the same two neighboring residues of the 5HT3A receptor into the negative ring of the muscle-type $\alpha 1$ subunit ($\alpha 1$ ST) and additionally the residue before the negative ring in the $\beta 1$ subunit ($\beta 1$ A272S) (see orange frame in **supplementary figure S3**), indicating a distinct or more complex binding area in the heteromeric muscle-type nAChR. Interestingly, as shown in **Figure 6 B**, the $\alpha 7$ -5HT3A-chimeras described above (3.4), the anionic $\alpha 7$ ($\alpha 7^{\text{Anion}}$) and the $\alpha 7^{\text{Anion}}$ E258R receptors were not blocked by 10 mM ACh, confirming that the open channel block by ACh is dependent on its charge and involves the same residues as the block by BPCs.

3.7 Correlation between typical physicochemical properties of the investigated BPCs and their potency towards the $\alpha 7$ nAChR

In order to further support our hypothesis, we performed a correlation analysis of physicochemical properties against the log-transformed potencies (pIC_{50}) of the tested BPCs at the $\alpha 7$ nAChR (**Figure 7A**). This revealed strong and significant correlations for the logP, van der Waals surface area, polarizability, van der Waals volume and associated molar refractivity. However, inclusion of QX-314 (**Figure 7C**) revealed that the logP as a measure of the hydrophobicity yielded a low correlation (**Figure 7A, B**) while the van der Waals volume and the more sophisticated molar refraction and polarizability (Zhu *et al.* 2017, Berinde 2021) were still strongly correlated with a higher potency providing additional structural properties except the linker length between the two pyridinium rings (Ring *et al.* 2015).

3.8 PTM0022 is not a resensitizer of the $\alpha 7$ nAChR

BPCs have been reported to recover muscle contractility in *in vitro* (Tattersall, 1993; Seeger *et al.*, 2012) and *in vivo* (Turner *et al.*, 2011; Timperley *et al.*, 2012) models of OPP intoxication in an AChE-independent way and to potentiate $\alpha 7$ currents (Scheffel *et al.*, 2018b). Since these findings indicate that BPCs can facilitate resensitization of desensitized nAChRs, we tested their potential to protect or recover the oocyte-expressed $\alpha 7$ nAChR from desensitization. Therefore, we exposed the $\alpha 7$ nAChR for 1 min to 1 mM ACh and accessed its recovery after 5 s of buffer application with and without 3 μ M PTM0022. As shown in **Figure 8A**, no current increase by PTM0022 was observed. Different application time points for PTM0022 (after 1 mM ACh-stimulation, co-applied with 1 mM ACh, before 1 mM ACh) did not alter the outcome. In contrast, co-application of the PAM II, PNU-120596, enabled the immediate activation and potentiation of the receptor and delayed desensitization, thus providing support for the concept of investigating nAChR PAMs as potential OPP treatment.

3.9 PTM0022 is selective for $\alpha 7$ and muscle-type nAChRs

Since the investigated BPCs showed some inhibition of the 5HT3A receptor, we further tested the ability of PTM0022 to inhibit other cation-selective ion channels (**Figure 8B-D**). Inhibition of the 5HT3A was voltage-dependent (**Figure 8C**), supporting their action as open channel blockers. Interestingly, no significant inhibition of the $\alpha 4\beta 2$ nAChR was found at 10 μ M PTM0022 at -50 and -100 mV while the trimeric purinergic P2X7 receptor was slightly inhibited at this concentration but in a voltage-independent way. The voltage-gated muscle sodium channel Nav1.4, which could be a relevant target for the treatment of OPP, was also not affected by 10 μ M PTM0022 (**Figure 8D**). Thus, PTM0022 appears to be rather selective for $\alpha 7$ and muscle-type nAChR subtypes.

4. Discussion

Here we investigated a series of BPC analogues and confirm that they act as antagonists of the $\alpha 7$ and muscle-type nAChRs and that inhibition is non-competitive and voltage-dependent. The simplest interpretation of our data is that BPCs act as channel blockers. A charge-dependent binding within the upper channel pore close to the ECD was supported by mutagenesis and computational analysis. Comparison of their potency at a variety of cation channels suggests a rather selective but non-specific binding to $\alpha 7$ and muscle-type nAChRs.

Our conclusion that BPCs act as channel blocker agrees with several previous reports, in which the action of the BPCs SAD-128 or MB327 were investigated by single channel patch clamp analysis of channels in isolated frog muscle cells (Alkondon and Albuquerque, 1989), murine muscle cells (Tattersall, 1993) and CN21 cells (human rhabdomyosarcoma cell line TE671 stably transfected with adult ϵ -nAChR subunit, (Beeson *et al.*, 1996)) (Turner *et al.*, 2011). However, in these studies on native receptors, selectivity of the compounds for defined human nAChRs, a possible involvement of other ion channels, and the specific binding site of BPCs was not determined.

In this study, we confirmed the channel blocking action of BPCs using defined oocyte-expressed human muscle-type and neuronal $\alpha 7$ nAChRs and show that they have clearly different effects to the $\alpha 7$ PAM PNU-120596. This is in contrast to a previous electrophysiological study (Scheffel *et al.*, 2018b) that found a positive allosteric modulation of CHO cell-expressed human $\alpha 7$ nAChRs by BPCs. The reason for this discrepancy is not clear. Differences in ion channel properties have been observed between ion channels expressed in mammalian cells and in oocytes and could influence the interaction with BPCs. For example, many ion channels, including pLGICs are allosterically modulated by lipids in the transmembrane domain (Velisetty, Chalamalasetti and Chakrapani, 2014; Howard, 2021) and even small changes in extracellular allosteric binding sites (Bertrand *et al.*, 1992; Young *et al.*, 2008; Collins and Millar, 2010; Gill *et al.*, 2011; Chatzidaki *et al.*, 2015; Newcombe *et al.*, 2018) or small modifications of compound (Gill-Thind *et al.*, 2015) can have a major influence on the activity of a compound or even change its mode of action entirely. Also, ligands acting via the same allosteric binding sites can induce potentiating, inhibiting or silent effects (Gill-Thind *et al.*, 2015; Brams *et al.*, 2020). Thus, differences in the membrane lipid composition could indirectly account for the different findings. However, all tested symmetrical C3-linker non-oxime BPCs showed a similar inhibitory behavior on the human $\alpha 7$ and muscle-type nAChRs (**Figure 1**) as well as on the 5HT3A receptor, indicating that their mode of action is rather unspecific and not affected by subtle differences in their structure or their binding areas. To definitely exclude an effect of the expression system, we confirmed the antagonistic properties

of MB327 by patch clamp analysis of CHO cells stable transfected with the human $\alpha 7$ nAChR. (Supplementary figure S6).

Due to the very fast desensitization of the $\alpha 7$ nAChR (Fucile, 2004; Williams, Wang and Papke, 2011) it is difficult to investigate BPC binding in the open state. Using PNU-120596, an $\alpha 7$ -selective PAM II with known binding site (Young *et al.*, 2008; Zheng *et al.*, 2021) and well-studied mode of action (Williams, Wang and Papke, 2011), we tested a direct competition between PNU-120596 and the BPCs. Based on the clearly faster different kinetics of channel closure and opening caused by PTM0022 compared to the kinetics of channel closure and opening caused by PNU-120596 alone, we excluded a direct interaction of PTM0022 with the PNU-120596 binding site. However, this interpretation does not consider the possibility that PNU-120596 binding is allosterically altered by PTM0022 binding. Interestingly, while 1 μM PTM0022 and 30 μM MB327 showed comparable inhibition of about 80-90% if applied without PNU-120596 (compare Fig. 1B), the same concentration of MB327 showed clearly reduced inhibition of the PNU-120596-potentiated open state. Even more striking, QX-314 was completely unable to block the potentiated channel. A possible explanation could be that the PNU-120596-potentiated open channel state differs significantly from the non-potentiated channel and PTM0022, as the larger compound, more efficiently occludes the potentiated state. This assumption is supported by the correlation analysis (**Figure 7**), which shows that BPCs with the larger van der Waals volume show stronger inhibition. While no structure of the short-lived $\alpha 7$ state is available, functional data indicate that both states differ in terms of subconductance levels (Williams, Wang and Papke, 2011), inward rectification (Sitzia *et al.*, 2011), Ca^{2+} permeability (Miller *et al.*, 2020), and sensitivity to channel blockers (Peng *et al.*, 2013; Quadri *et al.*, 2019). Alternatively, there might be a direct interaction between the specific MB327 binding residues and the PNU-120596 binding site. This would be in agreement with the potency increase of MB327 at the M253L PNU-120596 binding site mutant (**Figure 2**) and supported by our docking results (**Figure 5**).

BPCs may act as sequential channel blocker with similarities to permanently charged lidocaine derivatives

Like most channel blockers the BPCs used in this study are charged (Changeux, Pinset and Ribera, 1986; Hille, 2001; Moaddel, Jozwiak and Wainer, 2007). In agreement with a channel block, inhibition by BPCs showed a weak but significant voltage-dependency at the $\alpha 7$ receptor and strong voltage-dependency at the muscle-type nAChR, most likely as a result of facilitated channel entry and physical occluding of the pore at lower membrane potentials (Woodhull, 1973). Binding of some channel blockers depend on channel opening (Heginbotham and Kutluay, 2004; Phillips, Nigam and Johnson, 2020) and two principle modes of action have been distinguished: a sequential (“foot in the door”) mechanism as found for lidocaine-derivates like QX-222/QX-314 (Charnet *et al.*, 1990; Papke, Horenstein and Placzek, 2001) and a “trapped” binding mode (as described for mecamylamine) in which the compound can only enter and exit during the open state or depolarization (Giniatullin *et al.*, 2000). A clear differentiation requires single channel recordings. However, the fast washout of the BPCs (**Supplementary Figure S5**), the voltage-dependent inhibition (**Figure 2**), and the ability to block also other cation-selective ion channels (**Figure 9**) are in agreement with the previously defined sequential channel block (Tattersal 1993).

The binding site in the transition zone of ECD and TMD

The $\alpha 7$ nAChR is one of the best-studied nAChRs and high-resolution structures of antagonist-bound and apo-resting state, PNU-120596-bound open state, and epibatidine-bound desensitized state are available (Noviello *et al.*, 2021; Zhao *et al.*, 2021). Although the ICD has not been resolved, detailed experimental and modelling data are also available (Bondarenko *et al.*, 2022).

Its homomeric structure and homology with the homomeric 5HT3 receptor enable easy mutagenesis and generation of chimeras. These properties allowed us to extend previous studies and to investigate a possible binding region of the BPCs.

The binding site of QX-314 has been experimentally localized around L9' (L247) and T6' (T244) (Charnet *et al.*, 1990; Papke, Horenstein and Placzek, 2001) in the lower part of the channel pore. The reduced voltage-dependency of the BPCs compared to QX-314 (**Figure 3**) might indicate that the binding site is located more towards the ECD. This logic would indicate a deeper binding site for the muscle-type as well. However, the literature assumes a binding site in the ECD, either as competitive antagonist supported by radioligand binding assays of MB327 (C3-linker) with [³H]epibatidine on purified membranes *Torpedo californica* membranes (Niessen *et al.* 2018) and molecular dynamics simulations on a homology model of the human muscle nAChR with proposed additional allosteric action of MB505 (C8-linker) and MB442 (C5-linker) (Epstein *et al.*, 2021) or in the extracellular channel vestibule supported by docking studies on the *Torpedo* nAChR with MB327 (Wein *et al.*, 2018). In agreement with BPC and QX-314 binding within the $\alpha 7$ TM region, we showed that their potency was clearly reduced at a $\alpha 7$ -5HT3 chimera in which the TM and ICD domains were replaced by the respective 5HT3 sequences ($\alpha 7^{V201-5HT3A}$, **Figure 4**). Interestingly and for an unknown reason, inhibition by QX-314 and MB327 was slightly better if the $\alpha 7$ -ICD was re-introduced. A possible explanation is that this domain has an influence on the adjacent TM3 and 4 domains and influences gating as previously shown (Castelán *et al.*, 2007; Bondarenko *et al.*, 2022). Since we found MB327 to be localized a bit closer towards the channel gate, it could be more influenced by an ICD-dependent reorientation of these TMDs, in particular TMD3 with its prolonged cytosolic helix.

On the triple mutated anionic $\alpha 7$ ($\alpha 7^{Anion}$) nAChR (Galzi *et al.*, 1992) inhibition of MB327 and QX-314 was completely abolished at the used concentration (**Figure 4**) and that of PTM0022 significantly reduced. Here, the reason may be a combination of a direct effect of the V251T point mutation, which is close to the proposed binding site and the changed conductance. In any case, the $\alpha 7^{Anion}$ mutant tolerated the additional E258R mutation, which was not functional on its own. In agreement with its role in determining channel conductance (Imoto *et al.*, 1988) and the involvement in PTM0022 binding found in our computational modelling, this mutation completely abolished the inhibition by PTM0022 (**Figure 4**).

Our docking studies (**Figure 5**) predicted that MB327, PTM0022 and QX-314 (**Supplementary Figure S1**) have highest binding affinities in the transition zone of ECD and ICD (**Supplementary Table S2 –S4**). In agreement with their positively charged quaternary ammonium and lipophilic side chains, all three molecules were placed within a ring of negatively charged amino acid residues in the TMD, formed by E258 (E20') and were stabilized by lipophilic, and π -cation interactions. Interestingly, PTM0022 and MB327 bind close to the PNU-120596 binding pocket (Young *et al.*, 2008; Zhao *et al.*, 2021). We observed for both BPCs the highest binding affinity in the desensitized state. Interestingly, MB327 showed a poor binding affinity in the open state which could explain its weak inhibition of the PNU-120596 prolonged open state. However, the limitations of the open state structure mentioned in (Noviello *et al.*, 2021) and possible differences to the PNU-120596-free open state need to be considered. The here identified binding area, between ECD and TMD, is in close proximity to the second identified binding site in the molecular docking experiments of the *Torpedo* nAChR with MB327 (Wein *et al.*, 2018), further supporting our findings.

However, given the likely action as channel blocker, the usage of static molecular docking experiments is limited due to the lack of consideration of the ion conductance. BPCs act most likely as "big" ions competing of the pore with the general, conducting ions and penetrate into the pore depending on the properties of the ion channel. Sophisticated computational simulations (Xu *et*

al. 2006) with consideration of ion conductance and polarizability (Delemotte, Klein and Tarek 2012) would be necessary to clarify the exact depth.

5. Conclusion

Modulation of ion channels via allosteric binding sites has great therapeutic potential (Papke and Horenstein, 2021). In case of OPP, it has been hypothesized that resensitization of desensitized muscle-type nAChRs could provide a way to counteract OPC-induced muscle symptoms like respiratory failure and other nAChR-induced symptoms of the cholinergic syndrome (Scheffel *et al.*, 2018a). This principle concept is supported by the finding that the addition of PNU-120596 was indeed able to induce 4-5 fold increased current responses immediately after complete desensitization of the fast desensitizing $\alpha 7$ nAChR. However, the following needs to be considered:

i) the main target of interest is the muscle-type nAChR and so far, no PAM has been described for this subtype. Multiple allosteric binding sites have been identified in other nAChRs, ranging from compound-selective sites such as the quinacrine binding site (Arias, 1998) and the ethidium binding site (Pratt, Pedersen and Cohen, 2000), to less compound-selective binding sites within the TMDs (Newcombe *et al.*, 2018) and several others in the ECD, with the vestibule site seemingly be an important one (Papke *et al.*, 2014; Spurny *et al.*, 2015; Nys *et al.*, 2016).

ii) The receptor kinetics are clearly changed by the PAM co-application which might severely influence or even disable physiological muscle function, which critically relies on the accurate timing of ACh release and breakdown and associated receptor opening and desensitization. Although desensitization of the muscle nAChR is much slower, its kinetics might still be affected. PAMs that alter the desensitization of the receptor (PAM II) would probably be superior than compounds that primarily affect the current amplitude (PAM I). However, both kinds of PAM bear the risk of a superstimulation and subsequent facilitation.

Channel blocker would offer theoretically a therapeutic alternative to PAMs. Fast acting channel blocker would just decrease the ion flux during a burst without altering properties of the ion channel like PAMs or the activation pattern like antagonists and are already employed clinically as local anesthetics, antiarrhythmics and antiepileptics for other ion channels (Ågren, Nilsson and Åhrem 2019, Johnson and Kotermanski 2006). A channel block is use-dependent, thus the higher activation by accumulating ACh should result in a higher block. In principle a possible counter against ACh-induced depolarization block. The simplified overstimulation experiment in this study does not represent the complex muscle endplate enough to investigate this, but the muscle-preparation experiments are in support of this theory. However, the rather unspecific block by BPCs of cationic ion channels may pose a risk for side effects.

Conflict of Interest

The authors declare that the research was conducted in the absence of any commercial or financial relationships that could be construed as a potential conflict of interest.

Author Contributions

Conceptualization: AN, YH
Formal analysis: YH, TD, DL
Investigation: YH, TD, DL
Resources: KN, TS

Writing - Original Draft: AN, YH
Writing-Review and Editing: TD, DL, KVN, TS
Project administration: AN, YH
Funding acquisition: AN

Funding

This work was supported by the Deutsche Forschungsgemeinschaft DFG (German Research Foundation, Research Training Group GRK2338, P01) to AN.

Acknowledgments

We thank Han Shen Tae and David Adams (Illawarra Health and Medical Research Institute, Wollongong University, Australia) for providing adult muscle type nAChR cDNAs, Prof. Stefan Heine-mann (University of Jena, Germany) for providing the rat Nav1.4 cDNA, Monika Haberland for preparing oocytes and Veronika Iska for assistance with cloning. We further thank Sebastian Rappenglück (Department of Pharmacy–Center for Drug Research, Ludwig-Maximilians-Universität München, Germany) for the synthesis of the substituted bispyridinium compounds. This work received financial support from the State Ministry of Baden-Wuerttemberg for Economic Affairs, Labour and Tourism.

Supplementary Material

Supplementary material is provided as an additional file. They are added in the end of the manuscript.

References

- Adasme, M.F. *et al.* (2021) “PLIP 2021: expanding the scope of the protein–ligand interaction profiler to DNA and RNA,” *Nucleic Acids Research*, 49(W1), pp. W530–W534. doi:10.1093/NAR/GKAB294.
- Ågren R., Nilsson J. and Åhrem, P. (2019) “Closed and open state dependent block of potassium channels cause opposing effects on excitability – a computational approach,” *Scientific reports*, 9(1), pp. 1–9. doi:10.1038/s41598-019-44564-x
- Aldridge, W.N. and Reiner, E. (1972) *Enzyme inhibitors as substrates: interactions of esterases with esters of organophosphorus and carbamic acids*. Amsterdam: North-Holland research monographs, Frontiers of biology 26.
- Alkondon, M. and Albuquerque, E.X. (1989) “The nonoxime bispyridinium compound SAD-128 alters the kinetic properties of the nicotinic acetylcholine receptor ion channel: a possible mechanism for antidotal effects,” *The Journal of pharmacology and experimental therapeutics*, 250(3), pp. 842–52. Available at: <http://www.ncbi.nlm.nih.gov/pubmed/2476549>.
- Alozi, M. and Rawas-Qalaji, M. (2020) “Treating organophosphates poisoning: management challenges and potential solutions,” *Critical reviews in toxicology*, 50(9), pp. 764–779. doi:10.1080/10408444.2020.1837069.
- Amin, D.M. *et al.* (2018) “Morbidity and Mortality Indicators in Acute Organophosphate Poisoning in Zagazig University Hospital, Egypt: Retrospective Study,” *Occupational Diseases and Environmental Medicine*, 6(4), pp. 130–140. doi:10.4236/ODEM.2018.64011.
- Arias, H.R. (1998) “Binding sites for exogenous and endogenous non-competitive inhibitors of the nicotinic acetylcholine receptor,” *Biochimica et biophysica acta*, 1376(2), pp. 173–220. doi:10.1016/S0304-4157(98)00004-5.
- Banday, T.H. *et al.* (2015) “Predictors of Morbidity and Mortality in Organophosphorus Poisoning: A Case Study in Rural Hospital in Karnataka, India,” *North American Journal of Medical Sciences*, 7(6), p. 259. doi:10.4103/1947-2714.159331.
- Bataillé, N., Helser, T. and Fried, H.M. (1990) “Cytoplasmic transport of ribosomal subunits microinjected into the *Xenopus laevis* oocyte nucleus: a generalized, facilitated process.” *Journal of Cell Biology*, 111(4), pp. 1571–1582. doi:10.1083/JCB.111.4.1571.
- Beeson, D. *et al.* (1996) “Stable functional expression of the adult subtype of human muscle acetylcholine receptor following transfection of the human rhabdomyosarcoma cell line TE671 with cDNA encoding the ϵ subunit,” *Neuroscience Letters*, 207(1), pp. 57–60. doi:10.1016/0304-3940(96)12488-5.

- Bertrand, D. *et al.* (1992) "Unconventional pharmacology of a neuronal nicotinic receptor mutated in the channel domain," *Proceedings of the National Academy of Sciences of the United States of America*, 89(4), pp. 1261–1265. doi:10.1073/pnas.89.4.1261.
- Bondarenko, V. *et al.* (2022) "Structures of highly flexible intracellular domain of human $\alpha 7$ nicotinic acetylcholine receptor," *Nature Communications*, 13(1), p. 793. doi:10.1038/s41467-022-28400-x.
- Brams, M. *et al.* (2020) "Modulation of the erwinia ligand-gated ion channel (ELIC) and the 5-HT₃ receptor via a common vestibule site," *eLife*, 9. doi:10.7554/eLife.51511.
- Buckley, N.A. *et al.* (2004) "Where is the Evidence for Treatments used in Pesticide Poisoning? - Is Clinical Toxicology Fiddling while the Developing World Burns?," *Journal of toxicology. Clinical toxicology*, 42(1), p. 113. doi:10.1081/CLT-120028756.
- Buisson, B. and Bertrand, D. (1998) "Open-channel blockers at the human $\alpha 4\beta 2$ neuronal nicotinic acetylcholine receptor," *Molecular Pharmacology*, 53(3), pp. 555–563. doi:10.1124/mol.53.3.555.
- Castelán, F. *et al.* (2007) "Cytoplasmic regions adjacent to the M3 and M4 transmembrane segments influence expression and function of $\alpha 7$ nicotinic acetylcholine receptors. A study with single amino acid mutants," *Journal of Neurochemistry*, 100(2), pp. 406–415. doi:10.1111/j.1471-4159.2006.04202.x.
- Changeux, J.P. (2018) "The nicotinic acetylcholine receptor: A typical 'allosteric machine,'" *Philosophical Transactions of the Royal Society B: Biological Sciences*. Royal Society Publishing. doi:10.1098/rstb.2017.0174.
- Changeux, J.P., Pinset, C. and Ribera, A.B. (1986) "Effects of chlorpromazine and phencyclidine on mouse C2 acetylcholine receptor kinetics.," *The Journal of Physiology*, 378(1), pp. 497–513. doi:10.1113/jphysiol.1986.sp016232.
- Charnet, P. *et al.* (1990) "An open-channel blocker interacts with adjacent turns of α -helices in the nicotinic acetylcholine receptor," *Neuron*, 4(1), pp. 87–95. doi:10.1016/0896-6273(90)90445-L.
- Chatzidaki, A. *et al.* (2015) "The influence of allosteric modulators and transmembrane mutations on desensitisation and activation of $\alpha 7$ nicotinic acetylcholine receptors," *Neuropharmacology*, 97, pp. 75–85. doi:10.1016/j.neuropharm.2015.05.006.
- Collins, T. and Millar, N.S. (2010) "Nicotinic acetylcholine receptor transmembrane mutations convert ivermectin from a positive to a negative allosteric modulator," *Molecular Pharmacology*, 78(2), pp. 198–204. doi:10.1124/mol.110.064295.
- Dani, J.A. (2015) "Neuronal Nicotinic Acetylcholine Receptor Structure and Function and Response to Nicotine," in *International Review of Neurobiology*. NIH Public Access, pp. 3–19. doi:10.1016/bs.irn.2015.07.001.
- Dassanayake, T.L. *et al.* (2021) "Changes of attention-related brain activity over 6 months after acute organophosphate pesticide poisoning: a prospective follow-up study," *Clinical Toxicology*, pp. 1–9. doi:10.1080/15563650.2021.2010742.
- Delemotte, L., Klein, M.L. and Tarek, M. (2012) "Molecular dynamics simulations of voltage-gated cation channels: Insights on voltage-sensor domain function and modulation," *Frontiers in Pharmacology*, 3 MAY, p. 97. doi:10.3389/FPHAR.2012.00097/BIBTEX.
- Edgar, R.C. (2004) "MUSCLE: multiple sequence alignment with high accuracy and high throughput," *Nucleic Acids Research*, 32(5), pp. 1792–1797. doi:10.1093/NAR/GKH340.
- Eiselé, J.L. *et al.* (1993) "Chimaeric nicotinic-serotonergic receptor combines distinct ligand binding and channel specificities," *Nature*, 366(6454), pp. 479–483. doi:10.1038/366479a0.
- Epstein, M. *et al.* (2021) "Molecular determinants of binding of non-oxime bispyridinium nerve agent antidote compounds to the adult muscle nAChR," *Toxicology Letters*, 340, pp. 114–122. doi:10.1016/j.toxlet.2021.01.013.
- Franca, T.C.C. *et al.* (2019) "Novichoks: The Dangerous Fourth Generation of Chemical Weapons," *International journal of molecular sciences*, 20(5). doi:10.3390/IJMS20051222.
- Fucile, S. (2004) "Ca²⁺ permeability of nicotinic acetylcholine receptors," *Cell calcium*, 35(1), pp. 1–8. doi:10.1016/J.CECA.2003.08.006.
- Galzi, J.L. *et al.* (1992) "Mutations in the channel domain of a neuronal nicotinic receptor convert ion selectivity from cationic to anionic," *Nature*, 359(6395), pp. 500–505. doi:10.1038/359500a0.
- Gasteiger, J. and Marsili, M. (1978) "A new model for calculating atomic charges in molecules," *Tetrahedron Letters*, 19(34), pp. 3181–3184. doi:10.1016/S0040-4039(01)94977-9.
- Gibson, D.G. *et al.* (2009) "Enzymatic assembly of DNA molecules up to several hundred kilobases," *Nature methods*, 6(5), pp. 343–345. doi:10.1038/NMETH.1318.
- Gill, J.K. *et al.* (2011) "Agonist activation of $\alpha 7$ nicotinic acetylcholine receptors via an allosteric transmembrane site," *Proceedings of the National Academy of Sciences of the United States of America*, 108(14), pp. 5867–5872. doi:10.1073/pnas.1017975108.
- Gill-Thind, J.K.K. *et al.* (2015) "Structurally similar allosteric modulators of $\alpha 7$ nicotinic acetylcholine receptors exhibit five distinct pharmacological effects," *Journal of Biological Chemistry*, 290(6), pp. 3552–3562. doi:10.1074/jbc.M114.619221.
- Giniatullin, R.A. *et al.* (2000) "Rapid relief of block by mecamylamine of neuronal nicotinic acetylcholine receptors of rat chromaffin cells in vitro: An electrophysiological and modeling study," *Molecular Pharmacology*, 58(4), pp. 778–787. doi:10.1124/mol.58.4.778.
- Gloor, S., Pongs, O. and Schmalzing, G. (1995) "A vector for the synthesis of cRNAs encoding Myc epitope-tagged proteins in *Xenopus laevis* oocytes," *Gene*, 160(2), pp. 213–217. doi:10.1016/0378-1119(95)00226-V.
- Hagemans, D. *et al.* (2015) "A script to highlight hydrophobicity and charge on protein surfaces," *Frontiers in Molecular Biosciences*, 2(OCT), p. 56. doi:10.3389/FMOLB.2015.00056/BIBTEX.

- Hamill OP, Marty A, Neher E, et al (1981) "Improved patch-clamp techniques for high-resolution current recording from cells and cell-free membrane patches," *Pflug Arch* 391, pp. 85–100. doi:10.1007/BF00656997.
- Haslam, J.D. *et al.* (2021) "Chemical, biological, radiological, and nuclear mass casualty medicine: a review of lessons from the Salisbury and Amesbury Novichok nerve agent incidents," *British journal of anaesthesia* [Preprint]. doi:10.1016/J.BJA.2021.10.008.
- Heginbotham, L. and Kutluay, E. (2004) "Revisiting voltage-dependent relief of block in ion channels: A mechanism independent of punchthrough," *Biophysical Journal*, 86(6), pp. 3663–3670. doi:10.1529/biophysj.103.039412.
- Heidmann, T. and Changeux, J.P. (1986) "Characterization of the transient agonist-triggered state of the acetylcholine receptor rapidly labeled by the noncompetitive blocker [3H]chlorpromazine: additional evidence for the open channel conformation," *Biochemistry*, 25(20), pp. 6109–6113. doi:10.1021/BI00368A041.
- Hille, B. (2001) *Ion Channels of Excitable Membranes*. 3rd Editio, *The New Public Library*. 3rd Editio. Sinauer Associations, Inc., Sunderland. doi:10.4324/9780429449680-1.
- Howard, R.J. (2021) "Elephants in the Dark: Insights and Incongruities in Pentameric Ligand-gated Ion Channel Models," *Journal of Molecular Biology*. J Mol Biol, p. 167128. doi:10.1016/j.jmb.2021.167128.
- Huey, R. *et al.* (2007) "A semiempirical free energy force field with charge-based desolvation," *Journal of computational chemistry*, 28(6), pp. 1145–1152. doi:10.1002/JCC.20634.
- Hung, D.Z. *et al.* (2015) "The Long-Term Effects of Organophosphates Poisoning as a Risk Factor of CVDs: A Nationwide Population-Based Cohort Study," *PLoS ONE*, 10(9). doi:10.1371/JOURNAL.PONE.0137632.
- Hurst, R.S. *et al.* (2005) "A novel positive allosteric modulator of the alpha7 neuronal nicotinic acetylcholine receptor: in vitro and in vivo characterization.," *The Journal of neuroscience : the official journal of the Society for Neuroscience*, 25(17), pp. 4396–405. doi:10.1523/JNEUROSCI.5269-04.2005.
- Imoto, K. *et al.* (1988) "Rings of negatively charged amino acids determine the acetylcholine receptor channel conductance," *Nature*, 335(6191), pp. 645–648. doi:10.1038/335645a0.
- John, H. *et al.* (2018) "Fatal sarin poisoning in Syria 2013: forensic verification within an international laboratory network," *Forensic Toxicology*, 36(1), pp. 61–71. doi:10.1007/s11419-017-0376-7.
- Johnson, J. and Kotermanski, S. (2006) "Mechanism of action of memantine" *Current Opinion in Pharmacology*, 6(1), pp. 61-67. doi:10.1016/j.coph.2005.09.007
- Jokanović, M. (2018) "Neurotoxic effects of organophosphorus pesticides and possible association with neurodegenerative diseases in man: A review," *Toxicology*, 410, pp. 125–131. doi:10.1016/J.TOX.2018.09.009.
- Kassa, J. *et al.* (2020) "Influence of experimental end point on the therapeutic efficacy of the antinicotinic compounds MB408, MB442 and MB444 in treating nerve agent poisoned mice—a comparison with oxime-based treatment," *Toxicol. Mech. Methods*, 30(9), pp. 703–710. doi:10.1080/15376516.2020.1817218.
- Maksimović, Ž.M. *et al.* (2021) "Acute organophosphate and carbamate pesticide poisonings - a five-year survey from the National Poison Control Center Of Serbia," *Drug and chemical toxicology*, pp. 1–9. doi:10.1080/01480545.2021.2012481.
- Meyer, E.M. *et al.* (1998) "Neuroprotective and memory-related actions of novel alpha-7 nicotinic agents with different mixed agonist/antagonist properties.," *The Journal of pharmacology and experimental therapeutics*, 284(3), pp. 1026–32. Available at: <http://www.ncbi.nlm.nih.gov/pubmed/9495863>.
- Miller, D.R. *et al.* (2020) "Allosterically potentiated a7 nicotinic acetylcholine receptors: Reduced calcium permeability and current-independent control of intracellular calcium," *Molecular Pharmacology*, 98(6), pp. 695–709. doi:10.1124/MOLPHARM.120.000012.
- Moaddel, R., Jozwiak, K. and Wainer, I.W. (2007) "Allosteric modifiers of neuronal nicotinic acetylcholine receptors: new methods, new opportunities," *Medicinal research reviews*, 27(5), pp. 723–753. doi:10.1002/MED.20091.
- Morris, G.M. *et al.* (2009) "Software news and updates AutoDock4 and AutoDockTools4: Automated docking with selective receptor flexibility," *Journal of Computational Chemistry*, 30(16), pp. 2785–2791. doi:10.1002/jcc.21256.
- Muley, A. *et al.* (2014) "To identify morbidity and mortality predictors in acute organophosphate poisoning," *Indian Journal of Critical Care Medicine : Peer-reviewed, Official Publication of Indian Society of Critical Care Medicine*, 18(5), p. 297. doi:10.4103/0972-5229.132488.
- Neher, E. and Steinbach, J.H. (1978) "Local anaesthetics transiently block currents through single acetylcholine-receptor channels.," *The Journal of Physiology*, 277(1), pp. 153–176. doi:10.1113/jphysiol.1978.sp012267.
- Newcombe, J. *et al.* (2018) "Diversity of nicotinic acetylcholine receptor positive allosteric modulators revealed by mutagenesis and a revised structural model," *Molecular Pharmacology*, 93(2), pp. 128–140. doi:10.1124/mol.117.110551.
- Niessen, K.V. *et al.* (2018) "In vitro pharmacological characterization of the bispyridinium non-oxime compound MB327 and its 2- and 3-regioisomers," *Toxicology Letters*, 293, pp. 190–197. doi:10.1016/j.toxlet.2017.10.009.
- Noviello, C.M. *et al.* (2021) "Structure and gating mechanism of the $\alpha 7$ nicotinic acetylcholine receptor," *Cell*, 184(8), pp. 2121–2134.e13. doi:10.1016/j.cell.2021.02.049.

- Nys, M. *et al.* (2016) "Allosteric binding site in a Cys-loop receptor ligand-binding domain unveiled in the crystal structure of ELIC in complex with chlorpromazine," *Proceedings of the National Academy of Sciences of the United States of America*, 113(43), pp. E6696–E6703. doi:10.1073/pnas.1603101113.
- Papke, R.L. *et al.* (2014) "The activity of GAT107, an allosteric activator and positive modulator of $\alpha 7$ nicotinic acetylcholine receptors (nAChR), is regulated by aromatic amino acids that span the subunit interface," *Journal of Biological Chemistry*, 289(7), pp. 4515–4531. doi:10.1074/jbc.M113.524603.
- Papke, R.L., Horenstein, B.A. and Placzek, A.N. (2001) "Inhibition of wild-type and mutant neuronal nicotinic acetylcholine receptors by local anesthetics," *Molecular Pharmacology*, 60(6), pp. 1365–1374. doi:10.1124/mol.60.6.1365.
- Papke, R.L. and Horenstein, N.A. (2021) "Therapeutic Targeting of $\alpha 7$ Nicotinic Acetylcholine Receptors," *Pharmacological Reviews*. Edited by H. Khoshbouei, 73(3), pp. 1118–1149. doi:10.1124/pharmrev.120.000097.
- Pascual, J.M. and Karlin, A. (1998) "Delimiting the binding site for quaternary ammonium lidocaine derivatives in the acetylcholine receptor channel," *The Journal of general physiology*, 112(5), pp. 611–621. doi:10.1085/JGP.112.5.611.
- Peng, C. *et al.* (2013) "Multiple modes of $\alpha 7$ nAChR noncompetitive antagonism of control agonist-evoked and allosterically enhanced currents," *Molecular Pharmacology*, 84(3), pp. 459–475. doi:10.1124/mol.113.086462.
- Phillips, M.B., Nigam, A. and Johnson, J.W. (2020) "Interplay between Gating and Block of Ligand-Gated Ion Channels," *Brain Sciences*, 10(12), p. 928. doi:10.3390/brainsci10120928.
- Pratt, M.B., Pedersen, S.E. and Cohen, J.B. (2000) "Identification of the sites of incorporation of [3H]ethidium diazide within the Torpedo nicotinic acetylcholine receptor ion channel," *Biochemistry*, 39(37), pp. 11452–11462. doi:10.1021/BI0011680.
- Quadri, M. *et al.* (2019) "Macroscopic and Microscopic Activation of $\alpha 7$ Nicotinic Acetylcholine Receptors by the Structurally Unrelated Allosteric Agonist-Positive Allosteric Modulators (ago-PAMs) B-973B and GAT107," *Molecular Pharmacology*, 95(1), pp. 43–61. doi:10.1124/mol.118.113340.
- Rappenglück, S. *et al.* (2018) "Synthesis of a Series of Structurally Diverse MB327 Derivatives and Their Affinity Characterization at the Nicotinic Acetylcholine Receptor," *ChemMedChem*, 13(17), pp. 1806–1816. doi:10.1002/cmdc.201800325.
- Ring, A. *et al.* (2015) "Bispyridinium compounds inhibit both muscle and neuronal nicotinic acetylcholine receptors in human cell lines," *PLoS ONE*, 10(8), pp. 1–16. doi:10.1371/journal.pone.0135811.
- de Roos, A.J. *et al.* (2021) "Occupational insecticide exposure and risk of non-Hodgkin lymphoma: A pooled case-control study from the InterLymph Consortium," *International journal of cancer*, 149(10), pp. 1768–1786. doi:10.1002/IJC.33740.
- Sánchez-Santed, F., Colomina, M.T. and Herrero Hernández, E. (2016) "Organophosphate pesticide exposure and neurodegeneration," *Cortex; a journal devoted to the study of the nervous system and behavior*, 74, pp. 417–426. doi:10.1016/J.CORTEX.2015.10.003.
- Scheffel, C. *et al.* (2018a) "Counteracting desensitization of human $\alpha 7$ -nicotinic acetylcholine receptors with bispyridinium compounds as an approach against organophosphorus poisoning," *Toxicology Letters*, 293(December 2017), pp. 149–156. doi:10.1016/j.toxlet.2017.12.005.
- Scheffel, C. *et al.* (2018b) "Electrophysiological investigation of the effect of structurally different bispyridinium non-oxime compounds on human $\alpha 7$ -nicotinic acetylcholine receptor activity—An in vitro structure-activity analysis," *Toxicology Letters*, 293(September 2017), pp. 157–166. doi:10.1016/j.toxlet.2017.11.025.
- Seeger, T. *et al.* (2012) "Restoration of soman-blocked neuromuscular transmission in human and rat muscle by the bispyridinium non-oxime MB327 in vitro," *Toxicology*, 294(2–3), pp. 80–84. doi:10.1016/j.tox.2012.02.002.
- Sine, S.M. and Steinbach, J.H. (1984) "Agonists block currents through acetylcholine receptor channels," *Biophysical Journal*, 46(2), pp. 277–283. doi:10.1016/S0006-3495(84)84022-9.
- Sitzia, F. *et al.* (2011) "Voltage- and temperature-dependent allosteric modulation of $\alpha 7$ nicotinic receptors by PNU120596," *Frontiers in Pharmacology*, 2 DEC. doi:10.3389/fphar.2011.00081.
- Smelt, C.L.C. *et al.* (2018) "Identification by virtual screening and functional characterisation of novel positive and negative allosteric modulators of the $\alpha 7$ nicotinic acetylcholine receptor," *Neuropharmacology*, 139, pp. 194–204. doi:10.1016/j.neuropharm.2018.07.009.
- Spurny, R. *et al.* (2015) "Molecular blueprint of allosteric binding sites in a homologue of the agonist-binding domain of the $\alpha 7$ nicotinic acetylcholine receptor," *Proceedings of the National Academy of Sciences*, 112(19), pp. E2543–E2552. doi:10.1073/pnas.1418289112.
- Stigler, L. *et al.* (2021) "Post-VX exposure treatment of rats with engineered phosphotriesterases," *Archives of toxicology* [Preprint]. doi:10.1007/S00204-021-03199-6.
- Tattersall, J.E.H. (1993) "Ion channel blockade by oximes and recovery of diaphragm muscle from soman poisoning in vitro," *British Journal of Pharmacology*, 108(4), pp. 1006–1015. doi:10.1111/j.1476-5381.1993.tb13498.x.
- Thiermann, H., Worek, F. and Kehe, K. (2013) "Limitations and challenges in treatment of acute chemical warfare agent poisoning," *Chemico-Biological Interactions*, 206(3), pp. 435–443. doi:10.1016/j.cbi.2013.09.015.
- Timperley, C.M. *et al.* (2012) "1,1'-(Propane-1,3-diyl)bis(4-tert-butylpyridinium) di(methanesulfonate) protects guinea pigs from soman poisoning when used as part of a combined therapy," *MedChemComm*, 3(3), pp. 352–356. doi:10.1039/c2md00258b.

- T. Pournara, D. *et al.* (2020) "Design, Synthesis, and *in vitro* Evaluation of P2X7 Antagonists," *ChemMedChem*, 15(24), pp. 2530–2543. doi:10.1002/cmdc.202000303.
- Trimmer, J.S. *et al.* (1989) "Primary structure and functional expression of a mammalian skeletal muscle sodium channel," *Neuron*, 3(1), pp. 33–49. doi:10.1016/0896-6273(89)90113-X.
- Turner, S.R. *et al.* (2011) "Protection against nerve agent poisoning by a noncompetitive nicotinic antagonist," *Toxicology Letters*, 206(1), pp. 105–111. doi:10.1016/j.toxlet.2011.05.1035.
- Velisetty, P., Chalamalasetti, S. v. and Chakrapani, S. (2014) "Structural basis for allosteric coupling at the membrane-protein interface in *Gloeobacter violaceus* ligand-gated ion channel (GLIC)," *Journal of Biological Chemistry*, 289(5), pp. 3013–3025. doi:10.1074/jbc.M113.523050.
- Wein, T. *et al.* (2018) "New Resensitizers for the Nicotinic Acetylcholine Receptor by Ligand-Based Pharmacophore Modeling," *Current Computer-Aided Drug Design*, 15(1), pp. 104–109. doi:10.2174/1573409914666180703120201.
- Williams, D.K., Wang, J. and Papke, R.L. (2011) "Investigation of the molecular mechanism of the $\alpha 7$ nicotinic acetylcholine receptor positive allosteric modulator PNU-120596 provides evidence for two distinct desensitized states," *Molecular Pharmacology*, 80(6), pp. 1013–1032. doi:10.1124/mol.111.074302.
- Woodhull, A.M. (1973) "Ionic blockage of sodium channels in nerve," *Journal of General Physiology*, 61(6), pp. 687–708. doi:10.1085/jgp.61.6.687.
- Worek, F., Thiermann, H. and Wille, T. (2020) "Organophosphorus compounds and oximes: a critical review," *Archives of toxicology*, 94(7), pp. 2275–2292. doi:10.1007/S00204-020-02797-0.
- Xu, Y. *et al.* (2006) "Blocking of the nicotinic acetylcholine receptor ion channel by chlorpromazine, a non-competitive inhibitor: A molecular dynamics simulation study," *The Journal of Physical Chemistry B*, 110(41), pp. 20640–50648. doi:10.1021/jp0604591
- Young, G.T. *et al.* (2008) "Potentiation of $\alpha 7$ nicotinic acetylcholine receptors via an allosteric transmembrane site," *Proceedings of the National Academy of Sciences of the United States of America*, 105(38), pp. 14686–14691. doi:10.1073/pnas.0804372105.
- Zhao, Y. *et al.* (2021) "Structural basis of human $\alpha 7$ nicotinic acetylcholine receptor activation," *Cell Research*, 31(6), pp. 713–716. doi:10.1038/s41422-021-00509-6.
- Zheng, N. *et al.* (2021) "Discovery of Methylene Thioacetal-Incorporated α -RglA Analogues as Potent and Stable Antagonists of the Human $\alpha 9\alpha 10$ Nicotinic Acetylcholine Receptor for the Treatment of Neuropathic Pain," *Journal of Medicinal Chemistry*, 64(13), pp. 9513–9524. doi:10.1021/acs.jmedchem.1c00802.
- Zhu, Q. *et al.* (2017) "Entropy and Polarity Control the Partition and Transportation of Drug-like Molecules in Biological Membrane," *Scientific Reports 2017 7:1*, 7(1), pp. 1–10. doi:10.1038/s41598-017-18012-7.
- Zoi,ta, Z. and Berinde, M. (2021) "QSPR Models for the Molar Refraction, Polarizability and Refractive Index of Aliphatic Carboxylic Acids Using the ZEP Topological Index," *Symmetry 2021, Vol. 13, Page 2359*, 13(12), p. 2359. doi:10.3390/SYM13122359.
- Zwart, R. and Vijverberg, H.P.M. (1998) "Four pharmacologically distinct subtypes of $\alpha 4\beta 2$ nicotinic acetylcholine receptor expressed in *Xenopus laevis* oocytes," *Molecular Pharmacology*, 54(6), pp. 1124–1131. doi:10.1124/mol.54.6.1124.

Figure Legends

Figure 1: *Symmetrical bispyridinium compounds with C3 linker inhibit $\alpha 7$ and muscle-type nAChR currents with micromolar potency* (A) human $\alpha 7$ and $(\alpha 1)2\beta 1\epsilon\delta$ nAChRs were expressed in *Xenopus laevis* oocytes and clamped at -70 mV. Representative current traces in response to 100 μ M ACh ($\alpha 7$) or 30 μ M ACh (muscle-type) before and after 20 s preincubation with 300 nM PTM0022 (red) or 3 μ M MB327 (magenta) are shown. (B) Full dose inhibition curves of bispyridinium compounds with at least low micromolar potency at the indicated nAChR subtype. Error bars represent S.D. of the mean from n = 3 - 6 individual oocytes. (C) Dose response curves for ACh in the presence of the following concentrations of bispyridinium compounds: 3 μ M MB327, 3 μ M PTM0002, 10 μ M PTM0007, 3 μ M PTM0015, 300 nM PTM0022 as described in the method section. The lead compound MB327 (magenta) and the most potent derivate PTM0022 (red) are highlighted in colour (error bars represent S.D from the mean of 5-7 individual oocytes. Best-fit values from B and C are shown in **Tables 1** and **2**.

Figure 2: *Influence of the $\alpha 7M253L$ allosteric binding site mutation on BPC potency and interactions of BPC and PNU-120596 binding.* (A) Human $\alpha 7$ and $\alpha 7M253L$ were expressed in *Xenopus laevis* oocytes and clamped at -70 mV. Representative current traces in response to 100 μ M ACh (black bar) are shown before (black) and after preincubation (20 s) and co-application of the indicated compounds (coloured lines and bars). Note the more than tenfold increase of ACh-elicited

current amplitude by PNU-120596 (**B**) Dose-inhibition curves for the indicated BPCs at the human $\alpha 7$ and $\alpha 7$ M253L mutant ($n = 3 - 6$, mean and S.D. are shown). Dotted/solid lines represent data from Fig. 1B, for comparison. (**C**) Co-application of BPCs or QX-314 upon sequential pre-application of 10 μM PNU-120596 and 100 μM ACh. Averaged current traces from at least five different oocytes are shown. S.D. is shown in light gray. Current traces were normalized to the ACh elicited signal before the co-application. PNU-125096-amplified signals were between 20–30 μA .

Figure 3: Voltage-dependency of $\alpha 7$ and $(\alpha 1)_2\beta 1\epsilon\delta$ nAChR inhibition by selected BPCs. Representative current traces and statistical analysis of ACh (100 μM)-induced currents responses from $\alpha 7$ (A) and $(\alpha 1)_2\beta 1\epsilon\delta$ nAChRs (B) and their inhibition by the indicated compounds. Grey current traces represent equilibrated control currents at -50 mV (solid) and -100 mV (dotted). Colored lines represent the respective responses following 20 s of pre-incubation and co-application of the indicated compounds. Note that current traces are larger at -100 mV. Paired analysis comparing normalized responses upon antagonist application at a holding potential of -50 mV (filled symbols) and -100 mV (empty symbols) from 4 – 6 individual oocytes. Responses were normalized to the currents in the absence of an antagonist. Single values are shown with the mean displayed as black line. Statistical significance was determined with a paired t-test with $p < 0.05$ *, $p < 0.01$ **, and $p < 0.001$ ***. MLA (gray), PTM0022 (red), MB327 (magenta) and QX-314 (gold).

Figure 4: Inhibition of $\alpha 7$ chimeras and mutants by BPCs. Normalized responses of 1 μM PTM0022 (red triangle), 10 μM MB327 (magenta dot), and 30 μM QX-314 (golden dot) at the indicated chimeras and mutants (shown as pictograms, see supplementary figure S1 for more details). Single values are shown with the mean displayed as black line. Error bars represent 95% CIs ($n = 4 - 6$). Statistical analysis was done using Brown-Forsythe and Welch ANOVA with post-hoc Dunnett T3 test compared to $\alpha 7$ with $p < 0.05$ *, $p < 0.01$ **, and $p < 0.001$ ***, to - $\alpha 7$ with $p < 0.001$ #, and to 5HT3A with $p < 0.05$ °, $p < 0.01$ °°. Normalization was done to current evoked before (EC_{80} agonist) incubation and co-application of the indicated compound.

Figure 5: Molecular docking of PTM0022, MB327 and QX-314 in open, closed and desensitized states of the $\alpha 7$ nAChR. Results with the highest binding energy are shown for PTM0022, MB327 and QX-314 in the resting (7KOO, **A**), open (7KOX, **B**) and desensitized (7KOQ, **C**) state of the $\alpha 7$ nAChR. Cartoon structures of each receptor state with all three compounds are shown on the left. Detailed surface representation and interacting amino acid residues for PTM0022 (red), MB327 (magenta) and OX-314 (yellow) are shown on the right. Color coding follows YRB script (Hagemans *et al.*, 2015) with hydrophobic C-atoms in yellow and polar interaction partners in blue (positive) and red (negative). Black rings indicate the position of the labelled pore lining residues. Carbon, nitrogen and oxygen atoms of amino acid residues are colored in gray, blue, and red, respectively. ECD – extracellular domain, TMD – transmembrane domain, ICD – intracellular domain.

Figure 6: Generation of $\alpha 7$ nAChR mutants to identify residues involved in inhibition by PTM0022. (**A**) Representative current traces and statistical analysis showing inhibition of the indicated $\alpha 7$ mutants by 1 μM PTM0022 (red triangle). For details of the mutants refer to supplementary Figure S1. The mean of the individual values is displayed as black line. Error bars represent the 95% CIs from $n = 4 - 6$ experiments. Statistical analysis was done using Brown-Forsythe and Welch ANOVA with post-hoc Dunnett T3 test compared to $\alpha 7$ with $p < 0.05$ *, $p < 0.01$ **, and $p < 0.001$ ***, to 5HT3A with $p < 0.01$ °. Normalization was done to current response evoked before (EC_{80} agonist) pre-incubation and co-application of PTM0022. (**B**) ACh dose response curves for the indicated $\alpha 7$ mutants and chimeras with mean and S.D. (left panel) and detailed analysis of responses to 10 mM ACh showing single values with means and 95% CIs (right panel).

Figure 7: Correlation analysis of the potency of the bispyridinium compounds at the human $\alpha 7$ nAChR and their chemical properties. **(A)** Pearson correlation of the determined pIC₅₀ values and relevant QSAR chemical properties (see supplementary table S5) obtained from chemicalize.com (ChemAxon) with significance threshold of $p < 0.05$ (Holm corrected) with (+, $n = 8$) or without (-, $n = 7$) QX-314. Negative and positive correlations are indicated with red and blue, respectively. **(B)** Scatter plots of the five significant chemical properties from A without (-) QX-314 with smooth fit ($x \sim y$, dashed line) and 95% confidence interval (light gray) of the fit. QX-314 is shown as red point, independent from the fit. Note that pIC₅₀ values could not be determined for PTM0008 and 09 and they are not included in this analysis **(C)** Chemical structures of the symmetrical bispyridinium compounds and QX-314. Oxygen and nitrogen atoms are colored in red and blue, respectively. access, accessible; mol, molar, refract, refractivity; sol, solvent; top, topological; VdW, Van der Waals

Figure 8: BPCs do not resensitize oocyte-expressed $\alpha 7$ nAChR and show weak inhibition of some other cation-selective ion channels. **(A)** Oocytes were clamped at -70 mV and 5 s-pulses of 100 μ M ACh (grey lines) were applied in 1 min intervals until stable responses were obtained. Receptors were then desensitized by a 1 min application of 1 mM ACh (black lines) with or without 10 μ M PNU-120596 (blue line) or 3 μ M PTM0022 (red line). After a 5 s washout, 1 mM ACh was re-applied. Representative current traces from three different oocytes per experiment are shown. Note that PNU-120596 and PTM0022 were added 7 s after the beginning of 1 mM ACh exposure to allow complete receptor desensitization. **(B)** Superposition of representative current traces before (black) and after pre-incubation and co-application (red) of indicated PTM0022 concentrations for indicated ligand-gated ion channels. Scale bars represent 0.5 μ A (vertically) and 2 s (horizontally). **(C)** Voltage-dependency of the inhibition shown in B. Single values with mean as black line for -50 mV and -100 mV. Paired t-test with $p < 0.05$ *, $p < 0.01$ **, and $p < 0.001$ ***. **(D)** Left panel, typical current traces of Na_v1.4 before (black) and 12 min after (red) application of 10 μ M PTM0022. Currents were elicited by 50 ms pulses to -10 mV from a holding potential of -120 mV every 20 s. Right panel, sodium peak currents normalized to control pulse before application of PTM0022. Mean and S.D of different 4 oocytes.

Tables

Table 1: IC₅₀ values and Hill coefficients (n_H) of BPCs at human $\alpha 7$ and $(\alpha 1)_2\beta 1\epsilon\delta$ nAChRs as shown in Figure 1. Values in parentheses represent 95% confidence intervals (95% CI). IC₅₀ ratios relative to MB327 are shown.

Compound	$\alpha 7$				$(\alpha 1)_2\beta 1\epsilon\delta$		
	IC ₅₀	(95% CI) μ M	IC ₅₀ Ratio	n_H	IC ₅₀	(95% CI) μ M	n_H
MB327	3.50	(2.73 - 4.51)	1.00	-0.84	~ 30	-	-
PTM0001	3.13	(2.39 - 4.20)	1.10	-1.23	-	-	-
PTM0002	4.72	(3.60 - 6.27)	0.74	-1.14	-	-	-
PTM0007	6.96	(5.44 - 8.90)	0.50	-1.04	-	-	-
PTM0008	> 30		-	-	-	-	-
PTM0009	> 30		-	-	-	-	-
PTM0010	39.83	(30.95 - 51.75)	0.09	-0.91	-	-	-
PTM0015	0.49	(0.39 - 0.62)	7.14	-0.94	-	-	-
PTM0022	0.20	(0.17 - 0.23)	17.50	-1.07	0.29	(0.23 - 0.38)	-0.84
QX-314	4.98	(4.03 - 6.10)	0.70	-0.89	-	-	-

Table 2: EC₅₀ values and Hill coefficients (n_H) of ACh in the presence of the indicated concentrations of BPCs at human $\alpha 7$ and $(\alpha 1)_2\beta 1\epsilon\delta$ nAChRs. Values in parentheses represent 95% confidence intervals (95% CI). The corresponding dose-response curves are shown in Figure 1.

Compound	$\alpha 7$		$(\alpha 1)_2\beta 1\epsilon\delta$	
	EC ₅₀ (95% CI) μM	n_H	EC ₅₀ (95% CI) μM	n_H
ACh	36.5 (33.5 - 40.0)	1.90	15.4 (13.1 - 18.8)	1.22
+3 μM MB327	43.8 (33.6 - 58.2)	1.66	-	-
+10 μM MB327	-	-	13.0 (8.1 - 26.1)	1.10
+ 3 μM PTM0002	51.6 (42.5 - 63.2)	1.57	-	-
+ 10 μM PTM0007	35.8 (29.2 - 45.7)	1.93	-	-
+ 3 μM PTM0015	49.2 (31.7 - 82.2)	1.53	-	-
+ 0.3 μM PTM0022	58.8 (44.0 - 81.4)	1.46	-	-
+ 1 μM PTM0022	-	-	10.3 (7.3 - 17.2)	1.06

Table 3: IC₅₀ values and Hill coefficients (n_H) for MB327 and PTM0022 at human $\alpha 7$ and $\alpha 7M253L$ nAChRs. Values in parentheses represent 95% confidence intervals (95% CI). Corresponding dose-inhibition curves are shown in Figure 2.

Compound	$\alpha 7$		$\alpha 7 M253L$		$IC_{50}(\alpha 7)/IC_{50}(M253L)$
	IC ₅₀ (95% CI) μM	n_H	IC ₅₀ (95% CI) μM	n_H	
MB327	3.50 (2.73 - 4.51)	-0.84	0.84 (0.69 - 1.03)	-0.98	4.17
PTM0022	0.20 (0.17 - 0.23)	-1.07	0.30 (0.25 - 0.35)	-1.76	0.67

Table 4: Molecular docking results of the indicated compound in all three states (PDBs see experimental procedure or **Figure 5**) of the $\alpha 7$ nAChR. Compounds were docked in a grid covering interacting residues identified during the screening shown in supplementary figure S1 and supplementary tables S2, S3 and S4 according to the experimental procedure. Amino acid residues identified to be distinct between 5HT3A and $\alpha 7$ nAChR and mutated in this study are bold.

<i>a7 nAChR state</i>	<i>Compound</i>	<i>binding energy (Kcal/Mol)</i>	<i>RMSD</i>	<i>inhibition constant (Ki)</i>	<i>residues involved in interaction (protein chain)</i>
resting	PTM0022	-7.36	5.15	4.01 μ M	A257 (B), A262(B), F134(C), Y209(C), I259 (C) L247(A), V251(A), L247(B), V251(B), V251(C), L254 (C), L247(D), L254 (D), E258 (D), L254 (E)
	MB327	-7.69	0.9	2.31 μ M	D41(A), E44 (A), E172(A), W173(A), Y209(A), I259 (A), K45(E)
	QX-314	-6.79	1.01	10.49 μ M	L254 (B), A252(B), Y209(C), Y210 (C), N213(C), L214(C), V251(C), L255 (C), I259 (C) L45(B), E258 (B), Y210 (C), L214(C), L255 (C), I259 (C) K45(B), A262(B), D41(C), V42(C), E44(C), E172(C), W173(C), I259 (C)
open	PTM0022	-8.76	2.06	376.70 nM	Y209(A), L214(A), V251(A), F252(A), L254 (A), L255 (A), V256(A), E258 (A), I259 (A), L254 (E), A257 (E), E258 (E)
	MB327	-6.34	2.6	22.59 μ M	L246(C), L247(C), M253(C), N213(D), L214(D), P217(D), I221(D), V245(D), F252(D)
	QX-314	-7.72	1.95	2.18 μ M	M253(D), L254 (D), E258 (D), N213(E), L214(E), F252(E), L255 (E)
desensitized	PTM0022	-10.07	0.42	41.40 nM	Y209(A), L214(A), V251(A), F252(A), L254 (A), L255 (A), V256(A), E258 (A), I259 (A), L254 (E), A257 (E), E258 (E)
	MB327	-8.85	1.19	327.8 nM	L246(C), L247(C), M253(C), N213(D), L214(D), P217(D), I221(D), V245(D), F252(D)
	QX-314	-7.35	0.68	4.10 μ M	M253(D), L254 (D), E258 (D), N213(E), L214(E), F252(E), L255 (E)

Table 5: EC₅₀ values and Hill coefficients (nH) for the functional chimeras of human $\alpha 7$ and mouse 5HT3A receptors. Values in parentheses represent 95% confidence intervals (95% CI).

Chimera	Ligand	EC ₅₀ (95% CI) μM	nH
$\alpha 7$	ACh	35.5 (32.8 - 38.4)	2.06
$\alpha 7^{\text{V201-5HT3A}}$	ACh	38.6 (32.3 - 46.6)	1.85
$\alpha 7^{\text{4TM 5HT3A}}$	ACh	44.1 (41.6 - 46.8)	2.30
$\alpha 7$ SDT	ACh	15.4 (12.4 - 19.9)	1.17
$\alpha 7^{\text{Anion}}$	ACh	0.23 (0.19 - 0.27)	0.90
$\alpha 7^{\text{Anion E258R}}$	ACh	2.62 (2.17 - 3.19)	1.33

Figures

Figure 1

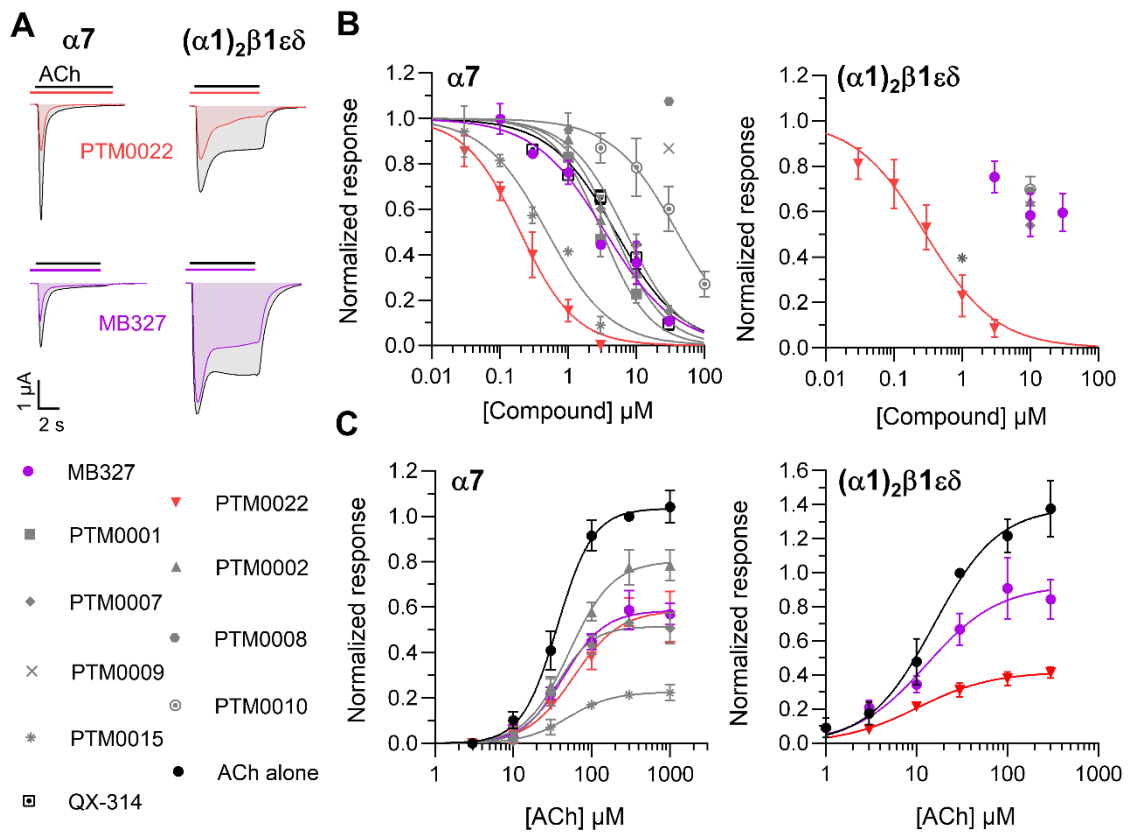


Figure 2

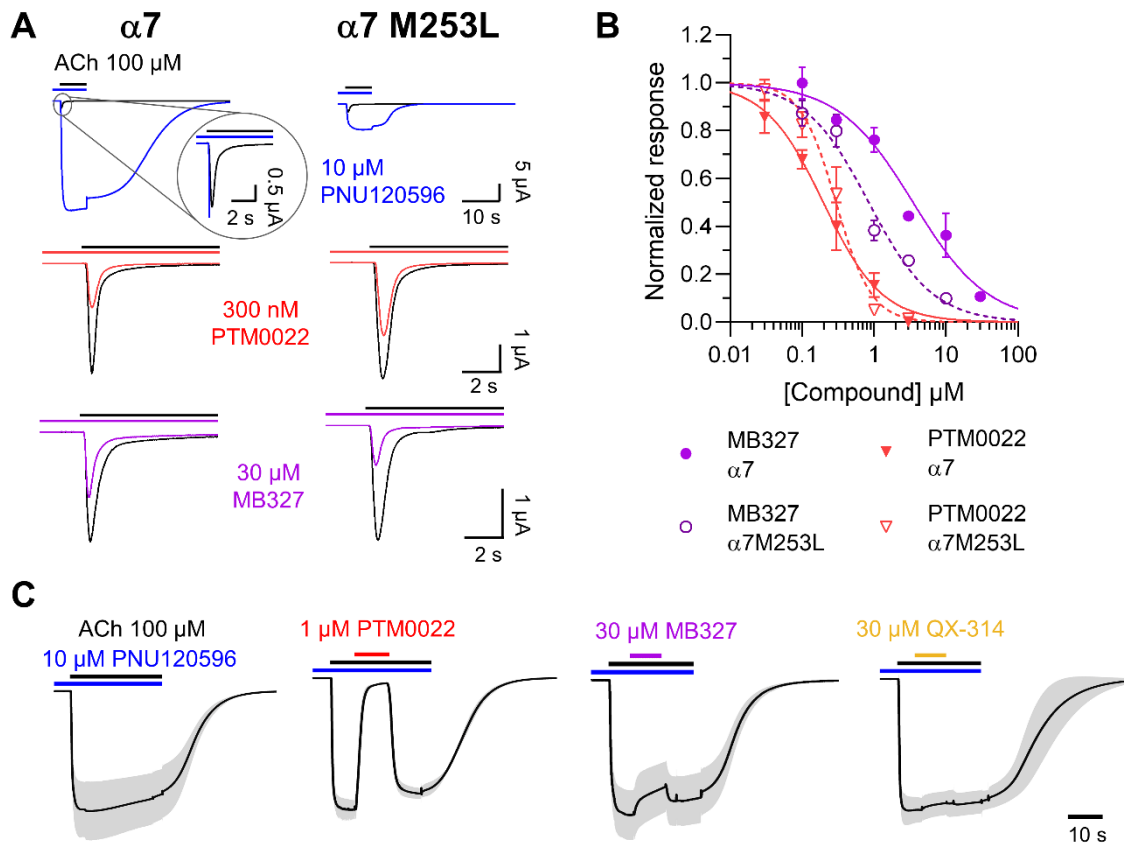


Figure 3

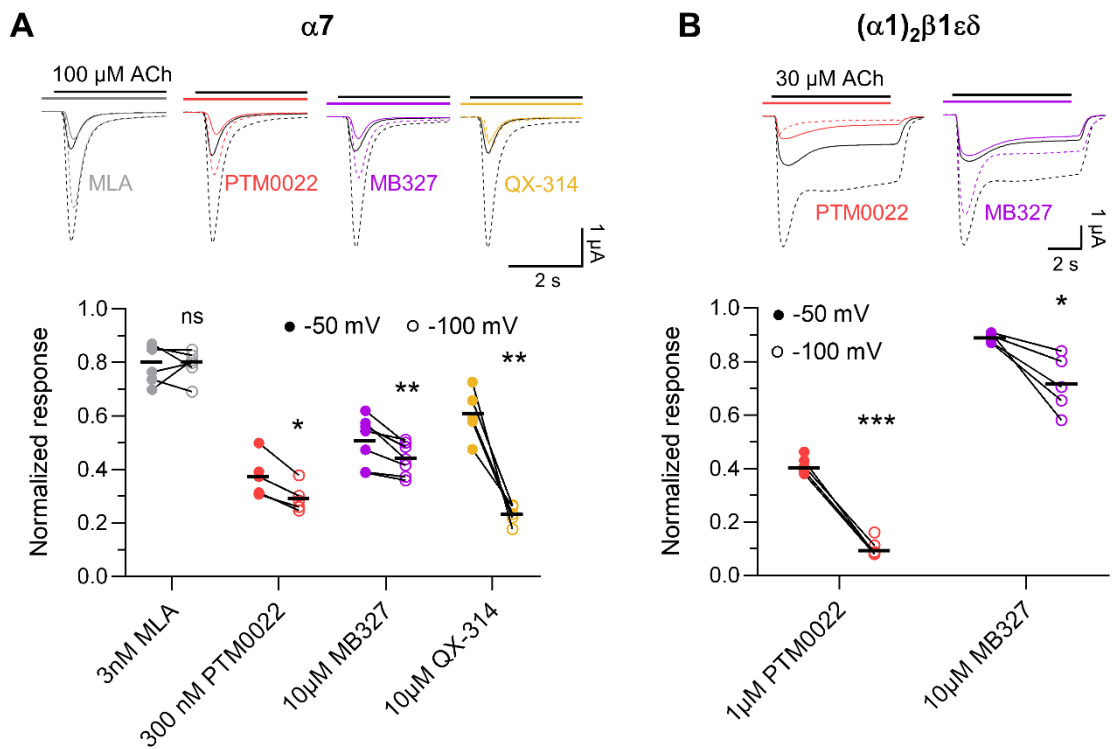


Figure 4

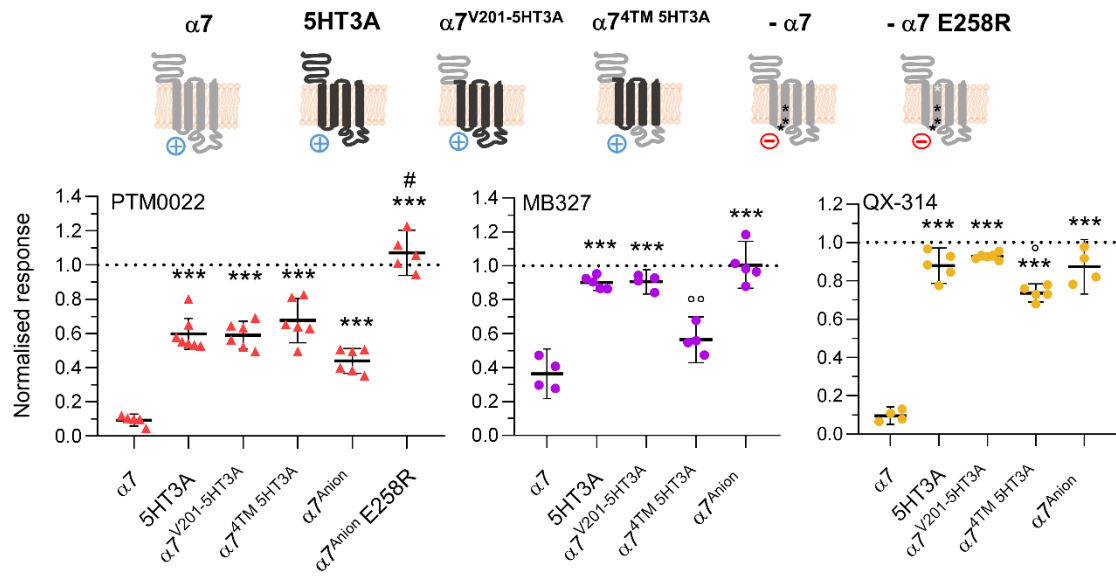


Figure 6

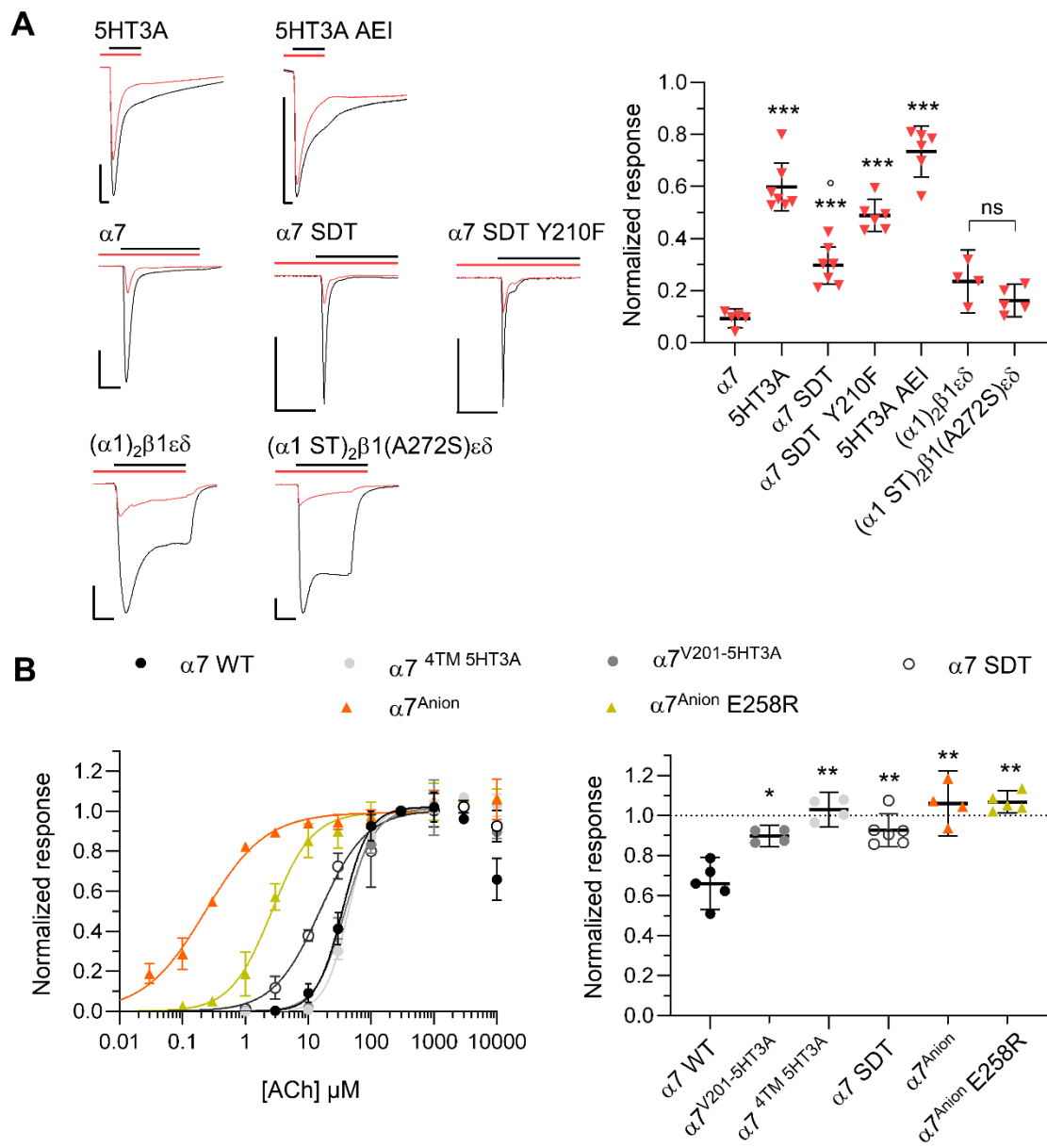
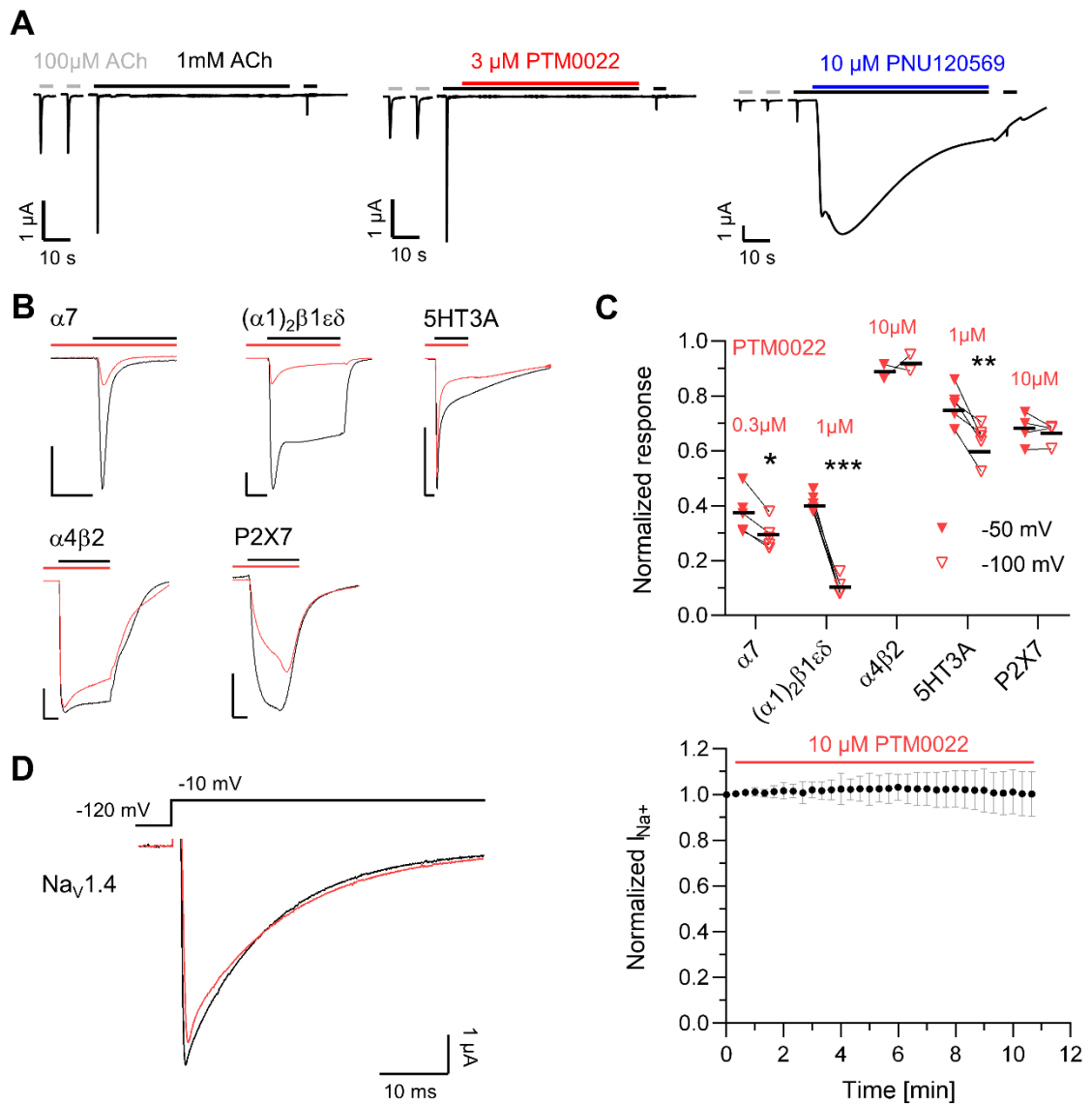


Figure 8



Supplementary Information

Symmetrical bispyridinium compounds act as open channel blockers of cation-selective ion channels

Yves Haufe¹, Dominik Loser², Karin V. Niessen³, Thomas Seeger³, Timm Danker², Annette Nicke^{1*}

¹ Walther Straub Institute of Pharmacology and Toxicology, Faculty of Medicine, LMU Munich, Munich, Germany

² NMI Natural and Medical Sciences Institute at the University of Tübingen, 72770 Reutlingen, Germany.

³ Bundeswehr Institute of Pharmacology and Toxicology, Neuherbergstr. 11, 80937 Munich, Germany.

*** Correspondence:**

Annette Nicke, annette.nicke@lrz.uni-muenchen.de

Supplementary Methods

Manual patch-clamp recordings

Patch-clamp experiments were performed in the whole-cell mode (Hamill *et al.* 1981) using an EPC 10 USB patch-clamp amplifier and the PATCHMASTER software (version 2x91; HEKA Elektronik, Germany). The extracellular solution contained (in mM): 140 NaCl, 5 KCl, 1 MgCl₂, 0.5 CaCl₂, 10 HEPES and 10 D-glucose, pH 7.4. The intracellular solution contained (in mM): 120 KCl, 2 MgCl₂, 10 HEPES, 10 EGTA, 1 sucrose and 31.25 KOH, pH 7.2. All substances were obtained from Carl Roth except EGTA, which was from Sigma Aldrich.

The patch-clamp experiments with CHO cells stably expressing human $\alpha 7$ nAChRs were executed using the Dynaflo Resolve System (Fluicell, Sweden), which allows a fast buffer exchange. The recordings were performed at room temperature and the cells were held at -60 mV in the voltage-clamp mode.

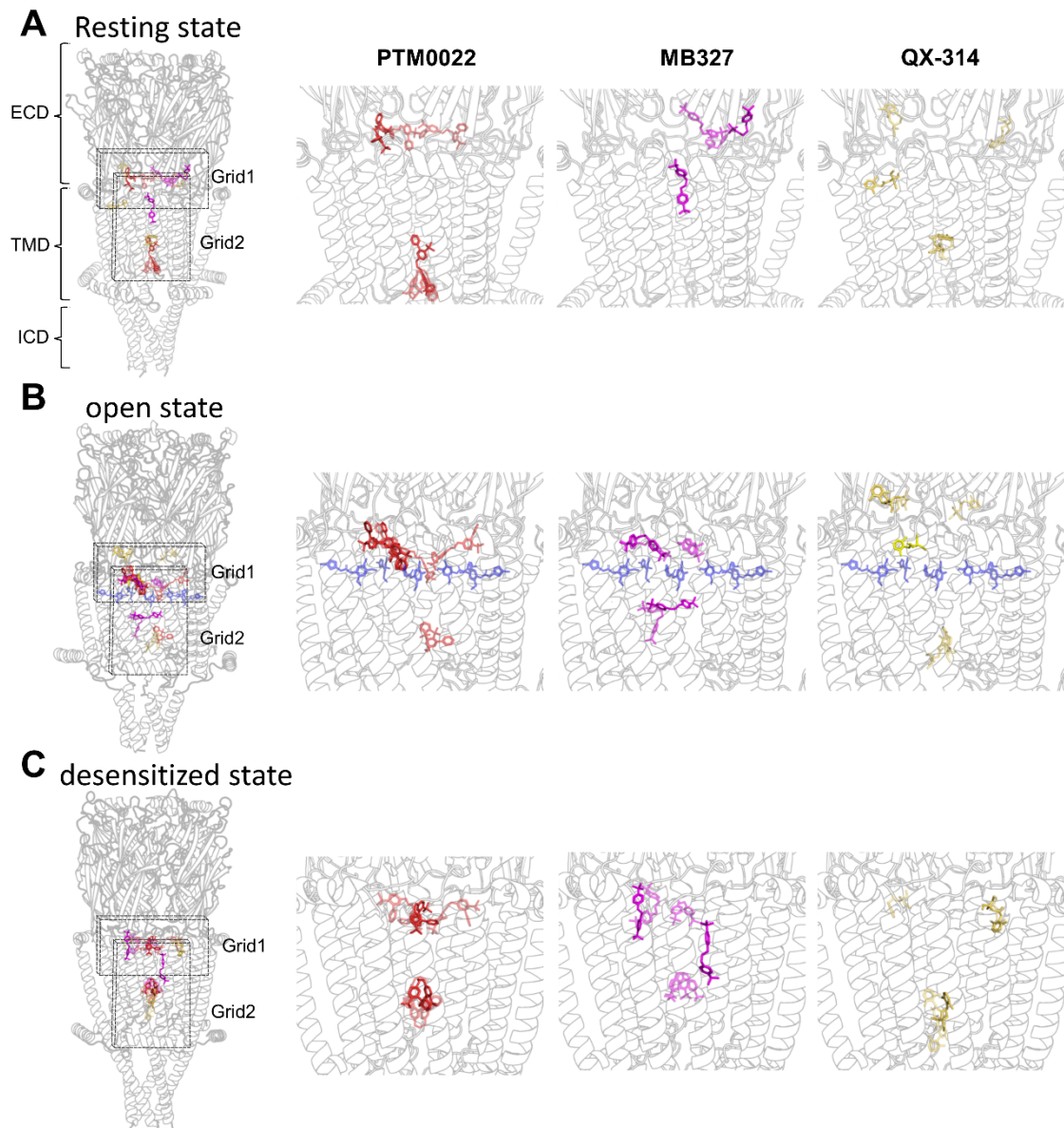
The following application protocol was used for each of the 10 sweeps of an experiment: After a baseline recording for 2 s, ACh (100 μ M) was applied for 0.5 s, followed by a washout for 10 s. The first three sweeps were used as a control (control phase). During the third sweep, the application of ACh (100 μ M) was followed by the washout of ACh and the simultaneous treatment of the cells with MB327 (30 μ M) or PNU-120596 (10 μ M) for 10 s. After the control phase, the next three sweeps (number four to six) were used for the compound tests (compound phase), where all steps of the application protocol were performed in the presence of MB327 (30 μ M) or PNU-120596 (10 μ M). During the sixth sweep, the application of ACh (100 μ M) was followed by a washout for 10 s, without MB327 (30 μ M) or PNU-120596 (10 μ M) present. The compound phase was followed by four additional sweeps (washout phase), which were performed like the first three sweeps (control phase). The negative control recordings were executed as described above but without MB327 (30 μ M) or PNU-120596 (10 μ M) present. Acetylcholine chloride and PNU-120596 were obtained from Sigma Aldrich.

The data of the manual patch-clamp recordings were analyzed and visualized with scripts written in R (R Project for Statistical Computing, RRID:SCR_001905) using the following packages: tidyverse (RRID:SCR_019186) and ggplot2 (RRID:SCR_014601).

The current responses were determined as peak currents.

Supplementary Table S1: Chimeras used in this work with representative traces. Mouse 5HT3A is shown in dark gray, human $\alpha 7$ nAChR in light gray. Chimeras marked with \times did not show expression in *X. laevis* oocytes. If accessory proteins were used, they are written with the construct name. Amino acids of transition points are labeled for the respective receptor. The numbering starts after a 23 amino acid long signal sequence for each receptor. In case of an insertion (V), the numbering of the original receptor is shown but marked with a +1 to address the shift in numbering. Scaling bars indicate 2s and 0.3 μ M, acetylcholine application with EC₈₀ is shown on top of each trace. Note that Eiselé et al. and Gee et al. have worked with rat $\alpha 7$ nAChR and mouse 5HT3A. Bertrand et al. worked with human constructs for both. $\alpha 7$ E258R and $\alpha 7$ E258A did not show expression.

Construct	Schematics		Trace	Ref.
	1-3 TMD	4 TMD		
$\alpha 7$ V201-5HT3A	$\alpha 7$ V201 5HT3A I218			Eiselé, J. et al. 1993
$\alpha 7$ 4TM 5HT3A	$\alpha 7$ V201 K303 5HT3A I218 P318 V434	C442		Gee, V. et al. 2007, Bertrand et al. 2008
$\alpha 7$ 3TM 5HT3A	$\alpha 7$ V201 K303 5HT3A I218 P318			Gee, V. et al. 2007, functional
$\alpha 7$ 2TMD 5HT3A	$\alpha 7$ A233 S264 5HT3A D250 T279			this work
$\alpha 7$ SDT + NACHO	$\alpha 7$ A257S E258D I259T 5HT3A			this work
$\alpha 7$ Anion	$\alpha 7$ 237P V251T E237A			Galzi, J. et al. 1992
$\alpha 7$ Anion E258R	$\alpha 7$ 237P V251T E237A E258R			this work
$\alpha 7$ Anion E258A	$\alpha 7$ 237P V251T E237A E258A			this work
5HT3A ^{V217-alpha7}	5HT3A V217 $\alpha 7$ T202			Bertrand et al. 2008, functional
5HT3A ^{4TM alpha7}	5HT3A V217 P318 Y433 $\alpha 7$ T202 G302 V443			this work
5HT3A ^{3TM alpha7}	5HT3A V217 P318 $\alpha 7$ T202 G302			this work
5HT3A ^{2TMD alpha7}	5HT3A P249 P277 $\alpha 7$ D234 M260			this work
5HT3A AEI	5HT3A S273A D274E T275I $\alpha 7$			this work



Supplementary Figure S1: Molecular Docking results to screen for potential binding sites at the $\alpha 7$ nAChR. Highest ranked 3 binding positions for the shown compounds (PTM0022 - red, MB327 - magenta, QX-314 - gold) in either of the two grids (Grid1 - upper channel pore, 90x90x70 (XxYxZ); Grid2 - channel pore, 60x60x126; spacing 0.375 Å) in the resting (**A**), open (**B**) and desensitized (**C**) state of the $\alpha 7$ nAChR. Refer to experimental procedure for docking parameters. PNU-120596 is shown in blue as orientation, based on PDB 7EKT (Zhao *et al.* 2021).

Supplementary Table S2: The 5 highest ranked dockings of *PTM0022* in the shown state of the $\alpha 7$ nAChR (PDB:7KOO, 7KOX, 7KOQ) either docked in the upper part of the pore or in the channel with a grid (X,Y,Z) of 90,90,70 or 60,60,126, respectively.

<i>nAChR</i> state	$\alpha 7$ Grid	Ranking	Binding energy (Kcal/Mol)	Inhibition constant (Ki)	Residues involved in interaction
Resting	Upper pore	1	-8.21	958.56 nM	Lys45(B), Lys45(C), Tyr210(C), Ile259(C), Tyr209(D), Tyr210(D), Glu258(D), Ile259(D)
		2	-7.52	3.09 μ M	-
		3	-7.36	4.04 μ M	-
		4	-7.28	4.58 μ M	-
		5	-6.55	17.83 μ M	-
	Channel	1	-6.60	14.42 μ M	Tyr244(C), Leu247(C), Tyr244(D), Ile243(E)
		2	-6.55	15.76 μ M	-
		3	-6.41	20.02 μ M	-
		4	-6.15	30.97 μ M	-
		5	-6.13	32.20 μ M	-
Open	Upper pore	1	-9.16	192.52 nM	Leu254(B), Glu258(B), Ala262(B), Tyr209(C), Tyr210(C), Asn213(C), Val251(C), Leu255(C), Ile259(C)
		2	-9.06	228.41 nM	-
		3	-8.99	258.47 nM	-
		4	-8.77	372.74 nM	-
		5	-8.55	536.83 nM	-
	Channel	1	-8.13	1.10 μ M	Leu254(A), Ala257(A), Glu258(A), Ala262(A), Leu214(B), Val251(B), Leu255(B), Ile259(B)
		2	-8.12	1.11 μ M	-
		3	-7.87	1.69 μ M	-
		4	-7.18	5.43 μ M	-
		5	-6.88	9.04 μ M	-

Continuous on next page.

Supplementary Table S2: continued

	1	-9.78	68.13 nM	Tyr209(A), Leu214(A), Val251(A), Phe252(A), Leu254(A), Leu255(A), Val256(A), Glu258(A), Ile259(A), Leu254(E), Leu255(E), Ala257(E)
Upper pore	2	-9.55	100.28 nM	-
	3	-9.49	110.40 nM	-
	4	-9.28	157.44 nM	-
Desensitized	5	-9.10	212.96 nM	-
	1	-8.88	308.01 nM	Thr244(A), Ile243(B), Ile243(C), Thr244(C), Thr244(D), Ile243(E), Thr244(E)
Channel	2	-8.53	556.19 nM	-
	3	-7.61	2.65 μ M	-
	4	-6.88	9.06 μ M	-
	5	-6.64	13.64 μ M	-

Supplementary Table S3: The 5 highest ranked dockings of MB327 in the shown state of the $\alpha 7$ nAChR (PDB:7KOO, 7KOX, 7KOQ) either docked in the upper part of the pore or in the channel with a grid (X,Y,Z) of 90,90,70 or 60,60,126, respectively.

<i>nAChR state</i>	$\alpha 7$ Grid	Ranking	Binding energy (Kcal/Mol)	Inhibition constant (Ki)	Residues involved in interaction (subunit)
Resting	Upper pore	1	-6.73	11.58 μ M	Asp41(A), Val42(A), Glu44(A), Glu172(A)
		2	-6.41	19.97 μ M	-
		3	-6.06	36.37 μ M	-
		4	-6.03	38.30 μ M	-
		5	-5.98	41.42 μ M	-
	Channel	1	-7.65	2.48 μM	Leu247(B), Val251(C), Leu254(C), Leu247(D), Val251(D), Leu254(D), Glu258(D), Leu247(E), Leu254(E)
		2	-7.62	2.60 μ M	-
		3	-7.61	2.64 μ M	-
		4	-7.61	2.64 μ M	-
		5	-7.59	2.74 μ M	-
Open	Upper pore	1	-6.77	10.96 μM	Leu254(B), Glu258(B), Tyr209(C), Asn213(C), Leu214(C), Val251(C), Leu255(C)
		2	-6.68	12.67 μ M	-
		3	-6.66	13.23 μ M	-
		4	-6.57	15.18 μ M	-
		5	-6.49	17.46 μ M	-
	Channel	1	-6.75	11.26 μ M	Ile243(A), Thr244(A), Leu246(A), Leu247(A), Thr244(B), Leu246(E), Leu247(E)
		2	-6.63	13.88 μ M	-
		3	-6.12	32.85 μ M	-
		4	-6.06	35.91 μ M	-
		5	-6.02	38.84 μ M	-

Continuous on next page.

Supplementary Table S3: continued

		1	-7.08	6.48 μ M	Thr250(A), Met253(A), Leu254(A), Ala262(A), Pro217(B), Leu255(B), Ile259(B)
Desensitized	Upper pore	2	-6.71	12.07 μ M	-
		3	-6.64	13.54 μ M	-
		4	-6.63	13.90 μ M	-
		5	-6.58	15.05 μ M	-
		1	-8.17	1.03 μM	Ile243(C), Leu246(C), Thr250(C), Leu254(C), Asn213(D), Pro217(D), Leu224(D), Val245(D)
Channel	2	-5.93	44.63 μ M	-	
	3	-5.88	49.18 μ M	-	
	4	-5.79	56.71 μ M	-	
	5	-5.76	59.64 μ M	-	

Supplementary Table S4: The 5 highest ranked dockings of QX-314 in the shown state of the $\alpha 7$ nAChR (PDB:7KOO, 7KOX, 7KOQ) either docked in the upper part of the pore or in the channel with a grid (X,Y,Z) of 90,90,70 or 60,60,126, respectively.

<i>nAChR state</i>	<i>$\alpha 7$ Grid</i>	<i>Ranking</i>	<i>Binding energy (Kcal/Mol)</i>	<i>Inhibition constant (Ki)</i>	<i>Residues involved in interaction (subunit)</i>
resting	Upper pore	1	-6.79*	10.47 μ M	Val256(C), Ala257(C), Ala275(C), Leu212(D), Asn213(D), Ile216(D)
		2	-6.34	22.41 μM	Glu44(A), Glu172(A), Tyr210(A), Ile259(A), Lys45(E), Ala262(E)
		3	-6.32	23.34 μ M	-
		4	-6.18	29.46 μ M	-
		5	-6.13	32.24 μ M	-
	Channel	1	-6.28	24.74 μ M	Thr244(A), Leu247(A), Ile243(B), Thr244(B), Leu247(B), Ile243(C), Leu247(C), Leu247(D), Thr244(E), Leu247(E)
		2	-6.18	29.50 μ M	-
		3	-6.12	32.56 μ M	-
		4	-6.03	37.81 μ M	-
		5	-6.01	39.27 μ M	-
Open	Upper pore	1	-7.36	4.00 μM	Lys45(B), Pro261(B), Asp41(C), Val42(C), Glu44(C), Glu172(C)
		2	-7.11	6.16 μ M	-
		3	-7.01	7.25 μ M	-
		4	-6.98	7.65 μ M	-
		5	-6.88	9.10 μ M	-
	Channel	1	-6.27	25.31 μ M	Leu254(A), Tyr209(B), Tyr210(B), Leu214(B), Phe252(B), Leu255(B), Glu258(B)
		2	-6.23	27.13 μ M	-
		3	-6.20	28.60 μ M	-
		4	-6.16	30.28 μ M	-
		5	-6.14	31.82 μ M	-

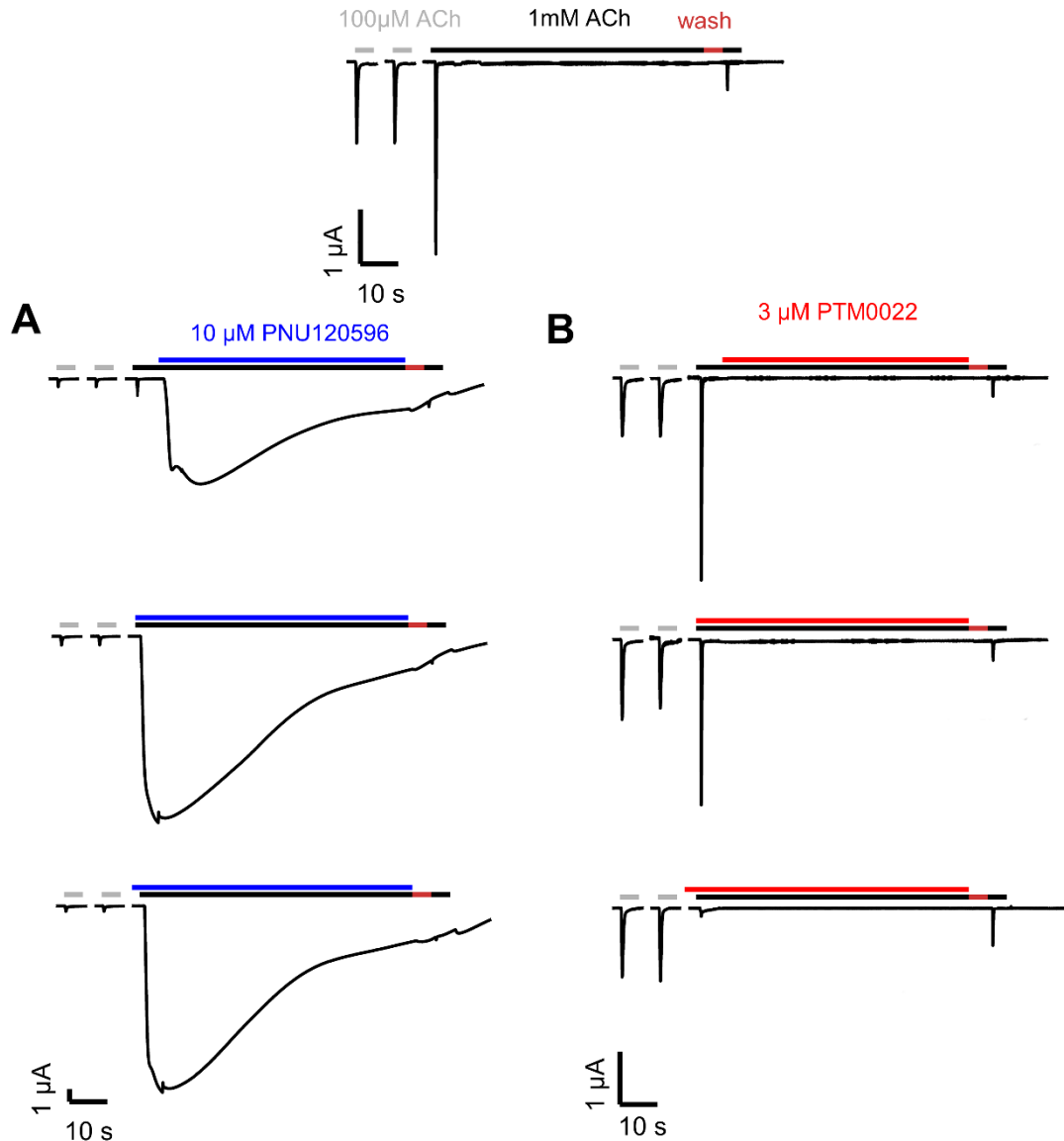
Continuous on next page.

Supplementary Table S4: continued

	1	-7.25	4.85 μ M	Met253(D), Leu254(D), Glu258(D), Asn213(E), Leu214(E), Phe252(E), Leu255(E)
Upper pore	2	-7.21	5.17 μ M	-
	3	-7.05	6.84 μ M	-
	4	-6.92	8.46 μ M	-
	5	-6.92	8.46 μ M	-
Desensitized				
	1	-6.87	9.23 μ M	Glu237(A), Glu237(B), Glu237(C), Ser240(C), Ile243(C), Glu237(D), Thr244(D), Glu237(E)
Channel	2	-6.70	12.17 μ M	-
	3	-6.51	16.80 μ M	-
	4	-6.40	20.19 μ M	-
	5	-6.26	25.90 μ M	-

Supplementary Table S5: Relevant chemical properties for QSAR studies of the symmetrical C3-linker bispyridinium compounds obtained from chemicalize.com by chemaxon. **Abbrev.** access. ... accessible, mol. ... molar, refract. ... refractivity, sol. ... solvent, top. ... topological, VdW ... Van der Waals

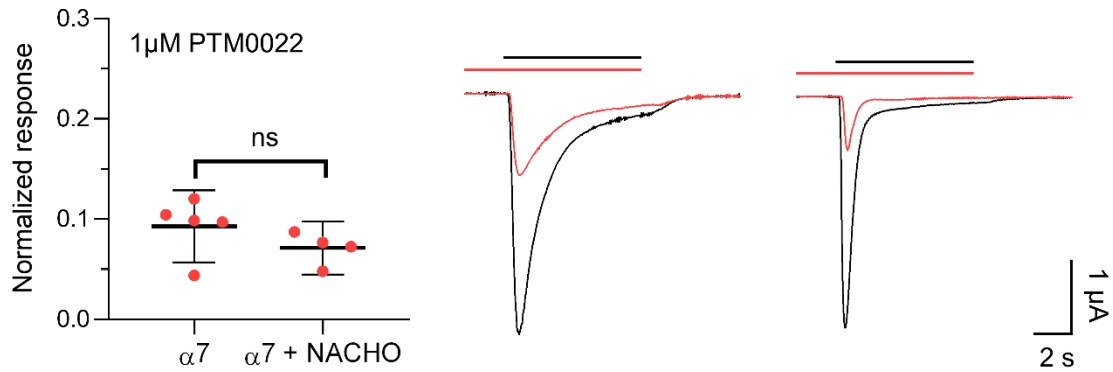
<i>Compound</i>	<i>pIC50</i>		<i>VdW Volume</i> (\AA^3)	<i>HLB</i>	<i>VdW surface area</i> (\AA^2)	<i>Sol. access. surface area</i> (\AA^2)	<i>Top. polar surface area</i> (\AA^2)	<i>Polarizability</i> (\AA^3)	<i>Mol. refrac.</i> (mol/cm^3)
	(<i>M</i>)	<i>logP</i>							
MB327	-5.46	-3.40	337.82	1	589.94	633.51	7.76	38.62	100.34
PTM0001	-5.50	-3.40	337.8	1	589.92	632.26	7.6	38.63	100.34
PTM0002	-5.33	-4.97	338.91	1	519.24	544.2	7.76	34.94	91.09
PTM0007	-5.16	-6.27	294.04	0.88	507.12	617.18	14.24	33.65	91.87
PTM0008	> -4.50	-6.80	252.99	4.43	430.54	564.5	26.22	29.02	75.94
PTM0009	> -4.50	-6.80	253.11	4.43	430.45	560.89	26.22	29.03	75.64
PTM0010	~ -4.30	-6.62	253.23	4.43	430.72	529.55	26.22	29.03	74.44
PTM0015	-6.31	-2.68	464.75	1.88	822.09	822.09	60.36	51.09	133.89
PTM0022	-6.70	-0.10	481.16	1	803.89	800.12	7.76	60.8	150.61
QX314	-5.30	-0.96	282.68	19.84	491.5	446.74	29.1	31.26	94.59



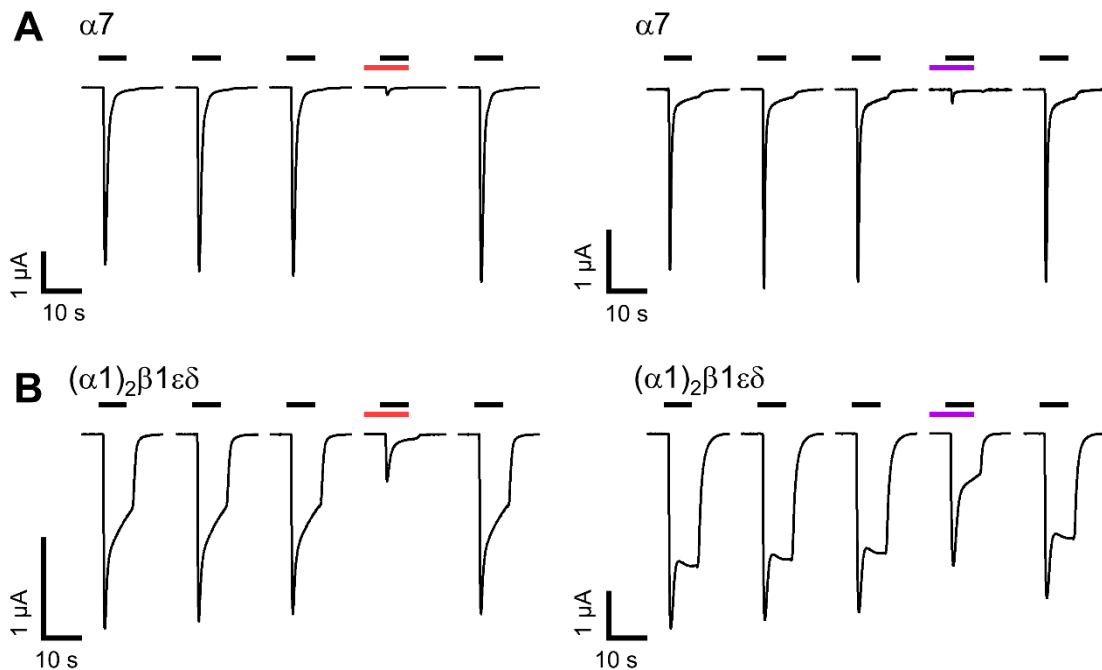
Supplementary Figure S2: PTM0022 does not overcome desensitization by prolonged ACh exposure of the $\alpha 7$ nAChR. Representative current traces of a simulated ACh-induced desensitization experiment (1 min prolonged exposure to 1 mM ACh) of the $\alpha 7$ nAChR. Top panel shows the control experiment with no compound application. The remaining panels show from top to bottom compound exposure after 7 s of 1 mM ACh, co-application of compound with 1 mM ACh and 20 s pre-incubation followed by co-application of compound for 10 μ M PNU-120596 (**A**) and 3 μ M PTM0022 (**B**). All three ways of compound exposure were performed on one *X. Laevis* oocyte. Whole experiment repeated on a total of three different oocytes. Note the effect of PTM0022 preincubation on the blockage of the 1 mM ACh-evoked current peak.

human_alpha7_nAChR	1	-----MRCSPGGWLLALAAS---LLHVSLOGEIFOR-----KLYKEIV--KNYNPLERPVANDSQPLTYFSLSLQIMDVDEK	68
mouse_5HT3A	1	-----MRLCIPQVLLALFLSMLTAPGEGSRRAATDITQPALLR	80
human_alpha4_nAChR	1	MELGGPGAPRLPPLLLLLGTGLL--RASSHVETRAHAE-----RLLKKLF--SCYNKWSRPVANI SDVVLVRFOLS IAQLIDVDEK	79
human_beta2_nAChR	1	-----MARRCGVALLLGFGLL--RLCSGV-WGTDTE-----RLVEHLLDPSRYNKLIRPATNGSELVTYQLMVSLAQLISVHER	73
human_alpha1_nAChR	1	-----MEPWP LLLLFLSCL--SAGLVLSGEHET-----RLVAKLF--KDYSSVVRVEDHRQVVEYVGLQLIQLINVDEK	66
human_beta1_nAChR	1	-----MTPGALLMLLGGALGAPLAPGV-RGSEAE-----RLREKLF--SGYDSSVVRAREYGDVVRVSVGLI LAQLISLNEK	69
human_delta_nAChR	1	-----MEGPVLTGLLAALAVC-----G-SWGLNEE-----RLIRHLFOEKGYNKLRLPVAHKEESVDALALATLSNLSLKEK	69
human_epsilon_nAChR	1	-----MARAPLGV LLLGLL-----GRGVKNEEL-----RLYHHLF--NNNDPGSRVREPEDTYTISLKVTLTNLISLNEK	66
human_alpha7_nAChR	69	NQVLT TN IWLQMS-----WTDHYLQNVSEYPGVKTVRF DGOIWKFDILL--YNSADERFDATFHTNVL	131
mouse_5HT3A	81	NQVLT TY IWRQY-----WDEFLQWTFEDFONVTKLS IPTDS IWPVDILINEFVDVGKSPNIPY--MY	142
human_alpha4_nAChR	80	NQMMTTN WVKQE-----WHDYKLRWDPADYENVTSIRIPSEL IWRPDI VL--YNNADGDFAVHLTKAH	142
human_beta2_nAChR	74	EQIMTTN WLTQE-----WEDYRLTKKPEEFONMKKVR LPSKH IWL P DVVL--YNNADGMVEVSFY SNAV	136
human_alpha1_nAChR	67	NQIVTTNVR LKQGDMDVLP RPSCVTLGVP LFSHLQNEQVVDY NLKWNPDYGGVKKIHI PSEKIWRPDLVL--YNNADGDFAI VKF TKVL	154
human_beta1_nAChR	70	DEEMSKY YLDLE-----WTDYRLSWDPAEHODISLRITAESVYLPDVVL--LNNNDGNFDVYALDISVY	132
human_delta_nAChR	70	EETL TNWIEHG-----WTDYRLSWDAEFGNISVLR LRPDMVWLRPEIVL--ENNDNSFQISYSNVL	132
human_epsilon_nAChR	67	EETL TS WIGID-----WTDYRLSNYKDDFGG IETLRVSELVWLRPEIVL--ENNI DGFVAYDANVL	129
human_alpha7_nAChR	132	VNSSGHCQYLPPGIFKSSCYIDWRWFPDVOHCKLKGWSVYGGWSLDLQMQE-----ADISGYIPNGEVDLVGIPGKRSE	207
mouse_5HT3A	143	VHHRGEVQNYKFLQLVTACSLDIYNFPFDVQNCSTLFTSWLHTIQDINI TLWRSPEEVR-----SDKSIFINOGEWELLEVFPQFKE	224
human_alpha4_nAChR	143	LFDGDRVQWTPPAIYKSSCSIDVTFPFDQOCTMKFGSWTYDKAKIDLVMHRSR-----VDOLFVWESGEWIVDAVGYNT	220
human_beta2_nAChR	137	SYDGSIFWLPPAIYKSAKIEVKHFPDQOCTMKFRSWTYDRTEIDLVLKSEV-----ASLDDFTPSGEWIVALPGRNE	214
human_alpha1_nAChR	155	LQYTGHIWTPPAIFKSYCEIIVTHFPDEQNCMKLGTWTYDGSVVAIPESDQ-----PDLNFMSEGEWIKESRQAKHS	232
human_beta1_nAChR	133	VSSDGSVRWQPPGIYRSSCSIQVTFPFDWQNTMVFSSYDSSSEVSLQTLGPDGGQHQEIH--IHEGTFIENGWEI IHKPSRLIQ	219
human_delta_nAChR	133	VYHYGFVYWLPPAIFRSSCPISVTFYFPDQOCTMKFSSSKYTAKEITLSLQDKAKENRTYVPEWIIIDPEGFTENGWEI VHRPARRV	222
human_epsilon_nAChR	130	VYEGGSVTLPPAIFYRVCAYEVTYFPFDQOCTMKFRSWTYNAEEVEFTFAVDNDGKTI NKID--IDTEAYTENGEWIVDFCPGIVR	216
human_alpha7_nAChR	208	RFYECC--KEP-YPDVTFVTMRRRTIYGLNLLIPCVLISALALLVFLPADS-GEKISLGI TVLLS LTFVMLVAEIMPATS DSVPLI	293
mouse_5HT3A	225	FSIDIS--NS--YAEMKFYIIRRRPLFVAVSLLLPSIFLMVVDIVGFC LPPDS-GERVSKITLLLGYSVFLIIVSDTLFAT-IGTPLI	308
human_alpha4_nAChR	221	RKYECC--AEI-YPDITYAFVIRRLPLFTINLLIPCLISCLTVLVFLPSEC-GEKITLCSVLLS LTFVFLLIITEIIPSTSLVPLI	306
human_beta2_nAChR	215	NPDDST-----YVDITYDFIIRRKPLFTINLLIPCVLITSLAIVLVFLPSDC-GEKMTLCSVLLALTFVLLISKIVPPTS LDVPL	297
human_alpha1_nAChR	233	VTYSCC--PDTPLDITYHFVMO RLPYFIVMMIIPCLLFSFLTGLVFLYLPDTS-GEKMTLCSVLLS LTFVFLLIIVELIIPSTSAVPLI	319
human_beta1_nAChR	220	PPGDRGGREGORGEVIFYLIIRRKPLFVLMVIAPCILITLLAIFVYFLPPDA-GEKMGLSIFALLTLTFVLLLLADKVPETSLSVPLI	308
human_delta_nAChR	223	DPRAPL--DSPSRDITFYLIIRRKPLFVIMINILVPCVLSIFMNVLVFLPADS-GEKTSVAI SVLLAQS VFLLLISKRLPATSMAIPLI	309
human_epsilon_nAChR	217	HGGAT--DGPGETDVIYSLIIRRKPLFVIMINII VPCVLSGLVLLAYFLPAQAGGOKTVAI NVLLAOTVFLFLIAQIIPETSLSVPLI	304
human_alpha7_nAChR	294	AQYFAS TMIIIVGLSVVVTVIIVLQYHHDPDGGKMPKWRVILMLMCAWFLR---MKRPG--EDKVRPACQHKQRCSLASVEMSAVAPP	378
mouse_5HT3A	309	GVYFVVCALLVLSLAETIFIVRLVVKQDLQRPV DWRHLVLDRIAWI LCL--GEOP---MAHRPPATFQANKTDDCGSD--385	385
human_alpha4_nAChR	307	GEYLLFTMI FVTL SIVITVFLVNVHRSRPTHMTPTWVRVFLDIPVRLLL---MKRPSVVKDNCRRRLIESMHKMASAPRFWPEPEGEP	393
human_beta2_nAChR	298	GKYLMTMVLVTF SIVTSVCLNVHRSRPTHTMAPWVKVYFLEKLPALLF---MQOP---RHHCARQLRLRRRORERE-----371	371
human_alpha1_nAChR	320	GKYLMTMVLVFIASIIITVIVINTHRSRPTHVMPNWRKVFIDTIPNIMFSTMKRPSREKQDKIIFTEIDISD ISGK-----399	399
human_beta1_nAChR	309	IKYLMFTMVLVTF SVIISLVVVLNLRHRSRPTHOMPLWVRQIFIHKLPLYLR---LKRPR---KPERDLMEPPHCSSPSSGSGWGR---385	385
human_delta_nAChR	310	GKFLFGMVLVTVVVIVCIIVLNIHFRTSTHVLSEGWKFLLETPELH---MSRP---AEDGSPGALVRRSSSLGYISK-----386	386
human_epsilon_nAChR	305	GRFLIEVMVVA TLI VMNCVIVLNVSRTEHTHMSRPLRHVLELLPRL---GSP---PPEAPRAASPPRRASSVGLLLR-----380	380
human_alpha7_nAChR	379	ASNGNLLYIGFRGLDGVHCVP TPD--S SVVCGRMA-----CSPTHDEHLL-----421	421
mouse_5HT3A	386	-----LLPAMGNHCSHV---GPP-----QDL-----L---PPPREASL-----L---AVRGLLQE	430
human_alpha4_nAChR	394	ATSGTQS--LHPPSPSFCVPLDVP AEPSPSCKSPDQLPQPQPLEAEKASPHPSPPGCRPHPGTQAPGLAKARLSVQHMS SPGEAVEG	480
human_beta2_nAChR	372	GAGALF FREAPGADSC TCFVNRASV-QGL-AGAFGAE-----PAPVAGPGRS-----416	416
human_alpha1_nAChR	400	-----PBP-----PPMGFHSF-----410	410
human_beta1_nAChR	386	GTDEYF--IRKPPSDFLPKPNRFQELSAPDL-----RRFIDGPNRA-----426	426
human_delta_nAChR	387	--AEEYF---LKSRS DLMFEKOSER-HGL-ARRLTTA-----RRFPASSEQA-----427	427
human_epsilon_nAChR	381	--AEEI---LKKRPSRLVFE GQRH-RQT-----WTA AFCQS-----412	412
human_alpha7_nAChR	422	-----HGGOPPEGDP-----DIAKILEE	439
mouse_5HT3A	414	-----L---PPPREASL-----L---AVRGLLQE	430
human_alpha4_nAChR	481	GVRCRSRSIQYCVPRDDAAPEADGQAAGALASRNTHSAELPPDQPSCKCTCKKEPSSVSPSATVKTRSTKAPPHLP LSPALTRAVEG	570
human_beta2_nAChR	417	-----GEPGCG-----GLREAVDG	430
human_alpha1_nAChR	411	-----L IKHP-----EVKSAIEG	423
human_beta1_nAChR	427	-----VALLF-----ELREVSS	439
human_delta_nAChR	428	-----QQLFN-----ELKPAVDG	441
human_epsilon_nAChR	413	-----LGA AAP-----EVRCVDA	426
human_alpha7_nAChR	440	VRYIANRFRCDSEAVCSEWKAFA CVVDR LCLMAFSVFTICTIGILMSAPNFVEAVSKDFA-----502	502
mouse_5HT3A	431	LSSIRHFLEKRDREMRVARDWLRVGYVLDRL LFR IYLLAVLAYSITLVTLWSIWHYS-----487	487
human_alpha4_nAChR	571	VQYIADHLKAEEDTDFSVKEDWKYVAMVIDRIFLWMMFII VCLLGT VGLFLP-PWLAGMI-----627	627
human_beta2_nAChR	431	VRFIADHMRSEDDDSQVSEDMKYVAMVIDRFLWLVFVVCVFTIGMFLQ-PLFQNYTTTTFLHS DHSAPSSK-----502	502
human_alpha1_nAChR	424	IKYIAETMKSQDQESNNAAEWKYVAMVMDHILLGVFMLVCIIGTLAVFAG-RLIELNQGG-----482	482
human_beta1_nAChR	440	ISYIARLQLOEQEDHDALKE DQFVAMVVDRLFWTFEIIFTSVGTGLVFLD-ATYHLPPDPFP-----501	501
human_delta_nAChR	442	ANFIVNHMRDQNNYNEEKDSINRVARTVDRLLCLFVYVTVMMVGTAWIFLO-GVYNRPPFPDGP DYSYNVODKRFI	517
human_epsilon_nAChR	427	VNFVAESTRDQEA TGEVSDIVRMGNALDNI CFWAALVLF SVGSSLI FLG-AYFNRPV DLPYAPCIQP-----493	493

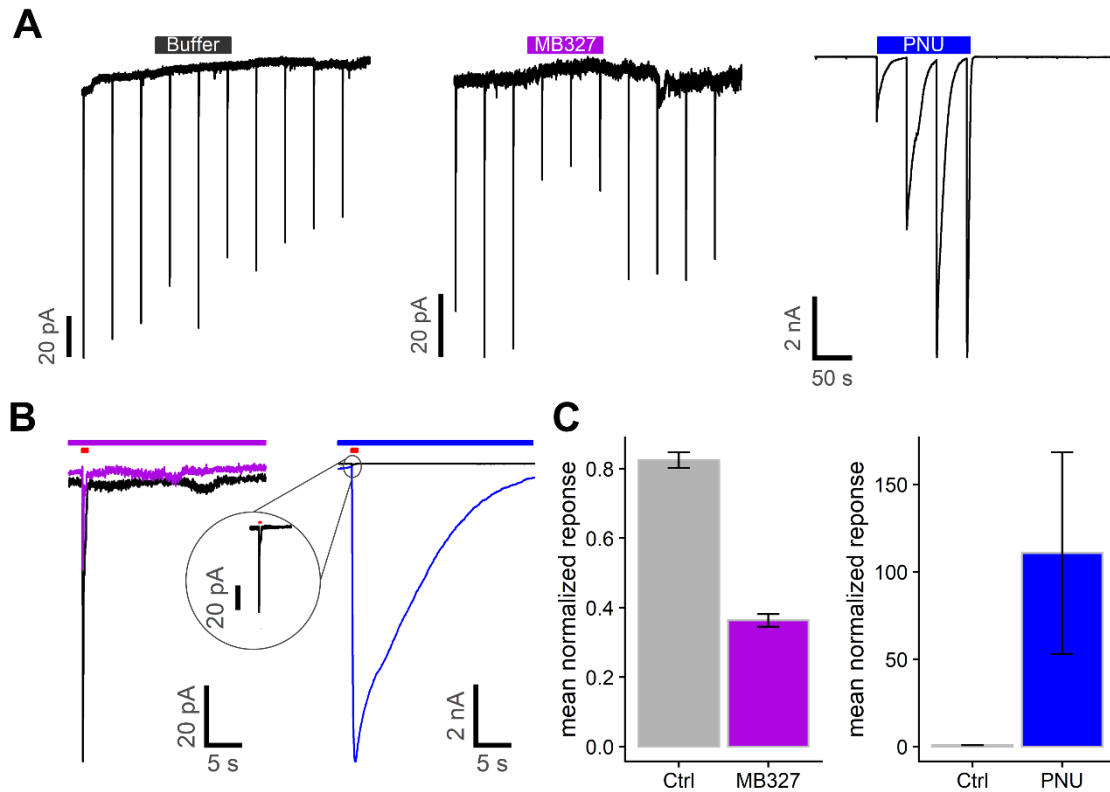
Supplementary Figure S3: Multiple Sequence alignment of cys-loop receptors relevant for this study. Coloring by “percentage identify” towards consensus sequence of the alignment, higher identity is indicated by darker blue. Important residues for PTM0022 binding at the $\alpha 7$ nAChR, identified by molecular docking studies, are framed red, critical residues identified in this study are counted in one cys-loop receptor, position 1 is framed green. Alignment performed using “muscle” algorithm with defaults in Jalview.



Supplementary Figure S4: Co-injection of $\alpha 7$ with NACHO does not affect compound binding. $\alpha 7$ SDT needed for functionality the co-injection of NACHO cRNA. Here we show that NACHO co-injected with WT $\alpha 7$ does not influence compound binding on the example of $1 \mu\text{M}$ PTM0022. Single values with mean as black bar and S.D. Note that co-injection with NACHO boosts currents signal development. In order to work with comparable currents, $\alpha 7$ alone was injected with 5 ng RNA per oocyte and measured after 2 days, whereas $\alpha 7 + \text{NACHO}$ was injected with $2.5 \text{ ng } \alpha 7 + 2.5 \text{ ng NACHO}$ per oocyte and measured after 1 days.



Supplementary Figure S5: Washout of BPCs from nAChR occurs quickly. Typical current traces of $100 \mu\text{M}$ ACh elicited $\alpha 7$ (A) and $30 \mu\text{M}$ ACh elicited muscle-type ($(\alpha 1)_2\beta 1\epsilon\delta$) nAChR (B) with 3 continuous stable control peaks and subsequent 20 s preincubation and co-application of $1 \mu\text{M}$ PTM0022 (red) or $10 \mu\text{M}$ MB327 (magenta). 2 min perfusion between ligand applications, indicated by bars on top of the current traces.



Supplementary Figure S6: MB327 inhibits human $\alpha 7$ nAChR in stable transfected CHO cells. (A) Manual patch-clamp recordings of the inward current responses of human $\alpha 7$ nAChRs evoked by the repeated application of ACh (100 μ M) for 0.5 s in the absence (negative control recording; left) or the presence of MB327 (30 μ M; middle) or PNU-120596 (10 μ M; right) during the compound phase (sweep 4-6). The first three ACh applications (sweep 1-3) were used as the control phase, followed by the compound phase (sweep 4-6) and the washout phase (sweep 7-10). Note the different y-axes. During the third sweep of the recordings with PNU-120596 (10 μ M), two inward current responses were evoked. The first response was triggered by ACh (100 μ M), which was similar to the two previous ACh-triggered responses, and the second response, which was much larger than the response before, was evoked by the application of PNU-120596 (10 μ M) during the washout phase. (B) Overlay of exemplary traces of the inward current responses of human $\alpha 7$ nAChRs triggered by ACh (100 μ M) in the absence (control phase; sweep 2; black) and the presence (compound phase; sweep 5) of MB327 (30 μ M; left; purple) or PNU-120596 (10 μ M; right; blue). The inset on the right side displays the response in the absence of PNU-120596 (control phase; sweep 2; black). The traces from the control phase and the compound phase originate from the same cell, respectively. Note the different y-axes. (C) Ratio of the peak current responses of human $\alpha 7$ nAChRs triggered by the second and the fifth application (sweep 2 and 5) of ACh (100 μ M) during negative control recordings ($n = 5$) and in the presence of MB327 (30 μ M; $n = 4$) or PNU-120596 (10 μ M; $n = 3$). The data are depicted as mean \pm SEM.

Acknowledgements

The research for this Dissertation was conducted within the graduate school “Targets in Toxicology, GRK2338” at the Walther-Straub-Institute for Pharmacology and Toxicology, medicinal faculty of the LMU Munich. To achieve this Dissertation, numerous people prepared the way and supported me along with it. Here, I want to express my gratitude to them.

Above all, I sincerely thank Prof. Dr. med. Thomas Gudermann for establishing the graduate school and creating a space of research and education in the field of toxicology. There would have been no place or funding for my work without his effort.

Next, I want to express my deepest gratitude to my supervisor, mentor, and scientific role model, Prof. Dr. Annette Nicke, for introducing me to the exciting research fields of electrophysiology and nicotinic acetylcholine receptors and allowing me to work with her. The shared ambitions, many discussions, and thoughtful critics shaped my research. Her support encouraged me throughout my Ph.D. and allowed me to grow, scientifically and personally, into the scientist I am today. I especially appreciate the cooperations and laboratory exchanges with other excellent researchers she made possible.

My thank also goes to my group, former and current members equally, for a comfortable work environment with mutual respect and teamwork. I want to especially thank Anna Durner, my yearlong lab partner in the work with *X. laevis* oocytes, for her numerous advice and helpful discussion regarding practical troubleshooting, the shared frustrating moments and her reliable character. Additionally, I thank Heinz Janser, the good soul of the lab, always lent a helping hand if needed and supported me through one or two delicate situations.

Outside of my working group, I would like to express my appreciation for the professional and friendly environment at the whole institute and the input and advice provided by many members during several occasions, such as the institute seminars. Particularly my two other thesis advisors, Prof. Dr. Ingrid Boekhoff and Prof. Dr. Stephan Kröger, provided essential ideas and advice for my Ph.D. work, for which I am very grateful.

Deep gratitude goes to Georgia Giotopoulou, my partner and closest friend, who stood with me throughout all the ups and downs during the exciting 3.5 years of my Ph.D and we came out of it victoriously.

In the end, I want to thank my parents and my whole family, although no words written here could ever really express the extent of my gratitude. Your unconditional support throughout my entire life provided the necessary base for me to thrive and pursue my aims.